Orientation aspects of growth during recrystallization

Juul Jensen, Dorte

Publication date:
1997

Document Version
Publisher's PDF, also known as Version of record

Risø-R-978 (EN)

Orientation Aspects of Growth during Recrystallization

Dorte Juul Jensen

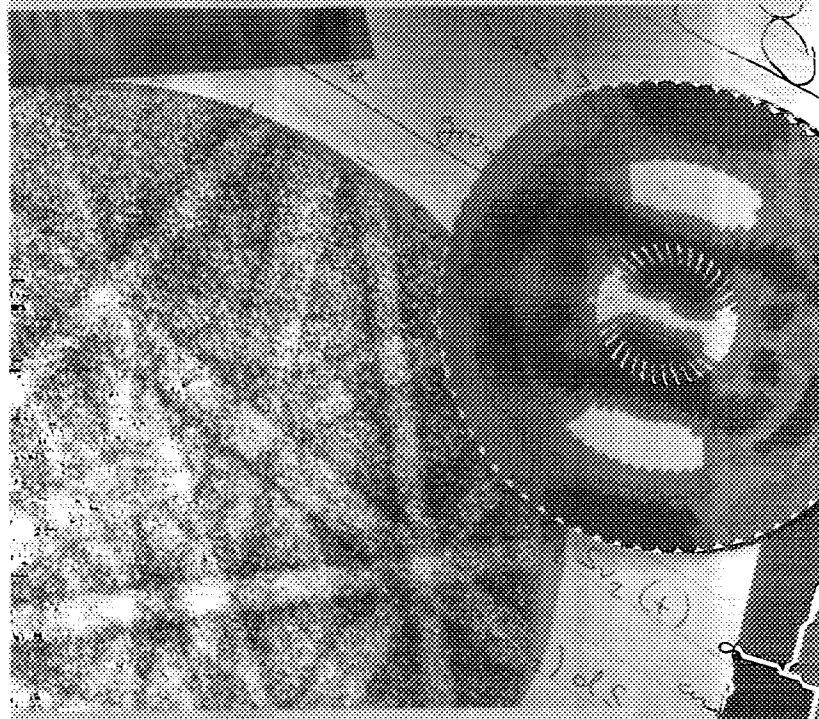

Materials Research Department
Risø National Laboratory
April 1997

ISBN 87-550-2295-2
ISSN 0106 - 2840

Risø-R-978 (EN)
Holbæk Center-Tryk

Risø-R-978 (EN)

Orientation Aspects of Growth during Recrystallization

Risø-R-978 (EN)

Orientation Aspects of Growth during Recrystallization

by

Dorte Juul Jensen

Materials Research Department
Risø National Laboratory
Roskilde, Denmark

Denne afhandling er af Danmarks Tekniske Universitet antaget til forsvar for den tekniske doktorgrad.

Antagelsen er sket efter bedømmelse af den sammenfattende redegørelse samt 8 publicerede artikler.

Lyngby, den 18. marts 1997

Hans Peter Jensen
Rektor

/Anne Grete Holmsgaard
Universitetsdirektør

This thesis has been accepted by the Technical University of Denmark for public defence in fulfilment of the requirements for the degree of Doctor Technices.

The acceptance is based on the summary and 8 articles.

Lyngby, March 18, 1997

Hans Peter Jensen
Rector

/Anne Grete Holmsgaard
University Director

CONTENTS

PREFACE

During recent years, techniques and methods for determining the crystallographic orientations in selected local regions of the microstructure, have been developed and automated to a level which allows rapid and accurate data collection. Thus, detailed characterisation, including orientation aspects, has become possible. This has led to breakthroughs in the quantitative description and understanding of basic metallurgical processes. Within the field of thermomechanical processes in particular, new knowledge about plastic deformation and the growth of new grains during recrystallization has been gained. The present work deals with growth during recrystallization. However, the new knowledge about plastic deformation has shown to be essential in the understanding of recrystallization, so some of the new results on deformation are also included. The work is in four parts covering experimental methods, experimental results, modelling and interpretation of results. Eight papers [A1-A8], published by the author alone, or together with colleagues, form the basis of this work and are reprinted in the Appendix.

The aim of this report is to give a coherent description of how the crystallographic orientation may affect growth during recrystallization. The aim is technical, in the sense that it describes how orientation growth dependencies can be measured experimentally, it gives examples of orientation-dependent growth rates and it discusses the effects hereof on the recrystallization texture and microstructure. Reasons for orientation-dependent growth rates are also discussed, but again, the primary aim is to provide a technical description of the most important mechanisms, rather than to derive fundamental and detailed conditions for grain boundary movements.

The hope is that this report, together with the eight selected papers, will give a comprehensive description of the topic. Therefore, some parts of this report are written as short summaries of the original papers, and the reader is referred to these for more detailed information. Other parts, however, describe, for example, data processing and data interpretation in more detail than it has been possible in the journal papers. So, altogether, the report and papers should enable a reader, first of all, to use the suggested methods and models and, secondly, to understand how the crystallographic orientation can affect the growth during recrystallization.

The selected papers cover work dating back for more than 10 years. In the report, major focus is placed on the more recent papers as these represent the present state of the art. The earlier papers have, however, been important for the development of the field and, therefore, are included in this work.

The eight selected papers are referred to in the report as A1 to A8 and other papers by the author (either as prime author or as co-author) are referred to as A9-A32. The works of other authors are presented in a separate list and referred to by numbers.

1. INTRODUCTION

When a material is plastically deformed, point defects and dislocations are introduced in the material. This content of defects and dislocations, and, thus, the associated stored energy in the material can be reduced by annealing. Basic processes taking place in the deformed material during annealing are recovery, recrystallization and grain growth.

That deformation and annealing can change the mechanical properties of metals, including hardness, strength, formability, fracture toughness etc. has been known empirically for thousands of years, and fundamental studies of these processes date back to more than 150 years. (For a historical overview see [1]). It is hence not surprising that vast amounts of knowledge have been accumulated. However, major progress in the understanding and quantification of the basic mechanisms of deformation and annealing has taken place over the last decade. Three factors have been of prime importance for this progress:

- New, advanced experimental techniques and methods have been developed. In particular, the development and automatization of local orientation techniques, which allow determination of the crystallographic orientation in selected, local volumes in the microstructure, have been shown essential. These techniques have enabled quantitative characterizations during all stages of deformation and annealing.

- More powerful computers, combined with more elaborate mathematical procedures, have offered new possibilities for modelling and for simulation of deformation and annealing processes. One trend has been to extend existing model and simulation codes to work on a more local scale (typically a μm-scale) and to include information about *both* microstructures and crystallographic orientations.

- The drive and stimulation from industries to quantify basic mechanisms that they can implement in their models for thermomechanical processing have also been essential for the recent progress. Keen competition between companies forces industries to optimize their products continuously, to give stricter specifications and to reduce the rejection rate. The trend in industry within the last 10-15 years has therefore been to replace costly empirical trial and error optimizations with more fundamentally based optimization wherever possible. (For a detailed discussion of the relevance of such optimizations of industrial thermomechanical processing in the aluminium industry see [2]).

The present work deals with recrystallization taking place during annealing. Recrystallization is generally separated into two distinct processes: nucleation and growth. During nucleation, almost defect-free nuclei form in the deformed microstructure. During growth, these nuclei grow by grain boundary migration. The nucleation and growth process may take place consecutively or simultaneously, in the sense that while already developed nuclei grow, new nuclei develop elsewhere in the deformed microstructure. The recrystallization process is completed when the entire deformed matrix is replaced by a new grain structure. Examples of a partly and a completely recrystallized microstructure

microstructure are shown in Fig. 1. Besides changing the microstructure, recrystallization generally results in a change in texture (in the preferred crystallographic orientations). An example is shown in Fig. 2.

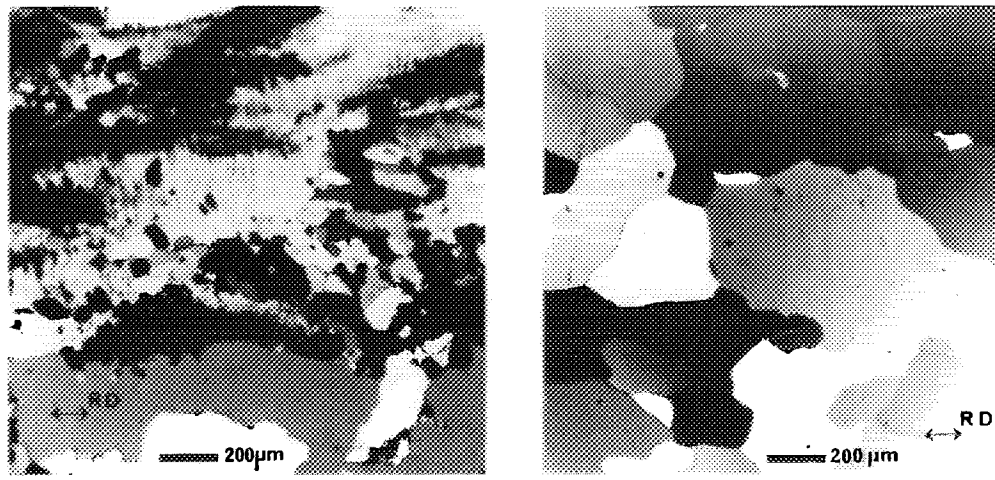

Fig. 1 Microstructure of pure aluminium. a) Partly recrystallized state. Regions with still deformed matrix material have a stripy appearance. b) Fully recrystallized state.

A key question in the understanding of recrystallization is: Does the crystallographic orientation of the nuclei or grains (nuclei/grains) affect their growth or not? Although, the discussion of this question began around 1930 (3 - 5), it has not been settled yet, and more than twenty-five keynote papers have been given on this topic within the last 10 years at international conferences on recrystallization and textures [A4,A7,A9,A10,6-29]. Recently, most attention has been paid to heavily deformed polycrystalline materials and interest has been focused on the development of recrystallization microstructures and textures. For scientists, it is, and has been, a challenge to understand the mechanisms controlling this development. For industry, it is essential to be able to optimize this development in order to improve technological properties of a given material. A notable example of the latter is the improvement of deep drawing characteristics of aluminium sheet for beverage can applications.

By using the newly-developed experimental techniques for local orientation determination mentioned above, it has now become possible to measure directly the growth rate of nuclei/grains with different orientations in polycrystalline materials [A3]. Thus it is possible, without assumptions to quantify whether the crystallographic orientation of the

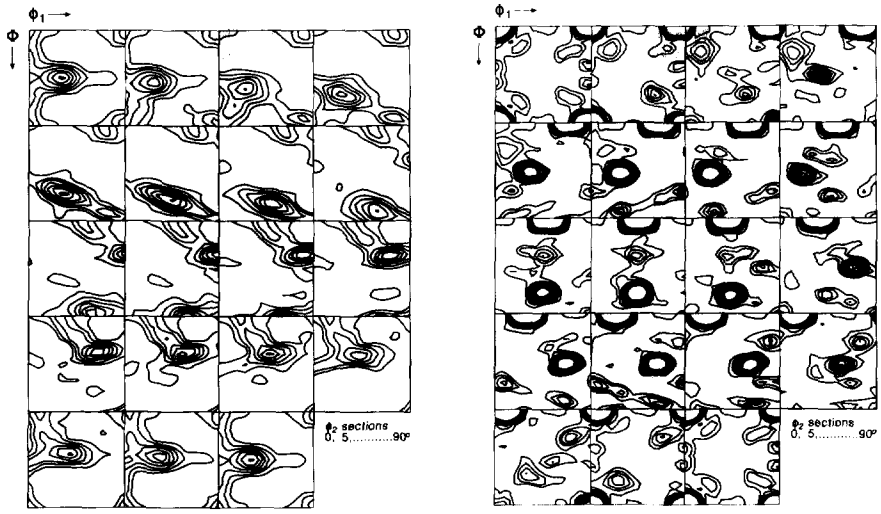

a b

Fig. 2 Texture of Cu (OFHC) represented by 3 dimensional orientation distribution functions. a) Cold rolled to 92% reduction in thickness. b) As a) but annealed to complete recrystallization at 121°C [A6]. (The contour levels are 1, 2, 3, ... x random intensity.)

nuclei/grains affect their growth or not, and to do so for the materials, deformation and annealing conditions which are of interest.

In the present work, it was chosen to study growth in heavily cold deformed, medium to high Stacking Fault Energy (SFE) fcc metals, and among these, cold-rolled aluminium and copper were selected. These metals typically develop medium to strong cube textures upon recrystallization, i.e. a microstructure with many grains having a crystallographic orientation close to cube (with a {100} plane parallel to the rolling plane and a <001> direction parallel to the rolling direction), but also many grains with other orientations. As such, the metals are ideal for studying whether nuclei/grains of the cube orientation grow differently (e.g. faster or slower) than the other nuclei/grains. If a material with a very strong texture has been selected, only nuclei/grains of almost one and the same orientation would develop, and no "competing orientations" could be detected. If a material with a very weak, almost random, texture was selected, identification of which nuclei/grain orientations to look at would be difficult and statistical limitations would emerge.

Other important reasons for choosing cold-rolled aluminium and copper for the present work are that they are of industrial interest and that a great deal of information has been gained recently on the development of deformation microstructures and local distribution

of orientations in these metals. Such information is necessary for understanding the growth mechanisms.

Both pure and commercial purity metals were studied to see the possible effects of impurities/second phase particles. No complex alloys, like heat-treatable aluminium alloys, are included. The growth rate measuring method would apply equally well to such alloys, but it was felt that data interpretation should be clearer and of a more basic nature in the more simple systems.

The outline of the present work is as follows:

The first part deals with the development of experimental methods to study growth rate orientation dependencies in the bulk of polycrystalline materials (Chapter 2 + A1,A2,A3,A5). The best among these experimental methods is then used to quantify growth rate orientation dependencies for a series of selected metals and deformation + annealing conditions. The results are the first of their kind and prove that crystallographic orientation can have a significant effect on growth rates (Chapter 3 + A3,A6,A7). When experimental observations display effects of crystallographic orientations, models for recrystallization have to be developed which take orientation into account. This has led to a new generation of recrystallization models - multicomponent models - which include information about both microstructure and texture (Chapter 4 + A4,A8). The new multicomponent models have been used to investigate recrystallization in a series of materials, deformed and annealed under selected conditions. Only a few results from this specific-case modelling are included in this report for illustration purposes; for more information, the reader is referred to the original papers. Instead, results from a more general type of simulation are included (Chapter 5 + A8). Here, one of the multicomponent models is used to predict the effects of orientation dependent growth (as that observed and reported in Chapter 3) on the development of recrystallization textures and microstructures under various nucleation assumptions.

Finally, knowledge about the characteristics of the deformation microstructures and distribution of orientations on a local scale, typical for the selected metals deformed to high strains has led to the discovery of a new mechanism which is important for growth, (Chapter 6 + A6,A7).

2. EXPERIMENTAL METHODS TO STUDY GROWTH RATES OF GRAINS WITH DIFFERENT ORIENTATIONS

In this chapter, experimental methods used to study the effects of crystallographic orientation on growth during recrystallization in polycrystalline materials will be described and evaluated. Some of these methods reveal growth in the bulk of large samples whereas others are suitable for studies in, or near, the surface. With the surface techniques, for example by in-situ annealing in a high-voltage electron microscope, very precise information about the movement of specific boundaries can be obtained. However, doubt always exist, whether the observations reflect the bulk processes, or whether they are controlled by surface effects, such as oxidation and surface geometry. Only bulk methods will, therefore, be considered here.

Before starting the description and discussion of such methods, impingement between nuclei/grains can have significant effects on the recrystallization process [A11] as well as on growth rate determinations and shall thus be described in some detail here: During recrystallization the nuclei may form far apart, fairly randomly distributed in the microstructure or closer together at special potential sites like triple junctions, original grain boundaries, deformation inhomogeneities or second phase particles. Then they grow, the driving force being provided by the energy stored in the plastically deformed matrix. Sooner or later the nuclei or grains, as they are called after some growth, will impinge upon other nuclei/grains. An example is shown in Fig. 3. Here several nuclei/grains are seen which have impinged upon each other. In the sketched version (Fig. 3b), the impinged grain boundary segments are shown by thick lines. These impinged grain boundaries or grain boundary segments will not experience further driving force from deformed matrix material and will not move further by recrystallization. When the aim is to determine growth rates during recrystallization, it is the velocity of the *free unimpinged* grain boundaries or grain boundary segments which has to be determined.

Among the bulk techniques, a traditional method to determine the growth rate is to measure the size of the largest grain in a partly recrystallized sample or in a series of partly recrystallized samples, and simply divide the size by the corresponding annealing time. Typically, this method has been used for growth rate determinations not taking the orientation of the nuclei/grains into account [e.g. 30,31]. However, if the orientations of the nuclei/grains are determined and categorized into preselected orientation groups (e.g. all nuclei/grains with orientations within x degrees from an ideal orientation "i" may be referred to as "i" nuclei/grains), effects of orientation on growth rates may also be determined [A12]. However, irrespective of whether orientations are included or not, several problems are associated with this method: (i) even when a major number of nuclei/grains are characterized, large uncertainties are associated with the determination of the largest grain sizes, (ii) the method can only be used in the earliest stages of recrystallization, where impingements between grains are not dominating the growth (typically less than 15% recrystallized) and, (iii) variations in growth rates of individual nuclei/grains within an orientation group, for example, due to different surroundings, are not registered, only the highest rate is determined. This method has, therefore, not been much used recently, and shall not be considered further here.

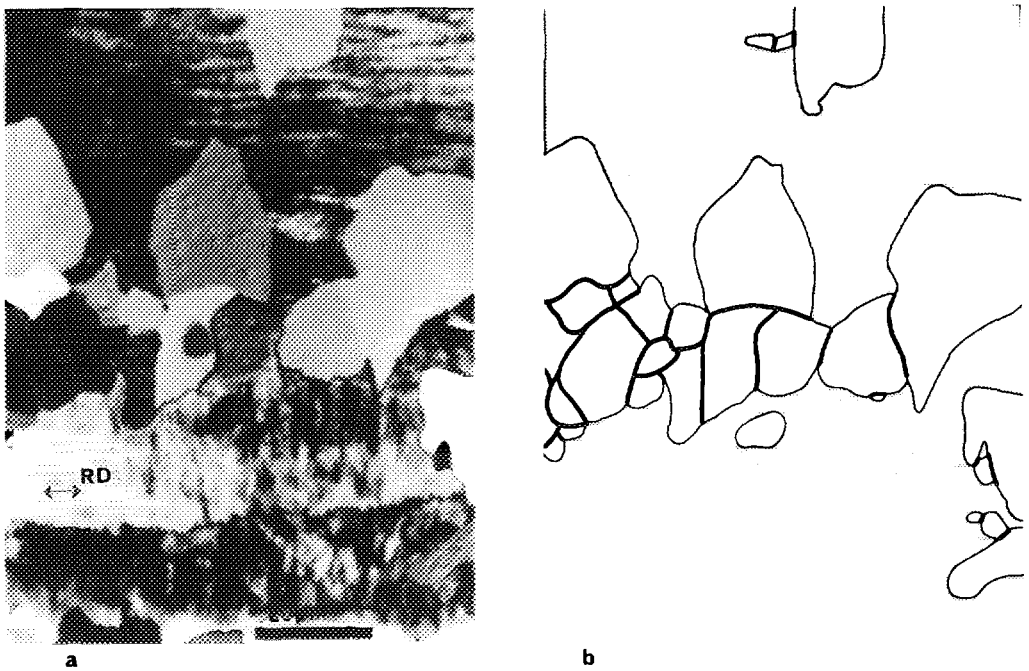

Fig. 3 Partly recrystallized microstructure of pure aluminium. a) Micrograph. b) Sketch of the micrograph; deformed regions are shown in grey and the nuclei/grain boundary segments which have impinged upon other nuclei/grains are shown by a thick line.

During the last 10-15 years, information about effects of orientation on growth rates has mainly been achieved from two other types of measurements: texture measurements and simultaneous size and orientation measurements. These types of measurements have been used both for static investigations, for example, looking at the fully recrystallized state and for kinetic investigations following the recrystallization process. But in neither case, direct information about growth rates is obtained; growth rate results can only be deduced indirectly, via an interpretation of the data. An example of such an interpretation could be: if it is observed that nuclei/grains of a specific orientation, "i", develop to become larger than other nuclei/grains, it is because the "i" nuclei/grains have a higher growth rate than the others. A main problem is, however, that information about nucleation sites and rates are not included and this may result in wrong interpretations of growth rates. If, for example, nuclei of a given orientation "i" form in clusters, they will, early in the recrystallization process, impinge upon each other and their growth will stop in the direction of the impingement. So, regardless of how high their true growth rate was, they will appear small in the grain size distribution, or, as a weak texture component. A data interpretation not taking the nucleation sites and, therefore, the impingements into account will in such a case conclude that the "i" nuclei/grains are characterized by slow

In spite of these difficulties, the two methods have in the 80s and early 90s been very important for the development in the understanding of growth during recrystallization. The two methods shall therefore be described shortly in the following.

The best method for the determination of orientation effects on growth rates available today is the so-called extended Cahn-Hagel method [A3]. It is based on a determination of both the development of recrystallized volume fraction and free unimpinged interfacial area of the individual nuclei/grains. Therefore, the method can determine directly the average growth rates of recrystallizing nuclei/grains without assumptions about nucleation sites and rates. This method will be described in detail in section 2.3. Finally, the benefits of a combined use of all 3 methods will be pointed out in section 2.4.

2.1 Texture methods

Recrystallization is typically associated with a significant change in texture [e.g. A9,32] and the texture changes may be used to gain information about growth during recrystallization. Textures are mostly determined by x-ray or neutron diffraction techniques. The main difference between the two techniques is that x-rays sample the texture within a relatively thin layer of material, whereas the neutrons typically sample complete bulk textures. Depending on the problem, the more suitable technique of the two may thus be chosen. With both techniques, first pole figures are measured for a series of (hkl) reflections, and then the corresponding three dimensional Orientation Distribution Function (ODF) is calculated. Standard procedures are available for both the experimental measurements and the data analysis [e.g. 33]. Both static and kinetic texture measurements have been performed.

Static measurements. The texture is measured before and after recrystallization and by comparing the two measurements, information about growth has been deduced. Typically this is done by applying a specific growth assumption to the deformation texture - for instance, all nuclei with a 40° <111> misorientation relationship to the deformed material grow twice as fast as the other nuclei. The "transformation texture" calculated in this way can then be compared to the measured recrystallization texture to test whether the growth assumption can simulate the experiment correctly [e.g. 13,16,34,35].

A problem with this method is that nothing is known about the orientation of the nuclei. So assumptions have to be made, and these can, of course, have significant effects on the calculated transformation texture and thus on the evaluation of growth assumption. In some studies [e.g. 36,37] this problem is overcome by measuring the orientations of a large number of nuclei in a lightly annealed sample using local texture techniques. The calculations of the transformation texture can then be based on this "nucleation texture", and a more reliable evaluation of the growth assumption is thus possible. However, even in this case, information about nucleation sites and rates is lacking, which, as discussed above, may affect the interpretation.

Kinetic measurements. A neutron diffraction texture instrument has been especially developed [A2,A13]. It is equipped with a position sensitive detector positioned with its axis vertical. So, instead of only measuring one point in a pole figure with a given sample setting, a whole section of a small circle (see Fig. 4) is measured simultaneously. With this

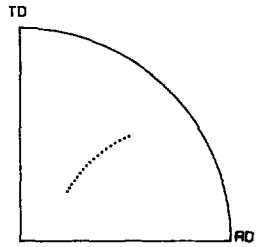

Fig. 4 Measuring points along the position sensitive detector with one sample setting covering 34° of a small circle in the pole figure plane [A2].

equipment, the measurement of a complete pole figure typically takes less than ½ hour, depending somewhat on the scattering cross section of the sample material. With the fast neutron texture equipment, the complete texture transformation during recrystallization may thus be followed in-situ while annealing the sample. An example of results from such an investigation is shown in Fig. 5. Alternatively, the kinetics of single texture components may be studied. For this type of measurement, the sample is positioned so that the position sensitive detector covers particularly interesting components. A time resolution in the order of seconds is thus achieved [A13]. An example is shown in Fig. 6.

The data give very precise information concerning how the concentration of different texture components evolves during recrystallization, and it is clear to see if a given component increases/decreases faster than another one. Furthermore, the data have the virtue of being in-situ data whereby any scatter or uncertainty introduced by using different samples annealed for different periods are illiminated.

2.2 Size and orientation methods

The aim of this method is to determine simultaneously the size and orientation of nuclei/grains. This can be done using local texture techniques, such as microdiffraction and Kikuchi-line techniques in TEM, channelling patterns and Electron Back Scattering Patterns (EBSP) in SEM, Kossel x-ray diffraction or crystallographic etching techniques. Among these, the EBSP technique has recently been the most widely applied. It has a better spatial resolution than the channelling pattern (SEM) and the Kossel x-ray diffraction, and a more precise orientation determination than the etching techniques. Compared to the TEM based techniques, the EBSP technique offers a much large area of inspection and easier sample preparation. The spatial and the orientation resolution are, however, significantly poorer in the SEM than in the TEM, but for recrystallization growth

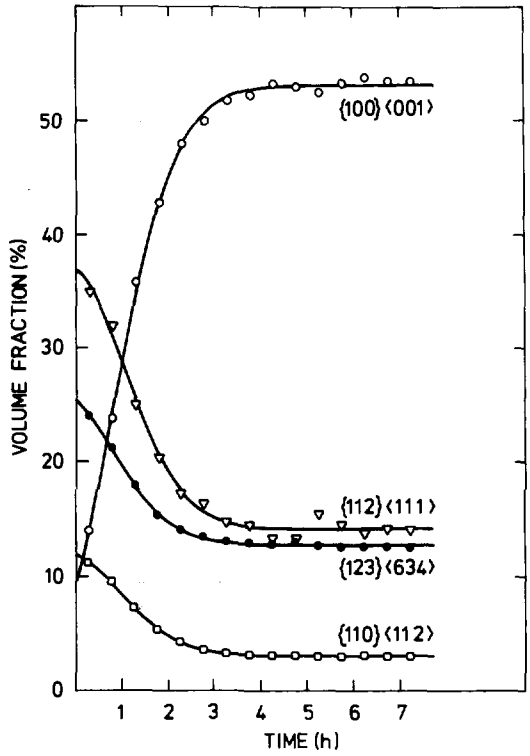

Fig. 5 The development of specific texture components during isothermal annealing at 95°C of copper (OFHC) cold rolled to 90% reduction in thickness [A2].

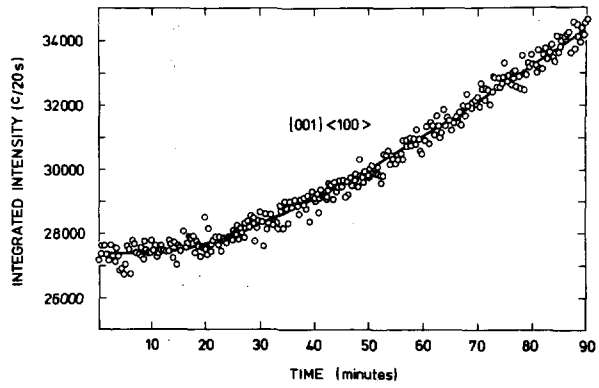

Fig. 6 Kinetic curve for the initial evolution of the cube texture component, {100} <001>, in commercially pure aluminium (Al-2S) cold rolled 90% measured during annealing at 253°C. The full line is a best fit to a kinetic equation. (The notation {100} <001> or more generally {hkl} <uvw> refer to a crystallographic orientation with a {hkl} plane parallel to the rolling plane and a <uvw> direction parallel to the rolling direction) [A2].

studies, where nuclei/grains larger than 1 μm have to be characterized and orientations are classified within orientation groups typically not less than 5-10° wide, the resolutions of the SEM based EBSP technique match the requirements, and the technique is thus ideal for simultaneous determination of size and orientation during recrystallization. (For a further discussion see [A5]).

Static measurements. The method may be used to characterize fully recrystallized samples. The size of a nucleus/grain may be determined looking directly at the microstructure. And the orientation may be determined by placing the electron beam inside the nucleus/grain and switching to EBSP mode. This procedure is, however, rather time consuming to use, and it is often preferable to stay in the EBSP mode and make line scans through the structure by moving the beam or the sample. By recording the vernier positions of the sample stage (in the case of sample movement) at which the EBSPs change, the chord lengths (linear intercept lengths) of the corresponding grains are determined. In the data-analysis the grains are catalogued, according to their orientation, into selected orientation groups, and size-orientation relationships may be deduced. From the data, one can see if grains of a specific orientation have exceeded the growth of the other grains.

Kinetic measurements. Information about the kinetics may be obtained, if size-orientation measurements are performed for a series of partly recrystallized samples annealed for various times. In this case, a distinction between recrystallized nuclei/grains and deformed matrix is necessary. This may be made based on the characteristics of the EBSPs (A5,A14,38): When the scan is through a recrystallized nucleus/grain, the EBSP is invariant (showing one, single, orientation) and sharp. Whereas the EBSP will often change rapidly (or the pattern moves around) due to misorientations between neighbouring volumes in the deformed microstructure, and the patterns may be blurred or non-existent when scanning through deformed material. For the recrystallized nuclei/grains, chord lengths and orientations are determined as described above.

Kinetic size-orientation measurements give precise information about how the sizes of the nuclei/grains with the selected orientations evolve during recrystallization. This type of measurement was, to the author's knowledge, first carried out using channelling patterns in an investigation of recrystallization in heavily cold rolled aluminium [A1,A15]. The results are shown in Fig. 7. In a publication by Hjelen, Nes and Høier at Int. Conf. on Al Alloys (1986) it was stated that "A new wave in this discussion has emerged with the recent investigation by Juul Jensen et al. [A1,A15] and by Nes and Solberg [39]". Indeed, nowadays a number of major laboratories studying recrystallization are measuring size-orientation relationships, for example Drexel/Los Alamos [e.g. 40,41], Trondheim [e.g. 42,43], Aachen [e.g. 27], Manchester [e.g. 44], Alcan [e.g. A16], Alcoa [e.g. 45] and Risø [e.g. A1,A6].

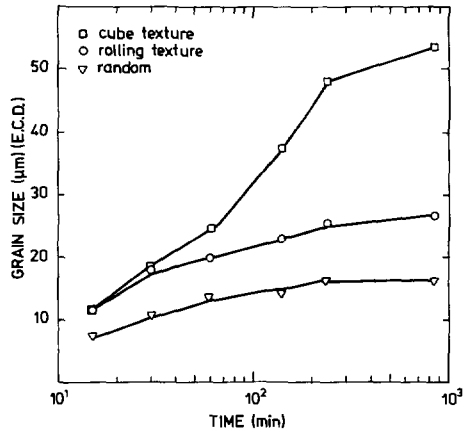

Fig. 7 The average size of nuclei/grains with different orientations (belonging to different texture components) measured in a series of partly recrystallized commercially pure aluminium (Al-2S) samples (cr 90%) annealed at 253°C [A1].

2.3 Extended Cahn-Hagel method

Using this method, average growth rates of nuclei/grains having different orientations are determined directly. The basic idea was originally suggested by Cahn and Hagel (46) for the formation of pearlite during austenite decomposition of steel.

Cahn and Hagel showed that the overall transformation rate is given by

$$\frac{dX}{dt} = <G> S_v \tag{1}$$

where, X is the volume fraction of transformed material, t is the reaction time, <G> is the spatially - averaged interface velocity, and S_v is the interfacial area per unit volume separating the parent and product phases.

It was later shown that the method is equally successful for characterizing recrystallization (30,40,41,47-49). In the recrystallization case, X is the volume fraction of recrystallized material, t is the annealing time, <G> is the average growth rate, and S_v is the total "free" unimpinged grain boundary of the nuclei/grains per unit sample volume - i.e. the interfacial area between recrystallized and deformed material.

The latest development of the Cahn-Hagel method has been to extend it to include crystallographic orientations [A3]. Thereby, average growth rates of grains of various specified orientations $<G_i>$ can be determined. This only requires that the crystallographic orientations of the individual nuclei/grains are determined. Then

$$\frac{dX_i}{dt} = < G_i > \cdot S_{vi} \qquad (2)$$

Where "i" refers to a specific orientation (or orientations within x degrees of a specific orientation).

To calculate $<G_i>$, X_i and S_{vi} first have to be determined. Often this is done by a lineal analysis of the microstructure. Stereologically it has been shown that X is equal to the line fraction of recrystallized material provided the test lines are chosen randomly (3D) in the microstructure [50,51]. X_i is thus equal to the line fraction of material with orientation "i".

The basic equation relating the number of intersections of test lines with a system of interfaces or surfaces in space was derived several times ([52] was the first). The derivation is based upon the geometrical probability of intersecting an element of surface area with a large number of test lines. The number of intersections N_L per unit length of test line is calculated, and when averaged over all orientations of test lines, the surface area or interfacial area per unit volume, S_v, is found to be

$$S_v = 2N_L \qquad (3)$$

and

$$S_{vi} = 2N_{Li} \qquad (4)$$

where N_{Li} is the number of intersections of boundaries separating a deformed region from a recrystallized nuclei/grain of orientation "i" per unit line length.

Using the EBSP technique in the SEM, it is possible to determine the orientation of volumes larger than 1 μm, and the technique is therefore very well suited to determining X_i and N_{Li}. The typical experimental procedure is to make line scans through the microstructure (see Fig. 8). As described in section 2.2, recrystallized regions are distinguished from deformed regions by the steadiness and blurring of the EBSPs. For each recrystallized nucleus/grain, the orientation is determined automatically by a computer [A5,A17,A18,53,54], and the nucleus/grain is then catalogued into one of a number of preselected orientation groups. In Fig. 8, the nuclei/grains are catalogued into 3 orientation groups, each represented by a colour: red, blue and green. For each nucleus/grain also the linear intercept length (chord length) is measured and stored in the computer. The number of transitions between deformed and recrystallized regions of orientation "i" (or vice versa), n_{Li}, is counted. When the linear scan is completed, X_i is calculated as the sum of all linear intercept lengths of i-oriented nuclei/grains divided by the total length L of the line scan. N_{Li} is equal to n_{Li}/L and thus $S_{vi} = 2 \cdot n_{Li}/L$.

The main concern in determining $<G_i>$ from (2) once X_i and S_{vi} are measured as a function of time, is in finding the time derivative of X_i. The same concern applies to the standard Cahn-Hagel approach where the orientations, "i", are not included. As discussed by

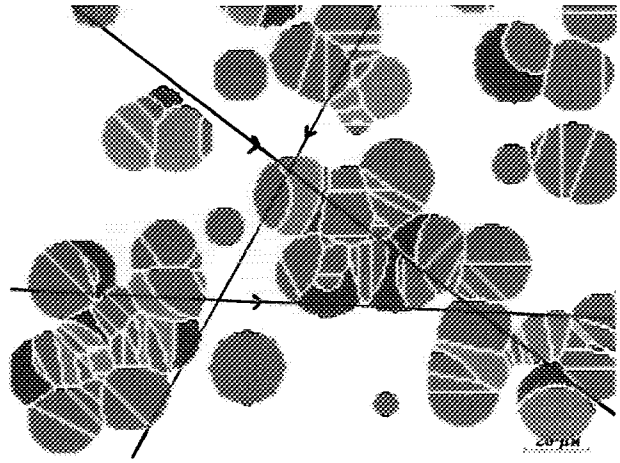

Fig. 8 Sketch of line scan through a partly recrystallized microstructure. Deformed regions are shown in white, and recrystallized nuclei/grains are shown in colour. The nuclei/grains are categorized into 3 orientation groups each represented by a colour - red, blue and green. For each scan along a randomly oriented line the following 5 characteristics are recorded: i) The chord length of each recrystallized nucleus/grain, ii) the length of deformed regions, iii) the number of interfaces between deformed material and recrystallized nuclei/grains of each orientation, S_{vi}, iv) the number of interfaces between recrystallized nuclei/grains of orientation "i" and "j", R_{ij} and v) the total length of the scan-line.

Vandermeer and Juul Jensen [A19] this concern is minimized if a suitable function describing X(t) can be deduced from which the time derivative can be calculated. Frequently, the Avrami equation [55-57] is used

$$X = 1 - \exp(-k \cdot t^{\beta}) \tag{5}$$

where k and β are constants. There are, however, many recrystallization studies where it has been observed that this equation does not describe X(t) sufficiently well over the entire annealing time period [e.g. A19,28,58-60]. An example is shown in Fig. 9. Other functions have to be chosen. It has been found [A6,A19] that better fits are obtained using an exponential function or a power law:

$$\log \ln\left(\frac{1}{1-X}\right) = A + B\exp\left[-C\,(\log t - D)^{E}\right] \tag{6}$$

$$\log \ln\left(\frac{1}{1-X}\right) = A + B(\log t) + C(\log t)^2 + D(\log t)^3 \tag{7}$$

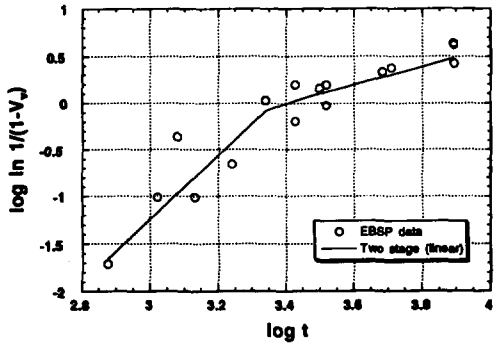

Fig. 9 Double-logarithmic plot of $\ln\frac{1}{1-X}$ versus t for annealing of 92% cold rolled, OFHC copper. (In the figure "V_v" is used instead of "X".) The fact that one straight line cannot fit the data well shows that the Avrami equation cannot represent the recrystallization kinetics [A19].

where A, B, C, D, E are fitting constants. Both functions generally describe the experimental data well. An example is shown in Fig. 10. As the exponential function (6) seems to give the most reasonable results just outside the investigated time interval, this function is generally chosen. It is however worth noticing that only insignificant differences are obtained between the growth rates calculated based on the two functions above, (6) and (7) [A6]. One concern could be the many fitting constants compared to the often fairly low number of experimental points (typically 5 to 10). But as the fitting constants are used only to gain a precise description of the experimental data not for any interpretation of physical phenomena, this is generally not important for the resulting growth rates.

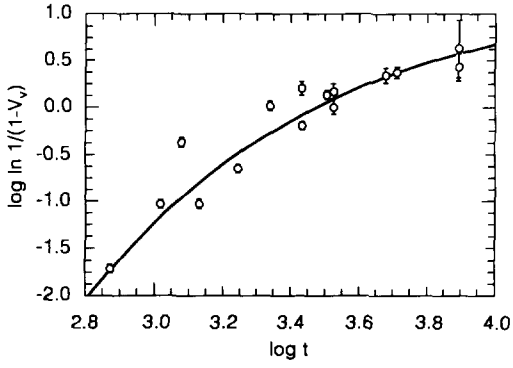

Fig. 10 Similar plot as Fig. 9 and the same experimental data. The full line is here the best fit to equation (6) with "E" fixed at one. It can be seen that the equation (6) represents the experimental data well over the entire annealing period. (Redrawn version of figure from [A19].)

The functions in (6) and (7) were also found to describe well the development of the individual orientation groups, X_i. When equation (6) or (7) is used to describe $X_i(t)$, the time derivative is calculated numerically.

When evaluating the potentials of the extended Cahn-Hagel method, a drawback is the time taken to collect the necessary EBSP data which typically requires a week (or more) hard work at the SEM. However it appears, at present, to be the best method available to study orientation effects on growth during recrystallization. Common to both the extended and the standard Cahn-Hagel method is that impingements between nuclei/grains do not cause problems, as it is only the movements of free-unimpinged boundaries (or boundary-segments) which are measured and included in the growth rate calculations. Also, there are no assumptions made about spatial distribution of the nuclei or the nucleation rate. Further, the growth rates may be anisotropic with respect to the sample axis. When the aim is to achieve true statistical average growth rates, the only requirement is that the test lines are selected randomly in the sample and, of course, that statistically sufficient data are collected. (In specific recrystallization studies, it may be decided not to use random test lines, but lines along major sample axes - for example along the rolling direction of rolled sheet metals. In that case, growth rates along the selected direction(s) are obtained.)

2.4 Combined use of the experimental methods

Recrystallization in general, is a complex process and to gain an as complete and precise description of the process as possible, it is, in most cases, beneficial to use several complementary methods in the characterization. This was discussed in [A2].

When the aim is to determine average growth rates for nuclei/grains of different crystallographic orientations, the extended Cahn-Hagel method is ideal to use. But even in this case, where one method can give the answer directly, it is advisable to also use bulk texture and size-orientation information.

Important examples for the present work are:

- Determination of the recrystallized texture in the complete bulk sample by static texture measurements eases the selection of suitable orientation groups and can be important when checking to see if the extended Cahn-Hagel analysis using EBSP measurements along discrete lines is representative for the entire material.

- Determination of the texture kinetics by the neutron measurements gives better statistical data than the EBSP measurements and may thus be used for comparisons, and to evaluate the suitability of kinetic functions for X(t) (as equation (6) and (7)).

- Size-orientation data are useful to evaluate reasons for orientation dependent growth rates (see section 3.4) and for modelling purposes (see Chapter 4). (It is worth noticing that the size-orientation data are obtained without any extra work when doing an

EBSP scan together with the other data necessary for the extended Cahn-Hagel analysis.)

3. GROWTH RATES DETERMINED BY THE EXTENDED CAHN-HAGEL METHOD

As the extended Cahn-Hagel method is the best technique available today for direct studies of effects of orientation on growth rates during recrystallization, results obtained by this method will be presented in the following. Whereas many results exist from traditional Cahn-Hagel analysis of recrystallization, the extended Cahn-Hagel analysis has, so far, almost exclusively been used by the present author and co-workers. The only exception is, to the author's knowledge, the work by Hutchinson and Ryde on the recrystallization of cold rolled steels presented at the Risø Symposium 1995 [28]. However, their growth rate analysis was limited to a narrow recrystallization range ($0.3 < X < 0.4$) and was, in that range, based on characterization of only 3 samples. These results will therefore not be included in the following. The data to be shown are those published in A3,A4,A6,A7. The full data analysis is described in detail (not possible in a journal publication) for one material and annealing condition, whereas only the final resulting growth-rate curves are presented for the other materials and annealing conditions.

The materials to be dealt with cover pure as well as less pure (commercial purity) aluminium and copper. By including the commercial purity aluminium in the investigation, information about influences of impurities is obtained. In the literature, it has been argued that a reason for the observed orientation effects in commercially pure aluminium could be impurity pinning. Also, an initial size advantage of special subgrains, has been suggested as an explanation for the observed results. Such interpretations are discussed in relation to the present data in the final section of this chapter.

3.1 Materials

The materials investigated were pure aluminium, aluminium of commercial purity and copper (OFHC) (see Table I). Three of the four starting materials were prepared in research laboratories (see Table I), whereas the aluminium AA1050 commercial purity material was prepared on an industrial scale by a combined effort from Hydro Aluminium, Norway and Alcan Int., UK as part of a Brite/Euram project. This Al AA1050 was cast as ingot with dimensions 0.6x1.2x3.3m and homogenized in accordance with standard industrial practice by Hydro Al. An almost random texture and a very homogeneous grain size distribution with an average size of 100 μm were achieved by break-down rolling and reheating at Alcan. All aluminium materials were rolled at room temperature at Risø to a total reduction in thickness of 90%, whereas the copper material was rolled also at room temperature in the University of Braunschweig to 92% reduction. (This is referred to as cold rolling or just cr.) The subsequent isothermal annealing was carried out in various air, vacuum and bath type furnaces. More details are given in Table I.

The EBSP scans were performed along principal, non - random, directions in the samples - along RD and/or ND and/or TD. The resulting growth rate data therefore represent the average growth rates along these principal directions. The scan directions were chosen to capture the main growth anisotropies. For example, for Al AA1050 annealed at 280°C, the

Table I Samples used for extended Cahn-Hagel analysis of orientation effects on growth rates

Material**	Initial Material prepared at	Purity	Initial heat treatment	Second phase particles	Initial grain size μm	Initial texture	Rolling reduction %	Annealing Furnace	Annealing temp. °C	EBSP scan directions
Pure Al	Risø	99.996	240°, 1h	-	230	Cube	90	Air	110	RD + TD
Al-2S	Risø	99.6	600°C, 24h vacuum, furnace cool	$FeAl_3$ 2.3 μm	50	Weak cube	90	He-furnace $\dot{T}$ = 50°C/min.	253	RD + TD
Al-AA1050	Hydro Al and ALCAN	99.5	600°C, 24h vacuum, slow cool to 500°C then furnace cool	$FeAl_3$ 1.7 μm	100	~random	90	Molten-tin bath	280	RD + ND *
								Air	245	RD + ND
Cu OFHC	Braun-schweig	99.96	450°C, 1½h in 5N argon	-	35	-	92	DSC-7 calorimeter	121	RD + TD

** In the report, the word "copper" is sometimes used instead of Cu (OFHC), and Al-2S and Al-AA1050 may be referred to as commercial pure aluminium or just aluminium.

grains were fairly equiaxed when seen in the rolling plane section (RD/TD aspect ratio = 1.1), whereas, in the longitudinal section, the RD/ND aspect ratio was 1.4. In this case, the EBSP scans were along RD and ND. For further details see Table I.

3.2 Growth rate analysis in aluminium AA1050

In this section the extended Cahn-Hagel analysis is described in detail for Al AA1050 cold rolled 90% and isothermally annealed in a bath at 280°C (the condition marked by an asterisk in Table I). The choice of this material and annealing condition for the detailed description was somewhat arbitrary.

A series of partly recrystallized samples was prepared by annealing for different times between 120 and 7200 seconds to achieve various degrees of recrystallization between 2% and 95%. The overall bulk texture was determined by neutron diffraction [A13,A20] in the deformed state and after complete recrystallization. The corresponding ODFs are shown in Fig 11. The deformation texture (Fig. 11a) is typical for aluminium with peak intensities around 7-9 times random along the skeleton line (running through the φ_2-sections from Br

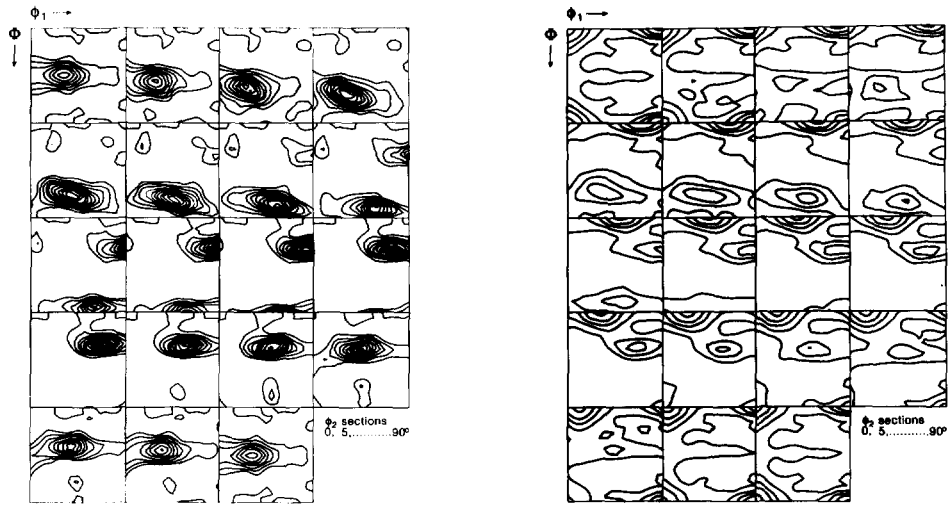

a b

Fig. 11 Textures represented by ODFs of aluminium AA1050. a) Cold rolled to 90% reduction in thickness. b) As a) but annealed to complete recrystallization at 280°C. (The contour levels are 1, 2, 3, ... x random intensity) [A6].

{110} <112> through S {123}<634> to Cu {112}<111>). The recrystallization texture (Fig. 11b) contains a cube component {100}<001>, retained rolling components (compare Fig. 11a and 11b) and a relatively large volume fraction of other components apparently randomly distributed in the Euler space. In the following, the last will be referred to as the random component. These 3 components, cube, rolling and random were selected for the

extended Cahn-Hagel analysis. The ODF (Fig. 11b) also shows that the full width half maximum of the cube and rolling texture components is about 15° in Euler space. Thus EBSP data were separated into these 3 components: cube - within 15° in Euler space from the ideal cube positions, rolling - within 15° from any of the 3 main rolling components (Br, S, Cu) and all the remaining orientations are catalogued as part of the random component.

EBSP scans were made along RD and ND in the longitudinal sample section. For each sample and in each direction, more than 1 mm long line scans were made. The EBSP results are listed in Table II. The table shows that some differences exist between the data measured along RD and ND respectively. This is most marked for the average grain sizes, showing that in the almost fully recrystallized state (7200 sec.) the grains have an aspect ratio of 1.4. In the following, the average values of the RD + ND results will be used. (If growth rates along RD and ND were to be determined separately, more data would have been required to improve the statistics.)

Information about the increase in average nuclei/grain size with annealing time for the 3 orientations is obtained directly from the data. The results are shown in Fig. 12. It is seen that initially the cube nuclei are similar in size to the other nuclei, but that the cube nuclei/grains grow to become the largest in the fully recrystallized state.

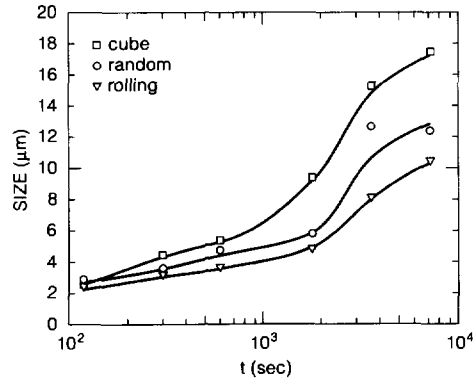

Fig. 12 The average size of nuclei/grains with different orientations (belonging to different texture components) measured for a series of partly recrystallized aluminium AA1050, cr 90% and annealed at 280°C [A6]

The number of intersections, n_L, between recrystallized nuclei/grains and deformed material and the total length of line scan, L, is used to calculate $S_{vi} = 2n_{Li}/L$ for each component. (It is important to note that for the sample annealed 7200 seconds to 95% recrystallization, the statistics on the n_{Li} data are poor. Therefore, this point is not used in

Table II Results of EBSP measurements in a series of partly recrystallized samples of Al AA1050, cr 90% and annealed at 280°C. (Ran = Random, Rol = Rolling and Cub = Cube orientations. Tot = total, including all orientations)

Anneal. time (s)	Scan dir.	L	Number of grains				Average size (μm)				X_i (%)				n_{Li}			
		(μm)	Ran	Rol	Cub	Tot	Ran	Rol	Cub	Tot	Ran	Rol	Cub	Tot	Ran	Rol	Cub	Tot
120	RD	14377	52	13	5	70	3.3	3.1	3.0	3.2				1.56	83	23	4	110
	ND	6465	39	26	2	67	2.2	1.8	1.5	2.0				2.09	65	48	4	117
	Aver	20842	91	39	7	137	2.8	2.2	2.6	2.6	1.22	0.41	0.09	1.72	148	71	8	227
300	RD	6520	69	19	5	93	4.4	4.4	4.8	4.5				6.35	87	25	2	114
	ND	4482	51	28	4	83	2.7	2.4	4.5	2.7				4.98	82	44	6	132
	Aver	11002	120	47	9	176	3.7	3.2	4.7	3.7	4.01	1.37	0.38	5.79	169	69	8	276
600	RD	5996	57	30	4	91	6.2	4.9	5.3	5.8				8.72	79	41	7	127
	ND	1840	50	43	0	93	3.3	2.7	-	3.0				15.27	58	57	0	115
	Aver	7836	107	73	4	184	4.9	3.6	5.3	4.4	6.69	3.35	0.27	10.26	137	98	7	242
1800	RD	1520	52	14	4	70	6.1	6.7	5.0	6.2				28.36	50	18	4	72
	ND	1035	30	32	2	64	5.5	4.2	18.0	5.2				32.37	37	35	4	76
	Aver	2555	82	46	6	134	5.9	5.0	9.3	5.7	18.94	9.00	2.18	29.98	87	53	8	148
3600	RD	2410	81	36	13	130	14.2	9.4	16.3	13.1				70.58	56	21	7	84
	ND	1829	76	52	11	139	11.1	7.0	13.8	9.8				74.30	43	21	7	71
	Aver	4239	157	88	24	269	12.7	8.0	15.2	11.4	47.04	16.61	8.61	72.19	99	42	14	155
7200	RD	1531	60	30	8	98	15.3	12.6	17.0	14.6				93.73	4	2	0	6
	ND	1605	90	46	12	148	10.3	9.0	17.9	10.5				96.76	7	2	1	10
	Aver	3136	150	76	20	246	12.3	10.4	17.5	12.1	58.83	25.20	11.16	95.28	11	4	0	16

the <G_i> calculation). The results for the cube and the random component are plotted against the total volume fraction of recrystallized material in Fig. 13. The typical shape of S_{vi} versus X_i curves are observed: early in the recrystallization process S_v increases with increasing X_i because nuclei form and grow, and thus have larger and larger interfacial areas (per sample volume). Later S_{vi} decreases with increasing X_i because more and more impingement between the grains is occurring.

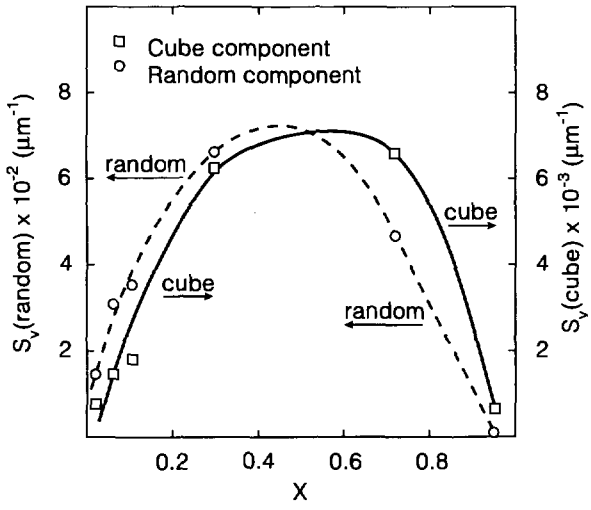

Fig. 13 Free unimpinged interfacial area for cube and random nuclei/grains as a function of the fraction recrystallized in aluminium AA1050, cr 90% and annealed at 280°C.

The calculated fraction of recrystallized material of each orientation $X_i(t)$, is fitted to the exponential function (6) given in section 2. The results for all three components are shown in Fig. 14. Due to the far lower number of cube nuclei/grains measured compared to random and/or rolling nuclei/grains, larger statistical errors are inherent for this component. However, as can be seen in Fig. 14, a reasonable fit between the experimental points and fitting equation is obtained in all cases.

Using the fitted constants, dX_i/dt is calculated for each component at the experimental annealing times, t, which, when divided by the corresponding S_{vi}-value, directly gives the average growth rate <G_i> for the given time and for the given component. The results are plotted separately for each component in Fig. 15. It can be seen that the growth rate of each component decreases by almost a factor 10 during the recrystallization.

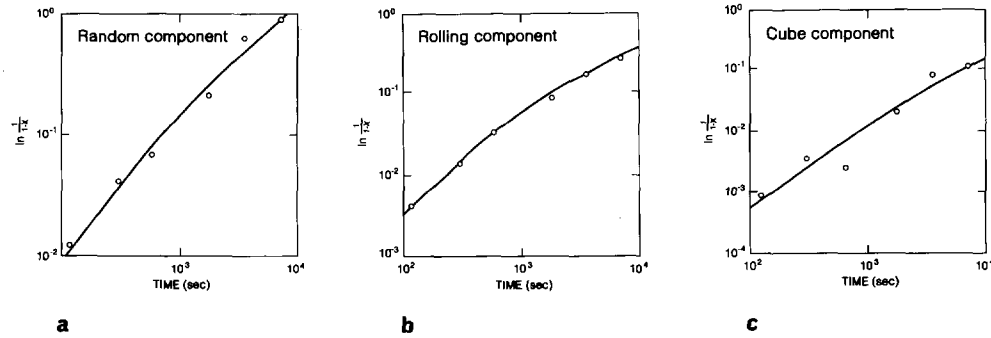

Fig. 14 Time dependence of the change in volume fraction of recrystallized material with a given orientation in aluminium AA1050, cr 90% and annealed at 280°C. a) Random, b) Rolling and c) Cube. The full lines are best fits to equation (6).

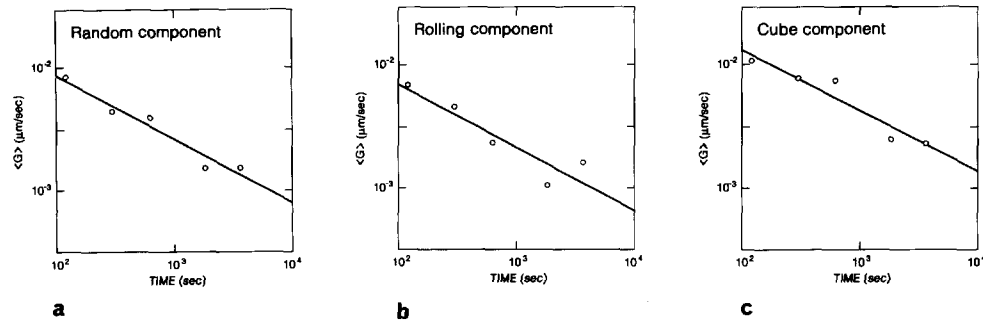

Fig. 15 Average growth rates as a function of annealing time in aluminium AA1050, cr 90% and annealed at 280°C. a) Random, b) Rolling and c) Cube.

When the growth rates of the different components are compared, it is seen that the cube nuclei/grains grow significantly faster than nuclei/grains having random and rolling orientations. In Fig. 15 the experimental growth rates are fitted to the equation

$$\langle G \rangle = k \cdot t^{-\alpha} \tag{8}$$

which is frequently used to represent this type of data (e.g. 47,49) and where k and α are constants. It can be seen that the equation gives a good fit to the data, and the fitting constants are listed in Table III. From the values in Table III, it can be seen that, for example, at t = 600 (X ≈ 10%) the cube nuclei/grain grow approximately 1.9 and 1.5 times faster than the rolling and random nuclei/grains, respectively. The growth advantage of cube nuclei/grains is maintained during the entire recrystallization process. This can be seen from Fig. 16c where the growth rate results for all 3 components are plotted on one graph.

Table III Fitted values for k and α in equation (8)

Component	k ($\mu m \cdot s^{\alpha-1}$)	α
Random	0.1085	0.53
Rolling	0.0820	0.52
Cube	0.1388	0.50

3.3 Growth rate results

Growth rate results for all the materials and deformation-annealing conditions listed in Table I are shown in Fig. 16. For each of the curves, an analysis as described in section 3.2 has been carried out*. The calculated growth rates are fitted to equation (8), and the full/broken lines show the best fits. From the figure, it is clear that the behaviour of the material described in Section 3.2 is fairly typical. In all cases it is observed that the growth rates decrease significantly during recrystallization. The decrease is most pronounced in the pure materials (pure Al and OFHC Cu) where the α-values are around 1.0. In the commercial purity Al materials, the decrease is smaller with α-values in the range 0.3-0.7. Decreasing growth rates are reported in the majority of the recrystallization studies using the standard Cahn-Hagel analysis [e.g. 41,47], and various explanations have been

*- The recrystallization texture of the commercial purity aluminium contained cube, rolling and random components for all the investigated deformation and annealing conditions. Therefore these 3 components were chosen for the analysis in all these cases. The texture of the pure aluminium and OFHC copper did not show significant retained rolling components after recrystallization. Therefore, no rolling component was included in the data analysis for these two materials. In copper, twin boundaries were treated like ordinary boundaries. With the view that a cube grain and its twin(s) can be regarded as a single growing geometrical entity, cube and cube twin nuclei/grains were classified as belonging to the same group. A further discussion of this is given in [A21].

- The data in Fig. 16b are the first data obtained by the extended Cahn-Hagel method [A4]. In this first analysis the Avrami equation [55-57] was used to fit the X versus t data. The EBSP X versus t data showed a reasonable linear relationship when $\ln \frac{1}{1-X}$ versus t was plotted on logarithmic scales, i.e. the Avrami equation seemed to give a reasonable fit to the data. When other methods, neutron diffraction, hardness and optical microscopy were also used to determine X for the partially recrystallized samples (see Fig. 17), a closer look, however, showed that the Avrami equation overestimates $\ln \frac{1}{1-X}$ for long annealing times. Therefore, for the present work, the exponential function (6) was used to fit the X(t) data, and a new growth rate curve was calculated. A comparison between the original and new result, however, reveal no major differences.

- In Fig. 16 sometimes <G> and sometimes G are used for the average growth rate, similarly the word "other" in Fig. 16a has the same meaning as "random" in Fig. 16b-e.

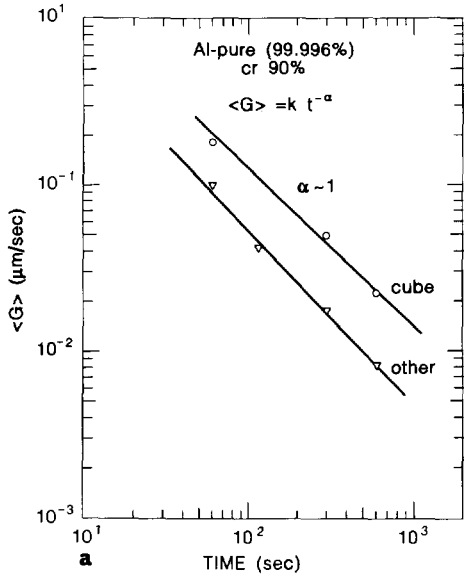

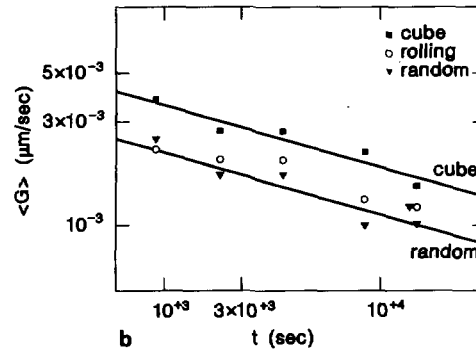

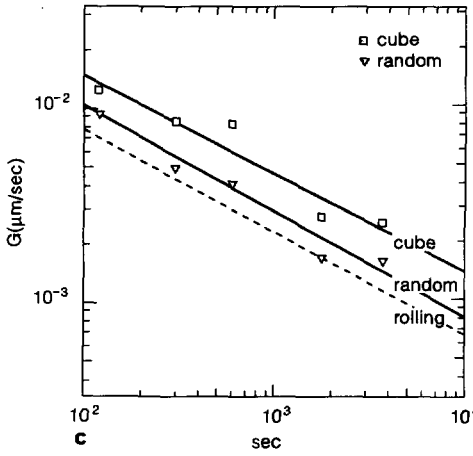

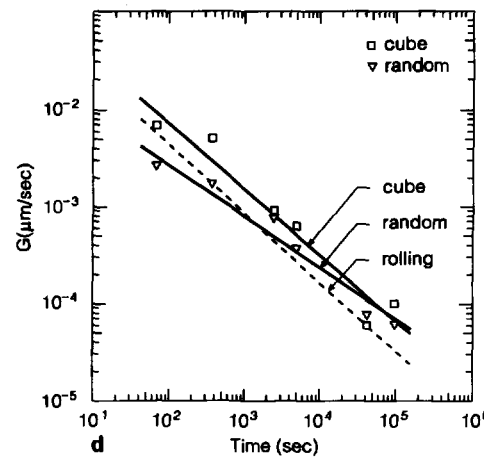

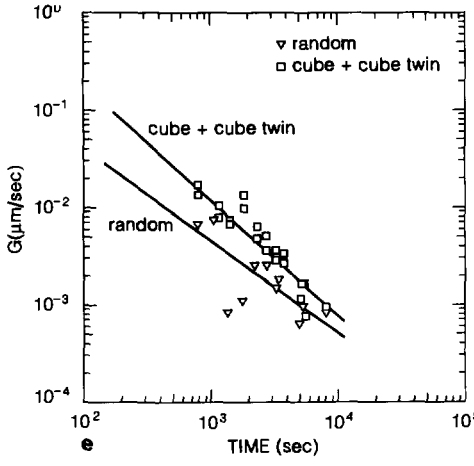

Fig. 16 Average growth rates as a function of annealing time. (Both <G> and G represent average growth rates.) The full and broken lines are best fits to equation (8). a) Pure Al, b) Al-2S, c) Al-AA1050 annealed at 280°C, d) Al-AA1050 annealed at 245°C, e) Cu (OFHC) [A7].

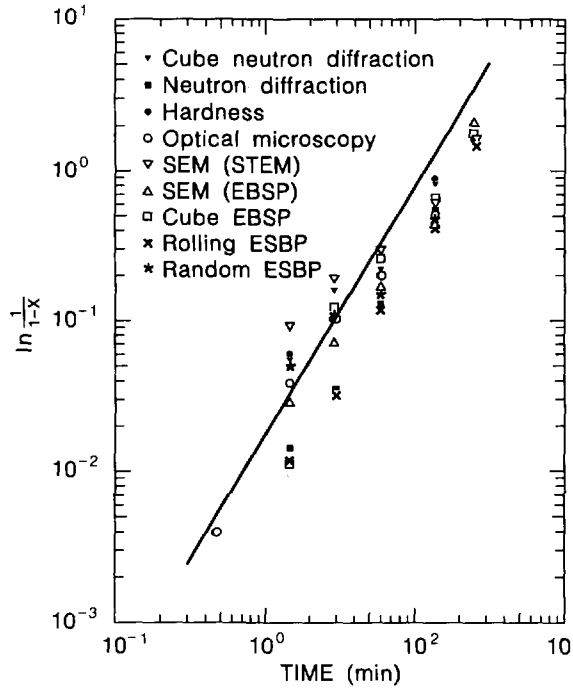

Fig. 17 Time dependence of volume fraction recrystallized in Al-2S annealed at 253°C determined by a variety of experimental techniques.

suggested: i) recovery of the deformed matrix occurring simultaneously with the recrystallization, thus reducing the driving force for recrystallization, ii) inhomogenous distribution of dislocations, and therefore stored energy, in the deformed matrix; regions with high stored energy recrystallize first resulting in high growth rates, and iii) impurities both in solid solution and present as small particles, pin the boundary motion; as the boundaries move, more and more impurities are collected and the growth rate will thus decrease. This latter explanation seems not to apply to the present data, as the decrease in growth rate is most pronounced in the pure materials where impurity effects should be less.

To further investigate the reasons for the decreasing growth rates, more measurements and analysis are under way: for the copper samples, the stored energy has been measured by calorimetry in the University of Braunschweig in the same samples used for the present growth rate analysis [A22]. From these data an analysis of relations between growth rate and remaining stored energy are being analyzed [A23]. For the commercial purity aluminium samples an analysis of effects of annealing temperature and heating rate are presently being carried out. However, as the aim of this work is to investigate effects of

crystallographic orientations, reasons for the decreasing growth rates shall not be discussed further here.

The crystallographic orientation has significant effects on the growth rates (see Fig. 16). In all the examples investigated, it was found that the cube nuclei/grains grow faster than the random and rolling nuclei/grains. Typically, the cube growth advantage is in the range 1.5 to 2.5 (except near complete recrystallization in the low temperature annealed Al AA1050 material - Fig. 16d).

3.4 Discussion of growth rate results

In the analysis described above, the random and the rolling components contain a selection of orientations, whereas the cube component only contains orientations near the cube (within 15°). This means that enclosed in the rolling and random components there are nuclei/grains of many orientations which may have different growth rates. Ideally, each individual orientation should be treated separately. This however, would require an enormous data collection (the actual amount being determined by the number of orientation classes and the frequency of their occurrence), in order to obtain statistically significant results. The present type of analysis which includes a few main components must, therefore, be considered as the best realistic solution at present.

The results presented in section 3.3 show that cube nuclei/grains grow faster than the others. A question could be if this is a genuine orientation effect, or if other factors could affect the results and lead to wrong conclusions about orientation effects. Three such other factors have been discussed at conferences and in the literature. The first relates to nucleation sites; it was suggested that the cube nuclei develop at more separated, less clustered sites than rolling/random nuclei which would result in a faster cube growth [39]. The extended Cahn-Hagel analysis, however, determines the growth rate of free-unimpinged boundaries or boundary segments, thus orientation-dependent nuclei clustering will not affect the results.

The second "other factor" relates to pinning of boundaries by impurities. If the boundaries of random/rolling nuclei/grains were more affected by impurities than the cube nuclei/grain boundaries, the cube nuclei/grains would grow faster [61]. This phenomenon should be expected to be most marked for the commercial purity Al, where resistivity measurements show that elements originally in solid solution precipitate during annealing [62]. There are, however, two reasons to believe that selective impurity pinning of the rolling/random grain boundaries is not the explanation for the present growth rate results: i) pure as well as less pure materials show the same type of behaviour and ii) selective impurity pinning of rolling/random grain boundaries during the annealing would cause a more significant decrease in the growth rate of these grains than of the cube grains. As can be seen from Fig. 16, this is not the case. The cube growth rate decrease at a similar rate (or in some cases even at a higher rate) than the rolling/random rate.

The third and last factor, which has been discussed, relates to the size of the nuclei. In hot rolled aluminium it was observed that the cube oriented subgrains and nuclei are larger

than the others [43,63]. Simply because of their size advantage, one may then expect the cube nuclei/grains to grow faster, a phenomenon called microgrowth selection [e.g. 64]. However, for the present materials and annealing conditions, no initial size advantage of cube nuclei was observed. For the Al AA1050 material, this can be seen in Fig. 12.

In the author's opinion there is, therefore, no doubt that the observed growth advantage of the cube nuclei/grains is a genuine orientation effect.

4. RECRYSTALLIZATION MODELLING INCLUDING ORIENTATION ASPECTS

The results presented in chapter 3 show that the orientations of the nuclei/grains can have significant effects on the growth rates during recrystallization. Realistic modelling of recrystallization therefore requires that nuclei/grains of individual orientations can be treated separately. This conclusion has led to a new generation of recrystallization models. These new generation models are developed by extending traditional microstructural models to include orientation aspects also. This is typically done by classifying the nuclei into a limited number of texture components and allowing nuclei of each class to have its own nucleation and/or growth characteristics. These new models will be referred to collectively as multicomponent recrystallization models.

Optimal recrystallization models have to contain information about both microstructure and texture. So, although the texture description in the multicomponent recrystallization models, is at present usually less detailed than that of the traditional recrystallization texture models (which include no information about microstructure [e.g. 34,35]) the multicomponent models are considered to be those of the future and only this type of models will be considered here. In the following, the various multicomponent modelling approaches are described.

At present 4 multicomponent modelling approaches exist. Three of these are numerical simulations: Monte-Carlo simulation, cellular automata/network models and the component model, and one is analytical: the microstructural path method.

The Monte-Carlo simulation is based on stochastic computer simulations using energy functions to define nucleation and growth. The method was first used to simulate grain growth (an overview is given by Anderson [65]) and extended later to simulate recrystallization also [66-69]. By introducing orientation dependent stored energies in the deformed matrix, the method was finally modified to simulate the textural development during recrystallization also [70-72]. The method was used in 1991 to simulate recrystallization in low-carbon steel, but has since then not been further developed or used to simulate other materials, and shall not be described in any further detail here.

The cellular automata [60,73] and node displacement network models [74,75] both operate from a predefined deformation microstructure. Various transition or growth rules are then applied to simulate what happens during nucleation and growth. Presently this type of modelling is being expanded to include crystallographic orientations in the deformed matrix as well as of the recrystallization nuclei/grains [76]. This expanded method seems very promising but is still in the development stage and no results have been published yet.

The remaining two methods have recently been used extensively and shall therefore be described in more detail in the following.

4.1 The component method

The component method belongs to the category of computer simulations which have been termed numerical geometrical models. This type of modelling to investigate recrystallization was first suggested by Mahin, Hanson and Morris [77], and later expanded to treat more complex nucleation conditions [78-81] and to operate in "extended" space as well as real space [82]. In the component method, this approach of recrystallization simulation, is further developed to treat nuclei/grains of different orientations individually [A4].

The simulations are carried out using a 3D cubic computer "sample" see Fig. 18. The size

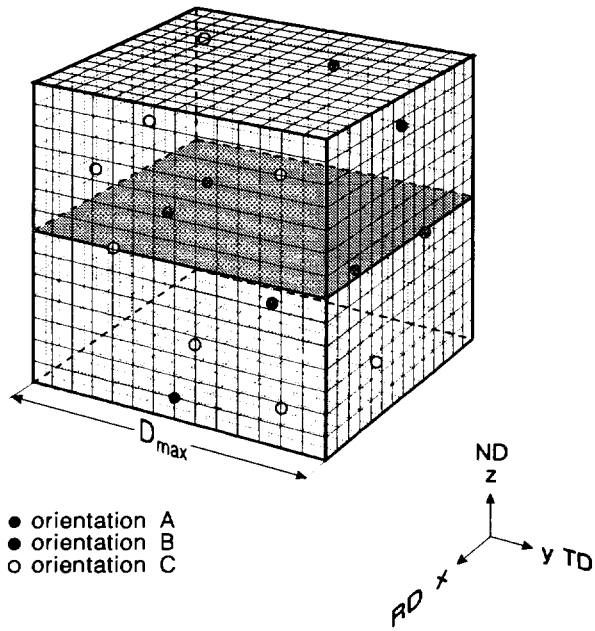

Fig. 18 Sketch of the 3D computer sample. Nuclei of 3 different orientations are distributed in the sample. A selected 2D plane of inspection is shown in grey [A4].

of the sample is determined by the number of grains, N, in the simulation and the nucleation density. As input the following information is needed:

General: Number of grains and number of different orientations (or components) here referred to by "i".

Nucleation: The total nucleation density, the size of the nuclei, r(i), the nucleation rate, $\dot{n}(t, i)$ and the spatial distribution of the nuclei which also may depend on the orientation "i".

Growth: Grain shape (i) and growth rate G(i, t).

First the N nuclei are distributed according to the nucleation information, after which each nucleus has a position (x, y, z) and a nucleation time t_o ascribed to it. For each grid point in the computer sample the time when each of the N nuclei/grains arrives there is calculated, and it is registered which nucleus/grain arrives there first and at what time. No grains are thus allowed to grow into already recrystallized sites. This corresponds to the assumption generally used in recrystallization modelling, that the nuclei/grains stop growing when and where they impinge upon each other but continue to grow freely in all other directions (see Fig. 19).

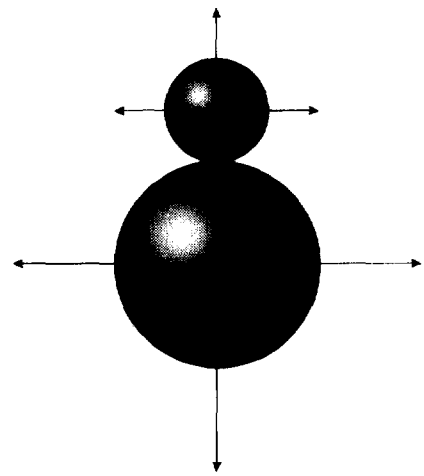

Fig. 19 Sketch of the impingement assumption. The two nuclei/grains will stop growing in the direction where they impinge upon each other but continue to grow unaffected in all other directions [A4].

From the stored data, it is straightforward to obtain output information about the simulated texture composition and microstructure at any time t during the annealing. The simulated microstructure can be seen in selected planes in the "computer sample", examples are shown in Fig. 20, and grain size data are obtained by the linear intercept method in these selected planes. Thereby data which are directly comparable to typical experimental grain size measurements are obtained.

For further information about the component method see [A4].

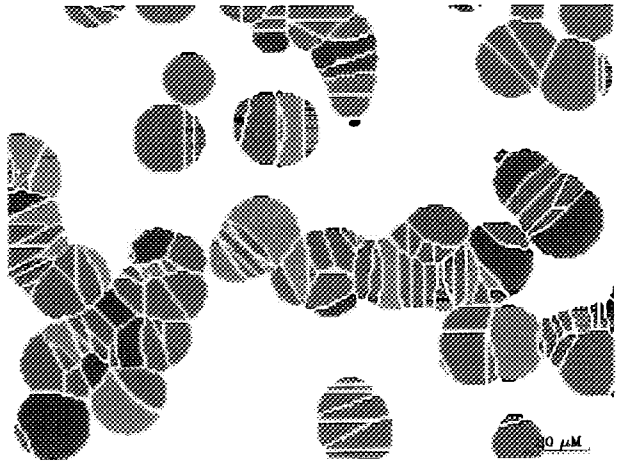

a

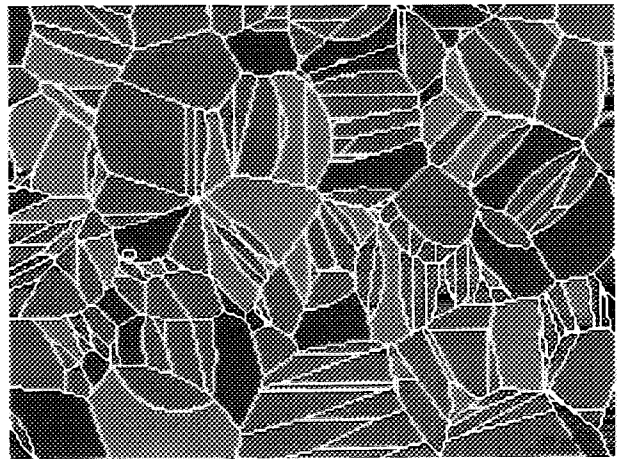

b

Fig. 20 Examples of simulated microstructures. The different colours represent nuclei/grains of different orientations. a) Partly recrystallized (the assumption of nucleation along lines in the microstructure is apparent). b) Fully recrystallized.

The component method has been used for simulations of the recrystallization of 90% cold rolled Al-2S (see Table I) [A4,A12,A24].

The advantages of using the component method relate to the facts that

i) the results contain a full microstructural description and the texture composition is also included,

ii) direct comparisons with experimental results are straightforward,

iii) it is relatively easy to define and change the nucleation and growth assumptions.

A drawback, however, is that the method requires significant computer memory and CPU-time, which in practice means that simulations often have to be limited to around 5000 grains and thus to acquire results without too much statistical scatter, the same calculation often has to be repeated several times using different seeds of nuclei describing the positions [A8,A25].

4.2 The microstructural path method

The microstructural path method, belongs to the category of recrystallization models which have been termed analytical geometrical models. The basic idea in the modelling is to operate in the so-called "extended space" i.e. in a space where impingements between nuclei/grains are ignored and the grains are assumed to nucleate and grow unhindered into already recrystallized volumes. Mathematical relationships are used to calculate the true volume fraction of recrystallized material from the extended volume fraction. This approach was first utilized assuming nucleation at random sites in the deformation microstructure by Kolmogorov [83] Johnson and Mehl [84] and in particular by Avrami [55-57]. In the random nucleation case the mathematical relationship transforming the extended volume X_{ex} to the true volume X is

$$\frac{dX}{dX_{ex}} = 1 - X$$

In recent years, this approach to recrystallization modelling has been expanded to consider complex nucleation and growth conditions [e.g. 49,82,85,86]. Very importantly, in these later works, not only X and X_{ex} but also the interfacial area per unit volume separating recrystallized nuclei/grains from deformed material, S_v and S_{vex}, are calculated [85]. S_v and S_{vex} have been shown to be very critical parameters describing characteristics of the recrystallization process. The interrelationship of X and S_v describes the so-called "microstructural path function" of the recrystallization [85], hence the name of this method, which in the following will be referred to as the MPM.

The newest developments of MPM have allowed modelling where individual texture components are treated separately [A21,A25-A27,85]. This has involved the development of mathematical models based on realistic nucleation and growth premises which take into account mutual impingement between the components. So far multicomponent MPM analyses are available for the following nucleation and growth conditions:

Nucleation sites: random, clustered along lines or clustered on planes
rate: pre-existing nuclei (site saturation) or constant nucleation rate

Growth rate: constant or time dependent
shape: spherical or spheroidal (oblate and prolate) (shape preservation throughout the annealing is assumed).

To analyse a given recrystallization process, first a model is selected from this library of available models and tested against experimental data ($X_i(t)$, $S_{vi}(t)$). If the match between model and experimental data is unsatisfactory, either the model parameters are refined or a new analytical model is developed. This is repeated until a good match is achieved. The thereby optimized recrystallization model contains full information about nucleation sites and rates as well as growth rates and shapes.

The multicomponent MPM analysis has so far been used for investigating recrystallization of 90% cold rolled Al-2S (see Table I) [A26] and 92% cr Cu (OFHC) (see Table I) [A21].

Once the mathematics of the MPM library models have been developed, the method is fast and relatively easy to use. It requires only limited (PC) computer power, and full kinetic information - not only selected discrete points - is obtained. A sound analysis of a given recrystallization process requires mainly that (i) a library model has been or can be developed which describes properly the actual nucleation and growth processes, and (ii) reliable experimental determination of $X_i(t)$ and $S_{vi}(t)$.

4.3 Combined approaches of multicomponent modelling

Both the component and the MPM method have strengths and limitations, as already discussed in the previous sections. Some of the main limitations can, however, be overcome by the combined use of the two methods.

A flow diagram of the combined modelling approach is shown in Fig. 21. First a MPM analysis is carried out based on experimental $X_i(t)$ and $S_{vi}(t)$ data. The resulting nucleation and growth models are then used as input for the component method simulation. Thereby, a full microstructural and textural description is obtained which can be compared to experimental data. Typically, the experimental data comprise the volume fraction of recrystallized material of orientation "i" at time t, $X_i(t)$ (i.e. the texture composition) the unimpinged interfacial area, $S_{vi}(t)$, the size distribution of each orientation, "i", and the interfacial area of mutual impingements between recrystallized grains of orientations "i" and "j", $R_{ij}(t)$. When a satisfactory match between simulated and *all* experimental results is obtained, it is believed that correct and complete nucleation and growth models have been deduced.

By the combined use of the component and the MPM method, only relatively few sets of input nucleation and growth assumptions, namely those predicted by the MPM analysis, have to be simulated numerically in the component method. Thereby, the main problem of the component method - the vast needs for memory and CPU-time, is reduced.

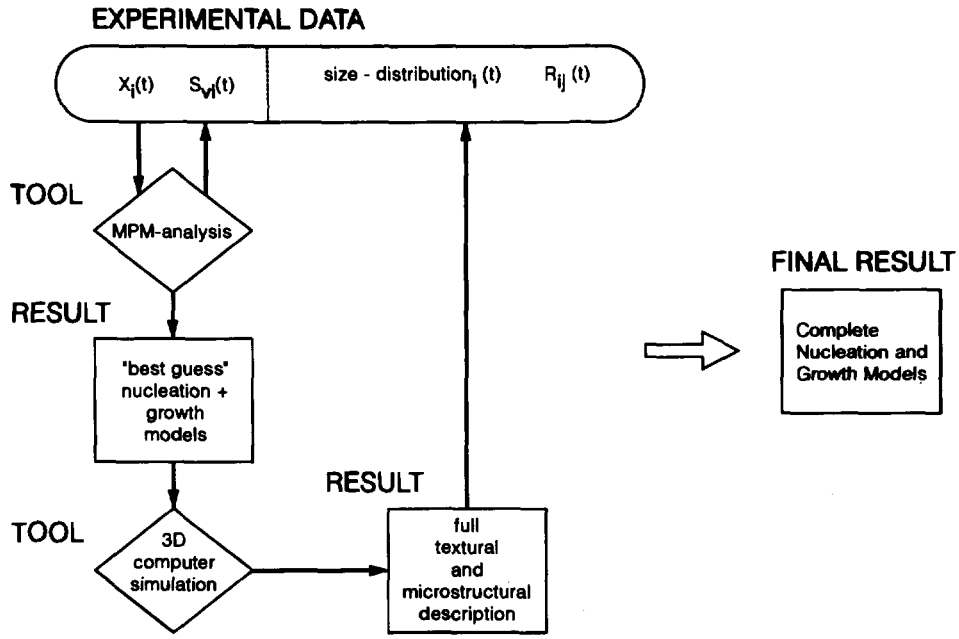

Fig. 21 Flow chart showing the combined MPM and component method approach of recrystallization modelling (revised version of figure in [A7]).

If the MPM analysis is used alone, there is no absolute assurance of the uniqueness of the solution; it can not be proven whether other nucleation and growth models, not yet in the library, could have described the experimental data better or equally well. One may therefore term the result of the MPM analysis a "best guess" [A25].

However, by combining the MPM with the component method, further microstructural characteristics than just X_i and S_{vi} are simulated. If these also match the experimental results, it makes the "best guess models" more reliable.

Furthermore, by the combined use of the methods more information about clustered nucleation may be obtained. The MPM analysis operates under idealized conditions, so if, for example, the assumption is that the nuclei develop in linear clusters, the MPM calculations are for infinite long, straight lines with random directions relative to the sample axes. With the component method, these idealized conditions may be relaxed and one can determine, for example, how long the lines need to be (equivalent to how many nuclei should form in each individual cluster), how should they be arranged in space and, whether the lines need to be straight or could they be jagged.

The combined modelling approach has been used to characterize recrystallization in 90% cold rolled Al-2S and Al AA1050 (T = 280°C) (see Table I) [A25,A27]. A main result of these investigations, is that very good agreements between simulated and experimental data are obtained. Examples of the agreement can be seen in Figs. 22-24.

It is believed that the combined modelling approach described above is at present the best choice to use when characterizing a given recrystallization process. It has, however, been argued that the methods (both the MPM and component method) depend too heavily on experimental data and do not really do what a model should, namely predict something. It is of course correct that the methods described are merely tools analysing complex sets of experimental data. However, the outcome of the analysis comprises for full descriptions of, or actually models for, the nucleation and growth processes taking place under the given recrystallization conditions. The necessity of collecting the required experimental data is clearly annoying, but in the author's opinion unavoidable with the present level of understanding of basic nucleation and growth mechanisms. Before more general recrystallization models can be developed, basic knowledge about, for example, stored energy - and misorientation - distributions in the deformed matrix, recovery and nucleation mechanisms, as well as grain boundary migration rate mechanisms are required.

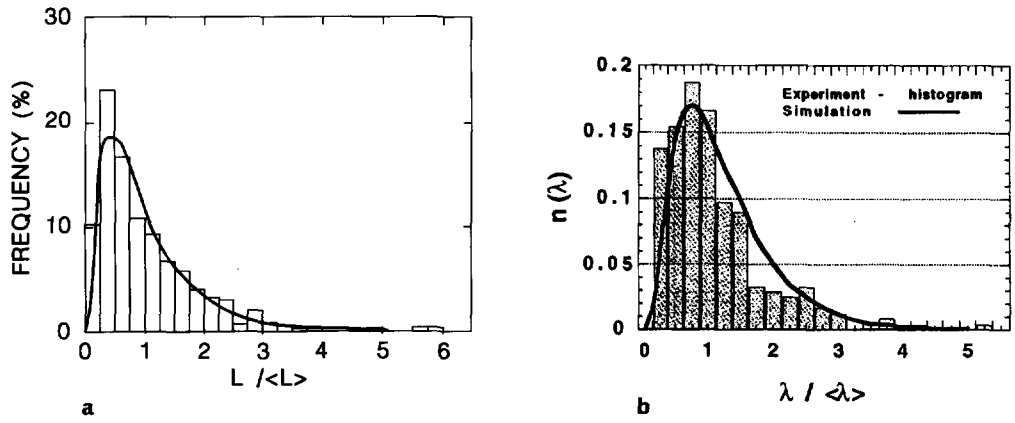

Fig. 22 Size distributions in fully recrystallized state including grains of all orientations. The histograms show the experimental results and the full lines represent the simulated results. L, λ both mean the chord lengths of the grains. a) Al-2S, cr 90%, recrystallized at 253°C [A25]. b) Al-AA1050, cr 90%, recrystallized at 280°C [A27].

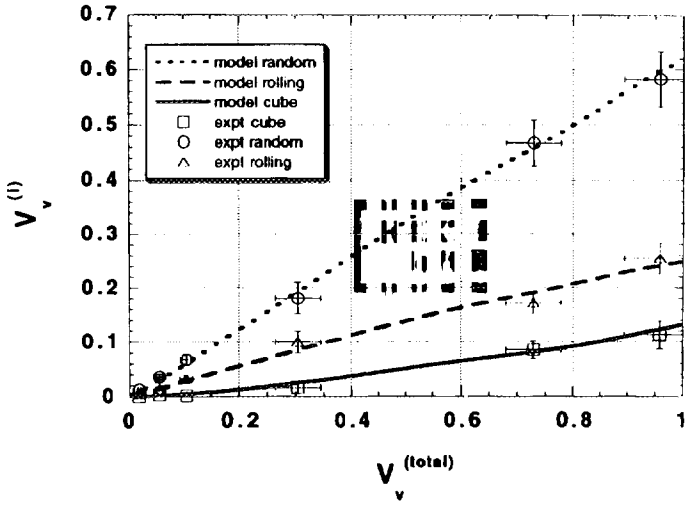

Fig. 23 Textural evolution during recrystallization of Al-AA1050, cr 90% at 280°C. $V_V^{(total)}$ is the total volume fraction of recrystallized material (= X) and $V_V^{(i)}$ is the volume fraction of the individual components (= X_i). The points show experimental results and the lines the simulated results [A27].

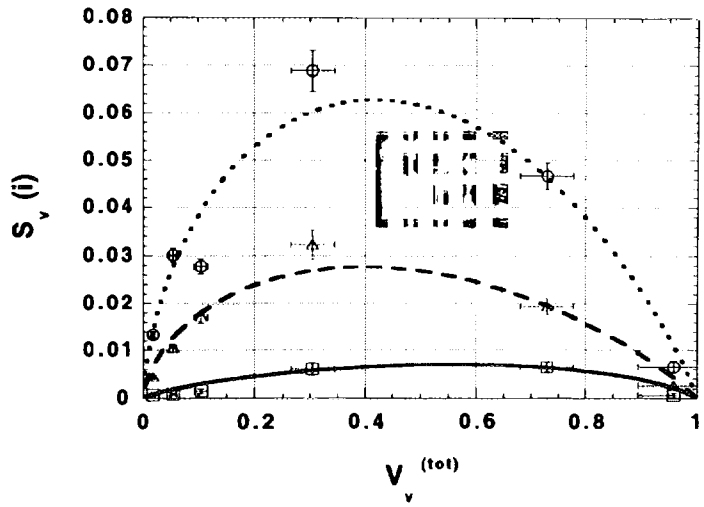

Fig. 24 Evolution in free unimpinged interfacial area of nuclei/grains of the various orientations in Al-AA1050, cr 90%, annealed at 280°C. Marks as in Fig. 23 [A27].

5. EFFECTS OF ORIENTATION DEPENDENT GROWTH RATES ON RECRYSTALLIZATION TEXTURE AND MICROSTRUCTURE

Technologically, it is extremely important to know and to be able to control textural and microstructural development during processing. A lot of money and effort is spent in improving reproducibility, in optimizing these two characteristics and, thus, the properties of the product. This was, for example, reflected in a recently-completed BRITE/EURAM project in which Risø was prime proposer and 6 other partners including 3 major European aluminium companies participated. For a synopsis report see [A28].

If the growth rate of the nuclei/grains depends on their orientation, the textural and microstructural development will be affected. It is intuitively obvious that if grains of a given orientation, "i", grow faster than the other grains, the "i" grains will become larger than the others and consequently a widening of the recrystallized grain size distribution should be observed. Also, the orientation dependent growth will lead to a strengthening of the i-type recrystallization texture. The magnitude of these effects is however difficult to predict as they depend critically on the nucleation conditions (density, sites and rates). With the aim of addressing typical industrial questions, the component method has been used to simulate the recrystallization microstructure, texture and kinetics for orientation-dependent growth conditions as those reported in chapter 3, and for various nucleation assumptions. These assumptions cover typical experimental findings in many metals at various deformation and annealing conditions. The results are thus believed to be of general value. The results are published in [A8] and in the following the main microstructural and textural results will be summarized.

5.1 Simulation assumptions

In the simulations it was assumed that the nuclei/grains may be categorized into 2 groups (type I and type II) and that type II nuclei/grains grow 1.0 to 2.5 times as fast as type I nuclei/grains. This choice of assumptions relates to the results presented in chapter 3. The nucleation was assumed either to be instantaneous, at the beginning of annealing (a condition often referred to as site saturation), or to continue at a decreasing rate during the annealing. The number of type II nuclei was either 10% or 30%. The nucleation sites were either randomly distributed or in predefined clusters. Three types of clusters were used: 1) 1-8 nuclei developing around random *points* in the microstructure, 2) 1-10 nuclei developing along random *lines* and 3) 1-100 nuclei developing on parallel *planes*. Either all nuclei, or only type I nuclei were assumed to form in such clusters. These nucleation assumptions were chosen to cover typical experimental findings. In all the cases the same nucleation density was assumed.

In the published paper [A8] the effects of all the variable nucleation and growth assumptions are described. Here emphasis will only be placed on the preferential growth effects.

5.2 Texture

The results of the simulations show that the texture development under all nucleation conditions is strongly affected by the preferential growth. This can be seen in Fig. 25. When all nuclei/grains are assumed to have identical growth rates, the texture composition is of course determined by the number percentage nuclei of the two types (here 10% or 30%). When the type II nuclei/grains grow 2.5 times faster than type I, the volume fraction of type II is 2 to 5 times as high. And when it is assumed that type II nuclei developed at non-clustered sites, type II textures up to 95 volume percentage can be obtained even though only 10-30 percent of the nuclei are of type II orientation.

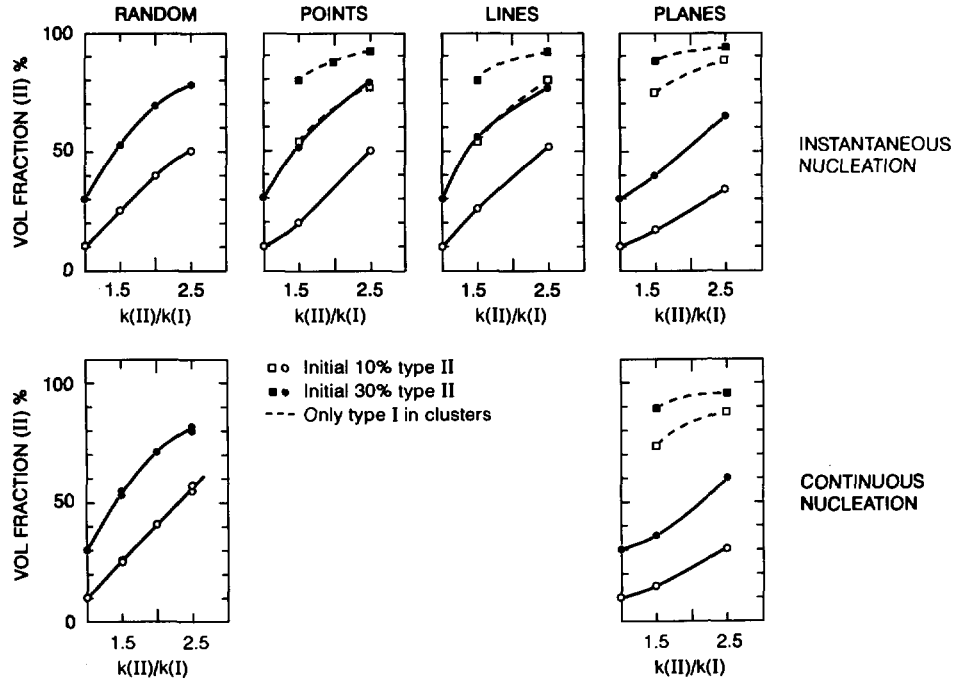

Fig. 25 Volume fraction of type II grains in the fully recrystallized state as a function of the growth rate advantage - k(II)/k(I) for various nucleation assumptions. "Random, points, lines, planes" refer to the nucleation site assumption [A8].

5.3 Microstructure

Examples of the simulated recrystallization microstructures are shown in Figs. 26. The average grain size, including grains of both types, is to a large extent determined by the

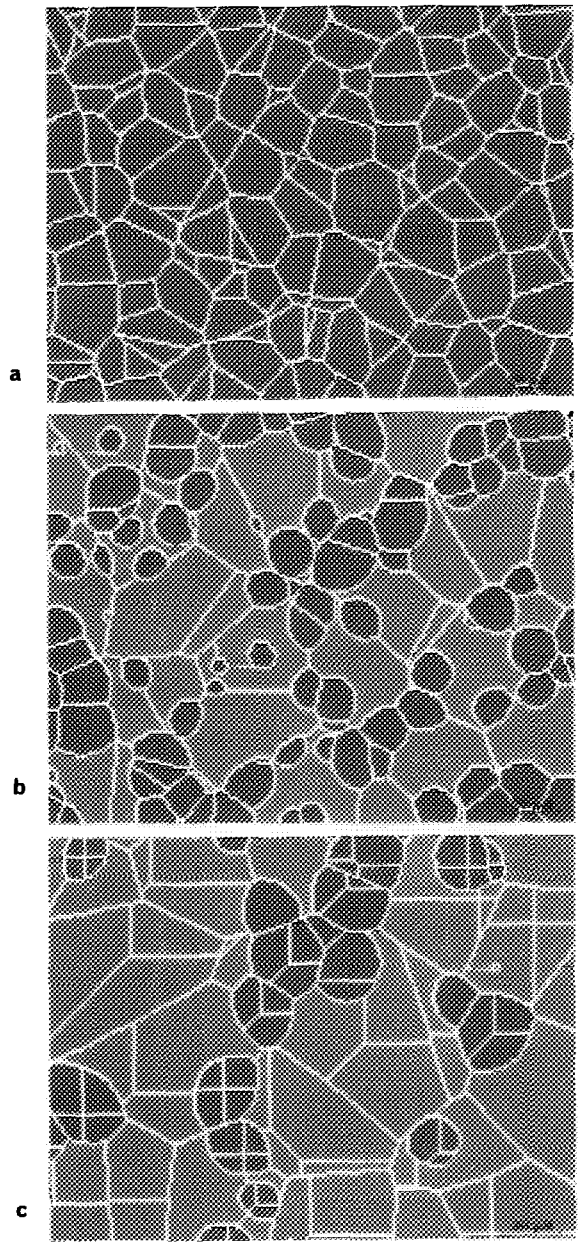

Fig. 26 Simulated fully recrystallized microstructures. Red grains are type I (slow growing) and green grains are type II (fast growing). a) Only type I grains - all growing at the same rate, instantaneous nucleation at random sites. b) 10% type II nuclei growing 2.5 times faster than type I nuclei, instantaneous nucleation at random sites. c) 30% type II nuclei growing 2.5 times faster than type I nuclei, instantaneous nucleation at sites clustered around random points [A8].

selected nucleation density; only a slight increase in the average size is observed when the growth rate of type II nuclei/grains is increased. This is because of the reduced probability of intersecting the small (type I) grains when measuring the grain size using the linear intercept method.

An increase in the growth rate of type II nuclei/grains leads to a significant increase in the size ratio between type II and type I grains. This is illustrated in Fig. 27. Typically, a

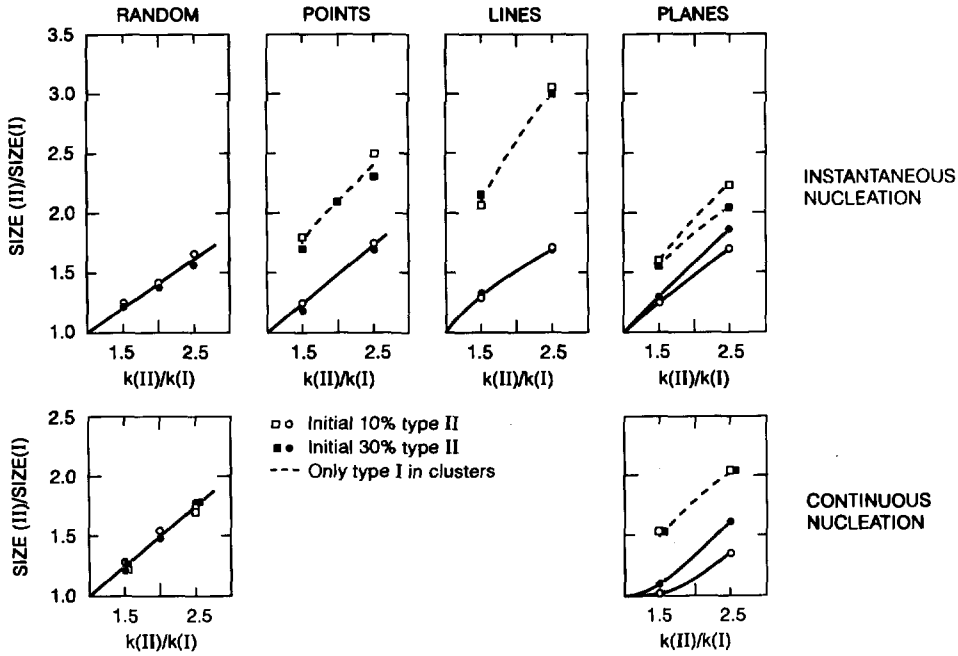

Fig. 27 Average recrystallized grain size of type II grains relative to type I grains as a function of the growth advantage (k(II)/k(I)) for the various nucleation conditions [A8].

growth advantage of 2.5 results in a size advantage in the range 1.5 - 1.8. That there is not a one to one relationship, in the sense that a growth advantage of x-times should result in a size advantage of also x-times, is due to the increased probability for impingements when the grains grow fast.

The grain size distribution is also strongly affected by orientation dependent growth. This is clear already from a visual inspection of the simulated microstructures (Fig. 26). If all

nuclei form instantaneously at random sites and grow with the same speed, a very narrow size distribution evolves with no grains larger than 3 times the average size. This is shown by the grey histograms in Fig. 28a, b. Already by introducing 10% type II nuclei growing 2.5 x faster than type I nuclei, the recrystallized grain size distribution widens significantly (see the white histogram in Fig. 28a). In this case, 2.4% of the grains are larger than 3 x the average size and the maximum size is 4 x the average. In case of clustering of the nuclei, further widening is observed. An example is shown in Fig. 28b. Here it is assumed there are 30% type II nuclei growing 2.5 times faster than type I nuclei and all nuclei form instantaneously along lines in the deformed microstructure. In this case a size distribution with many small and many large grains is observed: more than 15% of the recrystallized grains are less than half the average size and the maximum size is 6.5 x the average.

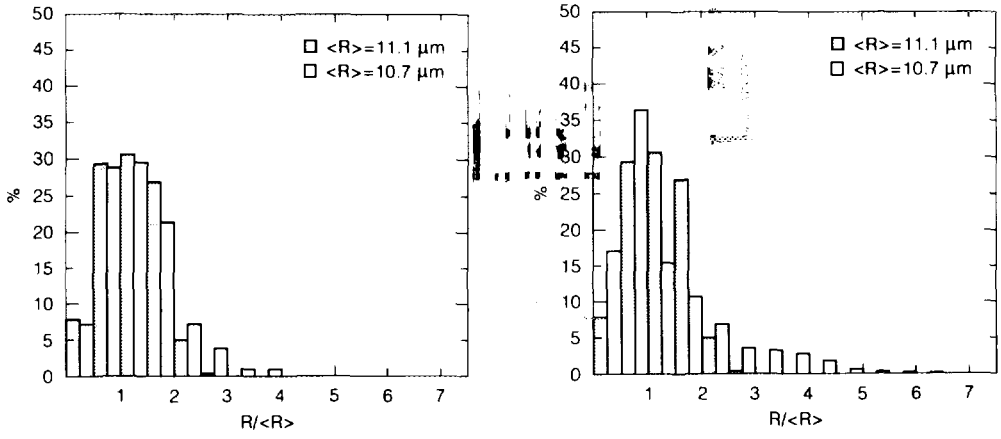

Fig. 28 Normalized grain size distributions. The grey histograms in both figures are for a simulation with only nuclei of one type (instantaneous nucleation at random sites - see also Fig. 26a). The width of each bar in the histograms (grey or white) corresponds to 0.5x<R>/R. The white histograms are for various conditions: a) 10% type II nuclei, k(II)/k(I) = 2.5, instantaneous nucleation at random sites (see also Fig. 26b), b) 30% type II nuclei, k(II)/k(I) = 2.5, instantaneous nucleation at sites clustered along lines [A8].

6. DISCUSSION OF REASONS FOR ORIENTATION-DEPENDENT GROWTH RATES

The results presented in chapter 3 show that in all the investigated cases crystallographic orientation has an effect on the growth rate: the cube oriented nuclei/grains grow faster than the other nuclei/grains. Reasons for such orientation dependent growth rates shall be discussed in what follows.

The growth rate of recrystallizing nuclei/grains depends on the driving force, F, provided by the stored energy in the deformed matrix and on the mobility of the boundaries, M. In most cases the simple relationship

$$G = M \cdot F$$

has been found to fit experimental data well [e.g. 87-89]. Both F and M may depend on crystallographic orientation - F on the orientations within the deformed matrix and M on the misorientation across the moving boundary.

That the driving force may depend on orientation relates to observations that the dislocation density, and therefore the stored energy, may be different in grains or single crystals of different orientations. The first serious observations of this dealt with measurements of cell size and misorientation across cell boundaries in 70% cold rolled iron [90] and it was concluded that $E_{110} > E_{111} > E_{112} > E_{100}$ (see also [91]). Here E_{hkl} refers to the stored energy within a region of hkl-orientation. Such orientation dependent stored energies have also been observed more recently in hot and cold deformed aluminium using similar measuring principles [92,93] and by x-ray line broadening measurement of cold and hot rolled steel [94].

It was Barrett [4] who first made the suggestion that grain boundary mobility depends on the misorientation across the boundary. The experimental verification of this idea was provided by the classic Beck experiment [95], in which the growth of artificially created nuclei into a well-characterized, deformed single crystal matrix was studied. In the fifties and early sixties, several groups performed experiments of this type, and for fcc metals, it was generally found that grains with an approximate 40° misorientation around a common <111> axis exhibit the highest growth rate [e.g. 95-99]. This fast growth misorientation relationship was recently confirmed by grain growth bicrystal experiments [100]. The magnitude of the preferential growth effect may depend on materials and process parameters, such as purity and solute content [101-103], as well as annealing temperature [104,105]. Also the actual grain boundary plane is of importance and as discussed by Beck et al. [106,107] in fcc metals tilt boundaries will move faster than twist boundaries. In spite of these "finer details", the 40° <111> misorientation fast growth result is so clear and convincing that it has been named "oriented growth" and has been used extensively to explain the recrystallization texture development in competition with the "oriented nucleation" hypothesis. (For a discussion of oriented growth versus oriented nucleation see Doherty et al. [9].)

When interpreting the present growth rate results, the classic observations and theories of orientation-dependent driving force, F, and mobility, M summarized briefly above, are, of course, essential. As it shall be discussed in the following, the growth of nuclei/grains in a heavily cold deformed polycrystalline matrix is, however, significantly different from that in the deformed single crystal Beck experiments referred to above. The single crystals in these experiments were either weakly deformed or had a stable orientation, whereby deformation microstructures with only small orientational spreads were developed. When a nucleus/grain grows in such a deformed matrix, the misorientation relationship between the nucleus/grain and the matrix will remain largely unchanged during the entire growth period, and will be almost identical at different segments of the boundary. Recent investigations have shown that in heavily cold deformed polycrystalline metals, the original grains are heavily subdivided, and the nuclei/grains experience growth in much more turbulent matrix surroundings during the recrystallization. After a description of the deformation microstructure typical for the investigated materials, reasons for orientation-dependent growth rates under these circumstances are discussed.

6.1 Deformation microstructures

During recent years, significant progress has been achieved in the characterization and understanding of the microstructural development during cold deformation (for overviews see [108-110]). Several medium to high SFE, fcc metals (Cu, Ni, Al) has been studied in detail after deformations to low, medium and high strain by rolling, torsion and compression (channel die). The morphology of the different dislocation configuration has been characterized using mainly TEM but also channelling contrast SEM. The local crystallographic orientations and their relations to the dislocation configurations have been quantified using the Kikuchi line technique in TEM and the EBSP technique in SEM.

It has been found that during deformation the original grains subdivide by the development of dislocation boundaries. At low and medium strain, the dislocation boundaries typically are dense dislocation walls (DDWs), microbands (MBs), S-bands and ordinary cell boundaries. Relatively large angular misorientations are observed across many DDW/MBs whereas the cell boundaries are of low angles [A29,111,112]. It is a common observation that most DDW/MB are aligned at an angle of about 40° and ~90° to the rolling direction when inspected in the longitudinal (RD-ND) and rolling (RD-TD) sample section, respectively [A30,109]. This directional alignment is sketched in Fig. 29.

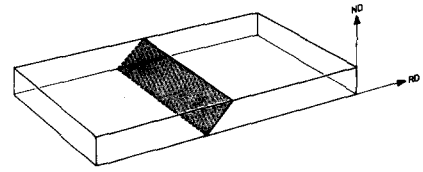

Fig. 29 Schematic drawing of the geometrical direction typical for DDW/MBs with respect to the sample axes [A30].

Depending on the orientation of the original grain, the grain size, the deformation conditions and sample material, the DDW/MBs may form on crystallographic <111> planes or may form by a combination of slip on several <111> planes whereby non-crystallographic macroscopic DDW/MBs evolve [e.g. 108-110]. It is an important observation that the original grains become subdivided, not only into volume elements with orientations having a random scatter around an average grain orientation, but also into volume elements having orientations belonging to different texture components [e.g. A31,110]. An example is shown in Fig. 30.

At higher strains also lamellar boundaries almost parallel to the rolling plane form and subgrains may develop.

At the strains relevant for this work (cr 90 and 92%), the deformation microstructure typically contains all the types of dislocation structures mentioned above: one sees areas where lamellar boundaries predominate, others where DDW/MBs delineate areas with few cells (cell blocks) and slightly larger areas with cells or subgrains. An example and a sketch of a typical structure are shown in Fig. 31. Many of these dislocation boundaries are associated with high misorientations. For example, in 90% cold rolled aluminium AA1050 (see Table I) a TEM-Kikuchi line analysis of misorientations across each dislocation boundary along ND showed that 20 out of 91 boundaries had a misorientation larger than 15° [113]. Some of these - approximately 5 - are expected to be original grain boundaries, whereas the remaining 15 have developed during the deformation.

The heavy subdivision and development of intragranular high angle boundaries can also be seen by EBSP scans through the structure [A6]. This is illustrated in Fig. 32 where the misorientation between neighbouring 1 μm areas is plotted versus position for 100 μm long linear scans along RD and ND in 90% cold rolled aluminium AA1050 (which had an initial grain size of 100 μm see Table I). Histograms showing the same data are shown in Fig. 33. In this example, the distance between high angle boundaries (> 15°) is 2.3 μm and 4.4 μm when measured along ND and RD respectively [A6]. Similar distances were observed in other aluminium materials with different initial grain sizes [93,110].

As for the lower strains (e.g. Fig. 30), the high angle boundaries separate material with orientations belonging to various of the typical rolling texture components [114,115]; in other words, each original grain divides into several different texture components. This may be seen by carrying on a 2-dimensional EBSP mesh scan through the deformed microstructure and by using different colours to represent the typical texture components. An example is shown in Fig. 34. The subdivision into small (<5 μm) blocks of material and the significant mix of texture components is obvious.

Finally, important for the interpretation of the growth rate data, is that no transition bands, cube bands or shear bands are observed in the present materials.

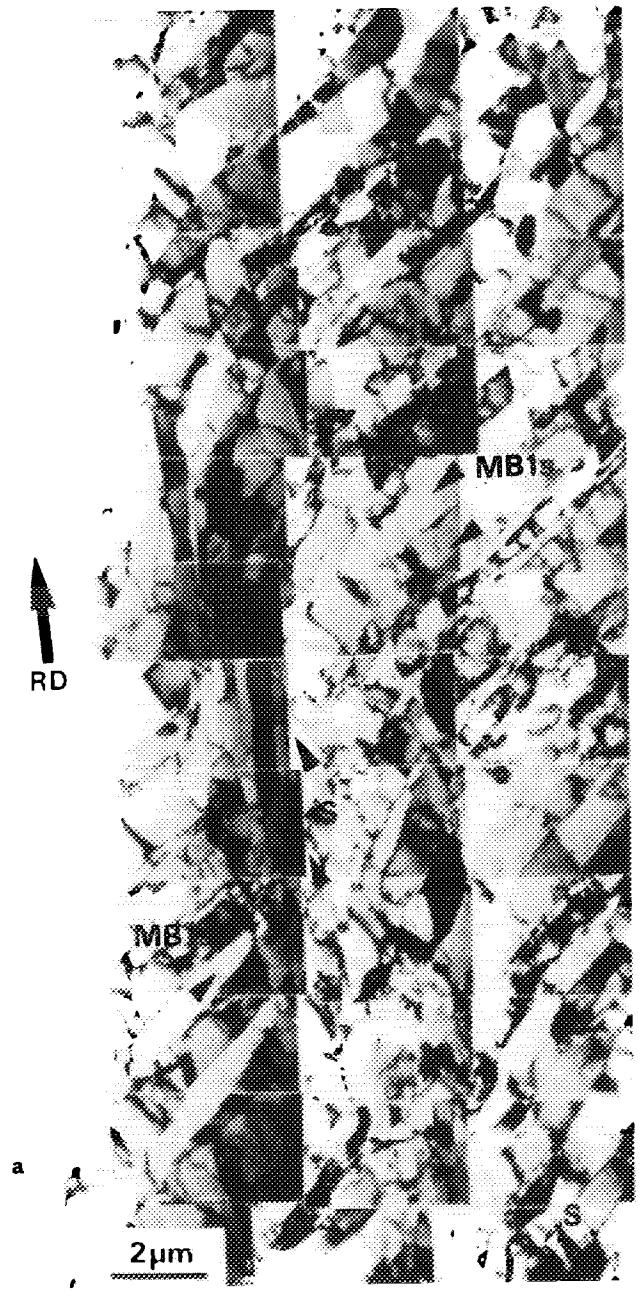

Fig. 30 Caption - next page.

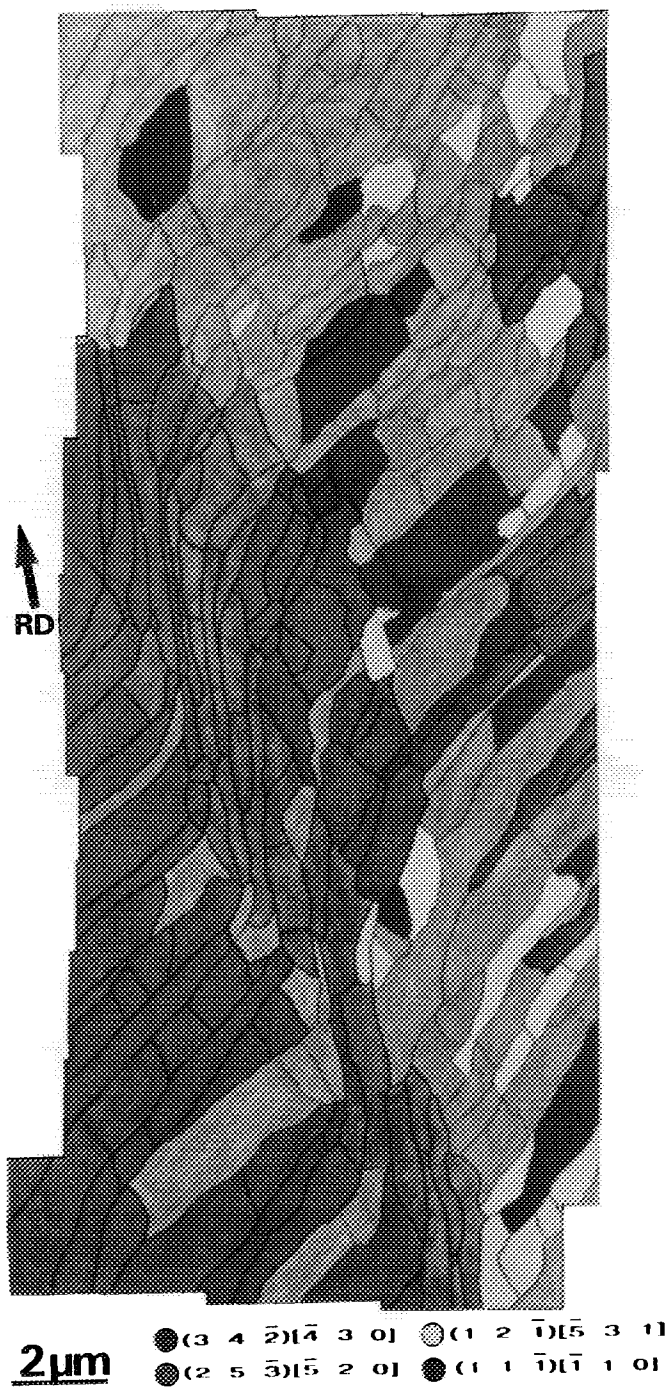

Fig. 30 Pure aluminium cold rolled 50%. a) Micrograph showing DDW/MBs (marked MB1s) and an S-band (marked S) b) same picture as a) but colours are used to show the local orientations. The subdivision into volume elements belonging to different texture components is apparent [A31].

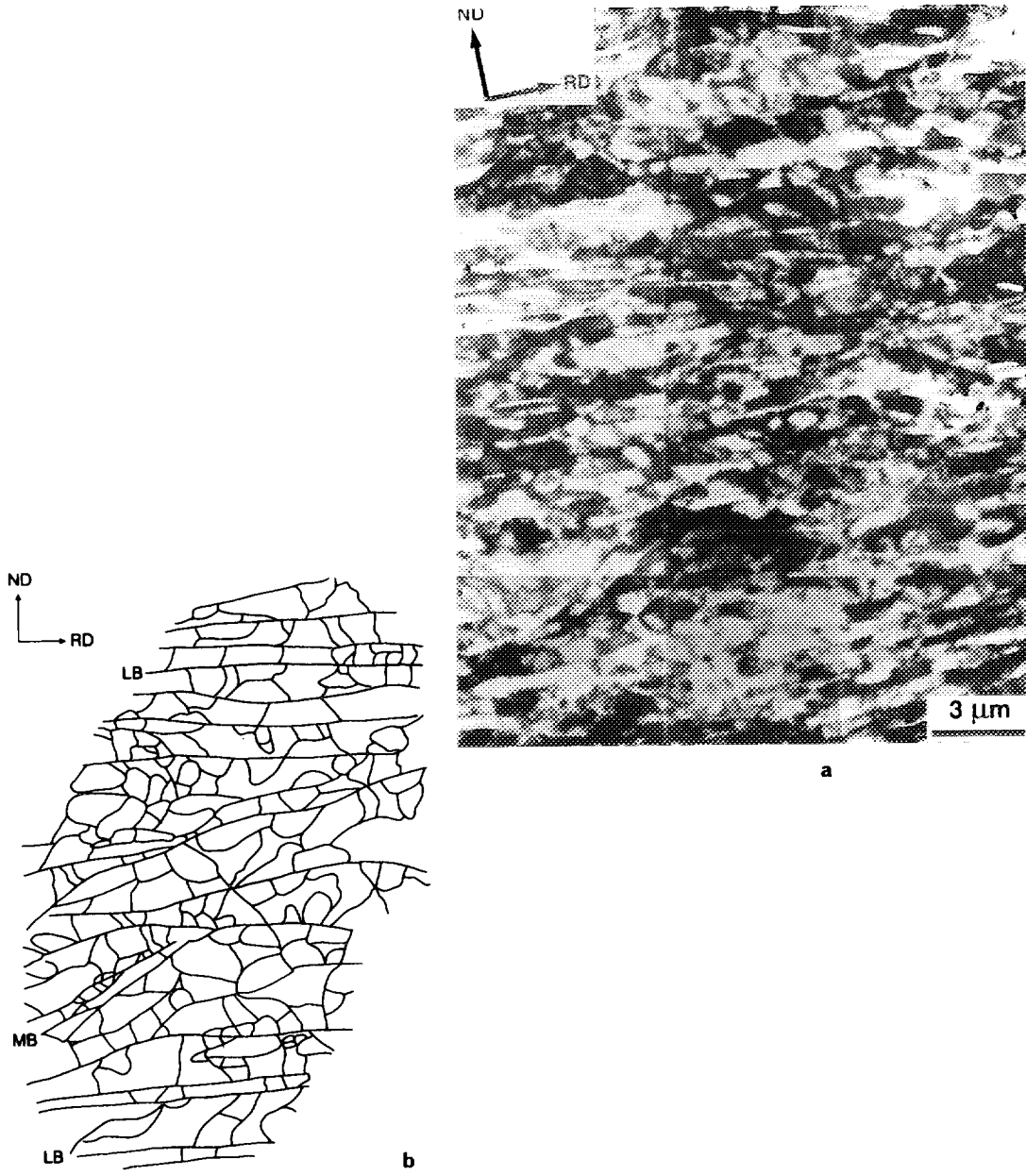

Fig. 31 Al-2S cold rolled 90%. a) Micrograph showing areas with lamellar boundaries (almost parallel to RD), with DDW/MBs (seen at angles of about 40° to RD) and with cells or subgrains [A32]. b) Sketch of a typical microstructure (LB marks lamellar boundaries and MB marks DDW/MBs).

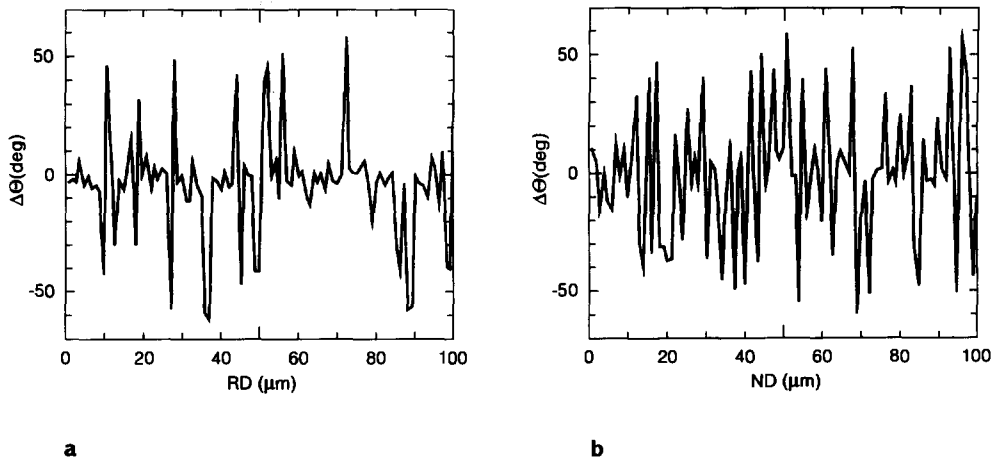

Fig. 32 Misorientation angles between neighbouring 1 μm areas in aluminium AA1050 cold rolled 90%. The sign of the angle is determined from the corresponding rotation axis: if the axis is in a right hand side triangle the sign is positive and it is negative if the axis is in a left hand side triangle. a) Scan along RD. b) Scan along ND [A6].

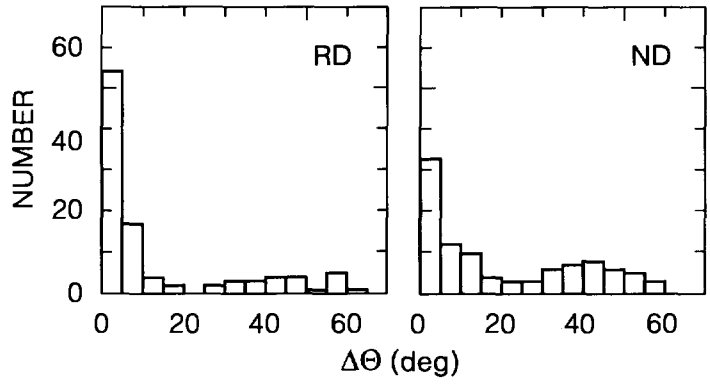

Fig. 33 Histograms showing the distributions of misorientation angles of Fig. 32 [A6].

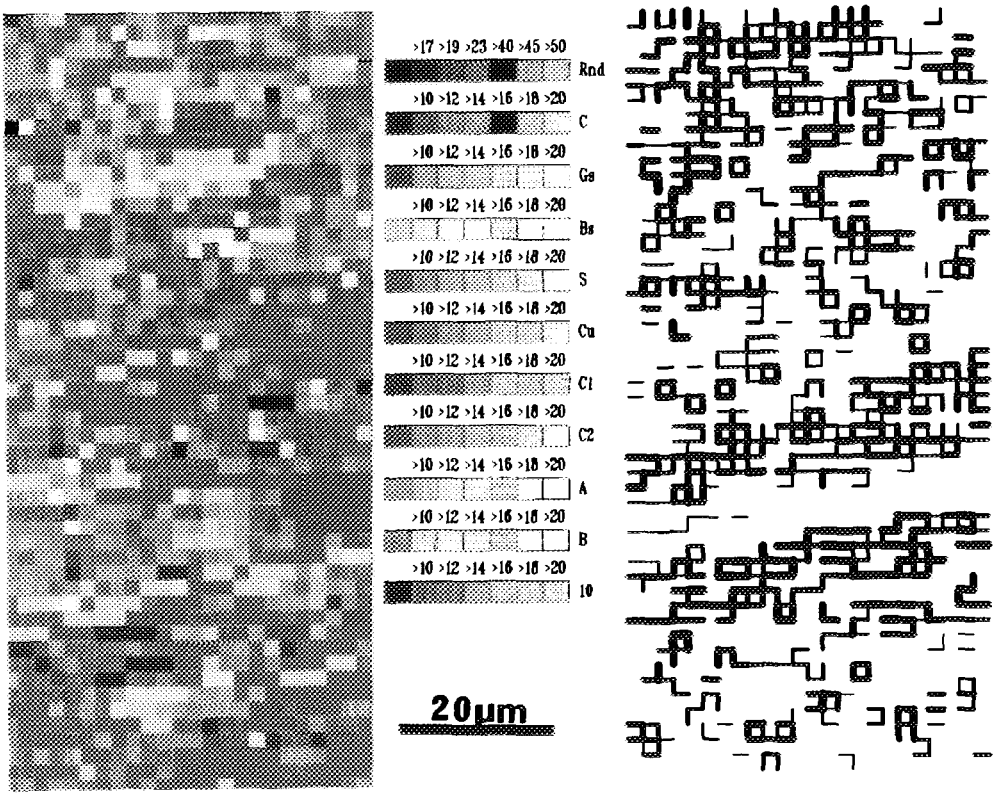

Fig. 34 Aluminium AA1050 cold rolled 90%. a) Orientation image micrograph (OIM) showing the distribution of crystallographic orientations in the deformed microstructure. Various orientations are represented by colours. Ten orientations are chosen: C - {100} <001>, Gs - {110} <001>, Bs - {110} <112>, S - {123} <634>, Cu - {112} <111>, C1 - {122} <221>, C2 - {001} <110>, A - {310} <130>, B - {310} <001> and 10 - {014} <041>. Distances in Euler space from these ideal orientations are represented by different shadings. b) As a) but here lines are used to show the magnitude of misorientation angles between neighbouring measuring points, the thinnest line corresponds to 15°-20°, the next thinnest line to 20°-25° etc. in 5° steps.

6.2 Nuclei and grains in heavily cold deformed matrices

Already when a nucleus is formed in a heavily cold deformed matrix such as that described above, it will typically be surrounded by matrix material of different orientations at various segments along its boundary. And during its growth, the boundary conditions will constantly change, as various segments of the boundary move to meet new deformed material with different orientations. An illustration of the "segmentation" of

nuclei/grain boundaries is given in Fig. 35. Here the EBSP technique was used to measure orientations in a 2 dimensional mesh along RD and ND in aluminium AA1050 cold rolled 90% and annealed for 600 seconds at 280°C in a bath furnace (see Table I). This annealing

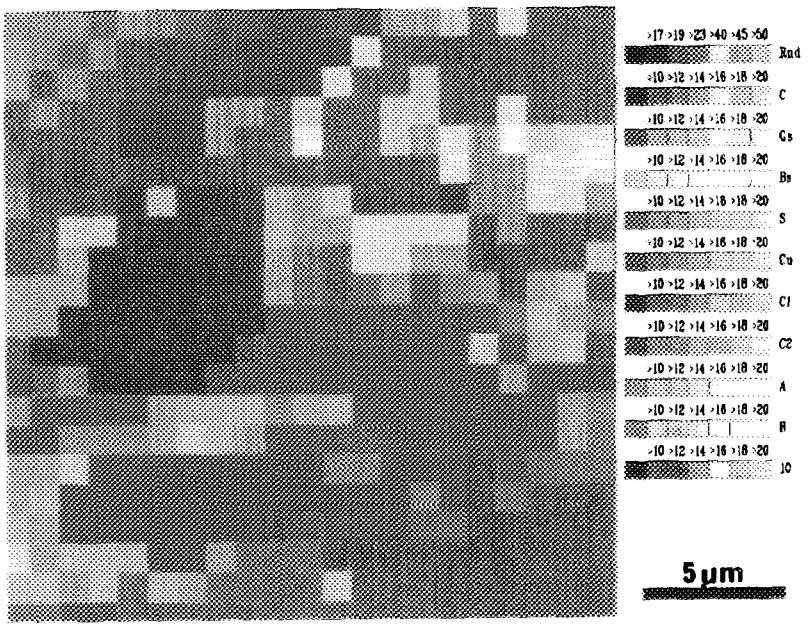

Fig. 35 As Fig. 34 but here for a sample annealed 600 seconds at 280°C in a bath furnace. A nucleus is seen in green colour.

treatment corresponds to approximately 10% recrystallization (see Table II). Selected orientations are represented by colours. One nucleus is seen surrounded by deformed matrix characterized by a wide variety of orientations and one can imagine how the nucleus/grain will constantly meet matrix material with "new" orientations during its growth.

A consequence of the heavy subdivision of the deformed matrix into small (< 5 µm, linear dimension) volume elements of different orientations, is that the misorientation relationship between a nucleus/grain and the surrounding deformed matrix can not be characterized by a single set of misorientation parameters (e.g. an axis/angle pair).

To study misorientation relationships one may choose to characterize the deformed matrix surrounding selected nuclei/grains [e.g. 115] in detail, or to use a statistical approach where very many nuclei/grains are studied, but the misorientation is only measured at one "random" point of each nucleus/grain boundary [A6]. Each method has advantages

and disadvantages, but when the aim is to obtain data which can be used to evaluate average growth rate data, as those presented in chapter 3, the statistical approach is most appropriate [A6]. It is worth noticing that a disadvantage common to both methods is that they are static, non-in-situ measurements. The probability of seeing a given misorientation relationship is thus inversely proportional to the corresponding mobility. In other words, when a boundary or boundary segment experiences a high mobility misorientation relationship, the nuclei/grain will quickly move to consume the corresponding deformed matrix and the probability of detecting this misorientation relationship will therefore be relatively smaller.

Statistical misorientation distributions were determined for copper (OFHC) and aluminium AA1050 (see Table I) in [A6], and the main results shall be summarized below.

From EBSP line scans through the microstructure of partly recrystallized samples, the orientations are measured of each recrystallized nucleus/grain and of the neighbouring deformed matrix point on the line - i.e. in the points marked by a double arrow in Fig. 36. The misorientations are calculated and expressed as axis-angle pairs choosing the minimum rotation relationship angle among the 24 equivalent solutions.

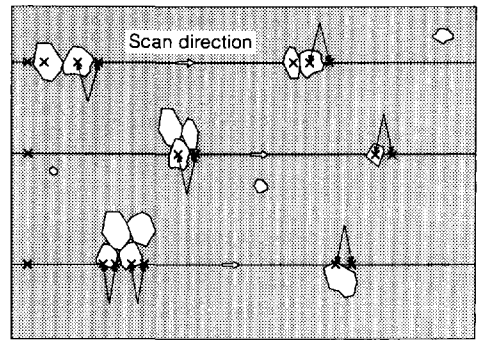

Fig. 36 Sketch of partly recrystallized microstructure, nuclei/grains are shown in white. EBSP orientation measurements were performed at positions marked by "X", and misorientations are calculated from sets of orientations as those marked by the double arrows [A6].

Results are shown in Fig. 37. As expected, the misorientation distributions are very wide. Typically the rotation axes cover the stereographic triangle fairly homogeneously and the rotation angles are in the entire range from ~0° to 62.8°.

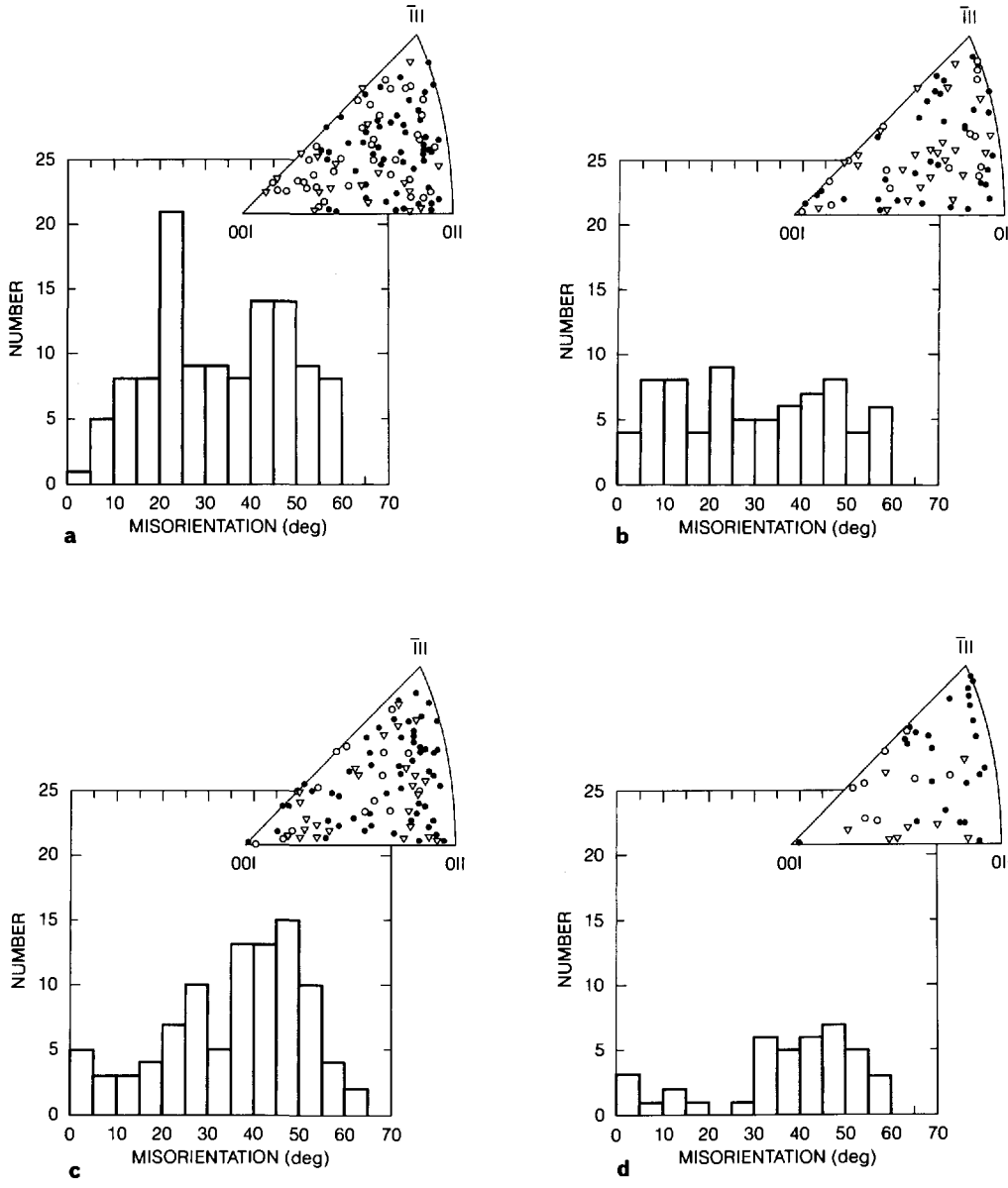

Fig. 37 Misorientations between nuclei/grains and the deformed matrix. Misorientation angles are shown in histograms and the axes are shown in unit stereographic triangles. In the stereographic triangles, different signatures are used for axes with different angles (θ): • $\theta \geq 35°$, ∇ $20° \leq \theta < 35°$, o $\theta < 20°$. a) Al AA1050 (X = 2%) b) Al AA1050 (X = 30%) c) Cu (X = 2%) d) Cu (X = 95%) [A6].

As in the growth rate determination, the recrystallized nuclei/grains are categorized into groups according to their orientation (typically cube, rolling and random). The misorientation angles for the different groups of nuclei/grains are shown in Fig. 38. It can be seen that for both copper and aluminium, the cube (cube-twin) nuclei/grains have larger misorientation angles than the random and rolling nuclei/grains. These results may be compared to the misorientation angle distribution in a completely random orientation distribution [116]. In Fig. 38 the "random distribution" is shown as an insert. By comparing the figures, it can be seen that the cube (cube-twin) misorientation distributions are fairly close to the random distribution, whereas the rolling and random nuclei/grains have a larger proportion of lower angle boundaries.

6.3 Growth of nuclei/grains in heavily cold deformed matrices

During the growth of a nucleus/grain in a heavily cold deformed matrix, the boundary will constantly meet new types of deformation microstructures (volume elements with lamellar boundaries, DDW/MBs, subgrains, cells) and new crystallographic orientations. Its growth conditions will, therefore, change constantly. Furthermore, even nearby segments of the boundary may experience quite different growth conditions because of small-scale variations in the deformed matrix. The nuclei/grains will therefore not have a constant mobility, M or driving force, F along their boundaries. In what follows, effects of driving force and mobility orientation dependencies on growth rates under such conditions are analyzed.

The energy stored in the deformed matrix, and therefore the driving force for recrystallization, may depend on the crystallographic orientation of the deformed matrix, also in heavily cold deformed metals. However, because of the subdivision into very fine-scale (< 5 μm, linear dimension) volume elements of different orientations and types of dislocation structures, the possible variations in F will be on similar fine scale. Each nuclei/grain may therefore, independently of its orientation, experience the local variations in F.

Preferential misorientation relationships between nuclei/grain and deformed matrix leading to high boundary mobilities, like the 40° <111> rotation relationship, may exist but only *locally* in time and space. Consequently, one can expect "orientation acceleration" of the boundary migration on a local scale whenever a grain boundary segment fulfils the preferential misorientation relationship. If such a preferential misorientation relationship is fulfilled more often for the cube nuclei/grains than the others, this may explain the observed cube growth advantages. This mechanism for explanation of preferential cube growth has been suggested [5,117,118] and is often referred to as a "compromise orientation" mechanism.

For the present aluminium (AA1050) and copper, however, the misorientation measurements show that all types of nuclei/grains (cube, rolling and random) have a broad range of misorientation axis/angle pairs to the deformed matrix [A6] (see section 6.2), with very few 40° <111> boundaries. The number of boundary segments with a

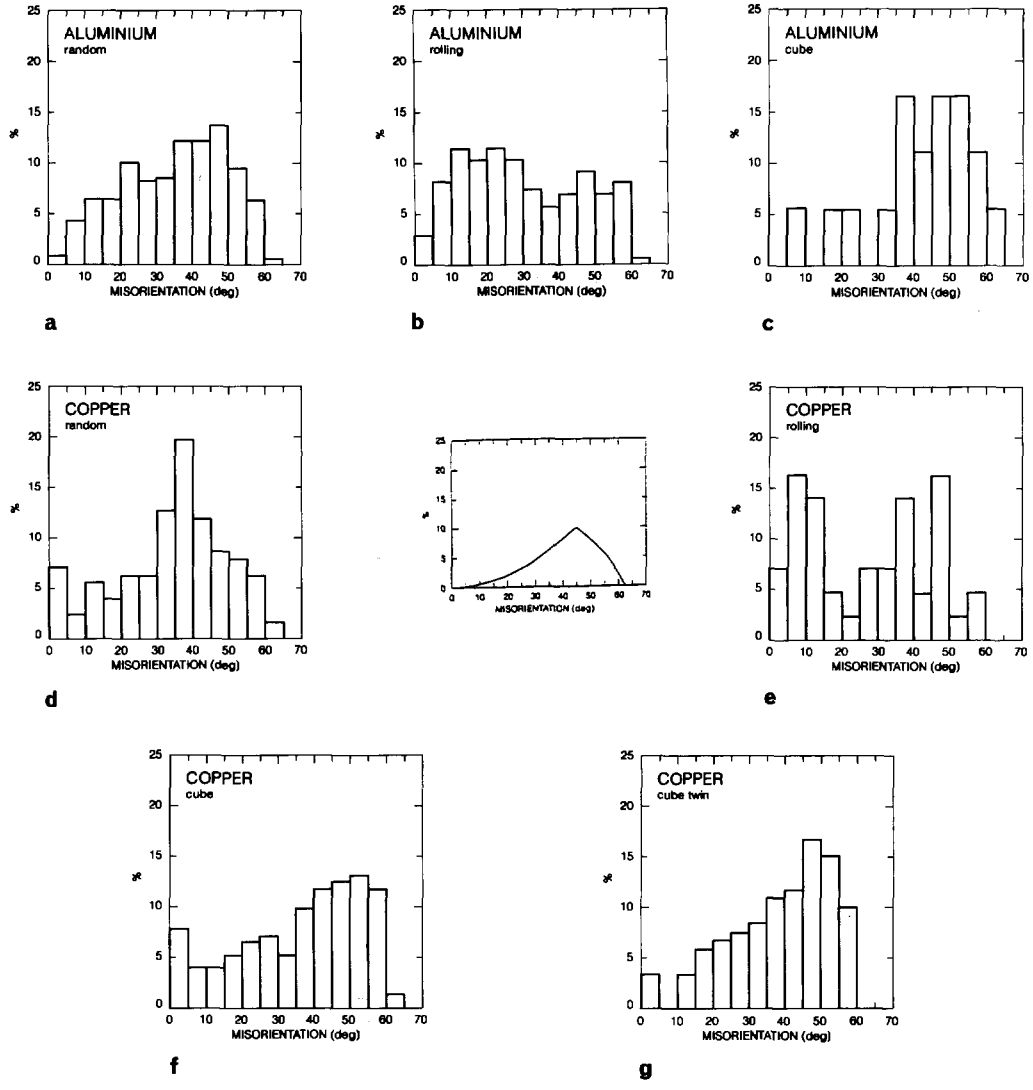

Fig. 38 Misorientation angles between nuclei/grains of various orientations and the deformed matrix. The data include all investigated annealing times. a) Al AA1050, random grains b) Al AA1050, rolling grains c) Al AA1050, cube grains d) Cu, random grains e) Cu, rolling grains (these are included in the analysis in spite the fact that the level of rolling texture in the recrystallized state is about random level, and the rolling grains may equally well be included in the random grains) f) Cu, cube grains g) Cu, cube twin grains [A6]. As an insert the distribution of misorientation angles in a completely random textured material is shown [116].

rotation axis within 5° of the <111> was determined, and among these, those with a 35°-45° misorientation angle were also determined. The results are listed in Table IV. In total, less than 3% of the boundary segments are within 5° of the <111> and less than 0.5% also fulfil the 35°-45° angle condition. In other words, extremely few boundary segments are of the 40° <111> type. This is also the case for the fast growing cube nuclei/grains (see Table IV).

Table IV Number of boundary segments within 5° of a <111> misorientation axis and number of boundary segments which in addition to the <111> axis also have a near 40° (35°-45°) misorientation angle.

Grain orientation	<111>	<111> + 40°
	Aluminium (AA1050)	
Random	2	1
Rolling	4	0
Cube	0	0
	Copper (OFHC)	
Random	4	1
Rolling	1	1
Cube	5	1
Cube twin	7	1

A third possibility for explaining the orientation dependent growth rates may relate to a newly found mechanism [A6,A7] where the presence of low angle boundaries between nuclei/grains and the surrounding deformed matrix is of importance. When twinning can be ignored, it is generally believed that the nuclei develop with orientations like those present in the deformation texture. During their formation and growth, the nuclei may therefore meet local volumes in the deformed matrix of their own, or almost their own, orientation resulting in a low angle boundary segment. As it is generally observed that the mobility of low angle boundaries is low [e.g. 119-121] such volumes will pin the boundary locally, and retard its movement. This mechanism has been called "orientation pinning" [A7] and is illustrated in Fig. 39. Here an imaginary nucleus of a given orientation, "i", is shown in grey. In the neighbouring deformed matrix, volume elements of "i", or near "i", orientation are also shown in grey. In the sketched example, it is clear that orientation pinning will hinder the movement of the top and right-hand side of the nucleus boundary, whereas the lower part is more free to move.

Depending on the volume fraction and distribution of the texture components in the deformed matrix, orientation pinning can affect to different degrees the average growth

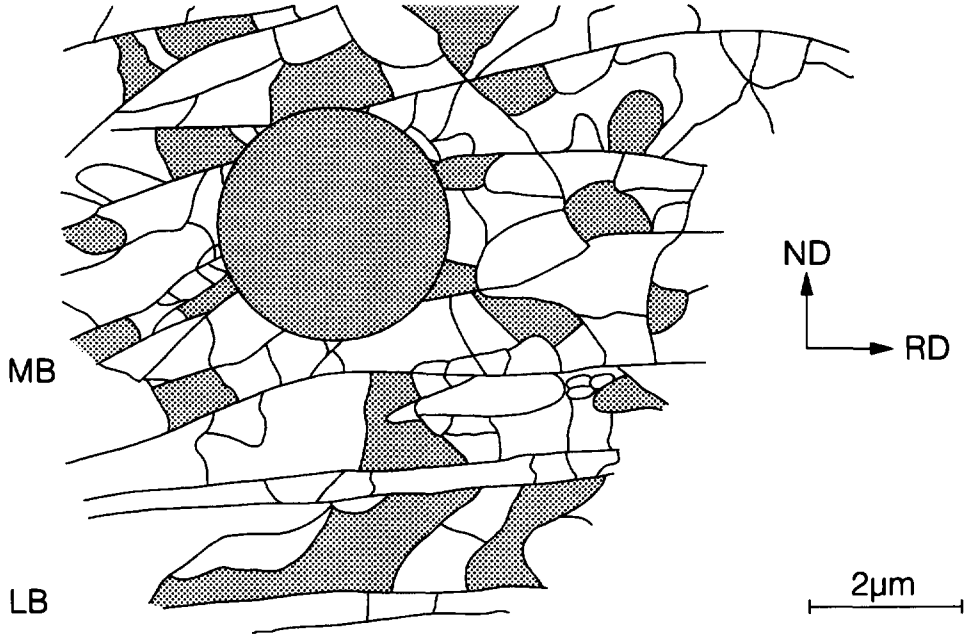

Fig. 39 Sketch illustrating orientation pinning. An imaginary circular nucleus is shown in a typical deformation microstructure. Areas of DDW/MBs and lamellar bands are marked by MB and LB, respectively. When the nucleus grows into areas of nearly its own orientations - as those shown in grey - the motion of the corresponding boundary segment will be retarded by orientation pinning [A7].

rate of nuclei/grains with different orientations. 3D numerical simulations were used to quantify the magnitude of orientation pinning for various typical deformation microstructures and nucleation conditions. It was found that if the nuclei develop at random positions in the deformation microstructure, not particularly associated with deformation Volume Elements of their Own (or nearly their own) Orientation (VEOO), the average area fraction being orientation pinned is equal to volume fraction of VEOOs. This is independent of the size and shape of the VEOOs and the size of the nuclei. However, the distribution of the pinned area fraction depends significantly on these parameters. This is illustrated in Fig. 40. The figure shows that if the VEOOs are small and uniformly distributed, almost all nuclei will experience the same orientation pinning (see Fig. 40a). If, on the other hand, the VEOOs are large (e.g. > 2 x the size of the nuclei), some nuclei will be very strongly pinned, whereas many other nuclei (still of the same orientation) will not be pinned at all (see Fig. 40b).

If the nuclei form at VEOOs, the average area fraction of orientation pinning increases significantly compared to the random nucleation case. And in this situation the deformation and nucleation parameters have significant effects on both the average

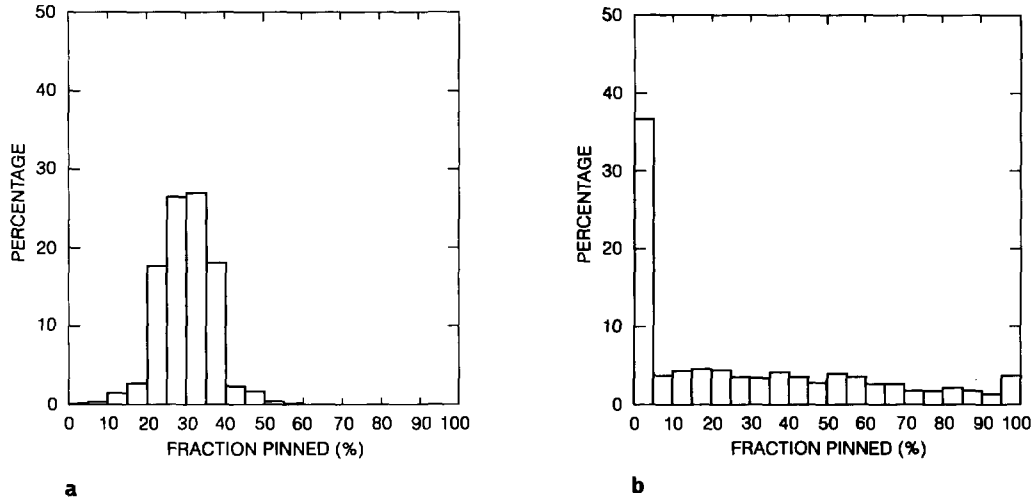

Fig. 40 Histograms showing distributions of nuclei surface area being pinned by orientation pinning (computer calculations). It is assumed that there is 30 vol % VEOOs in the deformed microstructure and that the nuclei size in 5 μm. a) VEOO radius = 1 μm. b) VEOO radius = 10 μm.

orientation pinning and the distribution. The results for the average pinning are shown in Fig. 41. It can be seen that even in the case where there is only 5 volume percent VEOO, an average pinning of up to 70% can be observed, depending on the sizes of the VEOOs and the nuclei.

The magnitude of orientation pinning in the present Al (AA1050) and Cu (OFHC) materials can be quantified from the statistical measurements of misorientations [A6]. In this investigation, it was found that the rolling and randomly oriented nuclei/grains in both Al and Cu are surrounded by 10%-25% low angle boundaries (< 10°). Cube (and in copper also cube twin) nuclei/grains, on the other hand, are only surrounded by 3-10% low angle boundaries. Orientation pinning therefore occurs about 3 times as often for rolling and random nuclei/grains as for cube nuclei/grains. This will clearly affect their relative average growth rates. If for simplicity it is assumed that the only difference between the two types of nuclei/grains is the difference in fraction of low angle boundaries, and all low angle boundaries move more than 10 times as slowly as the average of other boundaries, it is found that the growth advantage for the cube nuclei/grains compared to the other nuclei/grain should be about 1.3 times. In other words, orientation pinning can account for a significant fraction of the observed growth rate orientation dependency.

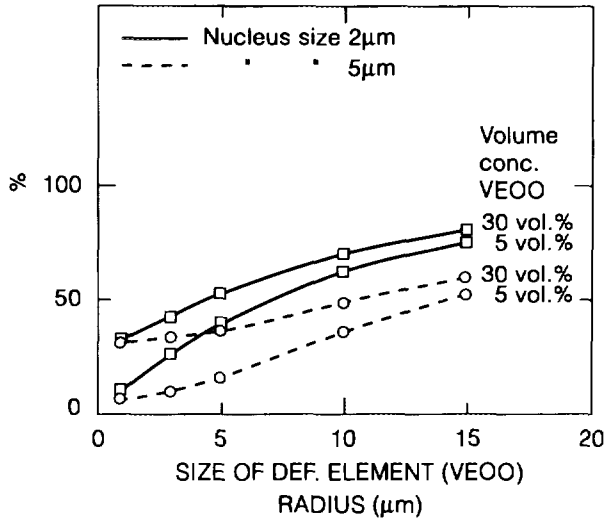

Fig. 41 Average percentage of nuclei surface area being pinned by orientation pinning, assuming that the nuclei develop at sites of their own orientation (at VEOOs) in the deformation microstructure (computer calculations). Two volume percentages of VEOO (5 and 30%) and two nucleation sizes (2 and 5 μm) are assumed.

7. CONCLUSIONS

The growth of nuclei and grains during recrystallization has been studied with the aim of investigating effects of crystallographic orientation in heavily cold rolled fcc metals. The work has involved the development of experimental methods, quantitative characterization, the development of recrystallization models and the proposal of a new physical mechanism important for orientation dependent growth. The main conclusions are:

- The development of automated techniques for the determination of the crystallographic orientation in selected local regions of the microstructure have allowed the standard Cahn-Hagel method for growth rate measurements to be extended to include the orientations of the nuclei/grains. It is, thus, possible to determine growth rates of nuclei/grains with different orientations individually. This extended Cahn-Hagel method is the most powerful technique available today for statistical studies of the average growth rate of nuclei/grains with different orientations in polycrystalline materials. The method applies to the entire recrystallization process and the velocity (migration rate) of the free unimpinged boundaries is determined directly, without any assumptions about nucleation sites, rates or orientations.

- By using the extended Cahn-Hagel method, it is proven that recrystallization growth rates may depend significantly on the crystallographic orientation of the nuclei/grains. This result is based on growth rate measurements in heavily cold deformed pure and commercially pure aluminium and copper recrystallized under several different annealing conditions.

- A consequence of the observed orientation dependent growth rates is that recrystallization models also have to take the crystallographic orientation into account. Combined use of analytical MPM and numerical component methods is very powerful when analyzing experimental data and thereby deducing complete nucleation and growth models, including orientation aspects. These nucleation and growth models describe in detail the microstructural development of individual orientations (or texture components) during recrystallization including: volume fraction of recrystallized material, texture composition, interfacial area between deformed matrix and recrystallized nuclei/grains, average grain size and grain size distributions of nuclei/grains of all orientations as well as interfacial area separating recrystallized nuclei/grains of the various orientations.

- By using recrystallization models which take orientation effects into account, it is shown that growth advantages, such as those observed experimentally, strongly affect, in particular, the texture development and the grain size distribution. Furthermore, when simulating recrystallization in specific materials under specific deformation and annealing conditions, the agreement between experimental and simulated results is significantly improved compared to that obtained with modelling techniques which do not consider orientation aspects.

- The orientation pinning mechanism is of importance for growth in deformed metals. In particular, when the material by the deformation is subdivided into volume elements belonging to different texture components which are small compared to the recrystallized grain size. This is typically the case for metals deformed to medium and high strains. Orientation pinning may affect the growth rate ratio between nuclei/grains of different orientations: Nuclei/grains with an orientation not very common in the deformed matrix, will, on average, not be much affected by orientation pinning, and will thus have a growth advantage compared to nuclei/grains which are more heavily pinned because of a high volume fraction of that texture component in the deformed matrix. It is shown that orientation pinning is an important mechanism which is necessary for the understanding of orientation dependent growth rates in heavily cold rolled aluminium and copper.

ACKNOWLEDGEMENTS

Acknowledgement is given to many present and former members of the Materials Department, the Physics Department, the Electronics Department and the Computer Group at Risø for their valuable assistance and interest in this work. Special thanks are due to Jørgen B. Bilde-Sørensen, Andy Godfrey, Niels Chr. Krieger Lassen, Jørgen Lindbo, Torben Leffers, Palle Nielsen, Helmer Nilsson, Jens V. Olsen, Henning F. Poulsen and Grethe Winther. For very skilful help with experimental work I am grateful to Preben B. Olesen. I also particularly wish to thank Roy A. Vandermeer, Naval Research Laboratory, Washington DC, with whom I have had a close and enjoyable collaboration over the last 4 years and who has had a major influence on the modelling part of this work. But, above all, I wish to thank Niels Hansen for the close collaboration, numerous fruitful discussions, his positive interest and for providing excellent working conditions and laboratory facilities.

I also wish to acknowledge Tora Skov for technical drawings, Jane Horsewell, for language corrections and Jytte Mortensen for the typing of this report.

REFERENCES

Authors Publications

A1. D. Juul Jensen, N. Hansen and F.J. Humphreys (1985). Acta metall., 33, 2155-2162.
A2. D. Juul Jensen and V. Randle (1989). Invited Paper Proc. 10th Risø Int. Symp.: Materials Architecture. Eds. J.B. Bilde-Sørensen et al., Risø, Roskilde, 103-126.
A3. D. Juul Jensen (1992). Scripta metall. mater., 27, 533-538.
A4. D. Juul Jensen (1992). Scripta metall. mater., 27, 1551-1556.
A5. D. Juul Jensen (1993). Textures and Microstructures, 20, 55-65.
A6. D. Juul Jensen (1995). Acta metall. mater., 43, 4117-4129.
A7. D. Juul Jensen (1995). Invited Paper. Proc. 16th Risø Int. Symp.: Microstructural and Crystallographic Aspects of Recrystallization. Eds. N. Hansen et al., Risø, Roskilde, 119-137.
A8. D. Juul Jensen (1997). Metall. Mater. Trans. A, 28A, 15-25.

A9. D. Juul Jensen, N. Hansen and F.J. Humphreys (1988). Proc. 8th Int. Conf. on Textures of Materials. Eds. J.S. Kallend and G. Gottstein. TMS, 431-444.
A10. F.J. Humphreys and D. Juul Jensen (1986). Proc. 7th Risø Int. Symp.: Annealing Processes - Recovery, Recrystallization and Grain Growth. Eds. N. Hansen et al., Risø, Roskilde, 93-106.
A11. D. Juul Jensen and R.A. Vandermeer (1996). Proc. 11th Int. Conf. on Textures of Materials. Eds Z. Liang et al., Int. Acd. Publ., 490-496.
A12. D. Juul Jensen and N. Hansen (1986). Proc. 7th Risø Int. Symp.: Annealing Processes - Recovery, Recrystallization and Grain Growth. Eds. N. Hansen et al., Risø, Roskilde, 379-384.
A13. D. Juul Jensen and J.K. Kjems (1983). Textures and Microstructures, 5, 239-251.
A14. N.C. Krieger Lassen, D. Juul Jensen and K. Conradsen (1994). Mat. Sci. Forum, 157-162, 149-158.
A15. D. Juul Jensen, N. Hansen and F.J. Humphreys (1984). Proc. 7th Int. Conf. on Textures of Materials. Eds. C.M. Brakman et al., Netherlands Soc. Mat. Sci., 251-256.
A16. R.K. Bolingbroke, T. Furu, D. Juul Jensen and K. Vernon-Parry (1996). Accepted for publication in Mat. Sci. Techn.
A17. D. Juul Jensen and N.H. Schmidt (1990). Proc. Int. Conf. Recrystallization '90. Ed. T. Chandra, TMS, 219-224.
A18. N.C. Krieger Lassen, D. Juul Jensen and K. Conradsen (1992). Scanning Microscopy, 6, 115-121.
A19. R.A. Vandermeer and D. Juul Jensen (1994). Scripta metall. mater., 30, 1575-1580.
A20. D. Juul Jensen (1990). Nondestr. Test. Eval., 5, 335-347.
A21. R.A. Vandermeer and D. Juul Jensen (1995). Metall. Mater. Trans. A., 26A, 2227-2235.
A22. E. Woldt and D. Juul Jensen (1995). Metall. Mater. Trans. A., 26A, 1717-1724.
A23. R.A. Vandermeer, D. Juul Jensen and E. Woldt (1996). Accepted for publication in Metall. Mater. Trans. A.

A24. D. Juul Jensen and N. Hansen (1990). Proc. Int. Conf. Recrystallization '90. Ed. T. Chandra, TMS, 661-666.
A25. D. Juul Jensen and R.A. Vandermeer (1995). Proc. 4th Europ. Conf. on Adv. Mat. Proc., F, 177-186.
A26. R.A. Vandermeer and D. Juul Jensen (1994). Acta metall. mater., 42, 2427-2436.
A27. R.A. Vandermeer and D. Juul Jensen (1996). Textures and Microstructures, 27, 263-279.
A28. D. Juul Jensen, R.K. Bolingbroke, T. Furu, F.J. Humphreys, C.M. Sellars, R. Shahani and R. Ørsund (1995). Synthesis report Brite-Euram project BREU-CT91-0399 (BE-4514-90), 1-16.
A29. N. Hansen, Q. Liu and D. Juul Jensen (1995). Proc. 4th Europ. Conf. on Adv. Mat. Proc., F, 211-216.
A30. D. Juul Jensen and N. Hansen (1990). Acta metall. mater., 38, 1369-1380.
A31. G.I. Rosen, D. Juul Jensen, D.A. Hughes and N. Hansen (1995). Acta metall. mater., 43, 2563-2579.
A32. N. Hansen, D. Juul Jensen, X. Huang and A. Bunsch (1996). Proc. 11th Int. Conf. on Textures of Materials. Eds. Z. Liang et al., Int. Acd. Publ., 1331-1338.

Other Publications

1. H. Hu, B.B. Rath and R.A. Vandermeer (1990). Proc. Int. Conf. on Recrystallization '90. Ed. T. Chandra, TMS, 3-16.
2. R.A. Ricks, R.K. Bolingbroke, R. Ørsund, J.L. Strid, R. Shahani and G.M. Raynaud (1994). Proc. 15th Risø Int. Symp.: Numerical Predictions of Deformation Processes and the Behaviour of Real Materials. Eds. S.I. Andersen et al., Risø, Roskilde, 99-108.
3. W.G. Burges and P.C. Louwerse (1931). Z. Physik, 67, 605-678.
4. C.S. Barrett (1940). Trans. AIME, 137, 128-145.
5. P.A. Beck (1954). Adv. in Physics, 3, 245-324.
6. P. Haasen (1986). Proc. 7th Risø Int. Symp.: Annealing Processes - Recovery, Recrystallization and Grain Growth. Eds. N. Hansen et al., Risø, Roskilde, 69-74.
7. H. Hu (1986). Proc. 7th Risø Int. Symp.: Annealing Processes - Recovery, Recrystallization and Grain Growth. Eds. N. Hansen et al., Risø, Roskilde, 75-92.
8. W.B. Hutchinson and E. Nes (1986). Proc. 7th Risø Int. Symp.: Annealing Processes - Recovery, Recrystallization and Grain Growth. Eds. N. Hansen et al., Risø, Roskilde, 107-122.
9. R.D. Doherty, G. Gottstein, J. Hirsch, W.B. Hutchinson, K. Lücke, E. Nes and P.J. Wilbrandt (1988). Proc. 8th Int. Conf. on Textures of Materials. Eds. J.S. Kallend and G. Gottstein, TMS, 563-572.
10. K. Lücke and M. Hölscher (1991). Proc. 9th Int. Conf. on Textures of Materials, Textures and Microstructures, 14-18, 585-596.
11. P. Haasen (1990). Proc. Int. Conf. Recrystallization '90. Ed. T. Chandra, TMS, 17-26.
12. M. Hatherly (1990). Proc. Int. Conf. Recrystallization '90. Ed. T. Chandra, TMS, 59-68.

13. H.J. Bunge and U. Köhler (1992). Int. Workshop on Fundamentals of Recrystallization, Scripta metall. mater., 27, 1539-1543.
14. R.D. Doherty, I. Samajdar and K. Kunze (1992). Int. Workshop on Fundamentals of Recrystallization, Scripta metall. mater., 27, 1459-1464.
15. B.J. Duggan and C.S. Lee (1992). Int. Workshop on Fundamentals of Recrystallization, Scripta metall. mater., 27, 1503-1507.
16. O. Engler and K. Lücke (1992). Int. Workshop on Fundamentals of Recrystallization, Scripta metall. mater., 27, 1527-1532.
17. P. Haasen (1992). Int. Workshop on Fundamentals of Recrystallization, Scripta metall. mater., 27, 1477-1484.
18. F. Haessner and K. Sztwiertnia (1992). Int. Workshop on Fundamentals of Recrystallization, Scripta metall. mater., 27, 1545-1550.
19. B. Hutchinson (1992). Int. Workshop on Fundamentals of Recrystallization, Scripta metall. mater., 27, 1471-1475.
20. J.J. Jonas and L.S. Tóth (1992). Int. Workshop on Fundamentals of Recrystallization, Scripta metall. mater., 27, 1575-1580.
21. D. Raabe and K. Lücke (1992). Int. Workshop on Fundamentals of Recrystallization, Scripta metall. mater., 27, 1533-1538.
22. P.J. Wilbrandt (1992). Int. Workshop on Fundamentals of Recrystallization, Scripta metall. mater., 27, 1485-1492.
23. T. Furu, K. Marthinsen and E. Nes (1993). Proc. Int. Conf. Recrystallization '92, Mat. Sci. Forum, 113-115, 41-54.
24. P. Haasen and P.J. Wilbrandt (1994). Proc. 10th Int. Conf. on Textures of Materials, Mat. Sci. Forum, 157-162, 887-898.
25. R.D. Doherty, I. Samajdar, C.T. Necker, H.E. Vatne and E. Nes (1995). Proc. 16th Risø Int. Symp.: Microstructural and Crystallographic Aspects of Recrystallization. Eds. N. Hansen et al., Risø, Roskilde, 1-23.
26. J.H. Driver (1995). Proc. 16th Risø Int. Symp.: Microstructural and Crystallographic Aspects of Recrystallization. Eds. N. Hansen et al., Risø, Roskilde, 25-36.
27. J. Hirsch and O. Engler (1995). Proc. 16th Risø Int. Symp.: Microstructural and Crystallographic Aspects of Recrystallization. Eds. N. Hansen et al., Risø, Roskilde, 49-62.
28. B. Hutchinson and L. Ryde (1995). Proc. 16th Risø Int. Symp.: Microstructural and Crystallographic Aspects of Recrystallization. Eds. N. Hansen et al., Risø, Roskilde, 105-117.
29. H. Weiland (1995). Proc. 16th Risø Int. Symp.: Microstructural and Crystallographic Aspects of Recrystallization. Eds. N. Hansen et al., Risø, Roskilde, 215-228.
30. J.E. Hilliard (1966). In Recrystallization, Grain Growth and Textures. Ed. H. Margolin, ASM, 267-286.
31. W.C. Leslie, F.J. Plecity and J.T. Michalak (1961). Trans. AIME, 221, 691-700.
32. K. Lücke (1984). Proc. 7th Int. Conf. on Textures of Materials. Eds. C.M. Brakman et al., Netherlands Soc. Mat. Sci., 195-210.
33. H.J. Bunge (1969). Mathematische Methodes der Texturanalyse, Akademie-Verlag, Berlin.
34. J. Hirsch (1986). Proc. 7th Risø Symp.: Annealing Processes - Recovery, Recrystallization and Grain Growth. Eds. N. Hansen et al., Risø, Roskilde, 349-360.

35. L. Kestens and J.J. Jonas (1996). Metall. Mater. Trans. A, 27A, 155-164.
36. A. Böttcher, M. Hastenrath, K. Lücke and J. Hjelen (1991). Textures and Microstructures, 14-18, 673-678.
37. F. Habiby and F.J. Humphreys (1994). Scripta metall. mater., 27, 1515-1520.
38. D.P. Field (1995). Mat. Sci. Eng. A, 190, 241-246.
39. E. Nes and J.K. Solberg (1986). Mat. Sci. Techn., 2, 19-21.
40. R.D. Doherty, K. Kashyap and S. Panchanadeeswaran (1993). Acta metall. mater., 41, 3029-3053.
41. C.T. Necker, R.D. Doherty and A.D. Rollett (1991). Textures and Microstructures, 14-18, 635-640.
42. J. Hjelen, R. Ørsund and E. Nes (1991). Acta metall. mater., 39, 1377-1404.
43. O. Daaland and E. Nes (1996). Acta mater., 44, 1413-1435.
44. M.G. Ardakani and F.J. Humphreys (1994). Acta metall. mater., 42, 763-780.
45. H. Weiland and J.R. Hirsch (1991). Textures and Microstructures, 14-18, 647-652.
46. J.W. Cahn and W.C. Hagel (1962). In Decomposition of Austenite by Diffusional Processes. Eds. V.F. Zackay and H.I. Aaronson, Interscience, 131-196.
47. A.T. English and W.A. Backofen (1964). Trans. AIME, 230, 396-407.
48. G.R. Speich and R.M. Fisher (1966). In Recrystallization, Grain Growth and Textures. Ed. H. Margolin, ASM, 563-598.
49. R.A. Vandermeer and B.B. Rath (1990). In Proc. Recrystallization '90. Ed. T. Chandra, TMS, 49-58.
50. E.E. Underwood (1968). In Quantitative Microscopy. Eds. R.T. Dehoff and F.N. Rhines, McGraw-Hill, 77-127.
51. K.J. Kurzydlowski and B. Ralph (1995). The Quantitative Description of the Microstructure of Materials. CRC Press.
52. S.A. Saltykov (1958). Stereometric Metallography, Metallurgizdat.
53. S.I. Wright and B.L. Adams (1992). Metall. Trans., 23A, 759-767.
54. K. Kunze, S.I. Wright, B.L. Adams and D.J. Dingley (1993). Textures and Microstructures, 20, 41-54.
55. M. Avrami (1939). J. Chem. Phys., 7, 1103-1109.
56. M. Avrami (1940). J. Chem. Phys., 8, 212-224.
57. M. Avrami (1941). J. Chem. Phys., 9, 177-184.
58. R.D. Doherty, A.R. Rollett and D.J. Srolovitz (1986). Proc. 7th Risø Int. Symp.: Annealing Processes - Recovery, Recrystallization and Grain Growth. Eds. N. Hansen et al., Risø, Roskilde, 53-67.
59. P. Kruger and E. Woldt (1992). Acta metall. mater., 40, 2933-2942.
60. H.W. Hesselbarth, L. Kaps and F. Haessner (1993). Mat. Sci. Forum, 113-115, 317-322.
61. H.E. Vatne, S. Benum, O. Daaland and E. Nes (1996). Textures and Microstructures, 27, 385-412.
62. E. Nes (1992). Private communication.
63. H.E. Vatne and E. Nes (1994). Scripta Metall. Mater., 30, 309-312.
64. B.J. Duggan, K. Lücke, G. Köhlhoff and C.S. Lee (1993). Acta metall. mater., 41, 1921-1927.
65. M.P. Anderson (1986). Proc. 7th Risø Int. Symp.: Annealing Processes - Recovery, Recrystallization and Grain Growth. Eds. N. Hansen et al., Risø, Roskilde, 15-34.

66. D.J. Srolovitz, G.S. Grest and M.P. Anderson (1986). Acta metall., 34, 1833-1845.
67. R.D. Doherty, A.R. Rollett and D.J. Srolovitz (1986). Proc. 7th Risø Int. Symp.: Annealing Processes - Recovery, Recrystallization and Grain Growth. Eds. N. Hansen et al., Risø, Roskilde, 53-67.
68. D.J. Srolovitz, G.S. Grest, M.P. Anderson and A.D. Rollett (1988). Acta metall., 36, 2115-2128.
69. A.D. Rollett, D.J. Srolovitz, R.D. Doherty and M.P. Anderson (1989). Acta metall. mater., 37, 627-639.
70. Ph. Tavernier and J.A. Szpunar (1991). Acta metall. mater., 39, 557-567.
71. Ph. Tavernier and J.A. Szpunar (1991). Acta metall. mater., 39, 549-556.
72. Ph. Tavernier and J.A. Szpunar (1991). Textures and Microstructures, 14-18, 667-672.
73. H.W. Hesselbarth and I.R. Göbel (1991). Acta metall. mater., 39, 2135-2143.
74. F.J. Humphreys (1992). Scripta metall. mater., 27, 1557-1562.
75. F.J. Humphreys (1993). Mat. Sci. Forum, 113-115, 329-334.
76. V. Marx, F.R. Reher and G. Gottstein (1995). Private communication.
77. K.W. Mahin, K. Hanson and J.W. Morris (1980). Acta metall., 28, 443-453.
78. T.O. Sætre, O. Hunderi and E. Nes (1986). Acta metall., 34, 981-987.
79. H.J. Frost and C.V. Thompson (1987). Acta metall., 35, 529-540.
80. I. Orgzall and B. Lorenz (1988). Acta metall., 36, 627-631.
81. K. Marthinsen, O. Lohne and E. Nes (1989). Acta metall., 37, 135-145.
82. R.A. Vandermeer, R.A. Masumura and B.B. Rath (1991). Acta metall. mater., 39, 383-389.
83. A.N. Kolmogorov (1937). Izv. Akad. Nauk. USSR-Ser. Matemat., 1, 355-359.
84. W.A. Johnson and R.F. Mehl (1939). Trans. AIME, 135, 416-458.
85. R.A. Vandermeer (1995). Proc. 16th Risø Int. Symp.: Microstructural and Crystallographic Aspects of Recrystallization. Eds. N. Hansen et al., Risø, Roskilde, 193-213.
86. R.A. Vandermeer (1992). Scripta metall. mater., 27, 1563-1568.
87. D.W. Demianczuc and K.T. Aust (1975). Acta metall., 23, 1149-1162.
88. G. Gottstein and L.S. Shvindlerman (1992). Scripta metall. mater., 27, 1521-1526.
89. R.A. Vandermeer and H. Hu (1994). Acta metall. mater., 42, 3071-3075.
90. I.L. Dillamore, C.J.E. Smith and T.W. Watson (1967). Met. Sci. J., 1, 49-54.
91. W.B. Hutchinson (1974). Met. Sci., 8, 185-196.
92. A. Bardal, I. Lindseth, H.E. Vatne and E. Nes (1995). Proc. 16th Risø Int. Symp.: Microstructural and Crystallographic Aspects of Recrystallization. Eds. N. Hansen et al., Risø, Roskilde, 261-266.
93. X. Huang (1996). Private communication.
94. R.L. Every and M. Hatherly (1974). Texture, 1, 183-194.
95. P.A. Beck, P.R. Sperry and H. Hu (1950). J. Appl. Phys., 21, 420-425.
96. B. Liebmann, K. Lücke and G. Masing (1956). Z. Metallk., 47, 57-63.
97. S. Kohara, M.N. Parthasarathi and P.A. Beck (1958). Trans. AIME, 212, 875-881.
98. H. Yoshida, B. Liebmann and K. Lücke (1959). Acta metall., 7, 51-56.
99. G. Ibe and K. Lücke (1966). In Recrystallization, Grain Growth and Textures. Ed. H. Margolin, ASM, 434-447.
100. G. Gottstein and L.S. Shvindlerman (1992). Scripta metall. mater., 27, 1515-1520.
101. K.T. Aust and J.W. Rutter (1959). Trans. AIME, 215, 119-127.

102. K.T. Aust and J.W. Rutter (1960). Trans. AIME, 218, 50-54.
103. P. Gordon and R.A. Vandermeer (1966). In Recrystallization, Grain Growth and Textures. Ed. H. Margolin, ASM, 205-266.
104. K.T. Aust and J.W. Rutter (1959). Trans. AIME, 215, 820-831.
105. K.T. Aust and J.W. Rutter (1962). Trans. AIME, 224, 111-115.
106. S. Kohara, M.N. Parthasarathi and P.A. Beck (1958). J. Appl. Phys., 29, 1125-1126.
107. M.N. Parthasarathi and P.A. Beck (1961). Trans. AIME, 221, 831-838.
108. N. Hansen, D. Kuhlmann-Wilsdorf (1986). Mat. Sci. Eng., 81, 141-161.
109. B. Bay, N. Hansen, D.A. Hughes and D. Kuhlmann-Wilsdorf (1992). Acta metall. mater., 40, 205-219.
110. D.A. Hughes (1995). Proc. 16th Risø Int. Symp.: Microstructural and Crystallographic Aspects of Recrystallization. Eds. N. Hansen et al., Risø, Roskilde, 63-85.
111. Q. Liu and N. Hansen (1995). Scripta metall. mater., 32, 1289-1295.
112. N. Hansen (1996). In Aluminium Alloys for Packaging II. Eds. J.G. Morris et al., TMS, 11-26.
113. N. Hansen and D.A. Hughes (1995). Phys. Stat. Sol. (b), 149, 155-172.
114. D.A. Hughes and N. Hansen (1995). Scripta metall. mater., 33, 315-321.
115. F. Haessner and K. Sztwiernia (1992). Scripta metall. mater., 27, 1545-1550.
116. J.K. Mackenzie (1958). Biometrika, 45, 229-240.
117. P.A. Beck (1953). Acta metall., 1, 230-234.
118. U. Schmidt and K. Lücke (1979). Textures Cryst. Sol., 3, 85-112.
119. R.D. Doherty (1978). In: Recrystallization of metallic materials. Ed. F. Haessner, Dr. Riederer Verlag, 23-61.
120. H. Hu (1981). Metall. Treaties. Eds. J.K. Tien and J.F. Elliott (AIME), 385-407.
121. F.J. Humphreys and M. Hatherly (1995). Recrystallization and Related Annealing Phenomena. Pergamon.

Dansk Resume
(Summary in Danish)

Sammenhængen mellem den krystallografiske orientering af kim/korn (kim og korn) og deres væksthastighed under rekrystallisation er blevet undersøgt med henblik på at forstå udviklingen af mikrostruktur og tekstur i polykrystallinske metaller. En sådan forståelse er meget vigtig, idet mange egenskaber afhænger af metallets mikrostruktur og tekstur. Det gælder f.eks. hårdhed, styrke, formbarhed, overfladeegenskaber og magnetiserbarhed. Emnet er således interessant både videnskabeligt og industrielt. Men på trods af en meget omfattende forskningsindsats, har emnet været (og er stadigt) kontroversielt. Dette skyldes især manglen af en velegnet eksperimentel teknik til kvantitativ bestemmelse af sammenhængen mellem orientering og væksthastighed. En sådan teknik er nu udviklet og beskrevet i dette arbejde. Teknikken er anvendt til bestemmelse af væksthastigheder i flere kraftigt deformerede fcc metaller - både rene metaller og gængse industrielle metaller. Det er blevet vist, at væksthastigheden kan afhænge signifikant af orienteringen, og rekrystallisationsmodeller/simuleringsmetoder er udviklet, som tager højde for dette. Endelig omfatter arbejdet en fortolkning af de målte væksthastigheder, hvilket har ført til definition og beskrivelse af en ny fysisk mekanisme "orientation pinning", der er vigtig for vækst i deformerede metaller.

Arbejdet er rapporteret i otte udvalgte publikationer (A1-A8), som er medtaget i appendiks.

1.
Formålet med arbejdets *første* del var at finde en velegnet eksperimentel metode til undersøgelse af sammenhængen mellem orientering og væksthastighed. Tre metoder blev analyseret: Metode 1 er baseret på teksturmålinger. Ud fra en sammenligning af den krystallografiske tekstur før og efter rekrystallisation kan det fastlægges, om nogle orienteringer udvikles specielt kraftigt og forskellige hypoteser for vækst kan analyseres.

Metode 2 er baseret på samtidig måling af størrelse og orientering af kim/korn. Ved at inddele alle kim/korn i orienteringstyper (f.eks. alle kim/korn med en orientering indenfor 15° fra en ideel "cube" orientering, {100} <001>, hører til typen "cube") kan man måle om kim/korn af specielle orienteringstyper vokser sig større end de øvrige.

Både metode 1 og 2 giver værdifuld information om rekrystallisationsprocessen, men kan kun benyttes til vækstanalyse hvis kimdannelsessteder og kimdannelseshastigheder kendes. Det der ønskes bestemt, er nemlig hastigheden af "frie" korngrænser, d.v.s. korngrænser hvis bevægelse ikke er stoppet på grund af "sammenstød" med andre kim/korn. Relationer mellem kimorientering og kimdannelsessteder/kimdannelseshastighed vil derfor have betydning for resultaterne af metode 1 og 2: Hvis for eksempel alle kim af orientering "A" dannes i klumper tæt sammen og alle andre kim dannes separat, fjernt fra hinanden, vil "A" kimene hurtigt støde sammen og deres vækst vil stoppe, hvorimod de andre kim/korn kan vokse mere frit. Resultatet vil derfor blive, at det rekrystalliserede

materiale vil have en svag "A" tekstur og "A" kornene vil være små, uanset hvor høj den sande væksthastighed af "A" kim/korn er.

I metode 3 er det frie overfladeareal af kim/korn inkluderet i analysen og metoden kan derfor benyttes uafhængigt af antagelser/undersøgelser af kimdannelsen. Metoden er udviklet baseret på en Cahn-Hagel analyse af væksthastighed:

$$\frac{dX}{dt} = <G> \cdot S_v$$

hvor X er den rekrystalliserede volumenfraktion, t er varmebehandlingstiden, <G> er gennemsnitsvæksthastigheden og S_v er det frie overfladeareal af kim/korn.

Ved at benytte moderne automatiserede elektronmikroskopimålemetoder kan man bestemme X_i og S_{vi} for kim/korn af orientering "i" og ved at udvide Cahn-Hagel analysen til også at inkludere den krystallografiske orientering, kan væksthastigheder bestemmes for kim/korn af forskellige orienteringer. Metoden skønnes at være den bedst mulige af de i dag eksisterende metoder til statistisk bestemmelse af væksthastighed under rekrystallisation. I det følgende vil den blive refereret til som "krystallografisk Cahn-Hagel analyse".

2.
Formålet med arbejdets *anden* del var at bruge den krystallografiske Cahn-Hagel analysemetode til at undersøge orienteringens indflydelse på vækst under rekrystallisation. Kraftigt kold valset rent og "industrielt rent" aluminium samt kobber blev anvendt, og væksten blev undersøgt for i alt 5 varmebehandlingsforløb. Samtlige undersøgelser viste at orienteringen er vigtig for vækst. Typisk blev det observeret at kim/korn med cube orientering (indenfor 15° fra den ideelle orientering {100} <001>) vokser 1,5 til 2,5 gange så hurtigt som kim/korn af andre orienteringer.

3.
Formålet med arbejdets *tredje* del var at udvikle modeller og simuleringsmetoder, der tager højde for at væksthastigheder kan være orienteringsafhængige; samt at benytte disse modeller/metoder til forudsigelse af mikrostruktur- og teksturudviklingen under rekrystallisation. To sådanne metoder blev udviklet: komponentmetoden og MPM (the microstructural path method).

Komponentmetoden er en 3-dimensional numerisk metode. Dannelsen og væksten af kim/korn med forskellige orienteringer (komponenter) behandles separat. Som input kræves information om kimdannelse og vækst for hvert komponent, og som output fås fuld information om mikrostruktur, tekstur samt kinetik. Metoden kan bruges både til simulering af specifikke rekrystallisationsforløb, hvor eksperimentelle data bruges som input og til mere generelle typer simuleringer, hvor forskellige antagelser - for eksempel om væksten - kan afprøves.

MPM er en analytisk metode, der er udviklet på "Naval Research Laboratory, Washington DC". Som led i et samarbejde, blev metoden udvidet til også at tage højde for orienteringsafhængigheder. Metoden benyttes oftest til analyse af specifikke rekrystallisationsforløb. Ved at udvælge matematiske funktioner der repræsenterer typiske kimdannelses- og vækstprocesser og sammenligne beregnede værdier for X_i og S_{vi} med eksperimentelle målinger, findes de funktioner der giver bedst overensstemmelse. Dermed opnås en beskrivelse af kimdannelses- og vækstprocessen for kim/korn af forskellige orienteringer.

Komponentmetoden og MPM har været anvendt separat og kombineret til to typer rekrystallisationsberegninger: i) konkrete tilfælde og ii) generelle beregninger af betydningen af orienteringsafhængig vækst.

I de konkrete tilfælde var målet at opnå korrekte og komplette beskrivelser af både kimdannelsen og væksten for kim/korn af alle orienteringer. Dette blev opnået ved detaljeret sammenligning med et stort antal eksperimentelle data for både delvist og fuldt rekrystalliserede prøver. Denne type beregninger blev med succes udført for kraftigt koldvalset kobber og industrielt rent aluminium.

Generelle beregninger blev udført for at forstå dannelsen af rekrystallisationsmikrostrukturer og -teksturer under vækstbetingelser som de eksperimentelt observerede (se 2. ovenfor). Beregningerne blev gennemført for en serie kimdannelsessituationer typisk for rene og for pratikelholdige metaller. Beregningerne viste, at både kimdannelsen og de orienteringsafhængige vækshastigheder har stor betydning for rekrystallisationsforløbet samt for mikrostruktur- og teksturudviklingen. Den orienteringsafhængige vækst er specielt vigtig for teksturens styrke og for kornstørrelsesfordelingen. Data af denne type kan benyttes til at forudsige mikrostruktur- og teksturdannelsen under givne kimdannelses- og vækstsituationer.

4.

Formålet med arbejdets *fjerde* og sidste del var at analysere betydningen af forskellige fysiske mekanismer for orienteringsafhængig vækst i kraftigt deformerede metaller. Det er vist, at opbrydning under deformation af de originale korn i små volumenelementer med hver deres krystallografiske orientering er særdeles vigtig for væksten under rekrystallisation, og en ny mekanisme "orientation pinning" er påvist. Ideen bag orientation pinning mekanismen er, at hvis et kim under sin dannelse eller vækst møder et volumenelement i den deformerede struktur med samme, eller næsten samme, krystallografiske orientering som det selv har, vil der lokalt dannes en lavvinkelgrænse med lav mobilitet, og væksten vil stoppe lokalt, eller blive forsinket. Betydningen af orientation pinning for den gennemsnitlige vækshastighed vil afhænge af kimets orientering, deformationsteksturen samt opbrydningen af deformationsmikrostrukturen. Kim med en orientering der ikke er særlig hyppig i deformationsteksturen vil i gennemsnit vokse hurtigere end kim med deformationsteksturorienteringer. Det er vist, at orientation pinning er særdeles vigtig for forståelsen af de eksperimentelt observerede vækshastigheder i kraftigt kold valset aluminium og kobber.

Det udførte arbejde har efter forfatterens opfattelse ført til følgende:

- *Udvikling af måleteknik*: Med nye elektronmikroskopimetoder kan den krystallografiske orientering bestemmes i små (≤ 1 μm) udvalgte volumenelementer i mikrostrukturen. Ved at inkludere denne krystallografiske information i en Cahn-Hagel analyse af vækst-hastighed, er det muligt direkte at måle vækshastigheder af kim/korn med forskellige krystallografiske orienteringer i polykrystallinsk materiale. Metoden refereres til som "krystallografisk Cahn-Hagel analyse" (på engelsk "extended Cahn-Hagel method").

- *Kvantificering af orienteringens betydning for vækshastighed*: Ved at bruge den krystallografiske Cahn-Hagel analysemetode er det vist, at orienteringen af kim/korn kan have kraftig indflydelse på vækshastigheden. Dette resultat er baseret på analyser af aluminium og kobber kold valset til reduktioner omkring 90%.

- *Udvikling og anvendelse af rekrystallisationsmodeller*: Nye metoder til modellering af rekrystallisation er blevet udviklet. Det specielle ved metoderne er, at de tager hensyn til at kim/korn af forskellig orientering kan opføre sig forskelligt under rekrystallisationsforløbet, f.eks. vokse med forskellig hastighed. Metoderne er benyttet til modellering af konkrete rekrystallisationsforløb samt til generelle beregninger af indflydelsen af orienteringsafhængig vækst for en række forskellige kimdannelsessituationer.

- *Definition af fysisk mekanisme*: Når kim/korn dannes og vokser i et polykrystallinsk metal, vil de med en vis sandsynlighed, afhængig af deres egen orientering og deformationsstrukturens opbrydning, møde områder i den deformerede mikrostruktur som har stort set samme orientering som de selv. Derved dannes en lavvinkelkorngrænse med lav mobilitet, som lokalt vil stoppe, eller forsinke, væksten. Denne mekanisme refereres til som "orientation pinning". Det er vist, at orientation pinning bidrager væsentligt til de eksperimentelt observerede forskelle i vækshastighed for kim/korn af forskellig orientering i kraftigt kold valset aluminium og kobber.

Til slut kan bemærkes, at dette arbejde blev påbegyndt for ca. 10 år siden med det primære formål at undersøge et fysisk fænomen. Som sådan må arbejdet betegnes som grundforskning. Men, at det også har industriel betydning er blevet dokumenteret inden for de sidste par år, hvor specielt aluminiumindustrien har vist stor interesse for de observerede vækstresultater. Desuden benytter flere industrier i dag de udviklede eksperimentelle teknikker og 2 store udenlandske aluminiumvirksomheder (Alcoa og Hydro Aluminium) er p.t. ved at implementere de nye rekrystallisationsmodeller til simulering af varmvalsning.

APPENDIX

A1. D. Juul Jensen, N. Hansen and F.J. Humphreys (1985). Acta metall., 33, 2155-2162.

A2. D. Juul Jensen and V. Randle (1989). Invited Paper Proc. 10th Risø Int. Symp.: Materials Architecture. Eds. J.B. Bilde-Sørensen et al., Risø, Roskilde, 103-126.

A3. D. Juul Jensen (1992). Scripta metall. mater., 27, 533-538.

A4. D. Juul Jensen (1992). Scripta metall. mater., 27, 1551-1556.

A5. D. Juul Jensen (1993). Textures and Microstructures, 20, 55-65.

A6. D. Juul Jensen (1995). Acta metall. mater., 43, 4117-4129.

A7. D. Juul Jensen (1995). Invited Paper. Proc. 16th Risø Int. Symp.: Microstructural and Crystallographic Aspects of Recrystallization. Eds. N. Hansen et al., Risø, Roskilde, 119-137.

A8. D. Juul Jensen (1997). Metall. Mater. Trans. A, 28A, 15-25.

A1

Acta metall. Vol. 33, No. 12, pp. 2155–2162, 1985
Printed in Great Britain.

0001-6160/85 $3.00 + 0.00

TEXTURE DEVELOPMENT DURING RECRYSTALLIZATION OF ALUMINIUM CONTAINING LARGE PARTICLES

D. JUUL JENSEN,[1] N. HANSEN[1] and F. J. HUMPHREYS[2]

[1]Metallurgy Department, Risø National Laboratory, DK-4000 Roskilde, Denmark and [2]Department of Metallurgy and Material Science, Imperial College, London SW7 2BP, England

(*Received* 3 *March* 1985; *in revised form* 2 *May* 1985)

Abstract—The recrystallization process in heavily deformed commercially pure aluminium containing large intermetallic particles was studied by *in situ* neutron diffraction texture measurements and various microscopical techniques including texture measurements in local areas and simultaneous determination of size and orientation of individual grains. The formation and growth of recrystallization nuclei at the particles and in the matrix were examined by correlating the measured change in texture to the observed change in microstructure. It was found that prolific nucleation of grains having a wide spread of orientations takes place close to larger particles or clusters of particles early in the recrystallization process. The texture of fully recrystallized material, however, contains only a relatively weak random component showing that the randomisation effect of the particles was limited. This was ascribed to a slower growth of randomly oriented grains compared with those with other orientations.

Résumé—Nous avons étudié la recristallisation dans un aluminium pur du commerce contenant de grandes particules, soumis à une forte déformation, par des mesures de texture par diffraction neutronique *in situ* et par diverses techniques microscopiques incluant des mesures de texture locale et la détermination simultanée de la taille et de l'orientation de grains individuels. Nous avons examiné la formation et la croissance de germes de recristallisation sur les particules et dans la matrice en reliant le changement de texture mesuré au changement de microstructure observé. Nous avons trouvé qu'une germination prolifique de grains ayant une large gamme d'orientation se produit près des plus grandes particules et des amas de particules, tôt dans le phénomène de recristallisation. Cependant, la texture du matériau complètement recristallisé ne contenait qu'une composante aléatoire relativement faible, ce qui montre que les grains les particules n'avaient qu'un effet limité pour orienter aléatoirement. Nous l'avons attribué à une croissance plus lente des grains orientés aléatoirement que des grains présentant d'autres orientations.

Zusammenfassung—Der Rekristallisationsprozeß stark verformten, kommerziell reinen Aluminiums mit großen intermetallischen Teilchen wurde untersucht. Hierzu wurde die Textur mit Neutronenbeugung *in situ* gemessen; außerdem wurden verschiedene mikroskopische Techniken angewendet einschließlich der Texturmessung in kleinen Bereichen und der Bestimmung der Größe und Orientierung einzelner Körner. Die Bildung und das Wachstum der Rekristallisationskeime an den Teilchen und in der Matrix wurde ausgewertet, indem die gemessenen Texturänderungen mit den beobachteten Änderungen in der Mikrostruktur korreliert wurden. Die Keimbildung von Körnern mit großen Orientierungsunterschieden findet zu Beginn des Rekristallisationsprozesses überwiegend in der Nähe großer Teilchen oder von Anhäufungen von Teilchen statt. Die Textur des vollständig rekristallisierten Metalles enthält jedoch nur eine relativ kleine zufällige Komponente, welches darauf hinweist, daß der störende Einfluß der Teilchen beschränkt ist. Die Ursache wird einem langsameren Wachstum der zufällig orientierten Körner im Vergleich zu des anderen Orientierungen zugeschrieben.

1. INTRODUCTION

Second phase particles in a metallic matrix may have a pronounced effect on the deformation and recrystallization behaviour. Studies have concentrated on the effect of particles on the development in microstructure and the changes in texture during deformation and recrystallization, respectively; these two aspects have been covered in recent conference proceedings [1, 2]. However, information about simultaneous changes in microstructure and texture is relatively limited, although such information would be very useful both from a fundamental and an applied point of view.

The present study is of the effect of large particles in a metal matrix on both the microstructural and textural changes during cold deformation and recrystallization. The material investigated was commercially pure aluminium containing a dispersion of large intermetallic iron–aluminium particles in aluminium. An aluminium system was chosen because detailed information exists about the microstructural changes during deformation and recrystallization of particle containing aluminium alloys [3–7]. Furthermore, the effects of variations in composition and fabrication parameters on the recrystallization textures have been examined in detail [8–17].

2. EXPERIMENTAL

2.1. *Sample preparation*

The material used was commercially pure alumi-

Table 1. Chemical composition (wt%)

Fe	0.33	Mn < 0.02
Si	0.09	Cr < 0.02

Less than 0.01 wt% Mg, Cu, V, Ti, Pb, Zn, Sn, Ni, Bi, Be.

nium with a chemical composition as given in Table 1. The amount of iron in solid solution was reduced by a heat treatment at 600°C for 24 h in vacuum followed by slow cooling in the furnace. A starting material with an average grain size of 50 μm was produced by cold rolling to 50% reduction in thickness followed by annealing at 350°C for 1 h. At this stage the material contained plate-shaped intermetallic $FeAl_3$ particles, which have an aspect ratio (diameter-thickness ratio) in the range 1–8. The mean size of the particles (average of thickness and diameter) is 2.3 μm and the size range is 0.2–7 μm. The texture of the starting material is shown in Fig. 1. It is seen that it is relatively weak, but not random, with the ideal orientations [18] $\{001\}\langle 100\rangle$ and $\{110\}\langle 001\rangle$ as the dominant texture components.

For the recrystallization experiments the starting material was cold rolled to 90% reduction in thickness, and circular discs with a diameter of 15 mm were stamped out. To avoid contribution from the surface texture, these discs were reduced in thickness by etching for 60 s in NaOH before they were stacked to form the final cylindrical composite specimens for the neutron measurements. The total height was 5.1 mm.

The annealing of the specimens was done isothermally in a furnace attached to the neutron texture spectrometer. The atmosphere in the furnace was helium and a typical heating rate was 50°C/min. The furnace temperature remained constant to ±2°C. The annealing temperatures were selected in the range 250–340°C resulting in recrystallization times of between 5 minutes and 20 h.

Annealed specimens were investigated microscopically (see sections 2.3 and 2.4). For light microscopy the samples were electropolished and anodized in a 1.8% HBF_4 solution using a current of 0.1–0.4 A/cm^2. Thin foil specimens for TEM and a few HVEM investigations were made by jet polishing [19] in an ethanol/perchloric acid at −20°C. For SEM the samples were electropolished as for light microscopy.

2.2. Neutron diffraction measurements

The texture of the bulk specimens was determined by neutron diffraction using a neutron spectrometer modified for fast texture measurements [20]. This spectrometer is specially equipped with an Euler goniometer and a linear position-sensitive detector placed to detect the diffracted intensity along several degrees of a Debye–Scherrer ring. A typical recording time for a complete 1/4 pole figure from the aluminium samples was 12 min.

During annealing of each specimen the development in texture was followed *in situ*. An overall picture of the changes was obtained by measuring two pole figures [in general (111) and (200)] continuously during the process; thus, the time resolution was 24 min. For more detailed kinetic investigations the development of specific texture components was measured. As the linear position-sensitive detector covers 34° of a small circle in the pole figure plane, it is possible to position the sample so that the detector records the change in intensity of one or even a few texture components simultaneously, in a matter of seconds.

For the deformed and annealed (partly or fully recrystallized) samples, 3 complete 1/4 pole figures [(111), (200) and (220)] were measured and the three-dimensional orientation distribution function (ODF) was calculated according to the series expansion method [21]. The series were truncated at $l_{max} = 22$ and only terms of an even rank in l were considered. This means that some loss in precision of the ODF occurs, but as the observed textures consist of relatively weak and broad components, the actual error in the main components is relatively small.

The ODFs were represented graphically as a function of the Euler angles, ϕ_1, Φ, ϕ_2 using equidensity lines in ϕ_2 = constant sections [22]. A measure for the volume fraction of each main texture component is calculated by integration over 15 deg around the respective points in the Euler space.

2.3. Electron diffraction measurements

2.3.1. Microtexture. Partial pole figures from regions of interest such as those containing second phase particles were determined from deformed or annealed specimens by a computer-controlled trans-

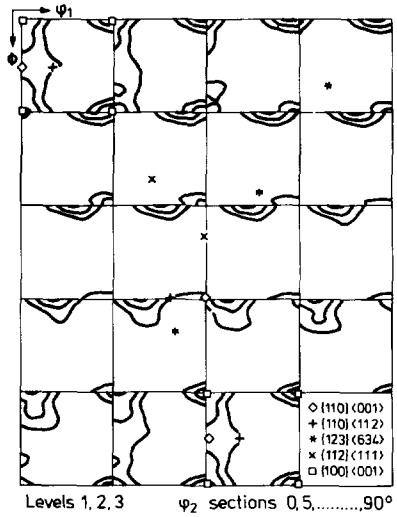

Fig. 1. The texture of the starting material before the final cold rolling.

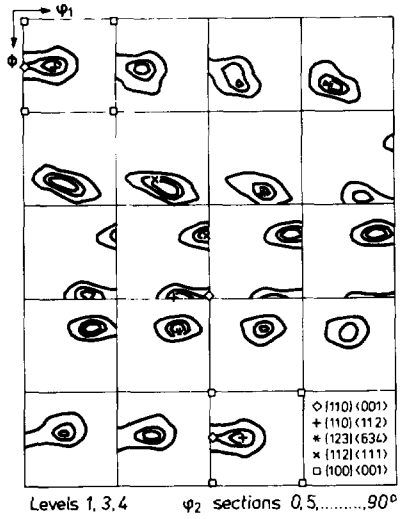

Fig. 2. The texture of a specimen cold rolled to 90% reduction.

mission electron diffraction (microtexture) technique [23]. In this method, a diffraction pattern of the selected area, of typical diameter 10 μm, is obtained by conventional methods from a thin foil under examination in a TEM/STEM instrument. The intensity of diffraction around a selected Derbye–Scherrer ring is measured and displayed graphically as the specimen is tilted in steps of 1.5° through $\pm 50°$.

2.3.2. Size and orientation measurements. A simultaneous determination of both the orientation and size of individual recrystallized grains, in partly and fully recrystallized specimens, was obtained from selected area channelling patterns (SACP). Electropolished specimens were placed in a JEOL 100 CX TEMSCAN set to detect SACPs from areas of ~ 1 μm diameter. As the specimen was mechanically traversed under the beam, using a calibrated stage, the SACP was noted and classified as being from either deformed material (diffuse or nonexistent pattern), or recrystallized material. In the latter case the patterns were compared with those from several ideal orientations $\{hkl\}\langle uvw\rangle$ corresponding to the main components found in the recrystallized texture. (For further details see [24].)

If the observed grain orientation was within $\sim 5°$ of $\{hkl\}$, and the rotation of the pattern was within $\sim 10°$ of $\langle uvw\rangle$ then the grain was classified as being $\{hkl\}\langle uvw\rangle$. Grains with other orientations, not being among the main recrystallized texture components, were designated as being of random orientation.

By noting the stage positions at which patterns changed, the size of the grains or unrecrystallized regions was estimated. Several traverses, each of 2 mm, were made on each sample, and thus the number and size of recrystallized grains of specific orientations could be measured rapidly (~ 3 grains/min). The grain size, here measured as a linear intercept, is transformed to the equivalent circle diameter (ECD) by multiplication with $(4/\pi)$.

2.4. Light microscopy

The electropolished and anodized specimens were examined under polarized light. The grains in the recrystallized material were approximately equiaxed and the grain size were measured in the rolling plane as the equivalent circle diameter using a computerized image analyzer (Kontron video-plan).

3. RESULTS

3.1. The deformed state

As the microstructure of similar specimens in the cold worked state has been discussed elsewhere [6], only the texture will be considered.

3.1.1. The rolling texture. After cold rolling to 90% reduction in thickness the aluminium samples have the texture shown by the ODF in Fig. 2. It consists of an orientation tube running through Euler space, plus some $\{110\}\langle 001\rangle$ texture. The calculated volume fraction of the main components in the tube and the $\{110\}\langle 001\rangle$ component is listed in Table 2.

The rolling texture has characteristics of both an alloy-type [25] and a pure metal (copper-type) [26] rolling texture. For example, the presence of the $\{110\}\langle 001\rangle$ component is typical of the alloy-type texture but the ratios of the components in the rolling tube (for example $\{110\}\langle 112\rangle/123\langle 634\rangle$) is more characteristic of the pure metal rolling texture.

Table 2. The volume fraction in % of the main texture components, calculated by an integration over 15 degrees in Euler space

	Rolling components					Cube component	Random components
	{110} ⟨001⟩	{110} ⟨112⟩	{123} ⟨634⟩	{112} ⟨111⟩	rolling total	{001} ⟨100⟩	
Cold rolled 90%	9	21	34	16	80	—	20
Annealed at 253°C	11	6	17	11	45	18	37
Annealed at 278°C	10	5	15	12	42	17	41
Annealed at 341°C	6	2	17	14	39	20	41

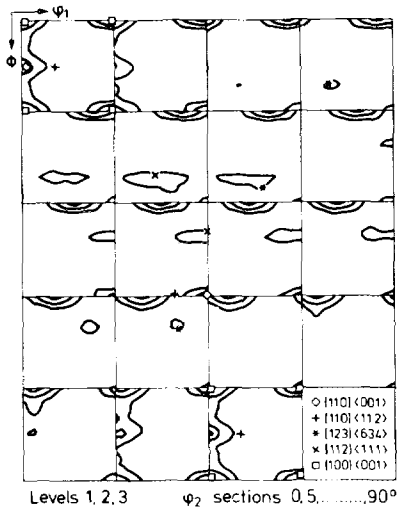

Fig. 3. The texture of a specimen cold rolled 90% and fully recrystallized at 253 C.

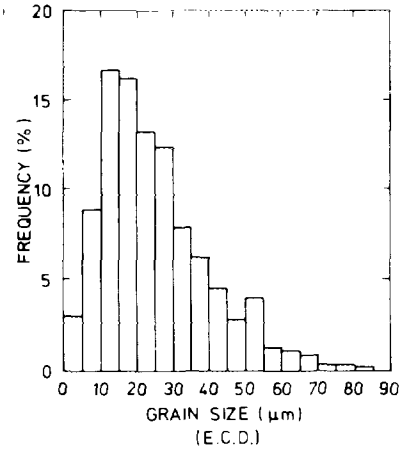

Fig. 4. Grain size distribution in the rolling plane in a specimen recrystallized at 253 C.

In similar materials given more or less equivalent pretreatments a rolling texture of the pure metal type is commonly found [14–16]. However, in some Al–Fe–Si alloys an alloy type texture has been observed for quenched materials, this being ascribed to the presence of relatively large amounts of iron in solid solution [16]. In the present material the amount of iron in solid solution was reduced by slow cooling in the furnace, so the presence of the {110}⟨001⟩ texture component is ascribed not to iron in solution but to the starting texture in the material before the final cold rolling (see section 2.1). This is supported by measurements of the deformation texture of less heavily deformed samples (cold rolled to 15, 30 and 50% reduction) where it was found that the amount of {110}⟨001⟩ texture was almost indcpendent of the degree of deformation [27].

3.2. *The recrystallized state*

3.2.1. The recrystallization texture. The recrystallization texture is shown by an ODF in Fig. 3. It is seen that this texture contains a cube texture component {001}⟨100⟩, the components of the rolling texture ({110}⟨001⟩, {110}⟨112⟩, {123}⟨634⟩ and {112}⟨111⟩) and a relatively large volume fraction of other components apparently randomly distributed in the Euler space. The calculated volume fraction of each of the texture components is given in Table 2. Annealing temperatures may have an effect on the recrystallization texture [14], but as shown in Table 2 there was little difference in texture between specimens annealed in the range 250–340 C.

During recrystallization the main components of the rolling texture are changed differently. {110}⟨001⟩ is almost constant and {112}⟨111⟩, {123}⟨634⟩, and {110}⟨112⟩ are reduced respectively to approximately 75, 50, and 25%. In total, the volume fraction of material with the rolling texture in the recrystallized state is approximately halved compared to the deformed state.

3.2.2. The microstructure in the recrystallized state. The grain size distribution in the recrystallized specimen was determined by light microscopy and the result of measuring 600 grains in a section parallel to the rolling plane for a sample annealed at 253 C is shown in Fig. 4. This distribution is relatively broad (range 1–85 μm) with an average grain size of 24.9 μm. An increase in the annealing temperature

Fig. 5. Light micrograph from a specimen recrystallized at 253 C (rolling plane), showing small grains associated with large particles (A) and cluster of particles (B).

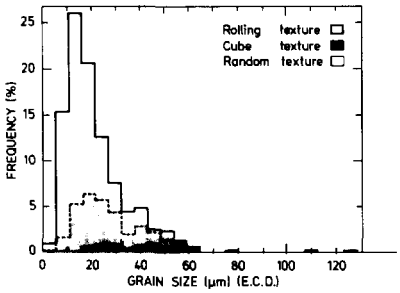

Fig. 6. The grain size distribution in the rolling plane in a specimen recrystallized at 253°C. The different shadings correspond to grains with different orientations.

(up to 340°C) has no significant effect on the grain size.

It is found that the smallest grains often are associated with large particles or a cluster of particles. A typical example of this is shown in Fig. 5. Here a number of grains with a diameter less than 10 μm are seen close to large particles (marked A) and to a cluster of particles (marked B).

Further details about recrystallized structure were obtained by a simultaneous determination of grain size and orientation in the SEM. The result from an examination of approximately 500 grains is shown in Fig. 6. The figure shows that there is a relationship between the size of a grain and its orientation. Recrystallized grains with the cube orientation ($\{001\}\langle 100\rangle$) are among the largest in the distribution, whereas randomly oriented grains are among the smallest.

3.3. *Recrystallization kinetics*

3.3.1. Development in texture. The development in texture during recrystallization was followed by measuring the (111) and (200) pole figures *in situ* during the annealing and calculating the corresponding ODFs. The volume fraction of each of the main components plotted as a function of time shows that the texture changes are continuous during the recrystallization process [28].

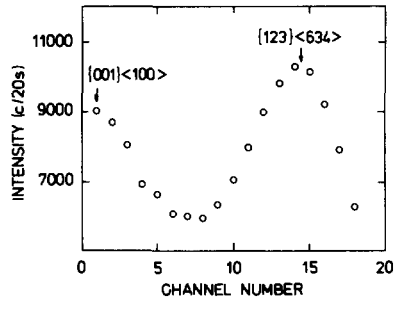

Fig. 7. Measured intensities along the detector for a specimen ~50% recrystallized at 253°C.

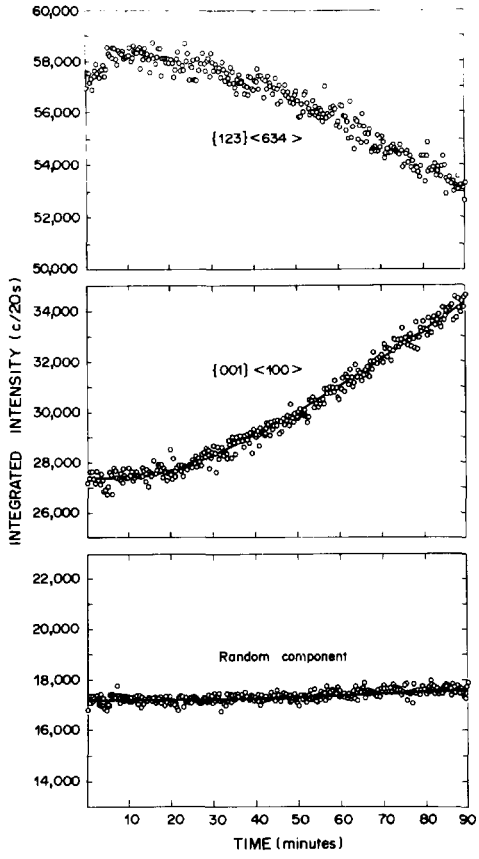

Fig. 8. Kinetic curves for the initial evolution of $\{001\}\langle 100\rangle$, $\{123\}\langle 634\rangle$ and a "random" component, measured close to the centre of the (200) pole figure during annealing at 253°C. ○: experimental points; ——: best fit to Avrami.

Detailed information about the development of the different components during recrystallization was obtained by measuring partial (200) pole figures keeping the sample fixed so that the detector covered the central cube component, the $\{123\}\langle 634\rangle$ close to the ND–RD line and the "random" component in between. Figure 7 shows an example of the intensity measured along the detector for the given setting of the sample at a state when the sample was approximately 50% recrystallized. The peak in the centre of the pole figure (low channel numbers) corresponds to the cube component, and the peak around channel 14 is the $\{123\}\langle 634\rangle$ component. By spatial integration over each of these peaks the development in the two components can be followed. For recrystallization at 253°C the initial development is plotted in Fig. 8. It can be seen that the cube component $\{001\}\langle 100\rangle$ at this annealing temperature starts to increase after an incubation period of approximately 10 min. The $\{123\}\langle 634\rangle$ rolling component increases slightly but after about 10 min a decrease in the intensity is

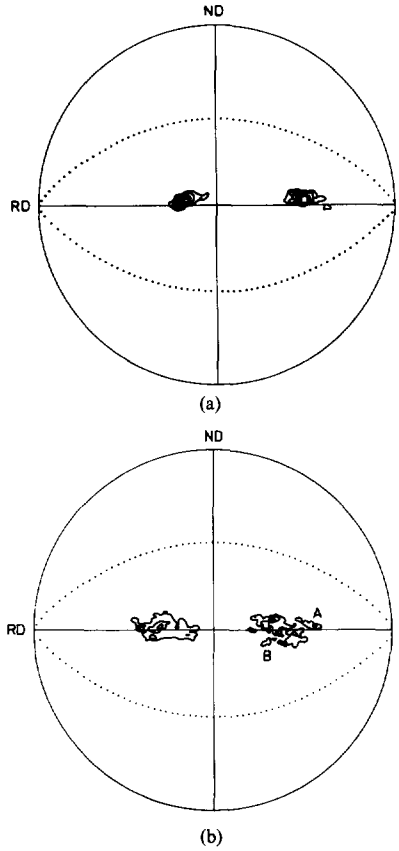

Fig. 9. Partial (111) pole figures obtained by the TEM microtexture technique of an approximately 10% recrystallized specimen. (a) Unrecrystallized matrix region. (b) Adjacent area containing nuclei associated with a large particle. A, B are the orientations of the nuclei.

observed. As this component is present in both the deformed and recrystallized state, it is not possible with neutron diffraction to distinguish between volumes of this texture as being either deformed or recrystallized. The evolution of the {123}⟨634⟩ component may be explained by an immediate development and growth of grains with the {123}⟨634⟩ orientation giving rise to the increase seen in the first 10 min. As new recrystallized grains with other orientations may develop and grow some of the deformed material with the {123}⟨634⟩ texture will disappear resulting in the observed decrease in the intensity.

A measure for the development in random component is obtained by integration over the central channels between the two peaks. It can be seen that the increase in the random component is not very large during the time interval in Fig. 8.

The kinetics for the growth of recrystallized grains in a deformed matrix are often described by an Avrami equation [29]

$$x = 1 - \exp(-Kt^{\beta})$$

where x is the volume fraction of recrystallized material, t is the time and K, β are constants characteristic of the process. An equation of this type has also been used to describe the development of single texture components [30]. As different texture components can start to develop at different times the Avrami equation has been modified to include an incubation time as a fitting parameter

$$I(t) = I_{\infty} - (I_{\infty} - I_0)\exp[-K(t - t_0)^{\beta}] \quad \text{for } t > t_0$$
$$I(t) = I_0 \quad \text{for } t \leq t_0$$

where I_0, I_{∞} are the measured intensities at time zero and infinity and t_0 is the incubation time. These equations have been used to fit the actual kinetic results for the cube and the random component. These fits based on the least squares method are in good agreement with the measured intensities from the beginning to the completion of the recrystallization. For the cube component the fit resulted in an incubation time $t_0 = 11 \pm 2$ min, whereas the best fit for the random component was with no incubation period. The initial part of the recrystallization curves for the two components are shown in Figs 8(b) and 8(c).

3.3.2. Development in the microstructure. The orientation of nuclei in partly recrystallized specimens was studied using the microtexture technique described in section 2.3, and an example is given in Fig. 9. Figure 9(a) is a (111) pole figure of a 10 μm diameter unrecrystallized region of a grain with the rolling texture {110}⟨112⟩. Figure 9(b) shows an adjacent

Table 3. Volume fraction and number of grains for the three texture components (cube, rolling and random) determined by SACP

Annealing time (min)		15	30	60	140	240	830
% Recrystallized		10	18	26	47	81	100
Volume fraction (%)	cube	1	2	4	12	15	18
	rolling	3	6	11	15	33	41
	random	6	10	11	20	33	40
Number of grains per unit volume (μm^3)	cube	$2\cdot10^{-6}$	$3\cdot10^{-6}$	$2\cdot10^{-6}$	$2\cdot10^{-6}$	$1\cdot10^{-6}$	$1\cdot10^{-6}$
	rolling	$2\cdot10^{-5}$	$1\cdot10^{-5}$	$1\cdot10^{-5}$	$1\cdot10^{-5}$	$2\cdot10^{-5}$	$2\cdot10^{-5}$
	random	$9\cdot10^{-5}$	$6\cdot10^{-5}$	$3\cdot10^{-5}$	$6\cdot10^{-5}$	$5\cdot10^{-5}$	$7\cdot10^{-5}$

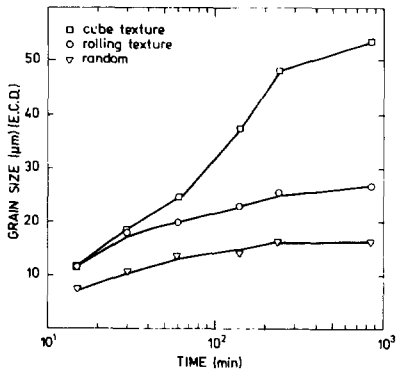

Fig. 10. The average size of grains with different orientations, measured for a series of specimens annealed at 253°C.

area of the same grain, containing a 2 μm diameter particle at which nucleation has occurred. The nuclei, marked with A and B, is seen to be misorientated up to 30° from the $\{110\}\langle 112\rangle$ orientation of the matrix. The results obtained in the present investigation are consistent with other work [31] in which the misorientation between the matrix and nuclei formed at particles was found to be between 15° and 40°.

Very few cube nuclei were observed in the TEM in specimens which were 5–10% recrystallized, and there was no evidence of their association with particles.

From a series of partly recrystallized samples all annealed at 253°C the development of each of the texture components was followed by the simultaneous determination of size and orientation of recrystallized grains in the SEM. From the size and number of grains of a particular texture component measured on the polished surface of a specimen, the volume fraction of the texture component was calculated, as was the approximate number of grains per unit volume, assuming the growing grains to be spherical. Table 3 shows the result of the investigation. It was found that nucleation of all the texture components had occurred by the time that the specimen was ~10% recrystallized. The table indicates that after this time, the number of grains remains approximately constant, implying no further nucleation. In Fig. 10 the size of grains with the different orientations is plotted as a function of time. It is seen that cube grains grow faster and grains of random orientation grow the slowest. Thus, there is a significant volume fraction of cube-oriented grains in the fully recrystallized sample, even though there are approximately fifty times as many grains of random orientation.

4. DISCUSSION

The recrystallization behaviour of aluminium may be greatly affected by small amounts of alloying elements which can be present in solid solution or as precipitated particles. The effect of such particles may depend on whether their precipitation occurs before the recrystallization heat treatment or if precipitation and recrystallization take place simultaneously [11, 14, 15]. In both cases important parameters are the size, shape, volume fraction and distribution of particles. In the present study the specimens are prepared in such a way that precipitation during recrystallization is eliminated. The starting structure consists of large intermetallic particles in an aluminium matrix, and it is assumed in the following that this structure is stable during the recrystallization process. This assumption is supported by the observation that the texture development during recrystallization is not significantly changed by a variation in the annealing temperature (see Table 2). This discussion will therefore be limited to the effect of particles on the microstructures and textures developing during deformation and recrystallization of aluminium.

It is a general observation [e.g. 2] that the presence of large particles in a metallic matrix may affect the texture changes both during deformation and during recrystallization. It appears, however, that a small volume fraction of particles has little effect on the deformation texture [14, 15] and the present results support these findings. However, the effect of particles is much more pronounced during the recrystallization process.

The components of the recrystallization texture have been classified as cube, rolling and random orientation. The cube orientation is characteristic of pure aluminium [25], whereas a combination of cube and other orientations is observed in aluminium containing alloying additions in solute solutions and as intermetallic precipitates [10–17]. In aluminium–iron alloys containing a very small amount of iron in solid solution earlier studies [14] have shown that the recrystallization texture consists mainly of a cube component. In the specimens investigated the amount of iron in solid solution is small and accordingly a relatively large cube component should be expected. However, the data show that the cube components accounts for only approximately 20% of the recrystallized texture and remaining part consists of approx. 40% random and 40% rolling components. The large percentage of components other than cube may be related to the presence of the particles. However, it is possible that elements in solid solution also may affect the recrystallization texture.

The microstructural development during cold rolling and recrystallization of aluminium containing large intermetallic particles has been dealt with in earlier work [6]. It has been observed that deformation zones form around the large particles and that nucleation occurs within such zones during recrystallization. In combination with the nucleation at particles other nucleation sites away from the

particles are operative. The orientation of a number of nuclei at intermetallic particles was analyzed in the present study by electron diffraction and it was commonly observed that the orientation is related to the orientation within the deformation zones at the particles (see Fig. 9). Such nuclei are misoriented from the matrix and it may be assumed that the growth of these nuclei will result in recrystallized grains with a large spread in orientation.

The texture of the fully recrystallized material not only reflects the orientation of the nuclei but also their rate of formation and growth. The neutron texture measurements indicate that grains having the rolling or random texture are nucleated almost instantaneously whereas grains of cube orientation appear after an incubation period (see Fig. 8). After an initial period of 15 min the number of grains of the different orientations remain constant during the remaining part of the recrystallization process (see Table 3). The number of grains of cube orientation is significantly smaller (of the order of 50 times) than the number of grains of the other orientations. However, the growth rate of the cube grains is much larger than for the two other components (Fig. 10), and this results in a significant contribution of cube grains to the final texture.

The grains close to the particles have a wide spread of orientations. However, such grains have a relatively low growth rate which may explain that the presence of large particles in aluminium randomizes the texture to only a limited extent.

5. CONCLUSIONS

In cold-rolled (90%) aluminium containing large intermetallic particles ($FeAl_3$) the recrystallization nuclei form at the particles and in the matrix. The orientation of the nuclei and their rate of formation and growth determines the recrystallization texture, which consists of cube, rolling and random orientations.

The grains nucleated at particles show a fast nucleation rate and low growth rate whereas the grains of cube orientations are relatively few but characterized by a high growth rate. As a result the presence of large nucleation stimulation particles randomizes the texture to only a limited extent.

REFERENCES

1. N. Hansen, A. R. Jones and T. Leffers (editors), *Proc. 1st Risø Int. Symp. on Recrystallization and Grain Growth of Multi-Phase and Particle Containing Materials*, Risø (1980).
2. K. Lücke, *Proc. 7th Int. Conf. on Textures of Materials* (edited by C. M. Brakman, P. Jongenburger and E. J. Mittemeijer), Noordwijkerhout, p. 195 (1984).
3. H. M. Chan and F. J. Humphreys, *Acta metall.* **32,** 235 (1984).
4. B. Bay and N. Hansen, *Metall. Trans. A* **15A,** 287 (1984).
5. S. Dermarkar, P. Guyot and J. Pellissier, *Acta metall.* **31,** 1315 (1983).
6. B. Bay and N. Hansen, *Metall. Trans. A* **10A,** 279 (1979).
7. F. J. Humphreys, *Acta metall.* **25,** 1323 (1977).
8. D. Altenpohl, *Aluminium und Aluminiumlegierungen.* Springer, Berlin (1965).
9. E. Nes, *Proc. 1st Risø Int. Symp. on Metall. Mater. Sci., Recrystallization and Grain Growth of Multi-Phase and Particle Containing Materials* (edited by N. Hansen, A. R. Jones and T. Leffers), Risø, p. 85 (1980).
10. S. E. Næss, *Am. Inst. Min. Engrs Fall Meeting*, Detroit (1984).
11. R. Rixen, R. Musick, H. Göker and K. Lücke, *Z. Metallk.* **66,** 16 (1975).
12. J. C. Blade and P. L. Morris, *Proc. 4th Int. Conf. on Texture* (edited by G. J. Davies *et al.*), Cambridge, p. 171 (1975).
13. B. Anderson and E. Nes, *ibid.* Ref. [9], p. 115.
14. K. Ito, R. Musick and K. Lücke, *Acta metall.* **31,** 2137 (1983).
15. K. Ito, K. Lücke and R. Rixen, *Z. Metallk.* **67,** 338 (1976).
16. D. H. Rogers and W. T. Roberts, *Z. Metallk.* **65,** 100 (1974).
17. G. J. Davies, I. S. Kallend and T. Ruberg, *Proc. 3e Coll. Eur. sur les Textures de Deformation et de Recristallisation*, Nancy, p. 299 (1973).
18. J. Hansen, J. Pospiech and K. Lücke, *Tables for Texture Analysis of Cubic Crystals.* Springer, Berlin (1978).
19. J. Lindbo and T. Leffers, *Metallography* **5,** 473 (1972).
20. D. Juul Jensen and J. K. Kjems, *Textures Microstruct.* **5,** 239 (1983).
21. H. J. Bunge, *Mathematische Metoden der Texturanalyse.* Akademie, Berlin (1969).
22. C. Esling, F. Wagner and H. J. Bunge, *Quantitative Texture Analysis* (Edited by H. J. Bunge and C. Esling), p. 319. Deutsche Gesellschaft Metallk. (1982).
23. F. J. Humphreys, *Textures Microstruct.* **6,** 45 (1983).
24. N. Hansen, D. Juul Jensen and F. J. Humphreys, *Proc. 5th Risø Int. Symp. on Metall. Mater. Sci., Microstructural Characterization of Materials by Non-Microscopical Techniques* (edited by N. Hessel Andersen *et al.*), Risø, p. 267 (1984).
25. K. Lücke, *Proc. 6th Int. Conf. on Textures of Materials* (edited by S. Nagashima), Tokyo, p. 14 (1981).
26. H. J. Bunge and J. Tobisch, *J. appl. Crystallogr.* **5,** 27 (1972).
27. N. Hansen, B. Bay, D. Juul Jensen and T. Leffers, *Proc. 7th Int. Conf. on the Strength of Metals and Alloys.* To be published.
28. D. Juul Jensen, N. Hansen, J. K. Kjems and T. Leffers, *ibid.* Ref. [24], p. 325.
29. M. Avrami, *J. chem. Phys.* **8,** 212 (1970).
30. N. Hansen, T. Leffers and J. K. Kjems, *Acta metall.* **29,** 1523 (1981).
31. H. M. Chan and F. J. Humphreys, *Metals Sci.* **18,** 527 (1984).

Reprint from: Proceedings of the Tenth Risø International Symposium
on Metallurgy and Materials Science: *Materials Architecture*
Editors: J.B. Bilde-Sørensen, N. Hansen, D. Juul Jensen, T. Leffers, H. Lilholt, O.B. Pedersen
Risø National Laboratory, Roskilde, Denmark, 1989

COMBINED ADVANCED TECHNIQUES IN THE STUDY OF ANNEALING PROCESSES

D. Juul Jensen[+] and V. Randle[*]

[+]Metallurgy Department, Risø National Laboratory,
Roskilde, Denmark

[*]*H.H. Wills Physics Laboratory, University of Bristol,*
Bristol, U.K.

ABSTRACT

Three recently developed techniques whereby information about local or global textures can be obtained, are reviewed, and their application to the study of annealing processes is considered. The three techniques are:

- the electron backscattering technique, whereby the crystallographic orientation of selected grains or areas down to ~0.5μm in diameter are determined in the scanning electron microscope;

- the microtexture technique, whereby the texture of selected local areas (typically 5-10 μm in diameter) in the microstructure are determined by transmission electron microscopy;

- the in-situ neutron texture technique, whereby the bulk texture and the texture transformation during annealing of typically 1 cm^3 samples are determined by neutron diffraction.

The experimental set-up and the data handling procedures are described for each of the three techniques; their potential for annealing investigations is discussed and illustrated via various examples. Finally, as an example of how the three techniques can complement each other, results from an investigation of the recrystallization process in a fibre reinforced metal matrix material - Al + SiC - are reviewed.

1. INTRODUCTION

Annealing is an essential part of thermomechanical processing of metals and alloys. The recovery, recrystallization and grain growth processes which occur during annealing are therefore of great importance both from a fundamental and an applied point of view (eg. Proc. Risø 7, 1986). Annealing processes can take place under static or dynamic conditions, i.e. take place either after a plastic deformation process is completed or together with the plastic deformation during hot working. This paper will be limited

to consider static annealing.

In the study of annealing processes the changes in microstructure and crystallographic orientation - texture - are of importance. Traditional microscopy techniques - optical microscopy, transmission and scanning electron microscopy - are still the most important tools used to characterize the microstructure at various stages during annealing. However, to get information about changes in crystallographic orientation many new powerful techniques have been developed which may be used to supplement the classic texture determination by X-ray diffraction. (For reviews, see Proc. Risø 5, 1984; Bunge 1986; Masteller and Bauer 1978). The present paper concentrates on three such techniques, the electron backscattering, the microtexture and the in-situ neutron texture technique.

Using these techniques the following important aspects of annealing can be addressed:

- Potential nucleation sites, i.e. areas with large local lattice misorientations, may be identified using the microtexture technique.

- Orientation relationships between a nucleus and the surrounding matrix may be determined by the microtexture technique.

- The growth rate of nuclei with different orientations may be determined using the electron backscattering technique.

- The overall recrystallization kinetics may be followed on-line using the neutron texture technique.

- Grain growth kinetics may be studied on-line using the neutron texture technique, and orientation relationships between neighbouring grains may be determined by the electron backscattering technique.

Although the three experimental techniques on which this paper is focussed each give important information about annealing, which otherwise is impossible or extremely time consuming to get, they do indeed not fully characterize the processes. In the attempt to get a complete, precise description of a given annealing process, it is therefore in most cases necessary to use several complementary techniques and combine the results. In the paper it is discussed how the three selected techniques can add new information to the general description of annealing and as an example of how the techniques may be combined, results from an investigation of the recrystallization in a metal matrix composite material are reviewed.

2. EXPERIMENTAL TECHNIQUES

2.1. Electron backscattering. The aim of the technique is to enable a determination of the crystallographic orientation of selected local areas - less than 0.5 μm diameter - in the microstructure. The technique operates in a scanning electron microscope (SEM), i.e. it is possible to inspect a large sample area. Selected area channelling or selected area diffraction techniques might be used as alternatives to the electron backscattering (EBS) technique giving equivalent information. However, the selected area channelling technique is limited by a more coarse spatial resolution than EBS and with the diffraction technique in a transmission electron microscope the sample areas which can be inspected are restricted to the thin areas. For more overall investigations of annealing processes the electron backscattering technique is therefore in general advantageous to use.

The principle of the electron backscattering (EBS) technique is similar to that of the SEM backscattered Kikuchi pattern technique (Alam, Blackman and Pashley 1954; Venables and Harland 1973; Venables and Bin Jaya 1977). . In the SEM the incident electron beam is focussed as a stationary probe on the specimen surface. If the specimen is perpendicular to the incident beam, a large proportion of the electron signal is absorbed. However, if the specimen is positioned so as to make a small angle (typically ~20°) with the incoming beam, a large fraction of the beam is backscattered or diffracted, and sufficient contrast is obtained to view the back-scattered diffraction patterns on an imaging screen or film placed directly within the microscope chamber, see Fig. 1. A considerable advance in the technique occurred when Dingley implemented the use of a low light television camera focussed on the phosphor screen to image the pattern and a microcomputer to interrogate it (Dingley, 1984). It was after these refinements were included that a texture analysis system based on electron backscattering became viable.

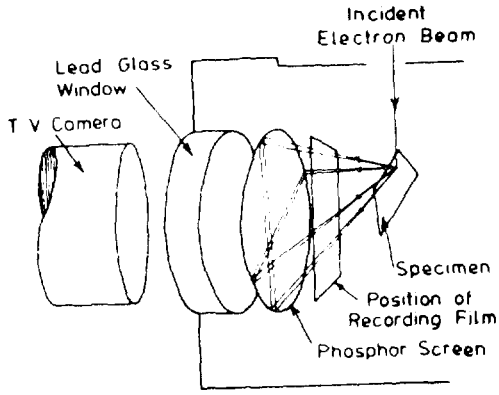

Fig. 1. Schematic diagram illustrating the experimental arrangement for imaging EBS pattern. (Dingley 1984).

The EBS system has been installed on several SEMs. The phosphor imaging screen and low light TV camera can be mounted in either the side or rear port of the microscope chamber, such that the specimen holder is about 40 mm from the screen. A consequence of the short specimen to screen distance is that the angular range of the EBS diffraction pattern is very large, typically greater than 60°, which greatly facilitates pattern recognition. An EBS diffraction pattern is shown in Fig. 2. Patterns may be obtained throughout a range of accelerating voltages and beam currents; typical values for nickel or iron based materials are 30kV and 3nA. The high spatial resolutions achievable are caused by the high proportion of back scattered electrons (due to the tilted specimen configuration) compared to the

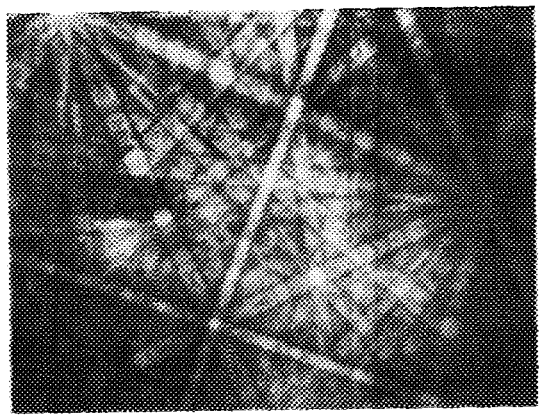

Fig. 2. An EBS pattern from germanium.

absorbed fraction, and thus the sample volume is governed by the probe size. Because the patterns arise from the 10-30nm below the specimen surface depending upon the atomic number, it is essential that this surface region is relatively undeformed. The specimen preparation must therefore include a final stage of either electropolishing or chemical etching in order to remove surface damage.

The geometrical parameters of the system are calibrated by use of a crystal of known orientation, such as single crystal silicon wafer cleaved along (001). The position of the sample volume with respect to tilt and rotation must remain constant between calibration and data acquisition; this is achieved by mounting the specimen in a special pre-tilted holder, inclined at 19 - 20° to the electron beam. The tilt and rotate controls on the microscope are maintained at zero. The inclination angle is chosen so as to make the [114] direction in the silicon calibration specimen the pattern centre (i.e. normal to the viewing screen) since the angle between [114] and the [001] specimen normal is 19.4° (Fig. 3a). During calibration the

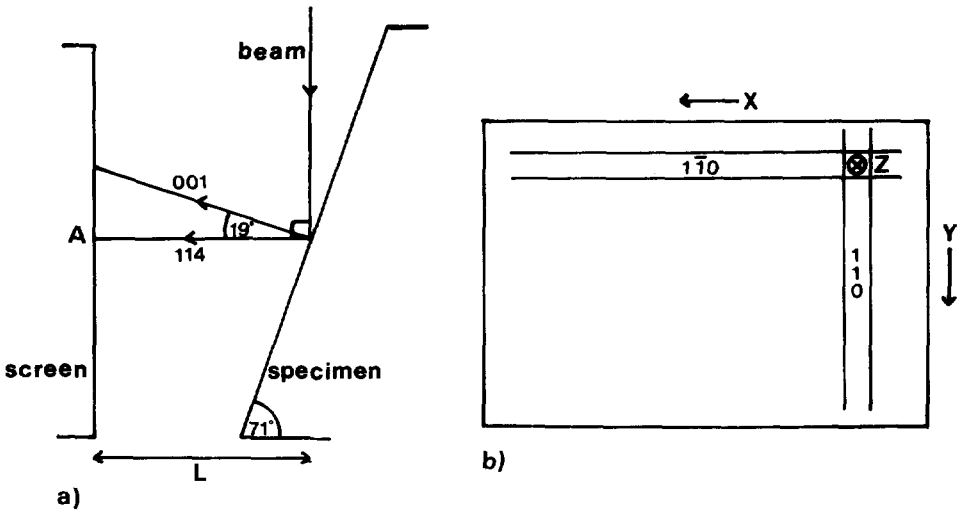

Fig. 3. a) Schematic illustration of how the specimen to screen distance L, the pattern centre (A) and the (001) normal from single crystal silicon are used to provide an angular calibration of the screen. b) The image screen as viewed by the operator during calibration, illustrating the XYZ reference axes. The X axis of the specimen coordinate system is parallael to the horizontal direction on the viewing screen, the Y axis is parallel to the vertical axis and the Z axis is parallel to the specimen normal coming out of the diagram to give right-handed axes.

distance between [001] and [112], which is positioned vertically below it in the Y direction (see Fig. 3), is measured on the screen and thus the specimen to screen distance, L, is known. Clearly, L will change if a different specimen height is chosen, and so data should be acquired with the specimen positioned at the same height as for calibration. In practice if patterns are collected along a line parallel to the X direction (see Fig. 3b) this constraint is unimportant, and for orientation relationships between neighbouring grains, it is irrelevant. Alternatively, the screen may be arranged to be parallel to the specimen.

Data collection and analysis from a selected region are semi-automatic. The operator is required to nominate two zone axes and position the cursor on each of them in turn. From this input, plus the working specimen height, the absolute orientation relative to the specimen coordinate system is computed to an accuracy of about 0.5°. This analysis takes about 30 seconds. Subsequently grain orientations, grain misorientations expressed as axis/angle pairs, pole figures and Rodriques-Frank maps (Frank 1988) are available. The computational methods are outlined elsewhere. (Dingley 1984).

2.2. Microtexture. The aim of the technique is to enable local texture measurements from selected areas in the microstructure. The size of the selected area is typically 5-10 μm in diameter, i.e. the area is so small that the measured texture really represents that of a local microstructural region, but on the other hand is so large that significant texture variations can exist within the area and hence a determination by individual diffraction measurements for example using selected area diffraction or the EBS technique becomes too comprehensive.

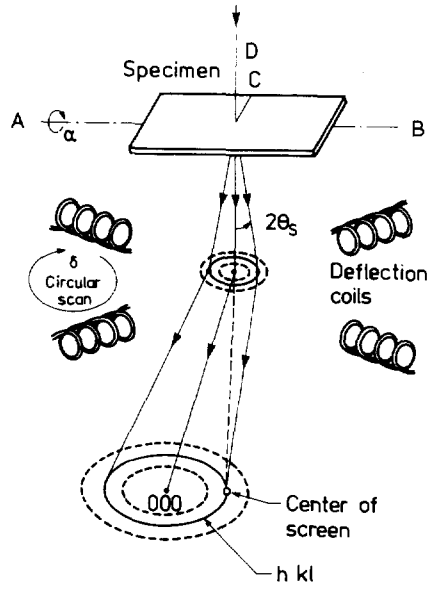

Fig. 4. Schematic diagram illustrating the experimental arrangement for the microtexture technique.

The microtexture technique was developed independently by Humphreys and by Weiland and Schwarzer (Humphreys 1983; Humphreys 1984a; Weiland and Schwarzer 1984; Schwarzer and Weiland 1986). In a transmission electron microscope (TEM) the indicent electron beam is focussed on a selected area of a thin foil specimen. From there some of the electrons will be diffracted to the different (hkl) Debye-Scherrer rings (see Fig. 4 and 5a) according to normal Bragg scattering

$$2d_{hkl} \sin \Theta s = \lambda \qquad (1)$$

where d_{hkl} is the distance between (hkl) lattice planes, Θs is the scattering angle (see Fig. 4) and λ is the wavelength. By a deflection of twice a Bragg angle Θs, the corresponding (hkl) Debye-Scherrer ring is brought to the center of the screen and the electron beam intensity can be measured by the transmission detector (see Fig. 4). This intensity is proportional to the volume fraction of crystallites having the normal to the (hkl) plane bisecting the angle $2\Theta s$ between the incident and the diffracted beam. The distribution of diffracted intensities around the entire (hkl) Debye-Scherrer ring is measured by making a circular deflection scan as illustrated in Figs. 4 and 5a. The data from such a scan may be presented in a (hkl) pole figure, and as the Bragg angles generally are less than 1°, the data fall on the edge of the pole figure as shown in Fig. 5b. If now the specimen is tilted the angle $\Delta\alpha$ around the specimen axis AB (see Figs. 4 and 5a) and the intensity of the

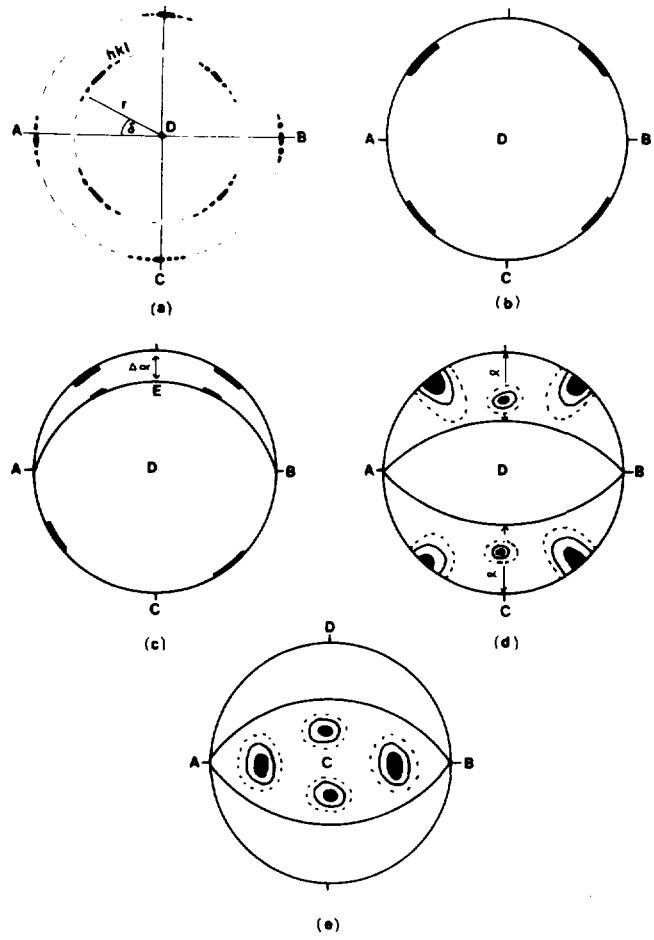

Fig. 5. a) Schematic diffraction pattern. b) Data from a) plotted as a (hkl) pole figure. c) Pole figure including data from specimen tilted $\Delta\alpha$ about AB. d) Partial pole figure obtained by tilting the specimen through $\pm$ α. e) Same data as d) replotted as a pole figure in the plane normal to C. (Humphreys 1983).

Debye-Sherrer ring from δ = 0 to 180° is measured, information about intensities along another great circle - AEB - in the pole figure is obtained (Fig. 5c). Thus by repeating this a number of times with different tilts up to $\pm$ $\Delta\alpha$, a partial pole figure as shown in Fig. 5d is determined. (Following the approach of Humphreys (1983) the partial pole figure data is replotted as a pole figure in the plane perpendicular to C, see fig. 5e).

The spatial resolution of the technique is limited by two factors: i) as the specimen is tilted the area being examined will move, and even with a good eucentric tilting stage this lateral movement will be ~1μm, ii) at a given tilt angle, α, a selected area of diameter X becomes an ellipse of major axis X/cosα, the volume of material contributing to the diffraction pattern therefore increases with increasing $|\alpha|$. These two effects restricts the smallest size of area which can be studied to about 5 μm.

The angular resolution, Δ, along a Debye-Scherrer ring is determined by (Humphreys 1983)

$$\Delta = \frac{P}{r} = \frac{P\, d_{hkl}}{L\lambda} \qquad (2)$$

where P is the diameter of the detector aperature, L is the camera length, λ is the electron wavelength, r is the radius of the selected (hkl) Debye-Scherrer-ring and d_{hkl} is the distance between the corresponding (hkl) lattice planes. For example operating the TEM at 200 kV with a camera length of 380 cm and a 3 mm detector aperature, this will result in an angular resolution equal to 4.2^{o} for the (111) pole figure of aluminium.

The microtexture technique may be used with any transmission electron microscope equipped with a transmission electron detector and an eucentric tilt stage. At Imperial College, London (Humphreys 1984a) and TU, Clausthal-Zellerfeld (Schwarzer and Weiland 1986) the complete operation of the technique is computerized. What is needed by the user is to select the area of interest and switch the microscope to diffraction mode. After adjusting alignment etc., the computer is started, and the scans in α and δ are performed automatically. Typically α is tilted between -50^{o} and $+50^{o}$ in steps of 1.5^{o} and δ is scanned from 0^{o} to 180^{o} in steps of 1.5^{o}. While measuring, the recorded intensities are displayed on a monitor and stored in the computer for further data analysis. Typically a complete run takes 10 minutes.

An unique option with the technique is that a particular texture component within a measured pole figure can be selected and by dark field imaging the corresponding microstructural region is seen.

2.3. In-situ neutron texture. The aim of the technique is to enable fast texture measurements of complete bulk samples. The penetration depth of neutrons in most metallic materials is rather large, typically several centimeters. If therefore the size of a sample is less than a couple of centimeters in each direction, a texture determined by neutron diffraction is the true bulk texture. With the more commonly used X-ray diffraction technique the limited penetration (less than 100 μm) restricts texture measurements to very small samples or selected layers of a larger specimen. The in-situ neutron texture technique further enables a complete texture to be determined rather fast, in less than 1/2 hour. This means that texture transformations during annealing can be studied on-line, which is not possible using standard X-ray or neutron diffraction techniques.

The in-situ neutron technique was developed at the Risø DR3 reactor (Juul Jensen and Kjems 1983; Juul Jensen, Hansen, Kjems and Leffers 1984). The basic principle is rather similar to that of the more well known X-ray diffraction technique (Schultz 1949; Welch and Puch 1982): A monochromatic X-ray or neutron beam is incident on the sample. From there the beam will be diffracted according to normal Bragg scattering (see Eq. (1)). At a given angle 2θs to the incident beam, the intensity of the diffracted beam is recorded. This intensity is proportional to the volume fraction of crystallites having the normal to the selected (hkl) planes bisecting the angle between the incident and the diffracted beam (see Fig. 6), and can be represented as one point in a (hkl) pole figure. By scanning the setting of the sample, a map of the crystallite orientations can be obtained and plotted as a pole figure. In general, a single (hkl) pole figure do not give the full information about the texture of a material. However, by

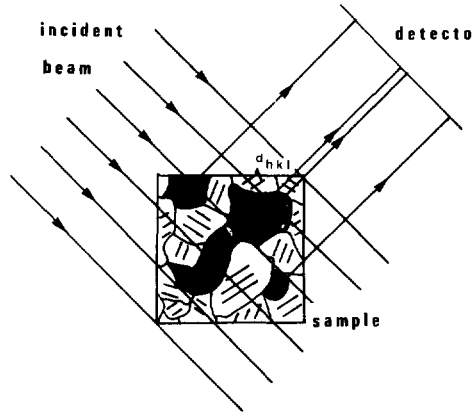

Fig. 6. Schematic illustration of the texture measuring principle. For each grain, lattice planes with the distance d_{hkl} are indicated. Only the grains shaded in grey fulfil the Bragg scattering condition.

combining the data of at least two pole figures from different (hkl) reflections the complete three dimensional orientation distribution function (ODF) describing the texture can be obtained. For a recent overview of standard experimental techniques and methods of ODF analysis see Bunge and Esling (1982).

The experimental set-up used for the in-situ texture measurements is shown schematically in Fig. 7a. It is a fairly standard set-up for neutron texture measurements except the detector which is a 50 cm long linear position sensitive detector (PSD) placed with its axis vertical. If the wavelength (see Eq. 1) of the incident neutron beam is selected so that the scattering angle 2θs is equal to 90°, the PSD simultaneously records the diffracted intensity along ~50° of a (hkl) Debye-Scherrer ring (see Fig. 7b). So for one setting of the sample not only one point of the pole figure but a large part (~34°) of a small circle is determined (see Fig. 8a). This means a considerable enhancement of the data collection rate compared to standard equipments.

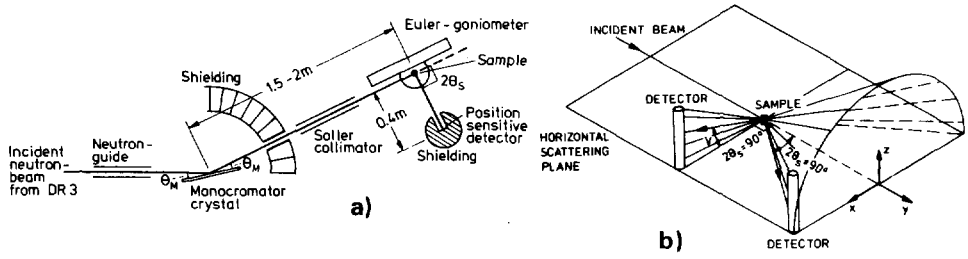

Fig. 7. a) Schematic illustration of the experimental arrangement as seen in a horizontal plane for the in-situ neutron texture technique. b) Illustration of the use of a position-sensitive detector to measure the intensity distribution along a (hkl) Debye-Scherrer cone. At 2θs=90° the cone degenerates to a plane and the detector axis lies completely in this plane. (Juul Jensen and Kjems 1983).

A complete pole figure, or any part of it, is obtained by rotating the sample discontinuously in the Euler goniometer (see Fig. 7a), with the sample fixed while counting. Typically 180 settings of the sample are required for a complete pole figure measurement. However owing to symmetry this number can in general be reduced. For example, for symetrically rolled materials only a quarter pole figure is needed. In this case 61 settings of the sample is used to obtain the sampling mesh shown in Fig. 8b. Typical measuring times for the quarter pole figure mentioned (with an accuracy of

2-3% as determined by counting statistics) are in the range 7 to 15 minutes depending on the scattering cross section of the sample material.

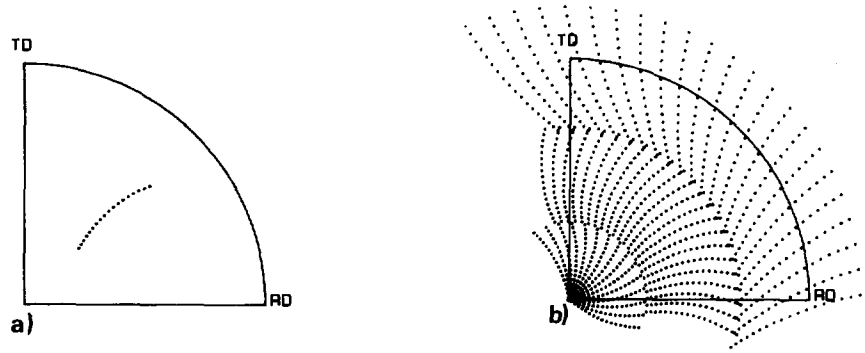

Fig. 8. a) With one sample setting the detector covers 34° of a small circle in the pole figure plane. b) The sampling mesh. (Juul Jensen and Kjems 1983).

On applying the calculation method introduced by Bunge (1969) at least two pole figures from different (hkl) reflections are needed to determine the ODF (assuming cubic crystallite and orthorhombic sample symmetry). A typical time resolution is therefore about 20 minutes. Thus, it is possible to make reasonably accurate ODF-based kinetic investigations of annealing processes, which involves a texture transformation over at least a couple of hours.

The kinetics of very fast processes, where this time resolution is insufficient, can be followed by means of partial pole figures that focus on selected texture components. Here the sample orientation is changed only between a few preselected positions. In the limiting cases the sample is kept fixed during the measurements, but as the position sensitive detector covers 34° of a small circle in the pole figure plane (Fig. 8a), it is possible to position the sample so that the detector records the change in intensity of one or even a few texture components simultaneously, and thus a time resolution of the order of seconds is obtained.

In general, cylindrical samples with a total volume between 0.1 and 2 cm^3 are used. For heavily rolled materials this relative large sample volume is achieved by stacking a number of circular discs on top of each other.

The complete operation of the measurements is computerized. What is needed by the user is to mount the sample, switch on the beam and start the computer. While measuring the recorded intensities are displayed as pole figures on a colour monitor and stored in the computer for ODF analysis. When the measurement of a pole figure is completed, the pole figure is automatically plotted by an 8 colour jet-ink printer.

3. NEW DEVELOPMENTS

Besides upgrading the computers used to control the microtexture and the in-situ neutron texture technique, at present there are no plans for major improvements or further developments of these two techniques. For the EBS technique two new procedures, namely i) a method for fully automatic EBS pattern recognition and analysis and ii) a measuring procedure for deter-

mination of grain boundary planes will be described briefly in the following.

Although techniques like the EBS technique, which are based on measurements of individual grains, yield very complete information, the greatest drawback to texture type investigations is the practical difficulty of obtaining sufficient data to achieve a statistically significant result in a reasonable time. This, for example, is a problem for the determination of growth rates of grains with different orientations during recrystallization. Reliable fully automatic diffraction pattern acquisition and analysis procedures would here be advantageous. At present such a procedure for EBS pattern analysis is being developed and tested (Juul Jensen and Schmidt 1989). Image processing procedures are used to find the most clear bands/lines in a pattern. Typically, for an annealed aluminium sample 2 - 4 lines are precisely identified. From these, the possible orientation solutions are calculated and by checking the positions of less clear lines, which could not be found using the image processing procedures the pattern is indexed. At present the method seems to work reasonably well but further tests are needed before it can be concluded if it is reliable enough to continue the development.

In order to give a complete description of a grain boundary geometry the orientation of the grain boundary plane needs to be determined. The significance of this parameter is that the grain boundary free energy, the mobility and other characteristics are strongly dependent upon the position of the boundary; a low Σ CSL* value alone is not sufficient criterion for the boundary to be identified as "special" with respect to its properties (Randle 1989a; Paidar 1987). Recently a method has been devised for measuring the orientation of the grain boundary plane (Randle and Dingley 1989a, b). The method relies on locating the position of the boundary trace both on the specimen surface from which EBS diffraction patterns are obtained and on adjoining specimen face which is perpendicular to it (Randle 1989b).

4. APPLICATIONS

The three techniques can each be used to address important aspects of annealing processes. In Table I their present potential for studies of deformation structure-texture relationships, nucleation processes, growth of nuclei, recrystallization kinetics and grain growth processes is shown. In the table + is used when the technique either can give information which is otherwise unattainable or when the technique can significantly reduce the required experimental work. - is used when the technique is of no or little value and (-), (+) indicate levels in between.

In table I it is marked that the EBS and the neutron texture techniques are rather unsuited for investigations of deformation structure/texture relationships. This might seem somewhat dubious as both techniques already have been used for this type of investigations. For example the EBS technique has been used to give information on localised dislocation densities in local areas of the deformation structure (Mackenzie and Dingley 1986, Quested Henderson and McLean 1988). As the strain is increased the EBS patterns become increasingly diffuse. By determining the diffuseness an estimate for the strain accumulated within individual grains is obtained. However, at high strains the quality of the EBS patterns becomes too poor,

*Σ refers to the reciprocal density of coinciding lattice sites in a coincident site lattice, CSL.

and at present the method is limited to strains below ~10% - 15%. To avoid this problem Ørsund, Hjelen and Nes (1989), in a study of local lattice curvatures in aluminium deformed to 90% reduction, prior to EBS examination annealed the specimen for short times in a salt bath to produce subgrains which were easyly detectable by the EBS technique. By a systematic examination of the orientation distribution within well defined texture components, they showed that the subgrain misorientation, in general, accumulated into a long range lattice curvature. An example is shown in Fig. 9.

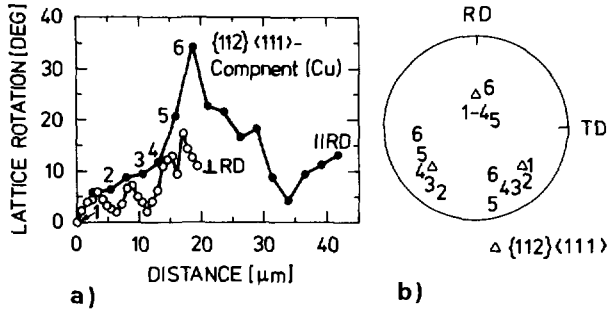

Fig. 9. Subgrain misorientations in Al cold rolled to 90% reduction. a) Misorientations within the Cu component ({112}<111>) measured both parallel and perpendicular to the rolling axis (RD). b) Pole figure showing the rotations (in three dimensions), the numbers refer to the position given in a). (Ørsund, Hjelen and Nes 1989).

Such a short time annealing procedure may be the solution in certain cases. However, in general, the rather coarse spatial resolution limits the potential of EBS for investigations of deformation microstructure/texture relationships at higher strains. Therefore the (-) in Table I.

Table I. Evaluation of the techniques for investigations of various aspects of annealing processes.

	EBS	Micro-texture	Neutron-texture
Deformation structure/texture	(-)	+	-
Nucleation	+	+	(-)
Growth of nuclei	+	-	(+)
Recrystallization kinetics	(+)	-	+
Grain boundary geometry and grain growth	+	-	+

The neutron texture technique has been used to determine the deformation texture in a variety of materials. However, as the technique determines the global texture, i.e. the statistical orientation distribution of a large number of grains, no information relating directly to the microstructure is obtained. Further, deformation textures often seem to be rather insensitive to changes in parameters such as composition of a given material (Hutchinson 1989) presence of particles (Juul Jensen, Hansen and Humphreys 1988) and development of shear bands (Hirsch, Lücke and Hatherly 1988). A change of these parameters can significantly alter the annealing process.

To get fundamental information about annealing mechanisms based on deformation texture measurements alone is therefore at present considered not to be possible (marked by the - in Table I).

In the following subsections examples of annealing investigations in which the selected techniques can really contribute with new and important information are reviewed. These examples represent the +'s in Table I.

4.1. Deformation structure/texture. In order to understand and characterize the early stages of annealing, information about the deformation microstructures and orientation relationships is needed.

The microtexture technique has been used to characterize lattice rotations associated with inhomogeneities in the deformation microstructure. For example, if large non-shearable particles (>0.1 μm) are present in the material, localized deformation zones with large lattice rotations are generated adjacent to the particles during the deformation (Humphreys 1978; Humphreys 1979). The textural spread within the complete deformation zone has been determined by microtexture measurements (Humphreys 1983; Humphreys 1984b; Humphreys and Kalu 1987, Kalu and Humphreys 1988; Juul Jensen, Hansen and Humphreys 1985). It was found that extremely large lattice rotations ($<40^{o}$) can be present in the deformation zone. Further it was found that the magnitude of the rotations depends on parameters such as particle size and shape, strain, strain rate and deformation temperature. However, for high strains ($\epsilon \geq 2$) the misorientations are in general quite large ($>15^{o}$).

Another type of deformation inhomogeneities studied by microtexture measurements is different types of bands (e.g. deformation bands, transition bands, microbands and shear bands). Schwarzer and Weiland (1988) studied the orientations within deformation bands and shear bands in titanium sheets. They found that the deformation bands have orientations similar to that of the matrix, whereas the orientations within the shear bands were distinctly different. Hansen, Kalu and Juul Jensen (1989) studied the rotations associated with microbands in aluminium cold rolled to 86% reduction. (For definition of microbands, see Bay, Hansen and Kuhlmann-Wilsdorf (1989)). A typical example of a microband and the measured microtexture is given in Fig. 10. The results show that microbands can cause large local misorientations.

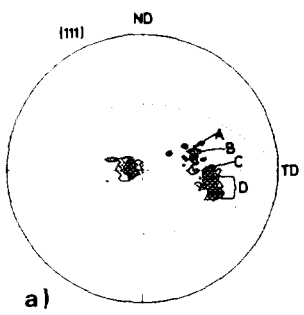

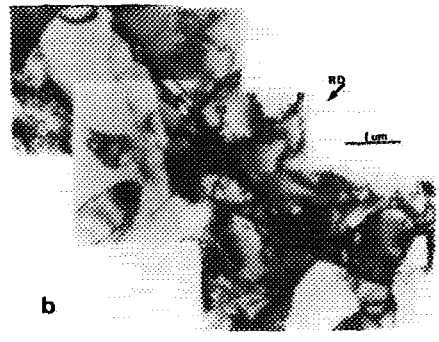

Fig. 10. a) (111) microtexture pole figure from aluminium cold rolled to 86% reduction. The selected region is a 7 μm area covering a microband and the surrounding matrix. A, B and C refer to orientations within the matrix and D represents orientations in the microband. b) Micrograph showing a typical microband marked M (rolling plane section, RD rolling direction).

Previously selected area diffraction, microdiffraction and X-ray transmission Kossel diffraction techniques have been used to determine local lattice misorientations associated with particles in deformed single crystals (Humphreys, 1978; Chapman and Stobbs 1969) and within deformation and shear bands (Hutchinson, Duggan and Hatherly 1979, Inokuti and Doherty 1978 and Bellier and Doherty 1977; Fukutomi, Suzuki and Kamijo 1989). Compared with these techniques a significant advantage using the microtexture technique is that the texture (and textural spread) is determined for a whole microstructural region (5 - 10 μm) automatically. This means reduction in the required labour.

4.2. Nucleation. The orientations of nuclei associated with deformation inhomogeneities in high purity aluminium cold rolled to 90% reduction have been studied by the EBS technique (Hjelen and Nes 1988). In agreement with earlier observations they found that transition bands, shear bands and grain boundaries were preferential nucleation sites. Further they found that there was a close correlation between the type of nucleation site and orientation of the nuclei. For example cube-oriented ({100}<001>) grains were found to grow out from transition bands in the {112}<111> deformation texture and S-oriented ({123}<634>) grains were nucleated in shear bands.

For investigations of this type the EBS technique is very powerful as it allows inspections of large sample areas and can classify the orientation of even small nuclei.

Large particles may act as potential nucleation sites, and the microtexture technique has been used to ascertain this role of the particles (Juul Jensen et al. 1985; Kalu and Humphreys 1988). An example is shown in Fig. 11. It can be seen that the orientations of the nuclei are within the deformation zone. In principle, the orientation of a nucleus may be anywhere within the orientation spread of the deformation zone. In agreement with earlier observations (Gawne and Higgins 1969; Chan and Humphreys 1984) it is, however, generally found that the misorientation between a nucleus and the local matrix is more than 15^{o}.

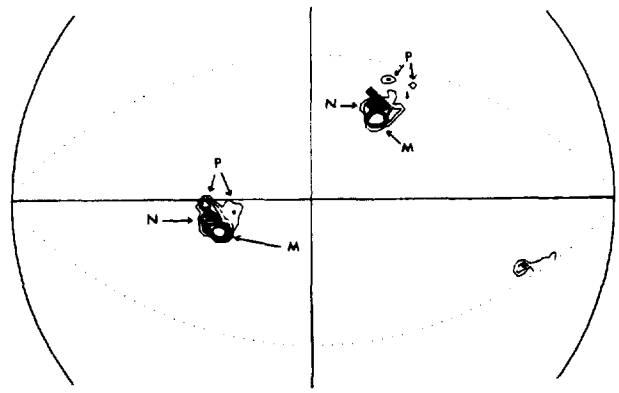

Fig. 11. (111) microtexture pole figure from a region containing a 2 μm silicon particle from a partly annealed Al-0.8wt% Si specimen. The orientations of matrix (M), recrystallization nucleus (N) and limit of the particle deformation zone (P) are marked. (Kalu and Humphreys 1988).

The possibility of getting directly the orientation relationship between a nucleus and the surrounding matrix using the microtexture technique is an important advantage compared to the more traditional microscopy techniques applied to study orientations of nuclei (eg. Gawne and Higgins 1969; Chan and Humphreys 1984; Ridha and Hutchinson 1982; Haratani, Hutchinson, Dillamore and Bate 1984; Ferran, Doherty and Cahn 1971).

4.3. Growth of nuclei. The growth of nuclei having different orientations has been followed using the EBS techniques (Hjelen and Nes 1986). For example Hjelen and Nes (1986) studied the growth rate of cube-oriented ({100}<001>) grains relative to the growth rate of grain otherwise oriented in commercially and high purity aluminium deformed to 90% reduction. They found that in the commercially pure material the cube grains tended to be bigger than the other grains whereas in the pure material the average cube grain size was almost equal to that of all grains. Previously the same type of investigations has been carried out using selected area chanelling patterns in a TEMSCAN and a SEM microscope (Juul Jensen et al. 1985; Nes and Solberg 1986). Compared to these techniques an advantage using EBS is the better spatial resolution (EBS: 0.5 μm, TEMSCAN: 1 - 2 μm, SEM: 10 μm) which enables identification of patterns already from the start of nucleation. In studies of this type, the orientation of a large number of grains needs to be determined. An easy analysis of diffraction patterns therefore is important. With the semiautomatic procedure used for the EBS patterns this analysis is rather fast and straight forward. A fully automatic analysis procedure would, however, further facilitate this type of investigations.

4.4. Recrystallization kinetics. During recrystallization a large lattice reorientation or change in texture usually occurs (Hu 1981). Using the neutron texture technique such changes can be followed on-line. An example is shown in Fig. 12. Here the variation in volume concentration of main texture components in copper cold rolled to 90% reduction is calculated by integration around the corresponding components in the ODF and plotted versus annealing time. From the data it can be seen how the cube texture component strengthen during recrystallization at the expense of the rolling components.

Results of this type can be used to evaluate kinetic models. The measured data shown in Fig. 12 are fitted to an Avrami type of equation (Avrami 1940):

$$X = X_\infty - (X_\infty - X_o) \exp(-A(t-t_o)^\beta) \text{ for } t > t_o \qquad (3)$$

where X is the volume concentration of a given texture component at time t, X_∞ and X_o are the corresponding volume concentrations at time ∞ and 0 (start of annealing), respectively, t_o is a possible incubation period and A, β are constants representative for the annealing process. It is seen that the equation gives a reasonable fit to the measured data and thereby an accurate determination of the fitted parameters A, β.

To get kinetic information about fast processes or for obtaining more precise information about specific events happening during a slower process, e.g. for investigations of incubation periods, the partial pole figure technique can be used. For example, the development in the {100}<001> and the {123}<634> components have been followed by measuring a partial (200) pole figure keeping the sample fixed so that the detector covered the two components during annealing (see Fig. 13a). By spatial integration over each of these peaks the development in the two components can be followed

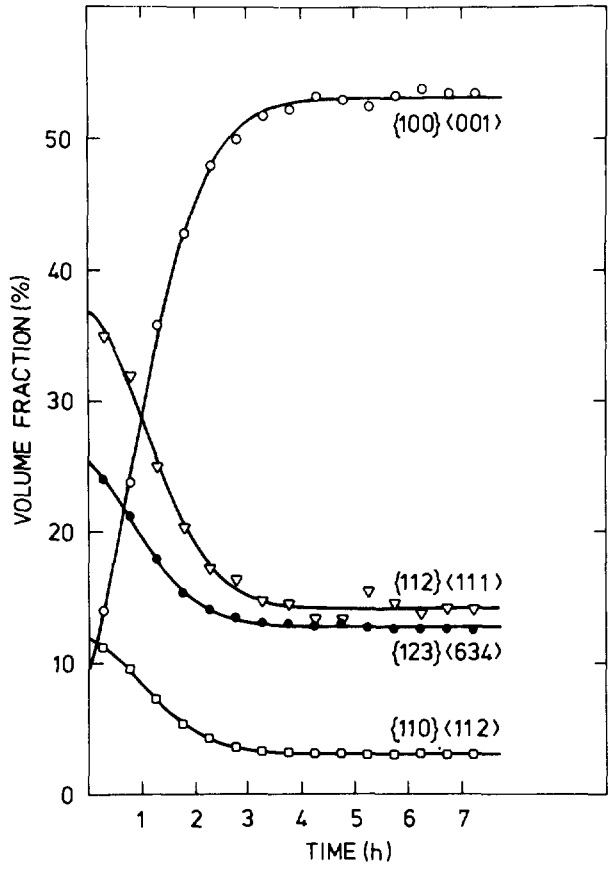

Fig. 12. The development of specific texture components during isothermal annealing at 95°C of pure copper, cold rolled to 90% reduction. (Juul Jensen and Hu 1989).

(Fig. 13b). Based on this type of data the incubation periods can be determined very accurately.

The neutron texture technique has also been used for controlled "texture tailoring" in aluminium (Juul Jensen and Hansen 1985). By adjusting the heating rate, the annealing time and temperature during on-line measurements, according to the actual texture development, it was possible to control the direction of the development. In spite, a rather limited range of annealing temperatures and large variation in the rolling to cube texture ratio was obtained. And an almost balanced texture (rolling/cube $\simeq$ 1) was achieved by annealing at 250°C for 1/2 hour followed by 36 hours at 230°C. Experiments of this type, where the kinetic texture information is used directly, may be a tool for optimizing the texture and thereby for example improve the formability of a given material.

Compared to other on-line techniques used in the study of recrystallization kinetics, eg. stored energy measurements (eg. Haessner and Schönborn 1985) the texture technique is considered to give data which are easier to corre-

late to the development and growth of nuclei, and therefore more direct information about the recrystallization is obtained.

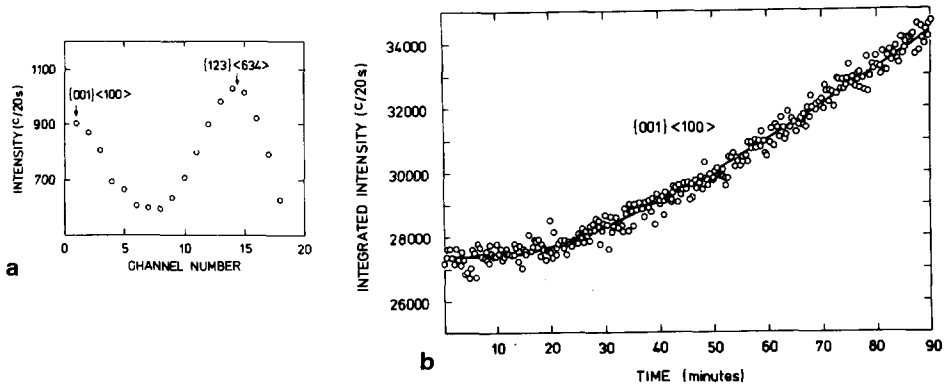

Fig. 13. a) Measured intensities along the position-sensitive detector for an aluminium specimen cold rolled to 90% reduction and annealed to ~50% recrystallization. b) Kinetic curve showing the initial development of the cube ({001}<100>) texture. (Juul Jensen et al. 1985).

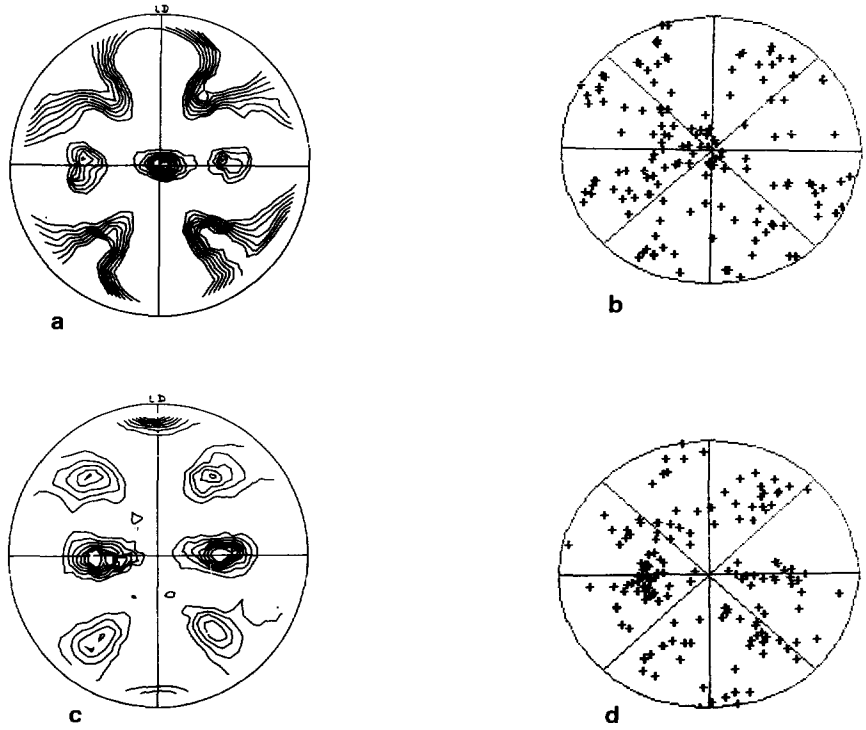

Fig. 14. (200) pole figures from the edge region (a and b) and the central region (c and d) of a rolled Al-Li based alloy obtained by EBS (b and d) and by conventional texture measurements (a and c).

4.5. Grain boundary geometry and grain growth. The majority of EBS investigations as yet reported in the literature pertains to fully recrystallized structures and to grain growth after completed recrystallization. A number of these studies has been concerned with the spatial distribution of grains having different orientations. For example in an investigation of a rolled and annealed aluminium-lithium alloy it was found that the centre grains have an elongated morphology whereas near the specimen edge, grains are much smaller and equiaxed. Here the two regions of differing grain structure are not intermixed and therefore it was possible to measure the texture both by EBS and by a conventional macroscopic means for comparison (Wismayer and Ralph 1989). Figure 14 shows (200) pole figures from the central and edge regions of the specimen sheet. Clearly the texture is markedly different between the sample populations and there is excellent agreement between the techniques, even though the sampled grains for EBS is fairly small (100 grains total).

As another example Randle, Ralph and Dingley (1988) studied the grain distribution in a nickel-base superalloy. They found a characteristic spatial arrangement of grains after recrystallization - bands of large grains are interspersed with much smaller grains. By selecting these two grain size extremes as separate populations, two texture variants are obtained, which compliment each other to give a random texture (Fig. 15). Similar measure-

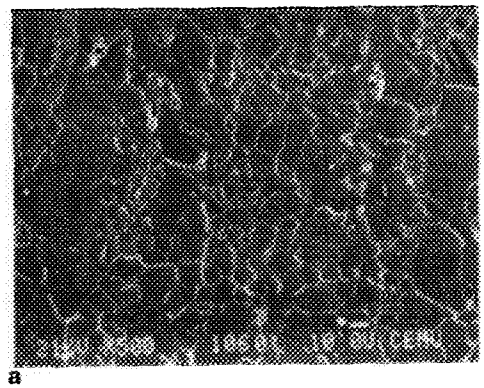

a

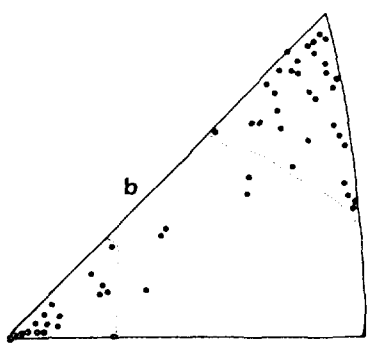

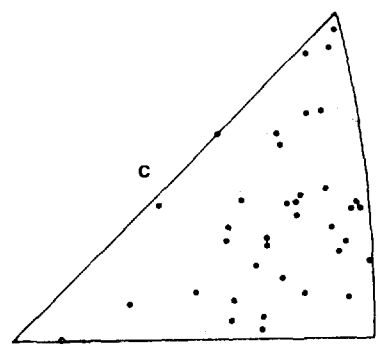

Fig. 15. a) Typical "banded" microstructure of nickelbase superalloy PE16, where bands of large grains are interspersed with smaller grains. Inverse pole figures in the grain normal direction for b) small grains in bands and c) large grains in bands. (Randle, Ralph and Dingley 1988).

ments taken for large and small grains from the same specimen, but where the juxtaposition of large/small grains does not form bands, show that here the textures of both sets of grain sizes are not differentiated as in the banded case.

When the orientation of contiguous crystals is known, orientation relationships can be derived and analysed in terms of models which describe interfacial geometry, e.g. the coincident site latice model, CSL, (e.g. Brandon 1966), the planar matching/coincident axial direction model (e.g. Randle and Ralph 1988a) and the interface-plane scheme (Wolf 1988). The essential point is that non-random geometry of some interfaces, e.g. CSLs, which may confer "special" physical properties. The identification and promotion of these "special" boundaries in polycrystals is termed "grain boundary design" (Watanabe 1984). Thus, the grain misorientation texture (GMT) may be equally important as the grain texture since many physical properties are related directly to the interfacial structure, such as grain boundary migration, grain boundary diffusion, precipitation, etc.

In this area EBS has been used to examine the link between carbide preicpitation on low CSLs compared to random boundaries (Randle and Ralph 1987), to investigate the fracture properties of Ni_3Al (Mackenzie, Vaudin and Sass 1988) to study the effect of prestrain on the GMT during the grain growth incubation period (Randle and Brown 1988, 1989) and to gain insight into the role that CSLs play during grain growth (Randle and Ralph 1988b). The two last mentioned studies show that the proportion of CSLs increases during the grain growth incubation period. For the case where large grains are surrounded by smaller ones, CSLs tend to be concentrated in the boundaries between small grain rather than in the boundaries between the large grain and the surrounding small ones (Randle and Ralph 1988b). Figure 16

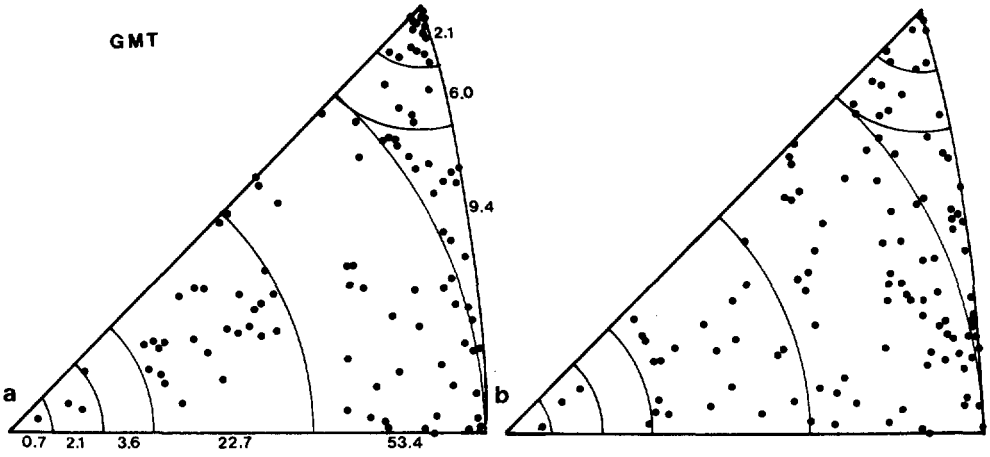

Fig. 16. Grain misorientation texture plots of a) boundaries between small grains and b) boundaries between large and small grains. The unit triangle is divided into regions which contain the indicated percentage of misorientation axes for a random distribution. (Randle and Ralph 1988b).

shows that this trend is apparent on a GMT plot. The GMT plot can be considered as the grain misorientation analogue for an inverse pole figure where axes of misorientation are plotted instead of a crystal direction. For the cubic system, it is possible to calculate the proportion of axes which will fall in each region marked on Fig. 16 if the GMT is random. In this case, a Student's t-test has been used to assess the non-randomness of

the distribution and shows that the distribution for boundaries between small grains is less random than those between large and small grains. The non-random spread tends to be accommodated in the (111) and (110) corners of the unit triangle which indicates the likelihood of a higher than average proportion of CSL boundaries.

The textural development during grain growth in cold drawn and recrystallized pure copper rods has been followed by the neutron texture technique (Grant, Juul Jensen, Ralph and Hansen 1984). It was found that grains having the (111) normal direction parallel to the fibre axis, grow at the expense of grain with the (100) direction along the fibre axis. The development of these two main texture components was followed via the partial pole figure method (as in the section about recrystalliztion kinetics) to determine the growth rate of the components for the various annealing temperatures.

Compared to other texture measuring techniques (based on X-ray or neutron diffraction) the main advantage is that the in-situ neutron texture technique is fast, enabling on-line studies of texture changes. Thereby the statistical scatter and the required experimental work is significantly reduced. Further the high penetration of neutrons ascertain that the measured textures are true bulk textures and coarse grained specimens are generally not a problem.

5. RECRYSTALLIZATION OF AL-SiC

The development of metal matrix composites for extremes of performance is at present one of the challenges for materials architecs. The mechanical properties of these materials depend heavily on the production and processing routes, and to get a scientific basis for optimizing the properties it is important to understand for example the microstructural and textural development taking place during various thermomechanical processing. Not much work has yet been concentrated on studies of this type. In the following results from on-going investigations of the recrystallization in heavily rolled fibre reinforced aluminium will be reviewed. (For further details, see Liu, Hansen and Juul Jensen (1989); Juul Jensen, Hansen and Liu (1989)). This is to illustrate how determinations of crystallographic orientations by the three selected techniques and microstructural investigations by TEM may be combined to further the understanding of annealing processes. It has to be noted, that the reported investigations still are far from being complete; several unsolved questions remain. Some of these will be considered in the following and it will be discussed how they might be addressed experimentally.

The material used is a powder blended Al-SiC composite containing 2 vol.% short whiskers. After processing the average dimensions of these fibres are 0.5 μm in diameter and 2 μm in length. Before the annealing experiments the material is cold rolled to 90% reduction in thickness.

In the deformed state, TEM and microtexture investigations show that deformation zones with large local lattice rotations - in general $>15^{o}$ - develop at the fibres; and adjacent to fibre agglomerates very complex zones with high dislocation densities and very rapid orientation changes develop. During the early stages of annealing also TEM and microtexture investigations reveal that nucleation predominantly takes place close to fibre agglomerates, and that these nuclei have a very wide range of orientations covering orientations which are present in the deformation zones, i.e. typical spread rolling texture components plus some {100}<013>. During the

annealing these nuclei grow, most of them with a rather low growth rate, but few with a significantly higher rate resulting in a rather broad grain size distribution in the recrystallized state. EBS investigations show that this variation in growth rate seems to be most pronounced for the {100}<013> grains out of which ~25% have a size larger than 3 x the average grain size in the recrystallized state. This large fraction of large {100}<013> grains corresponds well with the observed macroscopical texture development determined by neutron diffraction, namely that ~60 vol.% of the recrystallization texture is {100}<013>.

At present it is not known why some of the {100}<013> grow to become so large. It may relate to the spatial distribution of {100}<013> nuclei or to local variations in stored energy. EBS investigations of samples annealed to the beginning of nucleation may be used to study the spatial distribution of the {100}<013> nuclei and perhaps more detailed microtexture studies of similar samples can tell if these nuclei develop at special sites which are likely to have particular stored energy characteristics (for example if they nucleate predominantly within original grains of a specific orientation or at special deformation zones).

Fast kinetic, partial pole figure measurements by neutron diffraction indicate that {100}<013> grains grow at the expense of the various deformation texture components with various rates. This effect has to our knowledge not been observed for more conventional alloys. Complete ODF kinetic investigations can be used to get precise data on this point.

Further, it would be of interest to have growth curves for the various recrystallization texture components, i.e. curves that show the average grain size as a function of annealing time (isothermal annealing) for grains of different orientations. This type of data may be obtained by simultaneous measurements of size and orientations of recrystallized grains in a series of partly recrystallized samples using the EBS technique.

6. CONCLUSIONS

The three selected techniques, whereby information about local or global textures can be obtained, are all powerful tools for investigations of various aspects of annealing processes.

- The electron backscattering technique can determine the crystallographic orientation of grains down to ~0.5 μm in diameter over a large sample area. It is an efficient technique for achieving detailed and direct information about local microstructure/texture relationships and due to the good spatial resolution and large sample area it can be used to study entire annealing processes including the early stages of nucleation.

- The microtexture technique can determine the texture of selected local 5 - 10 μm areas in the microstructure. The technique is unique for studies of lattice rotation at deformation inhomogeneities and nucleation at particular sites like deformation zones and bands in the microstructure. It directly gives information about orientation relationships between the nuclei and the surrounding material.

- The in-situ neutron texture technique can determine the bulk texture of large specimens. It gives a precise description of the macroscopic texture, and the technique is especially developed to allow measurements of texture transformations, for example during annealing. Thereby orientation related on-line kinetic data is obtained which gives information

about overall recrystallization and growth processes and can be used to evaluate annealing models.

ACKNOWLEDGEMENTS

Dr. D.J. Dingley, Dr. N. Hansen, Prof. F.J. Humphreys and Dr. T. Leffers are thanked for valuable discussions and critical comments. VR also thanks the Royal Society for financial support.

REFERENCES

Alam, M.N., Blackman, M. and Pashley, D.W. (1954). High-angle Kikuchi patterns. Proc. Royal Soc. A. 221, 224-242.

Avrami, M. (1940). Kinetics of phase change II. J. Chem. Phys. 8, 212-224.

Bay, B., Hansen, N., Kuhlmann-Wilsdorf, D. (1989). Deformation structures in lightly rolled pure aluminium. To be published in Mat. Sci. and Eng.

Bellier, S.P. and Doherty, R.D. (1977). The structure of deformed aluminium and its recrystallization - investigations with transmission Kossel diffraction. Acta metall. 25, 521-538.

Brandon, D.G. (1966). The structure of high angle grain boundaries. Acta metall. 14, 1479-1484.

Bunge, H.-J. Ed. (1986). Experimental techniques of texture analysis. (DGM Informationsgesellschaft Verlag, Oberursel) 442 pp.

Bunge, H.-J. (1969). Mathematische Methoden der Texturanalyse (Akademie Verlag, Berlin) 330 pp.

Bunge, H.J. and Esling, C. Eds. (1982). Quantitative texture analysis. (DGM, Oberursel) 551 pp.

Chan, H.M. and Humphreys, F.J. (1984). Effect of particle stimulated nucleation orientation of recrystallized grains. Met. Sci. 18, 527-529.

Chapman, P.F. and Stobbs, W.M. (1969). The measurement of local rotations in the electron microscope. Phil. Mag. 19, 1015-1030.

Dingley, D.J. (1984). Diffraction from sub-micron particles using electron back scatter diffraction. Scanning Electron Microscopy 11, 569-575.

Ferran, G.L., Doherty, R.D. and Cahn, R.W. (1971). The Kossel line determination of the orientation of new grains formed by recrystallization of aluminium. Acta metall. 19, 1019-1028.

Frank, F.C. (1988). Orientation mapping. Met. Trans. A, 19A, 403-408.

Fukutomi, H., Suzuki, N. and Kamijo, T. (1989). The effect of shear bands on the recrystallization of copper single crystals. In this volume.

Gawne, D.T. and Higgins, T.T. (1969). A study of the recrystallization behaviour of iron containing coarse second phase particles. In: Textures in Research and Practice. Edited by J. Grewen and G. Wassermann. (Springer Verlag, Berlin) 319-330.

Grant, E., Juul Jensen, D., Ralph, B. and Hansen, N. (1984). Texture development during grain growth in pure copper. In: Proceedings ICOTOM 7. Edited by C.M. Brakman et al. (Neth. Soc. Mat. Sci., Holland) 239-244.

Heassner, F. and Schönborn. K.-H. (1985). Untersuchung der Rekristallisationskinetik in hochverformtem Kupfer und Silber mit Hilfe isothermer und anisothermer kalorischer Messungen. Z. Metallkde. 76, 198-207.

Hansen, N., Kalu, P.N. and Juul Jensen, D. (1989). Unpublished work.

Haratani, T., Hutchinson, W.B., Dillamore, I.L. and Bate, P. (1984). Contribution of shear banding to origin of Goss texture in silicon iron. Met. Sci. 18, 57-65.

Hirsch, J., Lücke, K. and Hatherly, M. (1988). Mechanism of deformation and development of rolling textures in polycrystalline fcc metals. Acta metall. 36, 2905-2927.

Hjelen, J. and Nes, E. (1988). The evolution of recrystallization textures in aluminium as determined by electron back scattering patterns. In: Proceedings ICOTOM 8. Edited by J.S. Kallend and G. Gottstein. (AIME, Warrendale) 597-602.

Hjelen, J. and Nes, E. (1986). Nucleation and growth of the cube texture component during recrystallization of aluminium. In: Proc. 7th Risø Symposium. Edited by N. Hansen et al. (Risø National Laboratory, Roskilde) 367-372.

Hu, H. (1981). Recovery, recrystallization and grain growth. In: Metall. Treatises. Edited by J.K. Tien and J.F. Elliott (AIME), 385-407.

Humphreys, F.J. (1984a). A method for determining textures by electron diffraction. In: Proc. ICOTOM 7. Edited by C.M. Brakman et al. (Neth. Soc. Mat. Sci., Holland) 771-776.

Humphreys, F.J. (1984b). The determination of local texture by electron diffraction methods. In: Proc. 5th Risø Symposium. Edited by N. Hessel Andersen et al. (Risø National Laboratory, Roskilde) 35-50.

Humphreys, F.J. (1983). The determination of crystallographic textures from selected areas of a specimen by electron diffraction. Textures and Microstructures 6, 45-62.

Humphreys, F.J. (1979). Local lattice rotations at second phase particles in deformed metals. Acta metall. 27, 1801-1814.

Humphreys, F.J. (1978). The deformation structure and the recrystallization behaviour of two-phase alloys. Metall. Forum 12, 123-135.

Humphreys, F.J. and Kalu, P.N. (1987). Dislocation-particle interactions during high temperature deformation of two-phase aluminium alloys. Acta metall. 35, 2815-2829.

Hutchinson, W.B. (1989). Recrystallization textures in iron resulting from nucleation at grain boundaries. Acta metall. 37, 1047-1056.

Hutchinson, W.B., Duggan, B.J. and Hatherly, M. (1979). Development of deformation texture and microstructure in cold-rolled Cu-30Zn. Met. Techn. 6, 398-403.

Inokuti, Y. and Doherty, R.D. (1978). Transmission Kossel study of the structure of compressed iron and its recrystallization behaviour. Acta metall. 26, 61-80.

Juul Jensen, D. and Hansen, N. (1985). Effect of thermal processing on the texture and microstructure of aluminium. In: Proc ICSMA7. Edited by H.J. McQueen et al. (Pergamon, Oxford) 263-268.

Juul Jensen, D., Hansen, N. and Humphreys, F.J. (1988). Effect of metallurgical parameters on the textural development in fcc metals and alloys. In: Proc. ICOTOM 8. Edited by J.S. Kallend and G. Gottstein (AIME, Warrendale) 431-444.

Juul Jensen, D., Hansen, N. and Humphreys, F.J. (1985). Texture development during recrystallization of aluminium containing large particles. Acta metall. 33, 2155-2162.

Juul Jensen, D., Hansen, N., Kjems, J.K., Leffers, T. (1984). In-situ texture measurements by neutron diffraction used in a study of recrystallization kinetics. In: Proc. 5th Risø Symposium. Edited by N. Hessel Andersen et al. (Risø National Laboratory, Roskilde) 325-332.

Juul Jensen, D., Hansen, N. and Liu, Y.L. (1989). Texture development during recrystallization of Al-SiC composites. In this volume.

Juul Jensen, D. and Hu, H. (1989). Unpublished work.

Juul Jensen, D. and Kjems, J.K. (1983). Apparatus for dynamical texture measurements by neutron diffraction using a position-sensitive detector. Textures and Microstructures 5, 239-251.

Juul Jensen, D. and Schmidt, N.H. (1989). A fully automatic on-line technique for determination of crystallographic orientations by EBSP. Submitted to Recrystallization '90.

Kalu, P.N. and Humphreys, F.J. (1988). A microtexture investigation of the deformation and recrystallization behaviour of particle-containing alloys. In: Proceedings ICOTOM 8. Edited by J.S. Kallend and G. Gottstein (AIME, Warrendale) 511-516.

Liu, Y.L. Hansen, N. and Juul Jensen, D. (1989). Recrystallization microstructures in cold-rolled aluminium composites reinforced by silicon carbide wiskers. To be published in Met. Trans. A.

Mackenzie, R.A.D. and Dingley, D.J. (1986). Computer analysis of diffuseness in wide angle Kikuchi patterns. In: Proc. XIth Int. Cong. on Electron Microscopy. 709-710.

Mackenzie, R.A.D., Vaudin, M.D. and Sass, S.L. (1988). Grain boundary characterization in Ni_3Al. Mat. Resh. Soc. Spring Meeting, 461-466.

Masteller, M.S. and Bauer, C.L. (1978). Experimental techniques. In: Recrystallization of metallic materials. Edited by F. Haessner (Dr. Riedere Verlag GmbH, Stuttgart) 251-279.

Nes, E. and Solberg, J.K. (1986). Growth of cube grains during recrystallization of aluminium. Mat. Sci. Techn. 2, 19-21.

Paidar, V. (1987). A classification of symmetrical grain boundaries. Acta metall. 35, 2035-2048.

Proceedings 5th Risø Symp. (1984). Microstructural characterization of materials by non-microscopical techniques. Edited by N. Hessel Andersen et al. (Risø National Laboratory, Roskilde) 605 pp.

Proceedings 7th Risø Symposium (1986). Annealing processes - recovery, recrystallization and grain growth. Edited by N. Hansen et al. (Risø National Laboratory, Roskilde) 601 pp.

Quested, P.N., Henderson, P.J. and McLean, M. (1988). Observations of deformation and fracture heterogeneities in nickel-base superalloy using electron back scattering patterns. Acta metall. 36, 2743-2752.

Randle, V. (1989a). The distribution of grain boundary plane orientations in a metastable grain aggregate. Scripta Met. 23, 773-778.

Randle, V. (1989b). $\Sigma = 3$ interfaces in nickel and austenitic stainless steel. In this volume.

Randle, V. and Brown, A. (1989). Development of grain misorientation texture in terms of coincident site lattice structures as a function of thermomechanical treatments. Phil. Mag. A59, 1075-1090.

Randle, V. and Brown, A. (1988). The effects of strain on grain misorientation texture during the grain growth incubation period. Phil. Mag. A58, 717-736.

Randle, V. and Dingley, D.J. (1989a). The measurement of grain boundar plane normal in polycrystals. Accepted for the Eur. Conf. on Adv. Mat. and Processes.

Randle, V. and Dingley, D.J. (1989b). Measurement of boundary plane inclination in a scanning electron microscope. To be published in Scripta Met.

Randle, V. and Ralph, B. (1988a). The coincident axial direction (CAD) approach to grain boundary structure. J. Mat. Sci. 23, 934-940.

Randle, V. and Ralph, B. (1988b). Local texture analysis associated with grain growth. Proc. Roy. Soc. A415, 239-256.

Randle, V. and Ralph, B. (1987). Application of electron back scattering diffraction to the determination of grain boundary parameters in bulk polycrystalline materials. In: Proc. EMAG'87, Inst. Phys. Conf. Ser. No. 90, 205-208.

Randle, V., Ralph, B. and Dingley, D.J. (1988). The relationship between microstructure and grain boundary parameters. Acta Met., 36, 267-273.

Ridha, A.A. and Hutchinson, W.B. (1982). Recrystallization mechanisms and the origin of cube texture in copper. Acta metall. 30, 1929-1939.

Schultz, L.G. (1949). A direct method of determining preferred orientation of a flat reflection sample using a Geiger-counter X-ray spectrometer. J. Appl. Phys. 20, 1030-1033.

Schwarzer, R.A. and Weiland, H. (1988). Measursement of local textures by electron diffraction-comparison with X-ray texture analysis. In: Proceedings ICOTOM 8. Edited by J.S. Kallend and G. Gottstein (AIME, Warrendale) 203-208.

Schwarzer, R.A. and Weiland, H. (1986). Electron diffraction polefigure measurements. In: Experimental techniques of texture analysis. Edited by H.J. Bunge (DGM Informationsgesellschaft Verlag, Oberursel) 287-300.

Venables, J.A. and Bin Jaya, R. (1977). Accurate microcrystallography using EBSPs. Phil. Mag. 35, 1317-1321.

Venables, J.A. and Harland, C.J. (1973). Electron back scatter patterns - a new technique for obtaining crystallographic information in the SEM. Phil. Mag. 27, 1193-1200.

Watanabe, T. (1984). An approach to grain boundary design for strong and ductile polycrystals. Rech. Mech. 11, 47-84.

Weiland, H. and Schwarzer, R.A. (1984). The determination of preferred orientations with the TEM. In: Proc. ICOTOM 7. Edited by C.M. Brakman et al. (Neth. Soc. Matls. Sci., Holland) 857-862.

Welch, P.I. and Puch, K.H. (1982). Practical considerations in the measurement of texture. In: Quantitative Texture Analysis. Edited by H.J. Bunge and C. Esling (DGM, Oberursel) 505-525.

Wismayer, S. and Ralph, B. (1989). Unpublished work.

Wolf, D. (1988). Comparison of the energies of symmetrical and asymmetrical grain boundaries. In: Proc. Ceramic Microstructures 86. Edited by Pask and Evans. (Plenum Publishing Corporation) 177-185.

Ørsund, R., Hjelen, J. and Nes, E. (1989). Local lattice curvature and deformation heterogeneities in heavily deformed aluminium. To be published in Scripta Metal.

Scripta METALLURGICA et MATERIALIA
Vol. 27, pp. 533-538, 1992
Printed in the U.S.A.
Pergamon Press Ltd.

GROWTH OF NUCLEI WITH DIFFERENT CRYSTALLOGRAPHIC ORIENTATIONS DURING RECRYSTALLIZATION

D. Juul Jensen
Materials Department, Risø National Laboratory
DK-4000 Roskilde, Denmark

(Received April 20, 1992)
(Revised June 22, 1992)

Introduction

To further the understanding of recrystallization, the growth process following nucleation has been studied. The present paper focuses on the following two aspects: (i) development of grain size distributions as a function of annealing time and crystallographic orientation of the grains and (ii) the average growth rate <G> also as a function of time and orientation. Experimental data on the development of size distribution and <G> versus time are very scarce (1-3), and to the author's knowledge nothing has been published about orientation effects on the two parameters. The electron back scattering pattern (EBSP) technique used in scanning electron microscopy enables determination of the crystallographic orientation within selected areas (> 1 μm) in the microstructure over a large sample area. The technique is thus well suited for studies of the recrystallization growth aspects outlined above.

Experimental

Material The material was commercially pure aluminium (99.4%), the main impurities being Fe (0.33 wt%) and Si (0.09 wt%). The amount of Fe in solid solution was reduced by a heat treatment at 600°C for 24h in vacuum, followed by furnace cooling. A recrystallized starting material with an average grain size of 50μm was produced by cold rolling to 50% reduction in thickness, followed by annealing at 350°C for 1h. The specimens were then deformed 90% by cold rolling and annealed at 253°C for periods ranging from 5 minutes to 15 hours. The preparation procedure is described in more detail in (4) and the specimens used for the present study are identical to those used in the previous investigation (4). For an overview of the samples see Table 1.

Electron back scattering measurements A simultaneous determination of the crystallographic orientation, the size of individual recrystallized grains, and the free surface area between deformed and recrystallized material was obtained from electron back scattering patterns (EBSP). The specimens were mechanically, chemically and electrolytically polished and were placed in a JEOL 840 SEM. This microscope was equipped with a phosphor screen, a back scatter detector and a very-low-light sensitive TV camera mounted in the side port. The EBSPs were recorded using a frame grabber and indexed according to the procedure described in (5). The spatial resolution of the EBSP technique is ~ 1μm. For regions in the deformed material the EBSPs are thus diffuse, whereas within recrystallized regions sharp EBSPs are observed. From previous neutron diffraction texture measurement, it is known that during recrystallization the texture changes from the typical Al deformation texture to a texture containing cube, retained rolling components and a rather large volume fraction (~40%) of grains which are fairly randomly distributed in Euler space (4). In the following these latter grains will be referred to as the random component. In the present investigation the orientation of recrystallized grains was calculated from the EBSPs and expressed in Euler angles φ_1, Φ, φ_2. If the observed grain orientation was within 15° from the cube ({100}<001>) or one of the rolling components, ({110}<112>, {123}<634>, {112}<111>) the grain was classified as cube or rolling respectively; otherwise; it was designated as being of part of the random component.

0956-716X/92 $5.00 + .00

Table 1 Overview of Samples and EBSP Data

Anneal. time (sec.)	Number of grains cube	roll.	random	all	Length of EBSP lines (μm)	Nuclei or grain density (μm^{-3}) $\cdot 10^{-5}$	X-overall (%)
900	10	21	145	176	29898	12	6
1800	9	24	152	185	17692	14	13
3600	18	68	139	225	17111	7	25
8400	18	60	149	227	7724	11	50
14400	19	51	136	206	4847	6	81
14400	14	117	151	282	10185	4	81
49800	31	106	201	339	11584	2	100

Each specimen was mechanically transversed under the beam. The plane of inspection was the rolling plane and the transverses were along the rolling direction. By noting the stage position at which patterns changed, the sizes (linear intercept values) of grains or deformed regions were measured, and the transitions between recrystallized and deformed regions were noted. From these data, grain size distributions for grains of the different orientations at the various annealing times were obtained. Also the average growth rates as a function of recrystallization time and orientation were determined.

Optical microscopy revealed that the grains are equiaxed in the rolling plane but slightly elongated (aspect ratio 1.5) in the longitudinal plane section, and that the recrystallization takes place homogeneously through the thickness of the samples. The latter is supported by the fact that almost identical results are obtained where two rolling planes at approximately 1/3 and 1/2 sample thickness of the sample annealed for 240 minutes are examined.The growth data presented in the following are therefore considered to be representative for growth in the rolling plane (along RD-TD) but not necessarily for growth perpendicular to the plane (along ND).

Calculation of average growth rates A method of determining the average growth rate has been suggested by Cahn and Hagel (6) and has been utilized and elaborated on (1,3,7,8). The increase in volume of recrystallized material, dX, during a short annealing interval dt is quite generally given by

$$\frac{dX}{dt} = \langle G \rangle \, S_v(t) \qquad (1)$$

where $S_v(t)$ is the free or unimpinged surface area per unit volume at time t, and <G> is the average growth rate, i.e. the average velocity with which the recrystallization interface moves normal to itself, at time t.

The free surface area per unit volume S_v is determined from line scans through the microstructure (9)

$$S_v(t) = 2 \, N_L \qquad (2)$$

where N_L is the average number of intersections (between deformed and recrystallized material) per unit length of a random test line. The only requirement for eq. 2 to be fulfilled is that the test lines are placed randomly (in random directions and at random inspection planes) (9).

The increase in volume of recrystallized material per unit time, dX/dt (eq. 1), may be determined directly from the EBSP data. However, as "only" 6 samples were used for the EBSP investigation, a statistically rather poor determination of dX/dt was achieved. Therefore, the EBSP data were used together with X versus t data determined previously by neutron diffraction, optical microscopy, hardness measurements and STEM for identical samples plus a few extra samples (4,10). The X versus t data were fitted to an Avrami equation

$$X = 1 - \exp(-K \cdot t^{\beta}) \qquad (3)$$

where K and β are constants. Considering the experimental scatter, equation (3) gives a good fit to the data for the entire annealing period and dX/dt is thus calculated directly from (3).

To determine the growth rate for grains of a specific crystallographic orientation (eg cube) equations 1,2 are used in a slightly modified form

$$\left(\frac{dX}{dt}\right)^c = \langle G \rangle^c \, S_v^c(t) \tag{4}$$

$$S_v^c(t) = 2 \, N_L^c \tag{5}$$

where c refers to grains of orientation c. The rolling and random grains seem to follow rather closely the development of "all grains". Therefore dX/dt for these two components were determined as described above. For the cube grains, the development in grain size distribution is significantly different from that of "all grains". It was therefore considered necessary to use dX/dt as determined for cube grains only. Two techniques were used for the sole measurement of cube grains: neutron diffraction

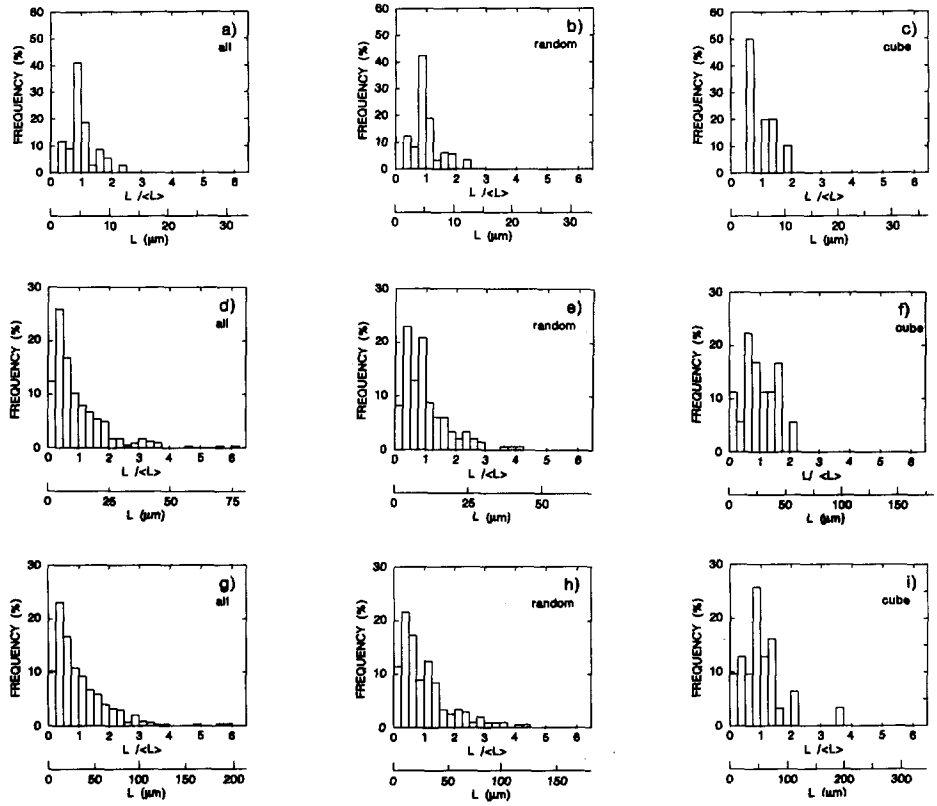

FIG. 1. Grain size distributions (linear intercept values) for grains of different orientations after different annealing periods a) b) c) 15 minutes (~6% recryst.), d) e) f) 140 minutes (~50% recryst.), g) h) i) 830 minutes (100% recryst.) ("All" includes grains of all orientations).

texture measurements (10) and the EBSP data. The X^c determined by neutron diffraction are equal to $V^c(t)/V^c(\infty)$, where $V^c(t)$ and $V^c(\infty)$ are the volume concentration of c-grains at time t and infinity (fully recrystallized), respectively. Thus, for each component, the X^c values represent volume fraction of recrystallized material, and values between 0 and 1 are obtained. Using EBSP, it is most straight forward to calculate X^c as the length fraction of c-grains of the entire test line (L), i.e. $X^c = L^c/L$. In this case, X^c represent volume fraction of c-grains in the material. This difference in definition of X^c gives rise to different definitions of N^c_L (see eq. 5). When neutron data are used, N^c_L is the number of interfaces between c-grains and deformed material per unit "c-length" of the test lines (i.e. it is taken into account that c-grains only occupy a certain fraction of the test lines). When EBSP data are used, N^c_L is number of c interfaces per unit length of the total test line. Both techniques were used to calculate the cube growth rate and rather similar results were obtained. However, using the neutron technique, all cube grains within the sample is determined. The data is therefore statistically much more reliable than the EBSP data, and the results shown in the following are thus based on the neutron diffraction data.

Results

Grain sizes For each sample, the size and orientation was determined for 175 - 340 grains (See Table 1). Grain size distributions were plotted for cube, rolling, random and all (including grains of all orientations) grains. For all samples, the rolling and random distribution are fairly similar and the rolling distributions will therefore not be shown in the following. In Fig. 1 the distributions are shown for samples annealed for 15, 140 and 830 minutes corresponding to approximately 6%, 50% and 100% recrystallization. Early in the recrystallization process the distributions (both average grain size and shape of grain size distribution) are fairly similar. Later in the processes, however, significant differences are observed. The distributions of cube grains continue to be rather narrow, whereas the random and overall distributions widen.

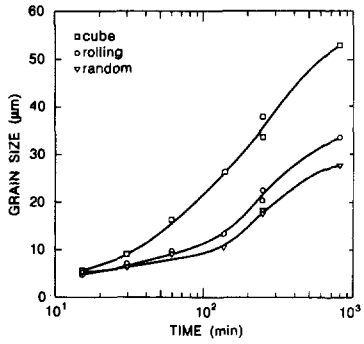

FIG. 2. The average size (linear intercept values) of grains with different orientations.

The average grain sizes of cube rolling and random grain are shown in Fig. 2. This curve is almost identical to that measured previously (4) and shows that in the fully recrystallized state, the average grain size of cube grain is about 1.7 times as big as grain of other orientations.

Growth rates The <G> versus t curves are shown in Fig. 3. It can be seen that <G> decreases with time for all components. It has been suggested that $\langle G \rangle = k/t$ where k is constant (1). The present data also shows that log <G> decreases linearly with log (t) for all components, however, the slopes are not equal to one. Instead the equation

$$\langle G \rangle = k \cdot t^{-\alpha} \qquad (6)$$

gives a good fit to the data when $\alpha = 0.3$.

A comparison between the <G> versus t curves for the cube and random component (Fig. 3b) shows that $\langle G \rangle_{cube} = 1.7 \langle G \rangle_{random}$ for all annealing times. The growth rate of rolling grains follows that of the random grains rather closely.

Discussion

Grain size distributions In the fully recrystallized state, the grain size distribution for grains of all orientations (Fig. 1g) is very wide. The maximum grain size is 6 times the average size. If new nuclei

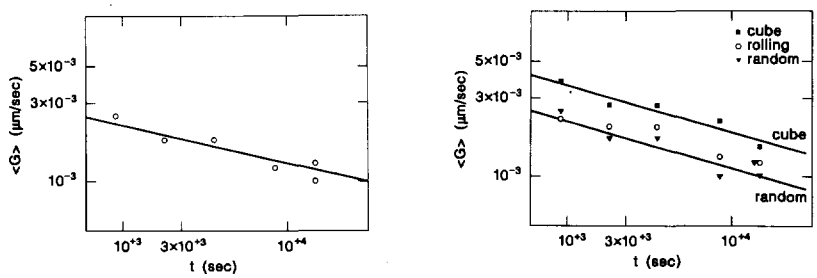

FIG. 3. The average growth rates <G>. a) all grains b) cube, rolling and random grains; the full lines are least squares fit to cube and random growth rates.

form constantly during the recrystallization process or if the distribution of nucleation sites is non-random it is expected that the grain size distribution in the fully recrystallized state will be wide. However, site saturation seemed to be fulfilled (considering the experimental scatter) for the present study (see Table 1 and (4)). A consequence of inhomogeneous distribution of nuclei would be that many grains were stopped by impingement early in the process and therefore remained small. This does not seem to be the case for the present results. Firstly, the number of very small grains (≤ 5 μm) decreases during the entire annealing period (see Fig. 4). Secondly, the number of neighbours along the EBSP test line was determined for very small grains (≤ 5 μm) and for larger grains (> 10 μm) in the sample annealed 140 minutes to ~ 50% recrystallization. It was found that 24%, 55% and 21% of the small grains were free (surrounded by deformed matrix on both sides), had one neighbour, or two neighbours, respectively. The same results for the large grains were 20%, 56% and 24%. It can therefore be concluded that the small grains are as free to grow as the large grains.

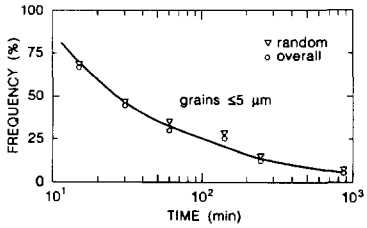

FIG. 4. The number fraction of grains less than 5 μm for grains of all orientations (o) and random grains (▽).

Another explanation for the wide grain size distribution relates to orientation dependent growth rates. Clearly, if all grains of one orientation grow fast and others more slowly, the resulting grain size distribution will be wide.

Average growth rates The average growth rates <G> were determined using $dX/dt = <G> S_v(t)$. In general, growth rates are determined as the largest grain size after a short anneal divided by the annealing time. For the present experiments,

the latter calculation method gives $G_{max} \approx 6\ 10^{-3}$ μm/sec for t = 15, 30 and 60 minutes corresponding to 6, 13 and 25% recrystallization. This value is about 2-3 times larger than <G> (see Fig. 3). If instead the average grain size is used for the calculation, the $G_{average} \approx 3\ 10^{-3}$ μm/sec which agrees fairly well with <G>. However, this easy method to determine G_{max} or $G_{average}$ is only applicable at short annealing times where impingement can be neglected. (The relative slow growth rates relate to the low annealing temperature).

For all orientations, it was found that the average growth rates decrease as $<G> = k\ t^{-\alpha}$ where $\alpha \sim 0.3$ (see Fig. 3). That <G> decreases with time agrees well with earlier findings (1). However the slope ($\alpha \sim 0.3$) is less than the value $\alpha \sim 1$ which have been found experimentally for silicon-iron (1) and is used extensively in recrystallization modelling (eg. 8). The decrease in growth rate with t has been related to recovery occurring simultaneously with the recrystallization, and it is well known that recovery depends strongly on the actual state (eg. impurity content, degree of deformation) of the material. It is therefore

not surprising that α may vary, as seen in a study of recrystallization in copper in which a wide range of α's were also found (3). To further clarify this, studies of temperature effects on <G> are in progress.

The average growth rate of cube grains is for all annealing times, about 1.7 times larger than that of rolling and random grains. The growth rates determined are the average speed at which free boundaries move. In other words, even if the cube grains were more isolated than the other grains, this will not affect the results since only unimpinged parts of the boundaries are included in the calculation. The reason that cube grains grow faster may relate to a 40° <111> rotation (11) or simply to a higher mobility of grain boundaries which have large misorientations to the surrounding matrix so that these nuclei have a growth advantage compared to nuclei with smaller misorientations (12). It is supposed that cube grains are nucleated at intergranular sites and will therefore have a large misorientation. Original grain boundaries and deformation zones around $FeAl_3$ particles on the other hand are preferential sites for rolling and random grains, and they may therefore have smaller misorientations.

Conclusions

The recrystallization of 90% cold rolled aluminium was studied during isothermal annealing. It was found that the crystallographic orientation has a significant effect on the growth during recrystallization.

The grain size distribution in the fully recrystallized state is very wide, which cannot be explained either by constant nucleation or inhomogeneous distribution of nucleation sites. Orientation dependent growth has to be considered.

The average growth rates decrease as $\langle G \rangle = k \cdot t^{\alpha}$ where $\alpha \sim 0.3$ for grains of all three orientations (cube rolling and random). However, cube grains grow on average 1.7 times faster than rolling and random grains.

Acknowledgements

Dr. Niels Hansen is thanked for valuable discussions and critical comments, and Helle Baastrup Christensen for preparing the manuscript.

References

1. A.T. English and W.A. Backofen, Trans AIME 230, 396 (1964).
2. L. Ryde, W.B. Hutchinson, S. Jonsson, In Recrystallization'90, p. 313, Ed. T. Chandra, TMS, Warrendale (1990).
3. C.T. Necker, R.D. Doherty and A.D. Rollett, Textures Microstr. 14-18, 635 (1991).
4. D. Juul Jensen, N. Hansen and F.J. Humphreys, Acta metall. 33, 2155 (1985).
5. N.H. Schmidt, J.B. Bilde-Sørensen and D. Juul Jensen, Scanning Microscopy 5, 637 (1991).
6. J.W. Cahn and W.C. Hagel, In Decomposition of Austenite by Diffusional Processen, p. 131, Eds. V.F. Zackay and H.I. Aaronson, Interscience, NY (1962).
7. J.E. Hilliard, In Recrystallization, Grain Growth and Textures, p. 267, Ed. H. Margolin, ASM, Ohio (1966).
8. R.A. Vandermeer and B.B. Rath, In Materials Architecture, p. 589, Eds. J.B. Bilde-Sørensen et al., Risø, Roskilde (1989).
9. E.E. Underwood, In Quantitative Microscopy, p. 77, Eds. R.T. Dehoff and F.N. Rhines, McGraw Hill, NY (1968).
10. N. Hansen, D. Juul Jensen and F.J. Humphreys, In Microstructural Characterization of Materials by Non-Microscopical Techniques, p. 267, Eds. N. Hessel Andersen et al., Risø, Roskilde (1984).
11. K. Lücke, In ICOTOM 7, p. 195, Eds. C.M. Brakman et al., NL Mat. Soc., Zwijndrecht (1984).
12. P. Haasen, In Annealing Processes-Recovery, Recrystallization and Grain Growth, p. 69, Eds. N. Hansen et al., Risø, Roskilde (1986).

Scripta METALLURGICA et MATERIALIA
Vol. 27, pp. 1551-1556, 1992
Printed in the U.S.A.
Pergamon Press Ltd.

CONFERENCE SET No. 1

MODELLING OF MICROSTRUCTURE DEVELOPMENT DURING RECRYSTALLIZATION

D. Juul Jensen
Materials Department
Risø National Laboratory
DK-4000 Roskilde, Denmark

(Received September 16, 1992)

Introduction

During recrystallization, grains of different crystallographic orientations may nucleate and grow with different characteristics; grains of one orientation may, for example, nucleate early at particular sites and grow faster than grains of other orientations. Such orientation dependencies can significantly affect the recrystallization microstructure and texture.

The aim of this paper is to demonstrate a computer model which can take into account the various nucleation and growth behaviour of different components (grains of different orientations). For each component, input information about the nucleation and growth characteristics is required. At any stage of recrystallization, simulated results for fraction recrystallized, 3-D or 2-D grain size distributions and texture are obtained. The model is used to simulate the recrystallization of 90% cold rolled aluminium. The input data are experimental data and the simulated results for recrystallization kinetics, grain size distributions and texture are compared to the experimental results. Finally the significance of using more than one component in the simulation is discussed on the basis of the aluminium data.

The Component Model

A 3 dimensional "computer sample" is considered (see Fig 1a). The size D_{max} of this sample is determined by the number of grains in the simulation N_g and the average recrystallized grain size. For spherical grains that is

$$D_{max}^3 = N_g \, 4/3 \, \pi \, \langle r \rangle^3 \qquad (1)$$

where <r> is the average recrystallized grain radius. The N_g grains are first distributed in the computer sample. This distribution may be random or in any predetermined form (e.g. nuclei in bands or clusters). The position (x,y,z), the crystallographic orientation (texture component no.) and the time of nucleation t_o are stored for each nuclei. The grains then grow. The growth rate may depend on direction (x,y,z), grain orientation (i) and annealing time (t). The size of a given grain which has not yet impinged upon a neighbouring grain at time t is thus

$$r_j(i) = ro_j(i) + \int_{t_o}^{t} G_j(i,t)\, dt \quad for \; t > t_o(i) \qquad (2)$$

where j refers to x,y,z direction, ro is the size of the nuclei and $G_j(i,t)$ is the growth rate in direction j of grains with orientation i at time t. t_o is the nucleation time.

For each point (x,y,z) in the computer sample, equation (2) used to calculate, which of the N_g grains arrived there first. For each x,y,z position, the grain number and the arrival time are stored in a "sample

0956-716X/92 $5.00 + .00

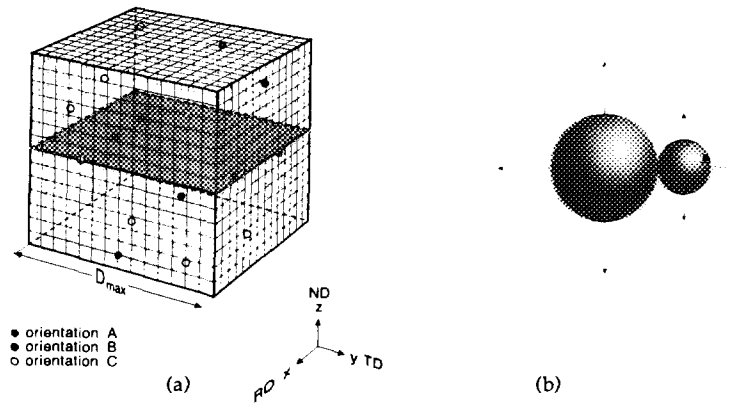

FIG 1. a) Sketch of the 3-D computer sample. Nuclei of 3 different texture components (crystallographic orientations) are distributed in the sample. b) Sketch of the impingement assumption.

table". This approach corresponds to the principles applied in most recrystallization modelling (1-4): namely, that the grains grow freely until they impinge upon another grain/nuclei. Growth is then stopped (for both grains) in that direction, but continues unhindered in any other direction (see Fig. 1b).

Using the "sample table", it is now straightforward to determine the volume fraction recrystallized and the volume concentration of each texture component at any annealing time. To obtain data comparable to that of microstructural measurements, selected planes in the computer sample may also be examined (Fig. 1a). Average grain sizes and grain size distributions for the different components, as well as for all grains, are obtained by the linear intercept method in these planes.

The following information is needed as input for the simulation: i) the overall average grain size, ii) the number of recrystallization texture components to be considered, iii) nucleation parameters (density, rate, size and spatial distribution of nuclei) and iv) growth parameters (rate and dimensionality). The nucleation and growth parameters must be determined for grains belonging to each texture component. Finally statistical information about the number of grains in the simulation and the number of inspection planes is needed. Typically, 5000 grains and 3 inspection planes are used. This resulted in CPU-times of around 10 hours on a VAX 8700.

Various approaches have been used for modelling recrystallization (1-11). All the models can be used for simulations of microstructural development. So far only the texture-Monte Carlo (3,8) and the component (this paper and (11)) models have been used for texture simulations.

Simulations using the component model is closely related to a specific experiment, and significant experimental work is required to obtain the necessary input data. One may argue that this is not really modelling since most of the data are measured experimentally. However, with precise experimental data on, for example, growth rates, the simulation allows evaluation of nucleation assumptions which are less well-known and experimentally much harder to determine. In general, it is felt that since so many different principal mechanisms can lead to the same recrystallization results (eg. recrystallized microstructure), further modelling should be based on as solid experimental data as possible.

Application to Experiment

The component model has been used to simulate the recrystallization of commercially pure aluminium (Al-99.6%). The material contained 0.5 vol% large (0.2-7 μm) intermetallic $FeAl_3$ particles; it was deformed by cold rolling to 90% reduction and was annealed at 253°C. The nucleation was characterized by TEM (12), the texture and recrystallization kinetics by neutron diffraction (13), and the growth rates and grain size distributions of grains of the different orientations by EBSP (14).

Input parameters for simulation The two first input parameters (see above) are fairly easily determined: (i) the average recrystallized grain size (including grains of all orientations) is 33 μm and (ii) the recrystallization could be described by 3 components (13): cube, retained rolling and other texture components more or less randomly distributed in the orientation space - here referred to as random texture. Thus, the number of components in the simulation is 3. (iii) Concerning the nucleation parameters (density, rate, size and distribution) the EBSP studies (14) have shown that ~7%, 26% and 67% of the nuclei/grains are of cube, rolling and random orientation, respectively, and that site saturation seems fulfilled. The size of the nuclei was determined to 3 μm (12) and the distribution of the nuclei seemed fairly random (a random site distribution is therefore assumed in the simulation). (iv) The growth parameters (rate and dimensionality) are determined from EBSP and optical measurements. It was found (14), that the average growth rates <G> of free (unimpinged) grains boundaries decreased with annealing time as

$$<G> = k \cdot t^{-\alpha} \qquad (3)$$

where $\alpha \approx 0.3$ for all 3 components and k is a different constant for the 3 components (see Fig. 2). For example, for the cube grains k was 1.7 times larger than k for the random grains (see table 1).

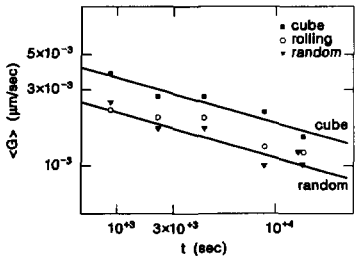

FIG. 2. The average growth rates <G> of cube, rolling and random grains; the solid lines are least squares fits to the cube and random growth rates. (14).

Optical microscopy revealed that the recrystallized grains were equiaxed in the rolling plane. In the longitudinal plane, the grains had an aspect ratio of 1.5, which is not too far from equiaxed. In the simulation spherical growth is assumed.

Although the component model is devised to take the individual behaviour of several texture components into account, it was also considered relevant for purposes of comparison to do the simulation using only one component (including grains of all orientations). In this case, results similar to those of other models were expected. In total, therefore, 2 simulations with different growth rates and number of components, but otherwise identical input parameters were carried out. For an overview see table 1.

Table 1 Growth rate input parameters for simulations (<G> (μm/sec) see eq. (3))

Simulation	Number of Components	k				α			
		all	cube	rolling	random	all	cube	rolling	random
I	3	-	0.027	0.012	0.017	-	.29	.24	.30
II	1	0.011	-	-	-	.23	-	-	-

Simulated Results

Examples of simulated microstructures are shown in Fig. 3. The simulated and experimental results for texture composition and average grain sizes in the fully recrystallized state are listed in Table 2. As can be seen, there is very good agreement between simulated and experimental results. Only the type I (with 3 components) simulation results are listed in the table. In the type II simulation (with 1 component - all grains) of course, no information about texture composition and grain sizes of individual grains is obtained. Only the average grain size of grains of all orientations is simulated and, as this is one of the input parameters, it is no surprise that the simulated result also is 33 μm.

The simulated grain size distributions (lines) are shown superimposed on the experimental data (histograms) in Fig. 4. Finally, recrystallization kinetics data are shown in Fig. 5. Both type I and II simulations give a reasonable fit to the experimental data. However, the 3-component case (type I) is closer to the experimental value, $\beta = 1.4$ (determined by a least squares fit to the experimental points).

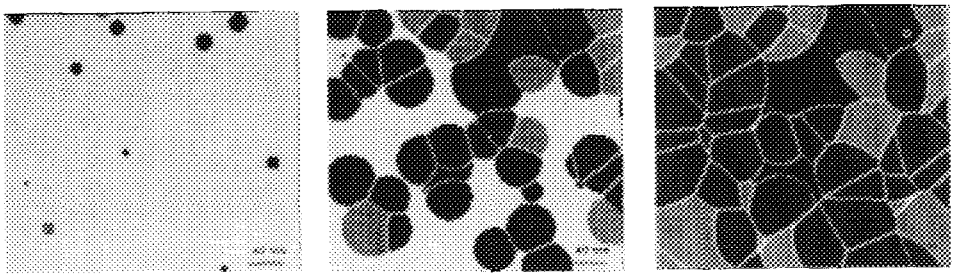

(a) (b) (c)

FIG. 3. Simulated microstructures (Type I simulation). The cube grains appear almost black, rolling grains light grey and random grains dark grey. a) 6%, b) 50%, c) 100% recrystallized.

Table 2 Simulated and Experimental Results (Fully Recrystallized State)

	Experiment		Simulation
TEXTURE (%)	neutrons	EBSP	(Type I)
cube	18	24	21
rolling	37	28	28
random	45	48	51
GRAIN SIZE (μm)		EBSP	
cube		53	49
rolling		34	34
random		28	32
all		33	34

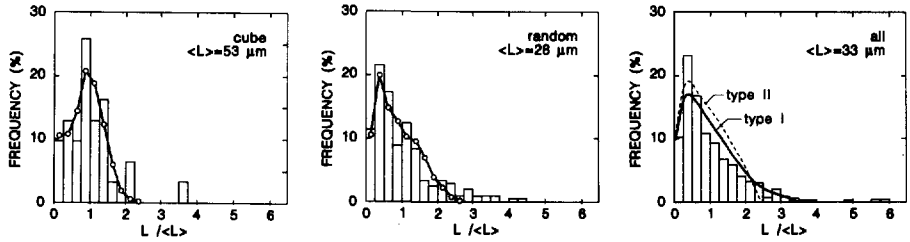

FIG. 4. Grain size distributions (linear intercept values). The histograms represent experimental EBSP data and the lines (solid and broken) represent simulated results.

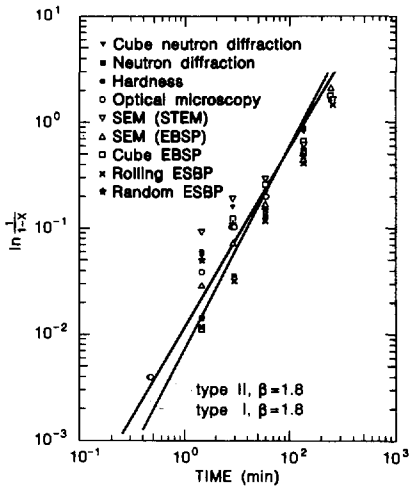

FIG. 5. Recrystallization kinetics, volume fraction recrystallized, X, versus annealing time. The lines are simulated results.

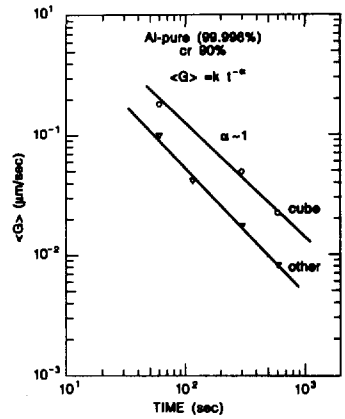

FIG. 6. The average growth rates of cube and random grains in pure aluminium.

Discussion

It has been shown experimentally that grains of different crystallographic orientations can grow with different rates (14). By modifying a computer code similar to that used by Mahin et al. (15) to allow for several texture components, it has been possible to introduce such texture effects and to model the recrystallization texture and average grain size of grains with different orientations. Good agreement between simulation and experimental results was obtained. The simulated grain size distribution is somewhat more narrow than the experimental one. Further consideration of the following may be needed: A) a further subdivision of the random component into specific texture components - note that the simulated/experimental agreement is not as good for random grains (see Fig. 4). B) a less random

distribution of nucleation sites - again this seems to be most important for the random grains. C) grain growth, in the sense that some large grains grow at the expense of smaller grains. Although the low annealing temperature (253°C) does not seem to support this argument, it has been observed experimentally that the nuclei/grain density decreased somewhat during annealing (14). D) finally a change in growth dimensionality from spherical to slightly elliptical (aspect ratio 1.5) may have some small effects on the simulated results.

The main effect of using 3 components in the simulation as opposed to 1, is to broaden the simulated grain size distribution. With 3 components, the maximum simulated grain size is 3.5 times the average grain size, whereas the corresponding value with 1 component is 2.5. Experimentally, the maximum size is 6 times the average.

It remains to be shown whether the general significance of texture effects is as great as observed in the present investigation. This may depend on the material and annealing conditions. However, the example demonstrated here is not unique as can be seen from Fig. 6, where the growth rates of cube and random grains in pure aluminium are shown.

An indication of significant texture effects is a broad grain size distribution and, in that case, whether grains of a specific orientation are large or small. From this data alone, it cannot be concluded whether it is a) growth effects b) orientation dependent inhomogeneous nucleation (eg. nuclei of one orientation being more clustered than others) or c) a combination of grown and nucleation effects which causes the broadening. Further measurements for example of growth rates are needed.

Conclusions

The crystallographic orientation can have significant effects on growth during recrystallization. This can be taken into account in the component model since grains of different orientations are treated separately. It was found that by using 3 components (= 3 orientations) and experimentally-determined growth rates, the recrystallization kinetics, texture and average grain size could be simulated very accurately. Further the agreement between experimental and simulated grain size distribution is significantly improved when 3 components are used in the model, instead of only one.

References

1. M. Avrami, J. Chem. Phys. 7, 1103 (1939).
2. A.D. Rollett, D.J. Srolovitz, R.D. Doherty, M.P. Anderson and G.S. Grest, In: Simulation and Theory of Evolving Microstructures. p. 103, Eds. M.P. Anderson and A.D. Rollett, TMS Warrendale (1990).
3. Ph. Tavernier and J.A. Szpunar, Acta metall. mater. 39, 549 (1991).
4. T. Furu, K. Marthinsen and E. Nes, Mat. Sci. Tech. 6, 1093 (1990).
5. R.A. Vandermeer and R.A. Musumura, Acta metall. 40, 877 (1992).
6. R.A. Vandermeer and B.B. Rath. In: Materials Architecture p. 589, Eds. J.B. Bilde-Sørensen et al., Risø, Roskilde (1989).
7. A.D. Rollett, D.J. Srolovitz, R.D. Doherty and M.P. Anderson, Acta metall. mater. 37, 627 (1989).
8. Ph. Tavernier and J.A. Szpunar, Acta metall. mater. 39, 557 (1991).
9. C.W. Price. Acta metall. mater. 39, 1807 (1991).
10. H.W. Hesselbarth and I.R. Göbel, Acta metall. mater. 39, 2135 (1991).
11. D. Juul Jensen and N. Hansen, In: Annealing Processes p. 379, Eds. N. Hansen et al., Risø, Roskilde (1986).
12. B. Bay and N. Hansen, Met. Trans. A 10A, 279 (1979).
13. D. Juul Jensen, N. Hansen and F.J. Humphreys, Acta metall. 33, 2155 (1985).
14. D. Juul Jensen, Scripta metall. mater. in press (1992).
15. K.W. Mahin, K. Hanson and J.W. Morris, Acta metall. 28, 443 (1980).

Textures and Microstructures, 1993, Vol. 20, pp. 55–65
Reprints available directly from the publisher.
Photocopying permitted by license only

AUTOMATIC EBSP ANALYSIS FOR RECRYSTALLIZATION STUDIES

D. JUUL JENSEN

Materials Department, Risø National Laboratory, DK-4000 Roskilde Denmark

The potential of local texture techniques for investigations of recrystallization are reviewed. The need for automatization of such techniques is discussed. It is shown how orientation measurements using one of these techniques, the electron back scattering pattern (EBSP) technique, can be made fully automatic.

KEY WORDS Recrystallization, image processing, EBSP.

1. INTRODUCTION

Traditionally, recrystallization has been studied using mostly microscopy and texture techniques. It has, however, proved to be very complicated to relate the microstructure development to the bulk texture results. Local texture techniques, which give information about the crystallographic orientation within selected areas of the microstructure can be used to link the microstructure to the bulk texture results and may thereby help to further the understanding of the recrystallization mechanisms.

2. LOCAL TEXTURE TECHNIQUES AND RECRYSTALLIZATION

2.1. *Techniques*

Several techniques may be used in the determination of the crystallographic orientation in selected local areas of the microstructure. Most of these techniques are electron microscopy techniques by which the microstructure is seen directly in the microscope and the orientation of individual subgrains/grains is determined from analysis of electron diffraction patterns. An overview of such techniques is given in Table 1.

The TEM techniques (Heimendahl, Bell and Thomas, 1964, Hirsch, Howie, Nicholson, Pashley and Whelan, 1965, Chapman and Stobbs, 1969, Ralph and Ecob, 1984, Humphreys, 1988) are characterized as having a very good spatial resolution, i.e. the crystallographic orientation of even small subgrains in highly deformed structures may be determined. TEM investigations are often limited by difficulties in preparing large areas of electron transparent material. However, new thinning techniques (Klepeis, Benedict and Anderson, 1988), as applied to semiconductor materials, may also give improved TEM foils in metals.

With the SEM techniques (Newbury and Yakowitz, 1975, Hall and Hutchinson, 1980, Dingley, 1981, Humphreys, 1988, Juul Jensen and Randle, 1989) large

Table 1 The main characteristics of three classes of local texture techniques

		Spatial resolution	*Angular accuracy*	
			Spot	*Kikuchi*
TEM	selected area diffraction	2 μm	2°	0.1°
	micro diffraction	20 nm	0.2°	0.1°
	convergent beam	2 nm	—	0.1°
TED	transmission electron diffraction (pole figures)	$\geq$5 μm	2°	
SEM	channeling	10 μm	0.5°	
	electron back scattering (EBSP)	1 μm	1°	

sample areas can be inspected routinely. However, the orientation of subgrains smaller than ~1 μm can not be determined, and fine details of the microstructure are not as well resolved as in the TEM.

The geometry of an X-ray transmission texture camera may be applied for transmission electron diffraction and a pole figure for a selected region (5 μm) can be obtained (Humphreys, 1983, Weiland and Schwarzer, 1984). The principle of this technique is to measure the diffracted intensity along an (*hkl*) Debye Scherrer ring, and to scan the tilting of the thin foil specimen from 0–60° to cover as large a part of the {*hkl*} pole figure as possible. Typically, the texture within 5–20 μm selected local regions of the microstructure is determined in this way (Humphreys, 1988). Once the pole figure measurement is completed, it is possible to identify elements in the microstructure corresponding to specific parts of the pole figure (Weiland, 1991a). This technique, in the following referred to as "TED", is ideal for measurements of all orientations within a selected region of the microstructure.

Other techniques, like the Kossel technique (Peters and Ogilvie, 1965, Bellier and Doherty, 1977, Dadson and Doherty, 1992) and synchrotron radiation techniques (Gottstein, 1988), have also been used to measure local crystallographic orientations. However, as no simultaneous information about the microstructure is obtained with these techniques, they will not be considered here.

2.2. *Recrystallization*

The three types of local texture techniques discussed above, the TEM, SEM and TED techniques, can each be used to address important aspects of the recrystallization process. In Table 2 the present potential of TEM/Kikuchi, TED and SEM/EBSP for the study of the various aspects of recrystallization are suggested. These aspects—nucleation, growth and recrystallized structure—will be discussed in the following.

Nucleation: Important questions which may be answered from the acquisition of local texture information are: i) What sites in the deformed microstructure are potential nucleation sites? ii) Is there a relationship between the nucleation site and the orientation of the nuclei? iii) What are the orientation relationships between a nuclei and the surrounding matrix?

Table 2 Potentials of 3 local texture techniques for studies of recrystallization

	TEM (*Kikuchi*)	*TED*	*SEM* (*EBSP*)
Nucleation	+	+	+
Growth	−	−	+
Recrystallized structure	−	−	+

It is very well known that two criteria must be fulfilled for a site to be a potential nucleation site (question i) (above); a large lattice misorientation is needed, and the driving force must be sufficient for the nucleus to grow. Also it is fully established that original grain boundaries, large second phase particles, transition bands and shear bands are nucleation sites (e.g. Doherty, 1980). However, it is not understood why for example only some of these sites become operational (e.g. only few nuclei develop along a grain boundary), why the nuclei may develop near but not at the transition band (Driver, 1992), or why some nuclei for no obvious reason stop growing very early in the recrystallization process (Bay and Hansen, 1979, Juul Jensen, Hansen and Humphreys, 1985, Humphreys and Juul Jensen, 1986). For studying this, it is of interest to measure the orientations of the individual deformation subgrains near the potential nucleation sites. For materials deformed to medium and high strain only the TEM techniques have the required spatial resolution, whereas for materials deformed to a low strain or by hot deformation, SEM/EBSP becomes important. Furthermore, TED and SEM/EBSP may be used for a spatially more coarse mapping of orientation distributions in the deformed structure, which may be used in the explanation of the limited growth of some nuclei.

All three types of techniques may also be used in studying question ii) and iii) above. The TEM techniques can give the most precise and detailed results to both questions. However, at present a serious draw back is the limited sample area in a typical thin foil and therefore the limited chance of finding nuclei. Furthermore, for studies related to question ii), the time involved in measuring all the individual orientations of nuclei and surrounding subgrains in the matrix may be overwhelming. For this the TED technique is clearly much more effective. With SEM it is straightforward to find, and to determine, the orientation of the nuclei. Due to recovery in the matrix during annealing to the start of nucleation, orientations of matrix subgrains can in general also be measured by EBSP (Hjelen, Ørsund and Nes, 1991). However, the microstructure is not so clearly resolved as in the TEM. For example it may be difficult to see whether a nucleus has developed at a transition band or if it is at an intragranular segment of a high angle grain boundary or a microband. As such it may be difficult to answer questions i) only using SEM. For a few particularly interesting nuclei, it may be valuable to locate the position of the nucleus in the SEM, and then produce a TEM foil from that region (Lindbo, 1991) and continue the investigation by TEM.

Growth. Important microstructure/texture questions are: i) How does the growth rate depend on the annealing time and does the growth rate and time dependence vary with the orientation of the grain? ii) Are there preferred orientation relationships between a growing grain and the matrix?

For studying the question i) the SEM/EBSP technique is very well suited since the size and orientation of the grains is easily determined. From a series of partly recrystallized specimens, the average growth rate G of each group of grain orientations may be determined using the equation (English and Backofen, 1964, DeHoff, 1968):

$$\frac{dX}{dt} = G \cdot A \tag{1}$$

where X is the volume fraction recrystallized, t is the time and A is the interfacial area separating recrystallized from unrecrystallized grains (the migrating boundary area).

Using this method, it is straight forward, but very time consuming, to determine statistically reliable results for the growth rates.

Question ii) is of course very difficult to answer. The local texture techniques considered here cannot be used for in-situ experiments and conclusions can therefore only be reached very indirectly.

Recrystallized structure local texture techniques may be used to study the following important questions i) Is there a relationship between the grain size and grain orientation? ii) What is the grain boundary geometry?

Also for these types of investigations the SEM/EBSP technique seems to be the most powerful (see Table 2), since the other techniques are restricted by the limited sample area.

The size and orientation of the grains may be determined by first measuring the size of a grain looking directly at the microstructure. Then the grain orientation may be determined from the corresponding EBSP pattern. This procedure requires a series of microscope manipulations and is therefore rather time consuming. A faster procedure is to stay in "EBSP-mode" and make line-scans by either moving the beam or the sample. When the pattern changes a new grain is reached. In this way the orientations are determined directly and linear intercept values for the grain sizes are obtained.

The potentials of SEM/EBSP for characterization of the grain boundary geometry are discussed elsewhere in these proceedings (Randle, 1992, Watanabe, 1992) and will not be considered here.

3. AUTOMATED TECHNIQUES AND EBSP

3.1. *Automated Techniques*

Reasonably fast and user-friendly procedures for semiautomatic analysis of the orientation patterns (Kikuchi, EBSPs etc.) are available for the local texture techniques discussed above (Venables, Harland and bin-Jaya, 1976, Carr, 1982, Schwarzer and Weiland, 1984, Dingley, Longden, Weinbren and Alderman, 1987, Schmidt, Bilde-Sørensen and Juul Jensen, 1991, Weiland 1991b). An important question is therefore, if it is worthwhile to develop fully automatic indexing procedures?

The answer to the question probably depends on the type of investigation in mind. For the recrystallization studies discussed above, the answer may be an equivocal yes. For example, for the TEM studies of the deformation microstruc-

ture and the SEM studies of nucleation, it is very important to locate precisely in the microstructure where for example the subgrain or nucleus is. A "blind" automatic scan through the structure would in general only give little relevant information. In these cases, it would be convenient to have an image processing procedure which directly could index a given pattern without the need for the operator to mark bands or poles. However, the extra time and effort required in marking the patterns using the semiautomatic procedures are in general of minor importance. For the SEM investigations of the growth rates and size-orientation relationships, on the other hand, line scans through the structure (in the EBSP mode) give the required information–the orientations, the sizes (linear intercept values) and the migrating boundary areas A (Eq. (1)) of the grains. It is of course possible to do such scans semiautomatically, but to collect statistically reliable data requires several days or often weeks of very exhausing work. Automatisation of the indexing of EBSP is thus clearly necessary. Such automation would not mean that a sample is placed in the SEM and the results come out directly. It is believed that for the investigations discussed, an initial microstructural inspection is always necessary. By this inspection, it is determined along which line or lines the scan should be made and what the appropriate step size is. The aim of the automation is then to develop a system, which, after calibration, allows automatic scanning along the predetermined line and determination of all orientations without any involvment of a human operator.

3.2. *Experimental Set-up*

The principles and experimental set-up for the EBSP technique are very well known (Dingley, 1981, 1984), and shall not be described here. However, it should be noted that the quality of the EBSPs depends strongly on the position in which the phospor imaging screen is placed in the SEM (Alam, Blackman and Pashley, 1954, Hjelen, 1990). This is illustrated in Figure 1. Here EBSPs taken with the phosphor screen mounted in the rear port (a standard commercial version of the EBSP set-up) and in the side port are shown. The difference in quality of the two patterns relates to the lower position of the screen relative to the sample when the side port is used (Figure 1b). Here the intensity of back-scattered electrons is higher, and the signal to noise ratio of the EBSP is therefore better. All following EBSP to be shown in this paper is taken with the phospor screen mounted in the side port.

3.3. *Automatic Indexing of EBSPs*

Several semi-automatic analysis procedures for the determination of crystallographic orientations from EBSPs are available (Dingley, Longden, Weinbren and Alderman, 1987, Schmidt, Bilde-Sørensen and Juul Jensen, 1991). Recently, work has been concentrated on developing image processing procedures by which the computer identifies elements (bands or poles) in EBSPs (Juul Jensen and Schmidt, 1990, Wright and Adams, 1991, Wright and Adams, 1992, Krieger Lassen, Juul Jensen and Conradsen, 1992). By combination of the two types of procedures, the analysis and image processing procedures, the indexing of EBSPs can be made fully automatic.

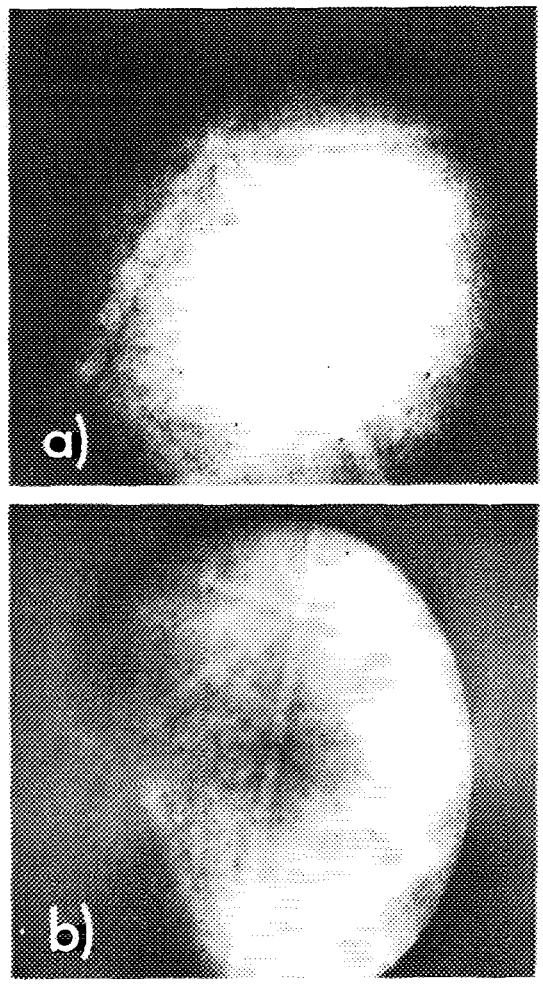

Figure 1 Typical EBSPs from aluminium a) Phosphor screen mounted in SEM rear port. b) Phosphor screen mounted in SEM side port.

Two such procedures are reviewed in the following:

1. Image processing: Computer identification of lines corresponding to bands in the EBSP (Krieger Lassen, Juul Jensen and Conradsen, 1992).

2. Analysis: Calculation of the crystallographic orientation based on the input of lines corresponding to bands in the EBSP (Schmidt, Bilde-Sørensen and Juul Jensen, 1991).

The two procedures have been shown to be very powerful in finding EBSP lines and indexing EBSPs, respectively. They are, however, not yet operating together. Indexing is thus not yet fully automatic, but it is discussed how this goal may be achieved.

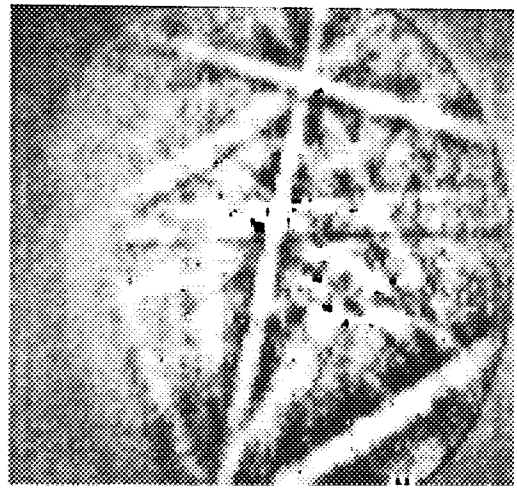

Figure 2 Reduced EBSP (corrected for background and reduced to 100×100 pixels) corresponding to Figure 1b.

Image processing The aim of this routine is to find lines corresponding to EBSP bands. First the original EBSP (see Figure 1b) is corrected for background and reduced to a 100×100 pixel picture by summation over 4×4 pixel squares in the original picture (only the central 400×400 parts of the original EBSP is considered). This reduction in the number of pixels significantly reduces the computer time needed later in the programme, and no important information is lost. The reduced picture corresponding to Figure 1b is shown in Figure 2.

The position of the bands in the reduced image is found using a Hough transform. The standard Hough transform (Hough, 1962) is designed to find lines in binary images. Each point, (x, y), in the picture different from zero is transformed to a sinusoidal curve

$$R = x \cos \theta + y \sin \theta \tag{2}$$

where θ is the range 0–180° (see Figure 3). If the points (x, y) lie on a straight line all the sinusoidal curves will intersect in a common point (R, θ) in the Hough space. The parameters R, θ describe the line (see Figure 3).

This simple procedure has to be somewhat modified to be optimal for finding lines in an EBSP picture (Figure 2). The EBSP picture is not binary, and too much information is lost in attempts to making it binary using various edge detection and thresholding techniques. Instead the EBSP picture is used as it is. Each pixel is transformed to the sinusoidal curve according to equation 2 with an intensity equal to the intensity of that pixel. This means, that an EBSP band will develop into a series of intense sinusoided curves which will intersect in a broad peak in the Hough space. The width of the peak depends on the width of the EBSP band. Figure 4 shows the result of this modified Hough transform.

Due to the nature of the Hough transform (Eq. 2) the peaks corresponding to lines of any width will be butterfly shaped (Van Veen and Groen, 1981, Leaves and Boyce, 1987). By using a butterfly filter the most intense points in the Hough

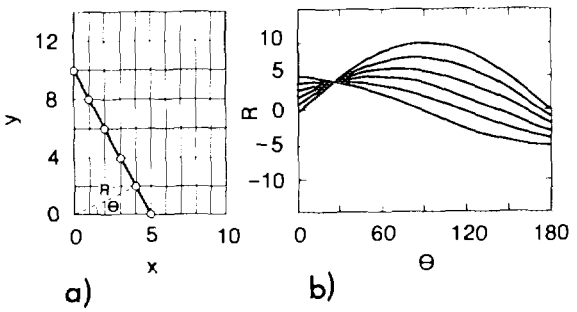

Figure 3 Principles of the Hough transform. a) straight line in the (x, y) image space. b) Hough curves of the (x, y) points in a) shown in the (R, θ) Hough space.

space (Figure 4) are enhanced and identified. The parameters of the lines corresponding to center lines of EBSP bands are calculated from these Hough points using the fact that EBSP bands cross in common poles (Krieger Lassen *et al.*, 1992). The result of this identification is shown in Figure 5. Here the computer identified lines are shown superimposed on the original EBSP. It can be seen that 15 lines have been identified. This very high number of correctly identified lines is typical. For a series of 25 EBSPs from commercially pure aluminium, from 12 to 16, lines were identified in the different patterns. On average 14 lines were found.

Compared to other image processing procedures used for EBSP analysis (Juul Jensen and Schmidt, 1990, Wright and Adams, 1991, Wright and Adams, 1992), the present procedure seems rather effective. It requires no a priori information about the sample or microscope conditions, it is relatively simple to implement and it finds a significantly larger number of EBSP bands. For further information about the routine, see Krieger Lassen *et al.* (1992).

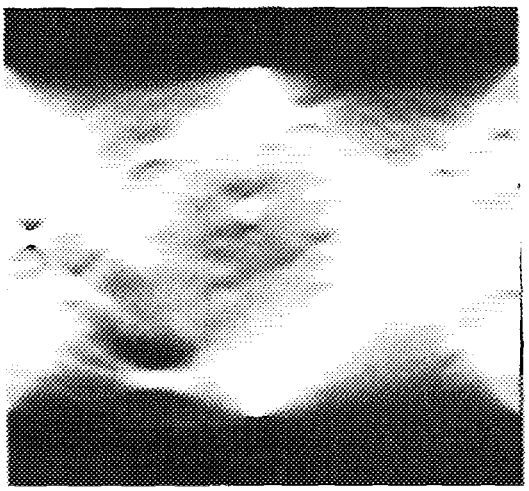

Figure 4 Peaks in the Hough space resulting from a modified Hough transform of Figure 1b.

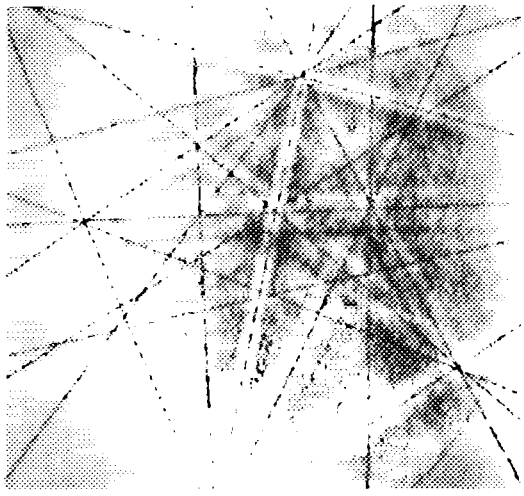

Figure 5 Lines identified by the image processing procedure (shown as dark lines) superimposed on the original EBSP (as in Figure 1b).

Analysis. The aim of this routine is to determine the crystallographic orientation from the input of lines corresponding to bands in the EBSP. Each EBSP band corresponds to crystal lattice plane (*hkl*), and the determination of the crystallographic orientation of the EBSP is, in the present programme, entirely based on a comparison of interplanar angles.

Before any EBSPs from a given sample material can be analysed, a reference table containing the interplanar angles characteristic for that sample material has to be created. Each table is based on input information about the number of atoms per unit cell (n), the atom positions (x_j, y_j, z_j) and the atomic form factor (f_j). The structure factor is calculated for all low index (*hkl*) reflections.

$$S(hkl) = \sum_{j=1}^{n} f_j(hkl) \exp\left(-i\,2\pi(hx_j - ky_j + lz_j)\right) \tag{3}$$

The diffracted intensity of an (*hkl*) EBSP band, is to a first approximation, proportional to $S(hkl) \times S^*(hkl)$ (Schmidt and Olesen, 1989).

Since only the strongest reflecting bands (bands with high values of $S(hkl) \times S^*(hkl)$) are seen in an EBSP (typically less than 100), the interplanar angles between these are calculated (Young and Lytton, 1972) and stored in the reference table. For a given material it is only necessary to calculate the reference table once.

For each experimental EBSP, two or more lines are identified (at present by an operator). These are transformed to a set of three dimensional planes, and the corresponding interplanar angles are calculated. By comparison with the angles in the reference table the most likely solution is calculated and the corresponding simulated EBSP is superimposed on the experimental EBSP. The operator can accept or reject the solution. If rejected other possible solutions are tested. When three bands, not intersecting in a common pole are used as input, the correct solution is obtained at the first attempt in 80% of the cases.

For further information about the procedure, see Schmidt *et al.* (1991).

For automated indexing, the next step is to use those lines identified by the Hough image processing procedure in the analysis procedure. Two approaches for doing this are considered:

One approach is to use three of the identified lines as input in the analysis calculation. Among the possible solutions, the correct one is selected by comparing the lines in the simulated EBSP to those found by the computer in the experimental EBSP. If *all* "experimental lines" correspond to one (and only one) of the simulated patterns, the solution is accepted. Another approach is directly to use all of the computer identified lines as input in the analysis calculation. In the latter case, the set of equations to calculate the orientation is largely overdetermined. A statistical estimation, taking into account the quality of the computer identified lines, is used to find a possible solution; only if this solution is unambigiously determined is the solution accepted.

4. CONCLUDING REMARKS

Microtexture techniques are powerful tools for studies of nucleation, growth of nuclei and the recrystallized structure. However, the time necessary to determine statistically reliable results is often a major problem. At present, work is underway to develop image processing procedures which automatically index EBSP patterns without the need for an operator to identify bands, poles etc. It is believed that during 1992 these routines will become as reliable as any of the semiautomatic procedures. Combined with computer controlled sample or beam movement, such routines will allow automatic orientation determinations. This will significantly improve the potential of the technique.

ACKNOWLEDGMENTS

N. Hansen, J. B. Bilde-Sørensen and N. C. Krieger Lassen are thanked for helpful discussions, and E. Sørensen for typing the manuscript.

References

Alam, M. N., Blackman, M. and Pashley, D. W. (1954). *Proc. Royal Soc.* A. **221,** 224–242.
Bay, B. and Hansen, N. (1979). *Met Trans.* A. **10A,** 279–288.
Bellier, S. P. and Doherty, R. D. (1977). *Acta met.* **25,** 521–538.
Carr, M. J. (1982). *JEOL News* **20E,** 35–37.
Chapman, P. F. and Stobbs, W. M. (1969). *Phil. Mag.* **19,** 1015–1030.
Dadson, A. B. C. and Doherty, R. D. (1992). *Acta metall. mater.* **40,** 345–352.
DeHoff, R. T. (1968). In *Quantitative Microscopy.* Eds. R. T. DeHoff and F. N. Rhines. McGraw-Hill NY 291–325.
Dingley, D. J., Longden, M., Weinbren, J. and Alderman, J. (1987). *Scanning Microsc.* **1,** 451–456.
Dingley, D. J. (1981). *Scanning Electron Microsc.* **1981 IV,** 273–286.
Dingley, D. J. (1984). *Scanning Electron Microsc.* **1984 II,** 569–575.
Doherty, R. D. (1980). *Recrystallization and Grain Growth of Multi-Phase and Particle Containing Materials.* Eds. N. Hansen *et al.*, Risø National Laboratory, Denmark 57–71.
Driver, J. (1992). In these proceedings.
English, A. T. and Backofen, W. A. (1964). *Trans. AIME* **230,** 396–407.
Gottstein, G. (1988). *ICOTOM* 8. Eds J. S. Kallend and G. Gottstein. TMS. Warrendale 195–202.

Hall, M. G. and Hutchinson, W. B. (1980). *Metallurgist* **12,** 371–375.
Heimendahl, M., Bell, W. and Thomas, G. (1964). *J. Appl. Phys.* **35,** 3614–3616.
Hirsch, P. B., Howie, A., Nicholson, R. B., Pashley, D. W. and Whelan, M. J. (1965). *Electron Microscopy of Thin Crystals* (Butterworth, London).
Hjelen, J. (1990). Thesis Universitetet Trondheim, 139 pp.
Hjelen, J., Ørsund, R. and Nes, E. (1991). *Acta Metall. Mater.* **39,** 1377–1404.
Hough, P. V. C. (1962). U.S. Patent 3 069.654 Dec. 18, 1962.
Humphreys, F. J. (1983). *Textures, Microstructures* **6,** 45–62.
Humphreys, F. J. (1988). *ICOTOM* 8. Eds. J. S. Kallend and G. Gottstein. TMS, Warrendale 171–182.
Humphreys, F. J. and Juul-Jensen, D. (1986). *Annealing Processes—Recovery, Recrystallization and Grain Growth.* Eds. N. Hansen *et al.*, Risø National Laboratory, Denmark 93–106.
Juul Jensen, D., Hansen, N. and Humphreys, F. J. (1985). *Acta metall.* **33,** 2155–2162.
Juul Jensen, D. and Randle, V. (1989). In *Materials Architecture,* Eds. J. B. Bilde-Sørensen *et al.*, Risø National Laboratory 103–126.
Juul Jensen, D. and Schmidt, N. H. (1990). *Recrystallization* '90. Eds. T. Chandra, TMS. Warrendale 219–224.
Klepeis, S. J., Benedict, J. P. and Anderson, R. M. (1988). *Specimen Preparation for Transmission Electron Microscopy of Materials.* Eds. Bravman *et al.*, MRS, Pittsburgh, 179–184.
Krieger Lassen, N. C., Juul-Jensen, D. and Conradsen, K. (1992). *Scanning Microscopy,* **6,** 115–121.
Leaves, V. F. and Boyce, J. F. (1987). *Image and Vision Computing* **5,** 161–166.
Lindbo, J. (1991). Risø private communication.
Newbury, D. E. and Yakowitz, H. (1975). In *Practical Scanning Microscopy.* Eds. Goldstein *et al.* (Plenum) 149–210.
Peters, E. T. and Ogilvie, R. E. (1965). *Trans. met. Soc. AIME* **233,** 89–95.
Ralph, B. and Ecob, R. C. (1984). *Microstructural Characterization of Materials by Non-Microscopical Techniques.* Eds. N. Hessel Andersen *et al.*, Risø National Laboratory, Denmark 109–129.
Randle, V. (1992). In these proceedings.
Schmidt, N. H., Bilde-Sørensen, J. B. and Juul Jensen, D. (1991). *Scanning Microscopy,* **5,** 637–643.
Schmidt, N. H. and Olesen, N. Ø. (1989). *Canadian Mineralogist* **27,** 15–22.
Schwarzer, R. and Weiland, H. (1984). *ICOTOM* 7. Eds. C. M. Brakman *et al.* Neth. Soc. Mat. Sci., Holland 839–843.
Van Veen, T. M. and Groen, F. C. A. (1981). *Pattern Recognition* **14,** 137–145.
Venables, J. A., Harland, C. J. and bin-Jaya, R. (1976). *Development in Electron Microscopy and Analysis.* Academic Press, London, 101–104.
Watanabe, T. (1992). In these proceedings.
Weiland, H. and Schwarzer, R. A. (1984). *ICOTOM* 7. Eds. C. M. Brakman *et al.* Neth. Soc. Maths. Sci., Holland 857–862.
Weiland, H. (1991a). Proc. 49th Ann. Meet. Elec. Micros. Soc. Am. 792–793.
Weiland, H. (1991b). Alcoa Technical Center Report DE. 56–91DE-9 pp. 36.
Wright, S. I. and Adams, B. L. (1991). *Metal. Trans.* In press.
Wright, S. I. and Adams, B. L. (1992). In these proceedings.
Young, C. T. and Lytton, J. L. (1972). *J. Appl. Phys.* **43,** 1408–1417.

Pergamon

0956-7151(95)00111-5

Acta metall. mater. Vol. 43, No. 11, pp. 4117–4129, 1995
Elsevier Science Ltd

0956-7151/95 $9.50 + 0.00

GROWTH RATES AND MISORIENTATION RELATIONSHIPS BETWEEN GROWING NUCLEI/GRAINS AND THE SURROUNDING DEFORMED MATRIX DURING RECRYSTALLIZATION

D. JUUL JENSEN

Materials Department, Risø National Laboratory, 4000 Roskilde, Denmark

(Received 20 June 1994; in revised form 2 February 1995)

Abstract—Average growth rates and misorientations between recrystallization nuclei (or grains) and neighbouring deformed matrix material have been studied for partially recrystallized samples by the electron back scattering pattern (EBSP) technique in heavily cold rolled aluminium and copper. It was studied how the annealing time and the crystallographic orientation of nuclei/grains affects the growth rates and distribution of misorientations. The two materials, aluminium and copper, develop a weak and a strong recrystallization cube texture respectively. Information about effects of cube texture strength was therefore also obtained. It was found that grains of cube orientation grow faster than grains of other orientations. A wide distribution of misorientation relationships was observed to exist between the growing grains and the neighbouring deformed matrix, and this distribution was not significantly affected by the annealing time. The faster growth of the cube oriented grains may be ascribed to a larger misorientation between cube grains and deformed matrix than that between other grains and the matrix.

1. INTRODUCTION

Growth of new grains in a deformed matrix during recrystallization is an integral part of thermomechanical processing. It is one of the basic processes that controls the microstructure and crystallographic texture, and may therefore significantly affect the mechanical properties of the material. It has long been discussed whether grains of certain crystallographic orientations grow preferentially. In the classic Beck experiments, where artificially nucleated new grains grow in deformed single crystal matrices, very clear evidence for oriented growth was observed [1–9].

More recently, several recrystallization experiments using deformed polycrystals have also shown oriented growth [10–12]. However, in other experiments, little or no oriented growth was observed [13–15]. In most of these polycrystal experiments, the conclusions about oriented growth were based either on simultaneous measurements of crystallographic orientations and size of recrystallized grains (i.e. are grains of a specific orientation larger than the other grains?) or on a comparison between nucleation and recrystallization textures. In the present work, average growth rates for grains of various orientations were measured directly, which eases the interpretation. For this, the Cahn–Hagel approach [16, 17] was used. It is a statistical approach, in which average growth rates of free, unimpinged boundaries can be determined throughout the entire recrystallization process for any nucleation distribution and nucleation rate. Optical microscopy was typically used for such measurements. However, by using modern electron back scattering pattern techniques, it is possible also to measure the grain orientation. Therefore such average growth rates can be determined for individual grain orientations [18].

Two heavily cold deformed polycrystalline materials, aluminium of commercial purity and pure copper, were chosen for the investigation because they, to a certain extent, resemble each other; in other aspects they are very different. The cold deformation microstructures and textures are of the same type [19] and both materials also develop cube texture upon recrystallization. However, the driving force for recrystallization is much larger and the cube texture is more than twice as strong in the copper than in the aluminium material.

A recrystallization nuclei/grain in a heavily deformed polycrystal during its growth meets very many different crystallographic orientations at various times and positions along its periphery. This means that the misorientation relationship between a grain and the deformed matrix is not characterized by a single set of misorientation parameters. In the present work, a statistical description of the misorientation distribution, representative for the entire sample, is obtained by measuring the misorientation between a nuclei/grain and the neighbouring deformed matrix at one point of the grain periphery for many nuclei/grains. Furthermore, the effects of annealing time, and crystallographic orientation of the nuclei/

Table 1. Overview of the alumimum samples together with the number of boundaries inspected and the average misorientation angles. The percentage of low, medium and high misorientations angles, and the percentages of rotation axes within zones I, II and III (see insert to Fig. 7) are also given

Annealing time (s)	X (%)	Scanning direction	No.	Misorientation angle Average	% 0–20	20–35°	>35°	Misorientation axis % I	II	III
120	1.7	RD	55	31.8	22	33	45			
		ND	59	35.0	17	36	47			
		RD + ND	114	33.5	19	34	47	26	39	35
300	5.8	RD	57	31.9	30	26	44			
		ND	66	35.4	20	24	56			
		RD + ND	123	33.8	24	25	50	19	48	33
600	10.3	RD	64	30.6	31	24	45			
		ND	58	36.6	21	22	57			
		RD + ND	122	33.4	25	24	51	19	37	43
1800	30.0	RD	36	26.5	38	22	38			
		ND	38	32.9	26	29	45			
		RD + ND	74	29.8	32	26	42	26	41	34
3600	72.2	RD	42	34.8	17	36	48			
		ND	36	40.0	11	17	72			
		RD + ND	78	37.2	14	27	59	29	39	32
7200	95.3	RD	3	25.2	33	33	33			
		ND	5	36.7	20	20	60			
		RD + ND	8	32.4	22	25	50	—	—	—
Σ all times	—	RD	257	31.2	28	28	44	30	39	31
		ND	262	35.9	19	26	55	20	42	38
		RD + ND	519	33.3	23	27	50	25	41	34

grains on such misorientation distributions are studied with the aim of correlating the data to the observed average growth rates.

2. EXPERIMENTAL

2.1. Materials

The aluminium material was of commercial purity (AA 1050) containing 0.32% Fe and 0.15% Si. It was prepared by DC casting, homogenization at 600°C, slow cooling, break down rolling and annealing. This starting material contained 0.5 vol.%, 1.7 μm eutectic particles. The average grain size was 100 μm. The starting texture was predominantly random with a small contribution from the cube orientation, $\{100\}\langle 001\rangle$, having a peak intensity of 2.4 × random [20]. For the recrystallization experiments the starting material was cold rolled to 90% reduction in thickness. The annealing of the specimens was done isothermally at 280°C in a molten tin bath. Six different annealing times in the range 2 min–2 h (see Table 1) were chosen to produce a series of partly recrystallized samples.

The copper material was 99.96% pure, the main impurities being Pb, As, Ni, Ag, Co and Fe. The initially cold drawn bars were sealed in glass tubes under 5 N argon gas and annealed at 450°C for $1\frac{1}{2}$ h. The average grain size was 35 μm. The samples were deformed by cold rolling to 92% reduction in thickness. The annealing was done isothermally at 121°C in a DSC-7 calorimeter made by Perkin Elmer. In total, 12 different samples annealed for various times in the range from 12.5 min to $2\frac{1}{2}$ h were prepared [21]. For the present investigations, ten of these samples were selected (see Table 2).

The bulk textures of both the Al and Cu samples were measured by neutron diffraction [22] and ODFs were calculated using the series expansion method [23].

2.2. EBSP measurements

For the EBSP investigations, the samples were mechanically polished down to 1 μm diamond paste, and finally electropolished in STRUERS A2 electrolyte for 30 s at a current of 2 A. The aluminium samples were inspected in the longitudinal plane section (the rolling direction, RD, and the normal

Table 2. Data as in Table 1 but here for copper

Annealing time (s)	X (%)	No.	Misorientation angle Average	% 0–20°	20–35°	>35°	Misorientation axis % I	II	III
750	2.0	110	33.3	27	22	51	22	38	40
1050	9.3	94	35.8	16	23	61	27	35	38
1200	34.3	75	36.1	17	23	60	30	31	39
2190	65.7	48	40.4	15	4	81	10	31	59
2670	57.4	26	42.4	8	19	73	12	35	54
3150	76.0	35	39.2	17	14	69	34	29	37
3300	70.8	39	36.4	18	26	56	21	38	41
4800	88.4	41	38.9	12	20	68	24	24	51
5100	90.4	43	32.7	28	16	56	14	47	38
7800	94.6	40	37.1	18	18	65	20	33	48
Σ all times	—	551	36.4	19	19	62	22	35	43

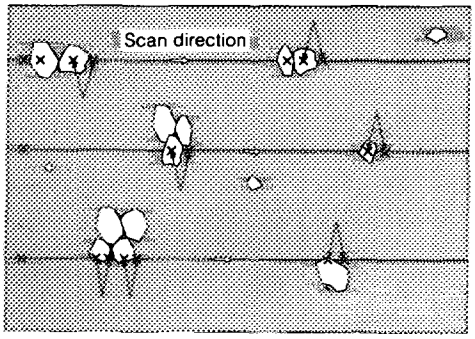

Fig. 1. Sketch of a partly recrystallized microstructure, grey areas indicate deformed matrix. Positions of EBSP orientation measurements are shown by "×". The double arrows mark sets of orientations from which misorientations are calculated.

direction, ND, section), whereas it was the rolling plane section RD and transverse direction, TD, which was studied in the copper samples.

The samples were mounted in an eucentric stage and inspected in a JEOL 840 SEM equipped with a phosphor screen and a CCD very-low-light camera mounted in the side port. The EBSP patterns were indexed using an automatic image processing procedure [24].

Each specimen was examined while it was manually traversed under the electron beam using a calibrated stage. Regions of deformed material were identified as regions with diffuse EBSPs with meandering crystallographic poles; whereas recrystallized regions (> 1 μm) have sharp patterns with stationary poles. Line scans were made along RD and ND in the aluminium samples and along RD and TD in the copper samples. Every time the pattern changed from a deformed to a recrystallized region or vice versa, or from one recrystallized orientation to another, the crystallographic orientation was determined. In Fig. 1, a sketch is given of where the orientations were measured, relative to the recrystallized grains.

The recrystallization appeared to happen fairly homogeneously throughout the samples of the aluminium material, whereas it was very heterogeneous in the copper material. For example, in a sample recrystallized 50%, one could find large areas which were close to 100 or 0% respectively [21]. Therefore long EBSP scans up to 20 mm, and many samples, were required for the copper investigation. The number of orientations measured in each of the partly annealed Al and Cu samples were in the range 200–350 and 250–750, respectively. In total 5697 orientations were determined for scans covering 9.16 cm in Cu and 4.96 cm in Al.

2.2.1. Determination of growth rates. A statistical method, originally suggested by Cahn and Hagel [16], was used to determine the average recrystallization growth rates. From the series of partly recrystallized samples, the spatially-averaged free interface velocity (or growth rate $\langle G \rangle$) was determined from

$$\frac{dX}{dt} = \langle G \rangle \cdot S_v$$

where X is the volume fraction of recrystallized material at annealing time t and S_v is the free/unimpinged surface area of the recrystallized nuclei/grains. As shown by Underwood [25], S_v can be determined statistically from line scans through the microstructure as $S_v = 2N_L$, where N_L is the number of intersections between recrystallized and deformed material. If also the crystallographic orientation of the recrystallized grains are determined, the method may be extended to also give average growth rates of grains with a given crystallographic orientation [18]. This is described in the Appendix.

From EBSP line scans through the microstructure of the partly recrystallized samples, as described in the section above, X, N_L and therefore $\langle G \rangle$ is directly determined provided a proper function for $X(t)$ is applied (see Appendix). The method is universal in the sense that there are no preassumptions about the nucleation or growth procedures; it applies also if the nuclei are clustered, if the nucleation continues during the recrystallization and/or if the growth is non spherical. And, as impingement between recrystallized grains is included, the method applies throughout the entire recrystallization process.

2.2.2. Determination of misorientation distributions. From sets of orientations like those marked by double arrows in Fig. 1, the misorientation between a recrystallized grain and the neighbouring deformed matrix is calculated. In other words, the misorientation is measured between a recrystallized nuclei/grain and one point of the neighbouring deformed matrix. This is done and for many nuclei/grains in two different scanning directions, a statistical description of the misorientation distribution is thus obtained. Alternatively, misorientation distributions can be obtained by measuring the orientation of the deformed matrix at many points around the single nuclei/grains. This clearly gives more detailed information about the misorientation situation for the single grains. However, due to the extended labour and measuring time required for this latter type of investigation, the number of nuclei/grains studied will be limited with the risk of only covering special nuclei/grains or sample areas. The present work aims at describing the misorientation generally for all grains or for all grains of a given crystallographic orientation, and does not focus on single selected grains. Therefore, the statistical approach with long line scans along the major sample axis were chosen. Furthermore, the data are used for comparison with average growth rates determined in the same statistical manner (see above) and not for evaluating the movement of single boundaries.

The misorientation results are expressed as angle-axis pairs; the minimum rotation angle among

the 24 equivalent solutions is selected. The recrystallized grains are classified according to their orientation; in aluminium as cube (within 15° from {100}⟨001⟩), rolling (within 15° from B: {110}⟨112⟩, S: {123}⟨634⟩ or C: {112}⟨111⟩) or random (any other orientation); and in copper as cube, cube-twin, rolling or random. This choice of orientation classes is based on the recrystallization texture developed in the two materials.

3. RESULTS

3.1. Texture and microstructure development

After cold rolling to 90% reduction, the two materials have typical copper type rolling textures [26]. The texture is somewhat stronger in the aluminium. In copper, some cube texture is still present (volume fraction of about 5%). Otherwise the two deformation textures are very similar. The cold deformed microstructures of both materials are typical deformation structures, which are subdivided by dislocation boundaries such as dense dislocation walls, microbands, lamellar bands and ordinary cell boundaries [27]. These boundaries are generally associated with large misorientations [12, 28, 29], hence large variations in crystallographic orientations exist in the deformed microstructure on a scale which is small compared to the recrystallized grain size. This is illustrated in Fig. 2, where the misorientation between neighbouring 1 μm areas is plotted vs position for 100 μm linear scans along RD and ND through the deformed aluminium microstructure. Note that the initial grain size before deformation was 100 μm; after deformation the grains will therefore on average be 1000 μm along RD and 10 μm along ND. This means that the many high angle misorientations ($>15°$) in Fig. 2(a) cannot be associated with original grain boundaries. In Fig. 3 the measured misorientations in the deformed matrix are plotted in histogram form. It can be seen that the deformed matrix contains a large fraction (>25%) of intergranular high angle dislocation boundaries, the distances between these are ≤ 5 μm and even within a very limited distance (<5 μm) inside an original grain, one may find several of the typical rolling components (e.g. Goss, B and S) [29].

After annealing to complete recrystallization at 280 and 121°C for aluminium and copper respectively, recrystallization textures as shown in Fig. 4 have developed. The aluminium texture contains a weak cube component plus retained rolling components whereas the copper texture is a strong cube plus cube twin texture. The volume fraction of "cube grains"—within 15° of the ideal cube orientation—is approx. 10 and 50 vol.% in the aluminium and copper respectively. The average recrystallized grain size is 12.1 and 7.5 μm in the Al and Cu, respectively.

The EBSP measurements on the partly recrystallized samples yield information about the development in grain size during recrystallization. In Fig. 5 the size of the grains with the different orientations is plotted as a function of annealing time in aluminium. It is seen that the cube grains grow to become the largest in the fully recrystallized state. This is similar to what has previously been found in another aluminium material annealed at a lower temperature [30]. Also, in the copper material, the cube grains grow to become larger than the random grains. In the fully recrystallized state the size of the cube grains is 1.6 times that of the random grains.

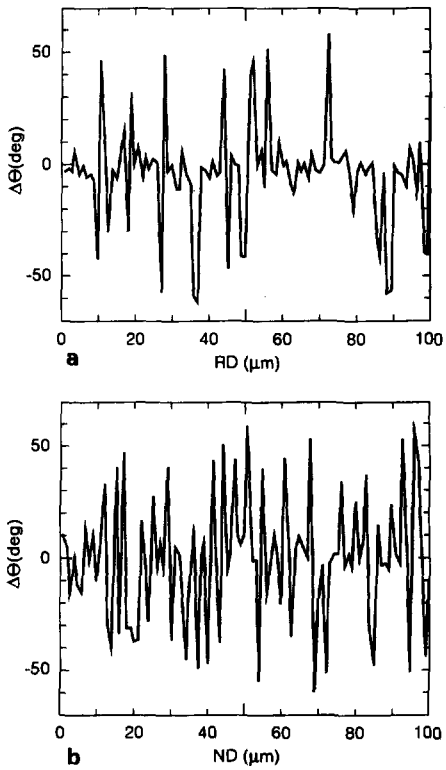

Fig. 2. Misorientation angle between neighbouring 1 μm areas is the aluminium deformed microstructure. The sign is determined from the corresponding rotation axis: if it is a right hand side triangle the sign is +, and −if it is in the left hand side. (a) Scan along RD; (b) scan along ND.

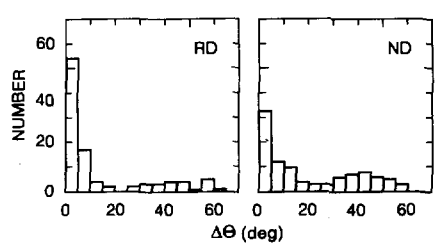

Fig. 3. Histograms showing the distributions of misorientations in the aluminium deformed microstructure in Fig. 2.

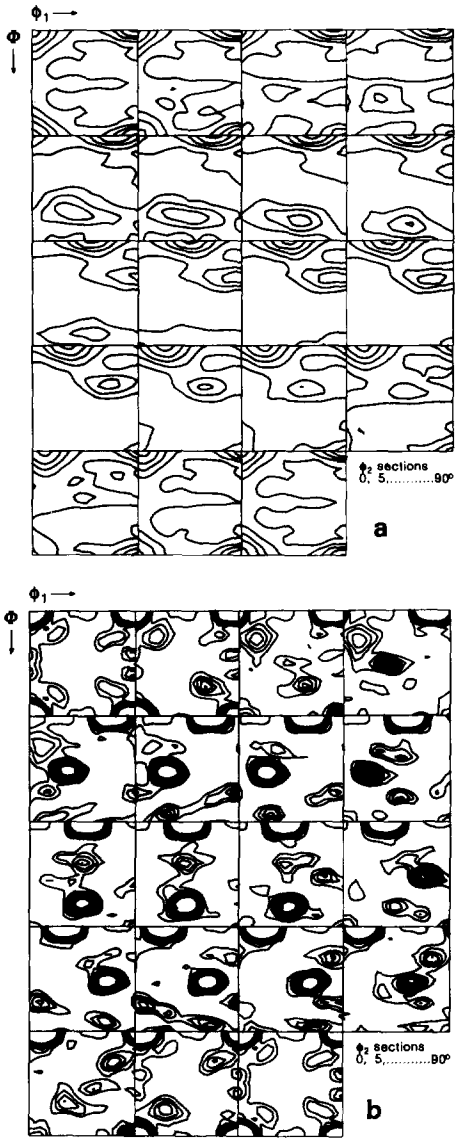

Fig. 4. Texture of the fully recrystallized specimens: (a) aluminium; (b) copper.

3.2. Growth rates

The average growth rates, G, of the grains of the different orientations were determined using the Cahn–Hagel approach [16, 17] (see the Appendix), and the G vs t curves are shown in Fig. 6. The experimental points are fitted to the equation [31]

$$G = k \cdot t^{-\alpha}$$

which gives a good fit to the data.

For both materials the cube grains grow faster than grains of other orientations. In the aluminium, the average growth rates of cube and other grains decrease with annealing time at almost identical rates ($\alpha \approx 0.5$ independently of grain type), and the cube grains always grow ~ 1.5 times faster than the random grains, and ~ 1.7 times faster than the rolling grains. In the copper, the growth rate of cube/twin grains decreases faster than that of the random grains during annealing; early in recrystallization ($t = 1000$ s, $X \approx 10\%$) $G_{\text{cube/twin}}/G_{\text{random}} = 2.5$, whereas later ($t = 5000$ s, $X \approx 90\%$) $G_{\text{cube/twin}}/G_{\text{random}} = 1.8$.

3.3. Orientation relationships

The misorientation angles are plotted as histograms and the rotation axes are plotted into unit stereographic triangles. Typical examples are shown in Fig. 7. The results show that as expected, a very wide variety of misorientation relationships exists between growing grains and the neighbouring deformed matrix for both aluminium and copper. Typically, the rotation axes cover the stereographic triangle fairly randomly and the rotation angles are in the whole range from 0° to 65°.

In Table 1 and Table 2 the average misorientation angles are listed together with the percentages of low (0°–20°), medium (20°–35°) and high (> 35°) angles for the two materials, respectively. The average misorientation angles are in the range 30°–37° in aluminium and 33°–42° in copper.

The misorientation axes were classified into three zones: I, II, III (see the insert to Fig. 7). The results are listed in Table 1 and Table 2, and show that the majority of axes are in zones II and III.

In the recrystallized state, the grains in aluminium were found to be equiaxed in the rolling plane section, whereas in the longitudinal plane section they were slightly elongated along RD with an aspect ratio (RD/ND) of 1.4. In Table 1 the results are therefore separated into two groups—scans along RD and ND respectively. The results show that the average misorientation angle is larger for ND than for RD scans. On average it is 35.9° along ND and 31.2° along RD. The misorientation axes cover the entire stereographic triangle for both types of scans.

In the copper material, the recrystallized grains were also found to be equiaxed in the rolling plane section. The misorientation results from EBSP scans along RD and TD were identical. In Table 2, therefore all results are summed without distinction of scanning direction.

3.3.1. Effect of annealing time. The annealing time does not seem to significantly affect the distribution of misorientation angles or rotation axes (some of the distributions are shown in Fig. 7). Both early and late in the recrystallization process, the distribution of misorientation angles is very wide, and there is no trend of any major changes in the distributions with time. This is illustrated for aluminium in Fig. 8. Here, the percentage of boundaries with low (< 20°) and high (> 35°) rotation angles are plotted vs annealing time (see also Table 1). It can be seen that the percentage of the two types of boundaries does not

change with annealing time. A similar result is observed for copper (see Table 2). A consequence of this is that also the average misorientation angle is independent of annealing time. A total average of 33.3° and 36.4° is observed for aluminium and copper respectively.

Also the distribution of rotation axis within the stereographic triangle is apparently independent of annealing time (see Fig. 7 and Table 1 and Table 2).

3.3.2. Effect of recrystallized grain orientation. For aluminium, the recrystallization nuclei/grains were classified according to their crystallographic orientation into three groups: cube, rolling (B + S + C) and random. "Random" is simply every orientation more than 15° outside cube and rolling. The same orientation groups plus cube twin were selected for the copper material. Since there are no significant effects of annealing time, the results to be shown in the following are summed over time, i.e. the results contain all the data measured for aluminium and copper respectively.

The misorientations to the deformed matrix for the grains of the different orientations are shown as histograms in Fig. 9. It can be seen that for both copper and aluminium, cube grains have larger and rolling grains smaller misorientations than the random grains. The average misorientations are listed in Table 3. Also, the distribution of misorientation axis is affected by the grain orientation. In Fig. 10, the percentages of boundaries within the three zones of the stereographic triangle (see insert to Fig. 7) are plotted. The percentages of high angle boundaries (>35°) relative to the total number of boundaries are also plotted in Fig. 10. The results show that cube and cube twin grains have the majority of the rotation axes in zone III, whereas the random grain axes are preferentially in zone II and the rolling grains have axes in all three zones. Furthermore, for the cube (and cube twin) grains, most of the misorientation axes in zone III also are of a large misorientation angle, whereas, for example for the rolling grains, many of the misorientation angles are low for the zone III axis.

4. DISCUSSION

The development of the recrystallization microstructure and texture depends on the nucleation and growth processes. In the present investigation the emphasis was on the growth aspects of recrystallization.

4.1. Preferential growth

The results clearly show that preferential growth is observed in the present experiment. In both aluminium and copper, the cube grains on average grow significantly faster than grains of other orientations. Further, as can be seen in Fig. 5, initially during the recrystallization process, the cube grains are of similar average size as the other grains. The faster growth rate of the cube grains is therefore not related to an initial size advantage of cube nuclei, but must be considered as a true selective growth effect. Also "microgrowth selection" [32, 33] can be excluded, as the growth advantage of the cube grains is observed during the entire recrystallization process.

The present observation that the cube grains grow faster is in agreement with earlier results for Al single crystals [34–39], as well as polycrystalline Cu [10, 11, 40] and Al [18, 30, 41–46]. However, in other polycrystalline Al investigations no preferential growth was observed [13–15, 47–49]. In the studies where preferential growth was excluded, but a cube

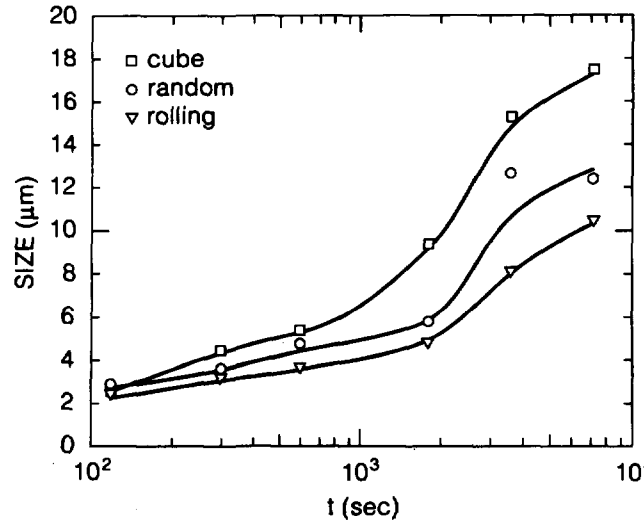

Fig. 5. The average size (linear intercept values) of grains with different orientations as a function of annealing time (aluminium).

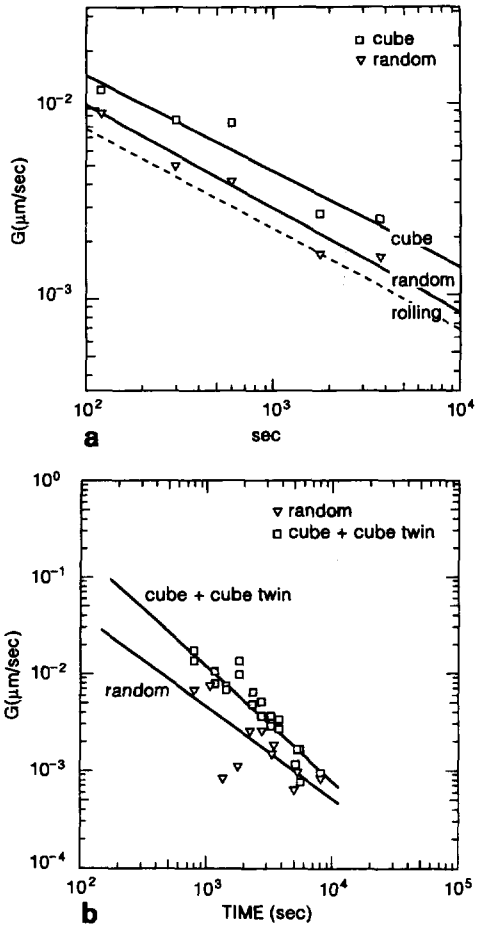

Fig. 6. The average growth rate of grains with different orientations as a function of annealing time. (a) Aluminium—for the rolling component, the experimental points are omitted, only the fitted line is shown by a broken line. (b) Copper—for the cube component two fit expressions to dX/dt were used (see Appendix), therefore the double set of experimental points per annealing time.

texture still develops upon recrystallization [13–15, 48, 49], it is remarkable that most of the materials are hot deformed. This would mean that the deformed microstructure in which the cube (and other) grains nucleate and grow may be different from those in the cold rolled materials. Weiland and Hirsch [50] and Vatne *et al.* [48] found that in hot deformed aluminium, bands of cube orientation (cube bands) are present even after large deformation, and that cube nuclei are formed in these cube bands [51, 52]. The cube bands are typically 1–5 μm wide, and can be quite close to each other (e.g. 10 μm apart) [53]. It is at present not clear how the presence of cube bands in the deformed microstructure and cube nucleation in cube bands affect the growth possibilities of these cube grains. However, it seems clear that when a cube nuclei is formed in a cube band it will be partly surrounded by cube oriented deformed materials and during its growth it will meet other cube bands. This may reduce the overall average cube growth rate because of the low mobility of such low angle boundaries.

In the present Al material, no cube bands were observed in the deformed microstructure, and cube nuclei were found to predominantly have B $\{110\}\langle 112\rangle$ and random oriented neighbouring material early in the recrystallization process (< 10% recrystallized).

4.2. Boundary mobility orientation dependence

Barrett [54] first made the suggestion that the grain boundary mobility depends on the orientation relationship between the growing grain and the surrounding matrix material. In the classical Beck experiment [2] this was studied, following the growth of artificially created nuclei of all orientations in a well characterized, deformed single crystal matrix. It was generally found that the fastest growing grains have a misorientation very close to 40° around a $\langle 111\rangle$ axis to the deformed matrix [1–6, 55]. In the present investigation the misorientations between recrystallized nuclei/grains and the surrounding deformed matrix were determined for a series of partly recrystallized polycrystalline Al and Cu samples. The results show that the distribution of misorientation angles and axes are very broad and that very few boundaries (<0.5%) have the 40° $\langle 111\rangle$ misorientation. Practically all possible rotation angles and axes were observed. This is the situation for both cube and grains oriented differently, and yet the cube grains are observed to grow faster than the other grains.

The difference in the two types of misorientation distributions, the sharp 40° $\langle 111\rangle$ and the present broad ones, relate to the distribution of orientations in the deformed matrices. In the Beck experiments the deformed matrices are single crystals, and even in the case where the single crystal is heavily deformed, the texture of the deformed crystal is very narrow [2, 55]. A growing grain will therefore meet a fairly homogeneous orientation distribution. In heavily deformed polycrystals, however, the deformed matrix is very turbulent, containing many different orientations even in a limited area (see Fig. 2 and Fig. 3). When a nuclei is formed in such a matrix it is therefore already surrounded by deformed matrix of different orientation at various places along its periphery. During the growth, the nuclei will meet matrix materials which are very differently oriented at different parts of its boundary and at different annealing times. This is illustrated in Fig. 11, where imaginary nuclei are shown superimposed on a sketch of the deformed microstructure of 90% cold rolled aluminium. The deformation microstructure is subdivided by dislocation boundaries such as

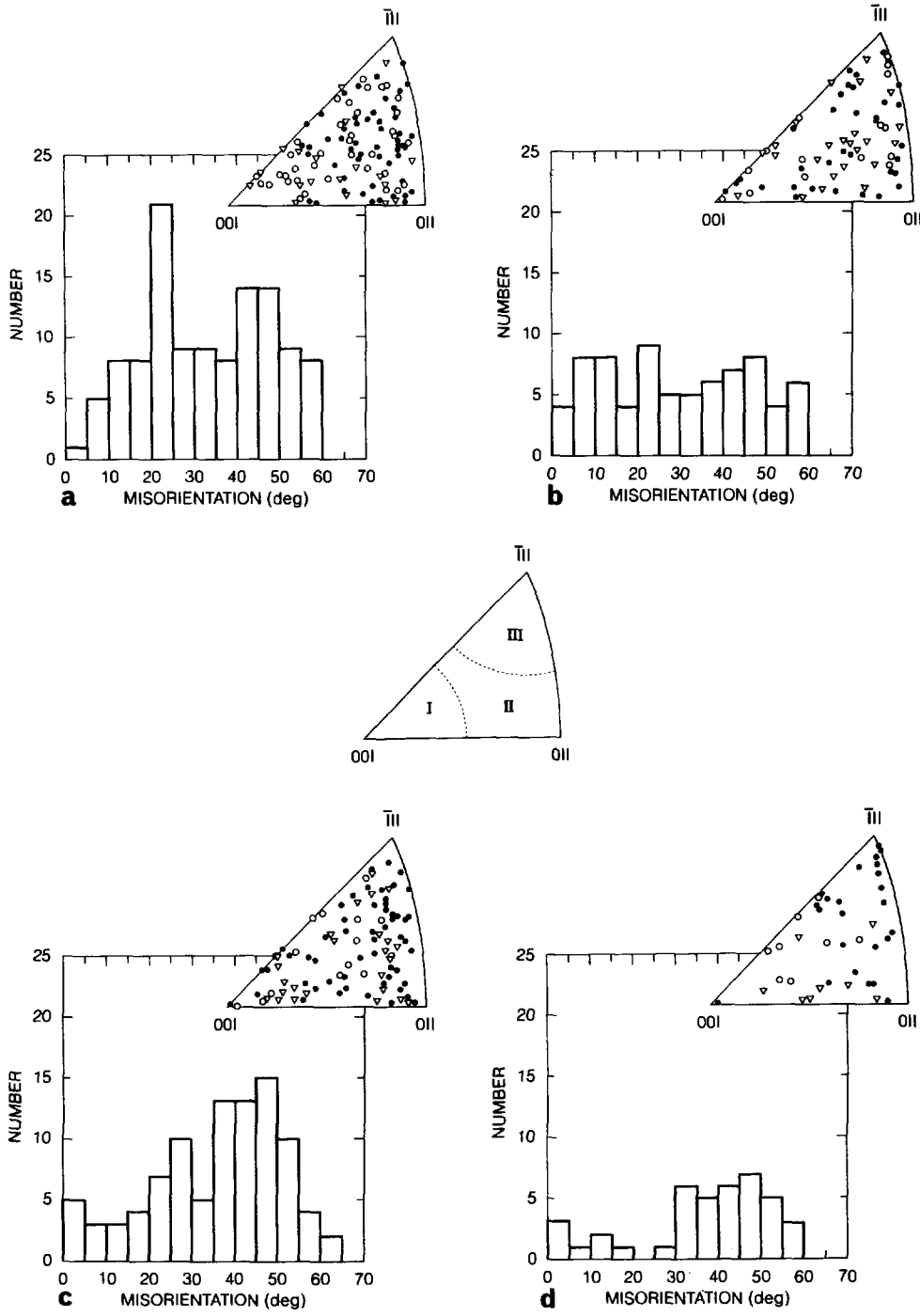

Fig. 7. Misorientations between growing nuclei/grains and the deformed matrix. The misorientation angles are shown as histograms and the axes are shown in unit stereographic triangles. Different signatures are used for axes with different misorientation angles: ● boundaries with high misorientation $\theta \geq 35°$, ▽ medium misorientation $20° \leq \theta < 35°$ and ○ low misorientations $\theta < 20°$. (a) Al annealed 120 s ($X = 2\%$). (b) Al annealed 180 s ($X = 30\%$). (c) Cu annealed 750 s ($X = 2\%$). (d) Cu annealed 7800 s ($X = 95\%$). For explanation of the insert see text.

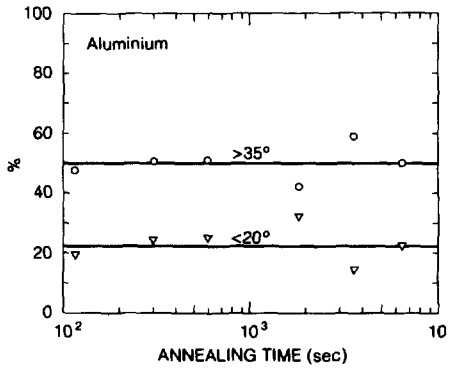

Fig. 8. Percentage of boundaries with low ($\theta < 20°$) and high misorientation ($\theta \geq 35°$) angles as a function of annealing time (aluminium).

microbands, lamellar bands and subgrain boundaries (see Fig. 11) which typically, at these high strains, are associated with large misorientations as well as ordinary cell boundaries. The intergranular high angle dislocation boundaries are typically less than 5 μm apart (see Fig. 2 and Fig. 3). Due to the large local orientation variations in the deformed matrix, the misorientation distribution between the nuclei/grains and the surrounding matrix must therefore, in heavily cold deformed polycrystals, be broad and not sharp, for example 40° ⟨111⟩, rotation. This is the situation for all nuclei/grains, also the faster growing cube ones. The assumption that 40° ⟨111⟩ rotations can explain preferential growth does therefore not apply to heavily deformed polycrystals. (Here it is chosen to use the term "preferential growth" for the faster growth of the cube grains, as the more usual "oriented growth" often is associated with a 40° ⟨111⟩ misorientation relationship.)

Other reasons for the observed preferential growth of the cube grains in the present materials must therefore be sought. When the misorientation distributions of the cube, rolling and random grains are compared (Fig. 9), it is clear that there is a difference in the fraction of low angle ($< 15°$) boundaries. The cube grains have few ($\leq 10\%$) and the rolling grains have many ($\geq 30\%$) of these types of boundaries. This could, at least in part, be the explanation for the preferential cube growth, as it is generally observed that the mobility of low angle boundaries is low. In deformed Al single crystals it was, for example, observed that the growth rate of boundaries with misorientation below 15°–20° (twist) or 10° (general boundaries) were close to zero (this was also the case for near first order twin boundaries), whereas other boundaries had a growth rate of 1–5 cm/s [56]. If it is assumed that the low angle boundaries on average move 10 times as slowly as other boundaries, this would in the present case result in an average growth advantage of cube relative to rolling grains of ~ 1.3.

4.3. Time dependence

It is observed that the growth rate of grains of any orientation decreases with annealing time throughout the entire recrystallization process in both aluminium and copper (see Fig. 6). This agrees with earlier observations [31]. It could be expected that this decrease may relate to changes in misorientation between the recrystallized nuclei/grains and the surrounding deformed matrix. The results, however, show that there are no significant effects of time on the misorientation distributions. It has also been suggested that the stored energy in the deformed material can be inhomogeneously distributed [57]. This would mean that the areas of highest stored energy recrystallize first and the recrystallization kinetics will change with annealing time [57]. However, as it should be expected that different levels of stored energy relate to grains of different initial orientations, the misorientation between the recrystallized grains and the deformed matrix should also change during the recrystallization. This seems not to be the case. In another investigation, the present EBSP copper data were compared to results of stored energy measurements [21]. Also in that investigation it was concluded that the stored energy could not be very inhomogeneously distributed. Extensive TEM studies of deformed aluminium also revealed that the deformation microstructure—cell size, average misorientation etc.—(and therefore the stored energy) is not very different from area to area.

Yet other explanations for the decreasing growth rates have to be sought. One of these could be recovery taking place simultaneously with recrystallization [58–60]. Investigations of the effects of heating rate on the growth rates are presently being carried out in an attempt to clarify this.

4.4. Recrystallized microstructure and texture

Both materials studied have cube texture in the recrystallized state. In the aluminium the cube texture is medium strong, whereas in the copper it is very strong. In the aluminium the strength of the cube texture relates to the preferential growth of the cube nuclei/grains. Whereas in the copper, which has about the same preferential growth behaviour as the aluminium, the stronger cube/twin texture is due to many more cube/twin nuclei than in the aluminium and than would be expected from random nucleation. The strong cube texture in the copper material is therefore a consequence of both preferential nucleation and growth.

The recrystallized grain size distributions in the two materials are fairly broad. The maximum grain size is respectively 3.7 and 3.9 times the average size in aluminium and copper. Preferential growth can clearly cause large size variations of the recrystallized grains [61]. Furthermore, if the material has a constant nucleation rate (in contrast to site saturation) or if the nucleation sites are inhomogeneously distributed in

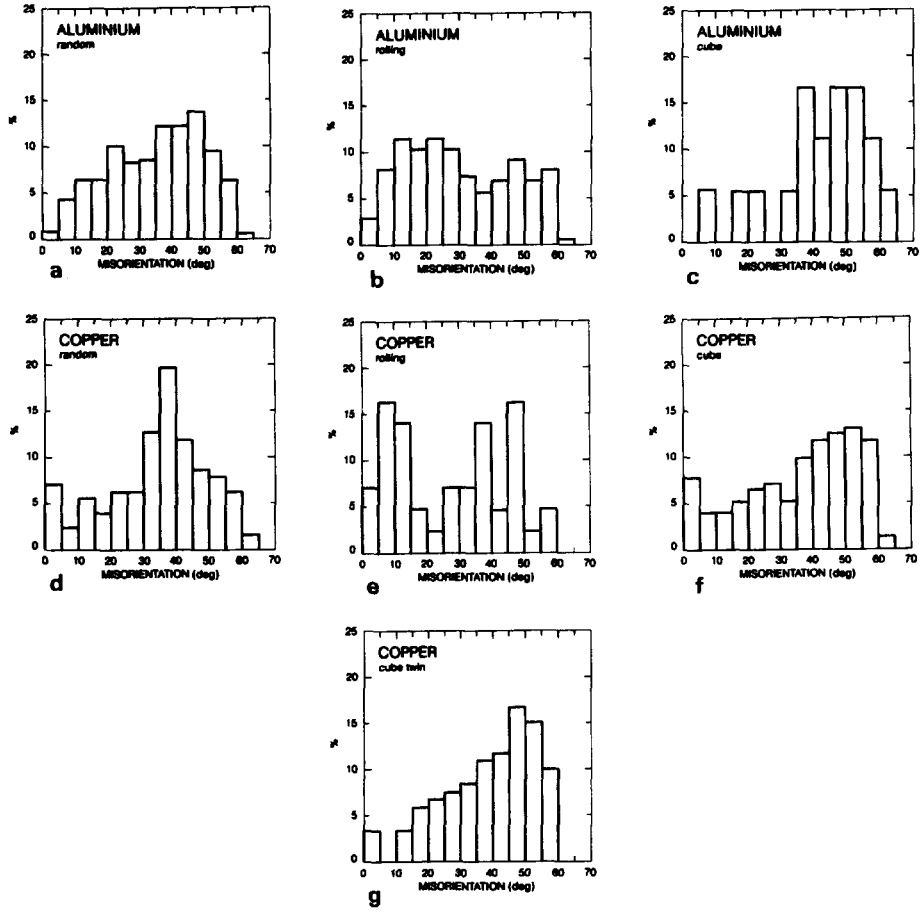

Fig. 9. Misorientation angles between growing nuclei/grains of various orientations and the deformed matrix. The data include all annealing times. (a) Al random grains. (b) Al rolling grains. (c) Al cube grains. (d) Cu random grains. (e) Cu rolling grains. (f) Cu cube grains. (g) Cu cube twin grains.

the microstructure, the grain size distribution will further widen.

In order to simulate a recrystallization behaviour, as observed in the present materials, where different texture components behave differently, it is clearly necessary to develop models that treat the individual components separately. Models of this type are starting to appear [61–63].

5. CONCLUSIONS

Growth rates and the orientation relationships between nuclei/grains and the surrounding deformed matrix have been studied for partially recrystallized heavily deformed aluminium and copper by the electron back scattering pattern technique. With this technique, it is possible to scan large sample areas and obtain results which are statistically significant for the entire sample. It was found that:

Table 3. Average misorientation angles in degrees for grains/nuclei of various orientations

	Aluminium	Copper
Random	35.1	34.2
Rolling	29.8	27.6
Cube	41.7	36.1
Cube twin	—	38.6

- In both aluminium and copper, the average growth rate of the cube grains is higher than that of the other grains. In aluminium it is ~1.5 times higher than that of the random grains throughout the entire recrystallization process. In copper, the growth advantage of the cube grains is found to decrease during the anneal, but the cube growth rate is always higher than that of the random grains. These faster growth rates relate well with the fact that the cube nuclei/grains have a lower volume fraction of low angle boundaries to the neighbouring deformed matrix than the other grains have.
- Misorientation distributions between recrystallized grains and the neighbouring deformed matrix are

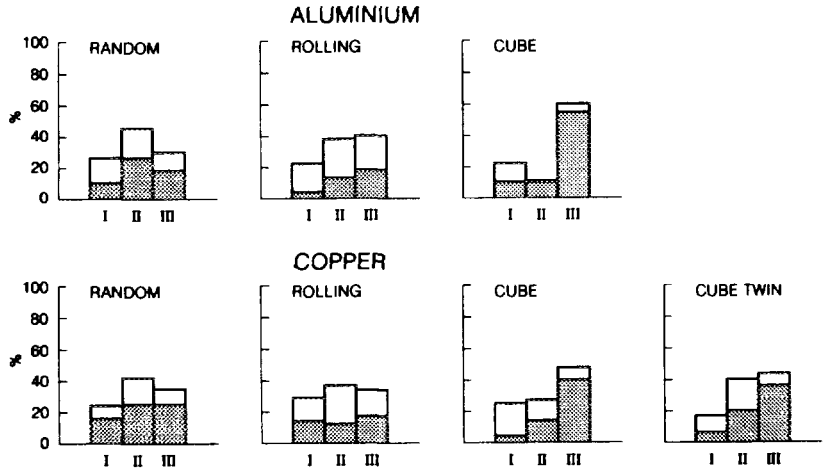

Fig. 10. Percentage of misorientation axes in the three zones (see Fig. 7) of the stereographic triangle for nuclei/grains of the various orientations. Data corresponding to Fig. 9. The percentage of high angle boundaries ($\theta \geq 35°$) relative to the total number of boundaries is shown in dark.

very broad, with no sharp preferred orientation relationships. This is due to the fact that the deformation microstructure of heavily cold deformed polycrystals is very turbulent with many intergranular high angle dislocation boundaries (typically less than 5 μm apart). The annealing time does not seem to affect the misorientation distributions significantly.

• The preferential growth of cube oriented grains can explain the strength of the recrystallization cube texture in aluminium. In copper, the strong cube recrystallization texture relates to a combination of the development of many cube nuclei and preferential growth of these.

Acknowledgements—Dr Niels Hansen and Dr Roy A. Vandermeer are thanked for fruitful discussions and important input to this work. The copper samples were provided by Dr Erik Woldt of the Technical University of Braunschweig, Germany and the aluminium starting material was prepared by Hydro Aluminium, Sunndalsøra, Norway and ALCAN International Ltd, Banbury, U.K. as part of a Brite/Euram project BREU-CT91-0399.

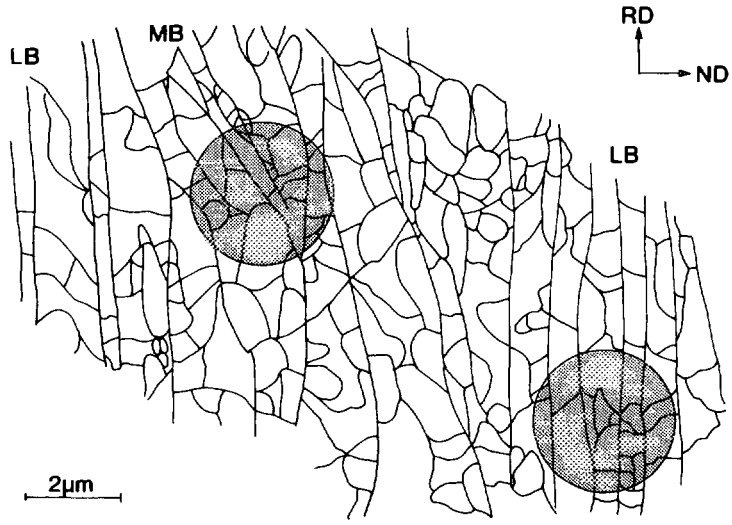

Fig. 11. Sketch illustrating the deformed microstructure in 90% cold rolled aluminium. Areas with microbands and lamellar bands are marked MB and LB respectively. Imaginary nuclei are shown in grey superimposed on the deformation microstructure.

REFERENCES

1. P. A. Beck, P. R. Sperry and H. Hu, *J. appl. Phys.* **21,** 420 (1950).
2. S. Kohara, M. N. Parthasarathi and P. A. Beck, *Trans. AIME* **212,** 875 (1958).
3. M. N. Parthasarathi and P. A. Beck, *Trans. AIME* **221,** 831 (1961).
4. B. Liebmann, K. Lücke and G. Masing, *Z. Metallk.* **47,** 57 (1956).
5. H. Yoshida, B. Liebmann and K. Lücke, *Acta metall.* **7,** 51 (1959).
6. G. Ibe and K. Lücke, in *Recrystallization, Grain Growth and Textures* (edited by H. Margolin), p. 434. Am. Soc. Metals, Materials Park, Ohio (1966).
7. K. T. Aust and J. W. Rutter, *Trans. AIME* **215,** 119 (1959).
8. K. T. Aust and J. W. Rutter, *Trans. AIME* **218,** 50 (1960).
9. K. T. Aust and J. W. Rutter, *Trans. AIME* **224,** 111 (1962).
10. K. Sztwiertnia and F. Haessner, in *Recrystallization* '90 (edited by T. Chandra), p. 535. TMS, Warrendale, Pa (1990).
11. K. Sztwiertnia and F. Haessner, *Text. Microstruct.* **14–18,** 641 (1991).
12. A. Böttcher, M. Hastenrath, K. Lücke and J. Hjelen, *ibid.* Ref. [11], p. 673.
13. J. Hjelen, R. Ørsund and E. Nes, *Acta metall. mater.* **39,** 1377 (1991).
14. O. Daaland, P. E. Dronem, H. E. Vatne, S. E. Naess and E. Nes, *Mater. Sci. Forum.* **113–115,** 115 (1993).
15. R. D. Doherty, K. Kashyap and S. Panchanadeeswaran, *Acta metall.mater.* **41,** 3029 (1993).
16. J. W. Cahn and W. C. Hagel, in *Decomposition of Austenite by Diffusional Processes* (edited by Z. D. Zackey and H. I. Aaronson), p. 131. Interscience, New York (1960).
17. J. E. Hilliard, *ibid.* Ref. [6], p. 267.
18. D. Juul Jensen, *Scripta metall. mater.* **27,** 533 (1992).
19. T. Leffers and N. Hansen, *Proc. 10th Risø Int. Symp. on Metallurgy and Materials Science, Materials Architecture* (edited by J. B. Bilde-Sørensen *et al.*), p. 127. Risø, Roskilde (1989).
20. D. Juul Jensen, R. K. Bolingbroke, H. Shi, R. Shahani and T. Furu, *Mater. Sci. Forum* **157–162,** 1991 (1994).
21. E. Woldt and D. Juul Jensen, *Metall. Trans A.* Accepted.
22. D. Juul Jensen and J. K. Kjems, *Text. Microstruct.* **5,** 239 (1983).
23. H. J. Bunge, *Mathematische Metoden der Texturanalyse.* Akademie, Berlin (1969).
24. N. C. Krieger Lassen, D. Juul Jensen and K. Conradsen, *Scan Microsc.* **6,** 115 (1992).
25. E. E. Underwood, in *Quantitative Microscopy* (edited by R. T. Dehoff and F. N. Rhines), p. 589. McGraw-Hill, New York (1968).
26. K. Lücke, *Proc. ICOTOM* 6 (edited by S. Nagashima), p. 14. Iron and Steel Institute, Japan (1981).
27. B. Bay, N. Hansen, D. A. Hughes and D. Kuhlmann-Wilsdorf, *Acta metall. mater.* **40,** 205 (1992).
28. J. H. Driver, D. Juul Jensen and N. Hansen, *Acta metall. mater.* **42,** 3105 (1994).
29. D. A. Hughes and N. Hansen, submitted for publication.
30. D. Juul Jensen, N. Hansen and F. J. Humphreys, *Acta metall.* **33,** 2155 (1985).
31. A. T. English and W. A. Backofen, *Trans. AIME* **230,** 396 (1964).
32. B. J. Duggan, K. Lücke, G. Köhlhoff and C. S. Lee, *ibid.* Ref. [14], p. 121.
33. H. E. Vatne and E. Nes, *Scripta metall. mater.* **30,** 309 (1994).
34. M. G. Ardakani and F. J. Humphreys, *Acta metall. mater.* **42,** 763 (1994).
35. A. W. Bowen, M. G. Ardakani and F. J. Humphreys, *ibid.* Ref. [20], p. 919.
36. M. Blicharski, J. Liu and H. Hu, *ibid.* Ref. [14], p. 109.
37. A. Akef, R. Fortunier, J. H. Driver and T. Watanabe, *ibid.* Ref. [11], p. 617.
38. J. F. Butler Jr, M. Blicharski and H. Hu, *ibid.* Ref. [11], p. 611.
39. P. Haasen, *Scripta metall. mater.* **27,** 1477 (1992).
40. F. Haessner and K. Sztwiernia, *Scripta metall. mater* **27,** 1545 (1992).
41. J. Hirsch, *ibid.* Ref. [57], p. 349.
42. J. Hirsch and K. Lücke, *ibid.* Ref. [57], p. 361.
43. J. Hirsch and K. Lücke, *Acta metall.* **33,** 1927 (1985).
44. O. Engler and K. Lücke, *ibid.* Ref. [40], p. 1527.
45. E. Nes and J. K. Solberg, *Mater. Sci. Technol.* **2,** 19 (1986).
46. D. Juul Jensen, *ibid.* Ref. [14], p. 335.
47. F. Habiby and F. J. Humphreys, *Scripta metall. mater* **30,** 787 (1994).
48. H. E. Vatne, O. Daaland and E. Nes, *ibid.* Ref. [20], p. 1087.
49. H. Weiland, T. N. Rouns and J. Liu, *Z. Metalk.* To be published.
50. H. Weiland and J. R. Hirsch, *ibid.* Ref. [11], p. 647.
51. I. Samajdar, R. D. Doherty, S. Panchanadeeswaran and K. Kunze, *ibid.* Ref. [20], p. 2025.
52. H. E. Vatne, T. Furu and E. Nes, submitted for publication.
53. O. Daaland, Ph.D. thesis, NTH, Trondheim (1993).
54. C. S. Barrett, *Trans. AIME* **137,** 128 (1940).
55. S. Kohara, M. N. Parthasarathi and P. A. Beck, *J. appl. Phys.* **29,** 1125 (1958).
56. C. D. Graham Jr and R. W. Cahn, *Trans. AIME J. Metals*, p. 517 (1956).
57. R. D. Doherty, A. R. Rollett and D. J. Srolovitz, *Proc. 7th Risø Int. Symp. on Metallurgy and Materials Science, Annealing Processes—Recovery, Recrystallization and Grain Growth* (edited by N. Hansen *et al.*), p. 53. Risø, Roskilde (1986).
58. R. A. Vandermeer and P. Gordon, in *Recovery and Recrystallization of Metals* (edited by L. Himmel), p. 211. Interscience, New York (1963).
59. B. B. Rath, R. J. Lederich, C. F. Yolton and F. H. Froes, *Metal. Trans.* **10A,** 1013 (1979).
60. C. W. Price, *Acta metall.* **38,** 727 (1990).
61. D. Juul Jensen, *ibid.* Ref. [40], p. 1551.
62. Ph. Tavernier and J. A. Szpunar, *Acta metall. mater.* **39,** 549 (1991).
63. R. A. Vandermeer and D. Juul Jensen, *Acta metall. mater.* **42,** 2427 (1994).
64. R. A. Vandermeer and B. B. Rath, *ibid.* Ref. [19], p. 589.
65. C. T. Necker, R. D. Doherty and A. D. Rollett, *ibid.* Ref. [11], p. 635.
66. R. A. Vandermeer and D. Juul Jensen, *Scripta metall. mater.* **30,** 1575 (1994).

APPENDIX

Calculation of average growth rates of free unimpinged boundaries

A methodology to determine average interface velocities in solids undergoing diffusional phase transformation was suggested by Cahn and Hagel [16], and the procedure is very well suited for the determination of average growth rates during recrystallization [17, 18, 31, 64–66]. The spatially-averaged free interface velocity or growth rate $\langle G \rangle$ is given by

$$\langle G \rangle = \frac{1}{S_v} \frac{dX}{dt} \tag{A1}$$

where dX is the increase in volume fraction of recrystallized material during a short annealing interval dt, and S_v is the interfacial area per unit volume separating recrystallized and deformed material, i.e. the migrating interfacial area.

For a series of partly recrystallized samples, X, S_v can be determined from line scans through the microstructure [25]

$$S_v = 2N_L \tag{A2}$$

where N_L is the number of intersections (between deformed and recrystallized material) per unit length of a random test line. X is directly determined as the linear fraction of recrystallized material along the random test line.

This methodology to determine $\langle G \rangle$, can be extended to also determine $\langle G \rangle^c$ for grains of specific crystallographic orientations c, which requires measurements of the orientation of the individual recrystallized nuclei/grains [18]

$$\langle G \rangle^c = \frac{1}{S_V^c} \cdot \left(\frac{dX}{dt} \right)^c \tag{A3}$$

$$S_V^c = 2N_L^c. \tag{A4}$$

The only concern in applying the equations above, once the properties X and S_v are measured as functions of annealing time, is in finding the time derivative of X. It requires a definition of a function $X = f(t)$ which describes the experimental data well. This problem was discussed by Vandermeer and Juul Jensen [66], and for the present materials, it was found that the Avrami equation

$$X = 1 - \exp(-Kt^b) \tag{A5}$$

could not be used. Instead a power law and an exponential function were used having the forms

$$\log \ln \left(\frac{1}{1-X} \right) = A + B(\log t) + C(\log t)^2 + D(\log t)^3 \tag{A6}$$

$$\log \ln \left(\frac{1}{1-X} \right) = A + B \exp\left[-C(\log t - D)^E \right] \tag{A7}$$

where A, B, C, D and E are fitting constants. It was found that both equations fit the experimental data well within the investigated time interval, but the exponential function (A7) seemed to give the most reasonable results just outside the investigated time interval. Therefore this function was generally applied. However, for the copper data, the power law function (A6) was also used, and reassuringly, the results for $\langle G \rangle^c$ using the two methods were very similar (see Fig. 6).

Proceedings of the 16th
Risø International Symposium
on Materials Science:
Microstructural and Crystallographic Aspects of Recrystallization.
Editors: N. Hansen, D. Juul Jensen Y.L. Liu and B. Ralph.
Risø National Laboratory, Roskilde, Denmark 1995.

EFFECTS OF ORIENTATION ON GROWTH DURING RECRYSTALLIZATION

D. Juul Jensen

Materials Department, Risø National Laboratory
DK-4000 Roskilde,Denmark

ABSTRACT

Direct and indirect methods to study effects of crystallographic orientation on growth during recrystallization are described and their potentials are discussed. Recent results obtained by these methods are summarized. Growth in heavily cold deformed polycrystalline materials are discussed with reference to new data on grain subdivision by dislocation boundaries during deformation. It is shown that in these materials, simple oriented growth relationships cannot describe faster growth of grains with specific orientations. Other possibilities are discussed. Effects of cube bands, present after hot deformation, are also analysed. Finally, a new simulation approach, which allows orientation dependent growth rates to be included, is outlined.

1. INTRODUCTION

Whether the crystallographic orientations of the nuclei have effects on their growth during recrystallization or not, has been the topic of discussions for decades. This was clearly reflected in a panel discussion at the ICOTOM8 texture conference (Doherty, Gottstein, Hirsch, Hutchinson, Lücke, Nes and Wilbrandt 1988). Here it was agreed that "recrystallization textures (RT) develop by growth selection from a limited spectrum of nuclei orientations" but that further investigations should be carried out to "help establish more clearly the relative importance of the oriented nucleation (ON) and oriented growth (OG) contributions to recrystallization textures (RT)". Since then, many such experiments have been carried out using modern advanced experimental techniques, and it is an aim of this paper to summarise and discuss the results. Both single crystals and polycrystalline materials have been studied. In another keynote paper at this conference, the behaviour of single crystals is reviewed (Driver, 1995). The present paper is therefore limited to polycrystalline materials.

Most of the recent polycrystal investigations, are for recrystallization after high strain ($\varepsilon \geq 2$) deformation. Furthermore the majority of the investigations has been for aluminium. This paper therefore concentrates on heavily cold and hot deformed, medium to high stacking

fault energy (SFE), materials; and with the aim of achieving a further understanding of the growth processes, the results are related to the characteristic microstructures and microtextures developed in these metals after deformation to high strains. Only growth during primary recrystallization is considered.

2. EXPERIMENTAL METHODS AND RESULTS

In recent years, new techniques and methods have been introduced which have significantly advanced the understanding of growth during recrystallization. In particular, local texture techniques have shown to be important. Examples are: microdiffraction and Kikuchi line techniques in TEM, channelling patterns and electron back scattering patterns (EBSP) in SEM and crystallographic etching techniques. Based on such techniques, various methods to study effects of orientation on growth during recrystallization have been developed. Some of these methods are of indirect nature in the sense that for example the texture changes or development in grain size of differently oriented grains are determined and therefrom information about the growth is deduced. Other methods follow more directly the growth of the grains either focusing on the motion of single grain boundaries or using statistical methods to determine the growth rates for categories grains with different orientations. In the following both these two types of methods are reviewed and typical results herefrom are given.

2.1 Indirect methods. An experimentally easy method, is to measure the crystallographic bulk texture by X-rays or neutrons before and after recrystallization. A "transformation texture" may be calculated from the deformation texture assuming specific preferential growth relationships, like nuclei with a 40° <111> misorientation to the deformed matrix (texture) grow faster than other nuclei. A comparison between the calculated transformation texture and the experimental recrystallization texture then shows if the assumed growth relationship(s) can simulate the experiment correctly. Recent results obtained using this technique are summarized in Table 1, and an example showing how good agreement can be obtained is given in Fig. 1.

Problematic with this method is that the orientation of the nuclei are based on assumptions, not experimental measurements. Typically, it is assumed that the nuclei have either random orientations (e.g. Hirsch 1986, Engler and Lücke 1992, Bunge and Köhler 1992) or have selected orientations corresponding to the deformed grains/orientations of the highest Taylor M-factor (Kestens and Jonas 1995). This may of course have significant effects on the results. In some studies (eg. Böttcher, Hastenrath, Lücke and Hjelen 1991, Habiby and Humphreys 1994), this is overcome by measuring the "nucleation texture" (orientations of a large number of nuclei) using local texture techniques like the Kossel or the EBSP technique. Then the measured nucleation texture is simply compared to the recrystallization texture, to determine if there is an orientation effect on growth. Results of this technique are listed in Table 1.

Another widely applied indirect method relies on measurements of size-orientation relationships for a series of partially recrystallized samples, thereby seeing if grains of specific orientations are larger than others. This may be done using channelling patterns or EBSP in the SEM, Kossel X-ray diffraction or crystallographic etching techniques. Recently, EBSP has been the most widely applied technique for this type of investigations. Typically line-scans are made through the structure by either moving the sample or the beam. When a recrystallized nuclei/grain is found, its orientation and chord length are recorded. If the nucleation/growth is anisotropic with respect to the sample axis, either random line

Table 1. Experimental data collected from literature on the effects of crystallographic orientation on growth during recrystallization.

	Effects of orientation observed *	Material	ε	Rex. Temp. xT_m	Method	Reference
	Yes	Al Pure	2.3	0.15	Extended Cahn-Hagel	Juul Jensen 1992b
	Yes	Al-1050	2.3	0.43	Extended Cahn-Hagel	Juul Jensen 1995
	Yes	Al-1050	2.3	0.38	Extended Cahn-Hagel	Juul Jensen 1992a
	Yes	Cu OFHC	2.5	0.11	Extended Cahn-Hagel	Juul Jensen 1995
	Yes	Al	--	--	Synchrotron	Gastaldi and Jourdan 1984
	Yes 2)	Al 1050	3.0	0.61	Size	Nes and Solberg 1986
	Yes	Al 1050	2.3	0.38	Size	Juul Jensen et al. 1985
	Yes 2)	Al 1050	3.0	0.61	Size	Hjelen et al. 1991
	Yes 1)	Al Mn Mg	3.5	0.45	Size	Daaland et al. 1993
Cold	No	Al Mn Mg	3.5	0.68	Size	Daaland et al. 1993
Deformed	Yes	Cu super pure	3.0	0.13	Size misorientation	Sztwiertnia and Haessner 1991
	Yes	Cu pure	3.0	0.16	Size misorientation	Sztwiertnia and Haessner 1990
	Yes 3)	Cu	~2.3	0.09-0.28	Size misorientation	Duggan et al. 1993
	Yes	Al	≥2.0	--	Texture	Engler and Lücke 1992
	Yes	Al	--	--	Texture	Hirsch 1986
	Yes	Al Cu	1.4-4.6	0.33-0.68	Texture	Engler et al. 1995
	Yes	ARMCO iron	--	--	Texture	Bunge and Köhler 1992
	Yes	IF steel	2.0	--	Texture	Kestens and Jonas 1995
	Yes	Si steel	0.9	0.47	Texture (incl. nuc.)	Böttcher et al. 1991
	No	Al Si	2.0	0.37	Texture (incl. nuc.)	Habiby and Humphreys 1994
Hot + Cold	No	Al Pure	2.3	0.68	Size	Hjelen et al. 1991
Deformed	No	Al Mn	2.0	0.42	Texture (nucl.)	Weiland et al. 1995
	No	Al 1050	Ext. 90%	0.55 - 0.67	Size	Samajdar et al. 1994
	No	Al 1050	Ext. 90%	0.71	Size	Doherty et al. 1993
Hot	No	Al Mn Mg	--	0.5	Size	Daaland et al. 1993
Deformed	Yes 3)	Al Mn Mg	--	0.5	Size	Vatne et al. 1994
	Yes	Al Mn	2.3	0.75	Texture	Rickert et al. 1991

* The "Yes, No" etc. in this column are the authors conclusions.

1) Ascribed to precipitation effects 2) Ascribed to location of nuclei (cluster effects) 3) Ascribed to micro growth selection

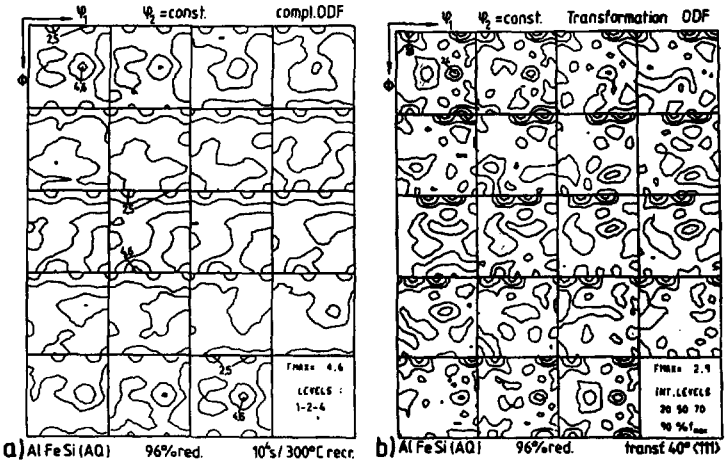

Fig. 1. Recrystallization texture in 96% deformed Al Fe Si annealed at 300°C for 10^4 sec.
a) Experimental result, b) simulated result assuming the deformation texture is statistically transformed by all possible 40° <111> rotations (Hirsch 1986).

directions or preselected principal directions have to be chosen, for the line scans. Deformed material is separated from recrystallized grains based on the characteristics of the EBSPs (Krieger Lassen, Juul Jensen and Conradsen 1994). When scanning through deformed microstructure, the EBSPs will change rapidly due to misorientations between neighbouring volumes and the EBSPs may be blurred. But when scanning through a recrystallized nuclei/grain, the EBSP is invariant and sharp. This distinction between deformed and recrystallized material, is easiest if the deformed matrix consists of small cells/subgrains with relatively large misorientations across the dislocation boundaries (i.e. the EBSPs are very blurred) and/or if the recrystallized grains are large.

Recent results using this technique are summarized in Table 1 and two examples are shown in Fig. 2. It is seen that in the one case (Fig. 2a), the cube grains grow to become significantly larger (~1.6 times) than the other grains, whereas in the second case (Fig. 2b) only a small difference between the cube and other grain sizes is observed.

Common to both these indirect methods (also the texture method including nucleation) is that information about nucleation (sites and rates) is not included. This may affect the interpretation if the results are used for analysis of growth rates. If, for examples, nuclei of a given orientation develop in clusters, their growth will be stopped early in the process due to impingement and they will appear small in the grain size distribution or as a weaker texture component no matter what their growth rate is. This is illustrated in Fig. 3. The figure shows, that even if the fast growing grains (here cubes) grow 2.5 times as fast as the other grains, the two types of grains will have identical average recrystallized grain sizes if the fast growing grains nucleate on clustered lines and the other grains at random sites.

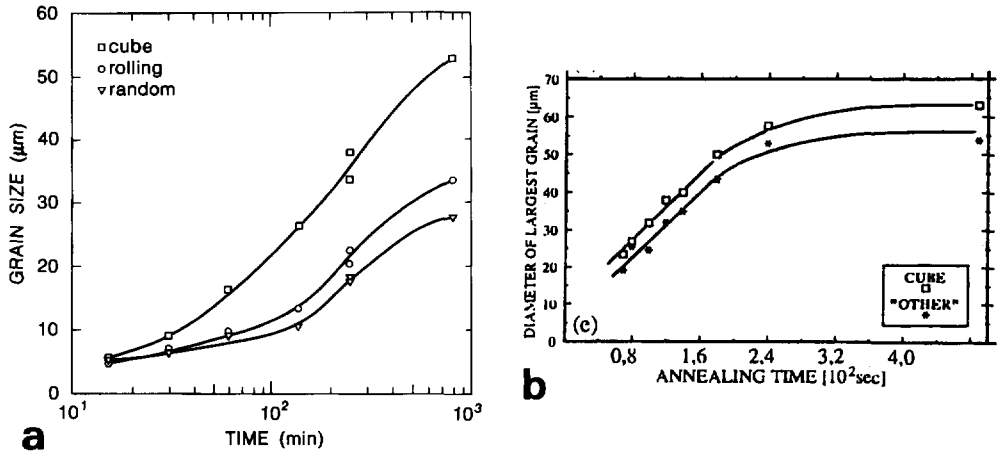

Fig. 2. The average sizes of grains with different orientations determined by the EBSP technique for a series of partially annealed samples. a) Al (99.4%) cold rolled 90% and annealed at 253°C (Juul Jensen 1992a). b) Al Mn Mg hot rolled and annealed at 330°C (Daaland, Dronen, Vatne, Naess and Nes 1993).

2.2 Direct methods. The most direct method to study orientation effects on growth rates is to monitor the movement of a selected boundary in-situ. HVEM, TEM and SEM techniques have been used for this. However, these techniques only reveal surface motions and here the focus is on bulk processes. Alternatively, the average growth rate <G> may be determined statistically from a series of partially recrystallized samples. Following the Cahn-Hagel approach (1962)

$$\frac{dX}{dt} = < G > A \tag{1}$$

where X is the volume fraction of transformed material after annealing for time t and A is the surface area of the migrating boundaries.

If also the crystallographic orientations of the individual growing grains are determined, as it is possible by the EBSP technique, the average growth rates of grains of various orientations $<G_i>$ can be determined (Juul Jensen 1992a)

$$\frac{dX_i}{dt} = < G_i > A_i \tag{2}$$

It can be shown (Underwood 1968) that A or A_i can be determined statistically from line scans through the microstructure in random direction relative to the sample axes

$$A = 2N_L \text{ or } A_i = 2N_{Li} \tag{3}$$

where N_L is the number of intersections per unit length of the test line between recrystallized grains and surrounding deformed matrix (in determination of A_i, the N_L's are categorized according to the orientations, i, of the recrystallized grains).

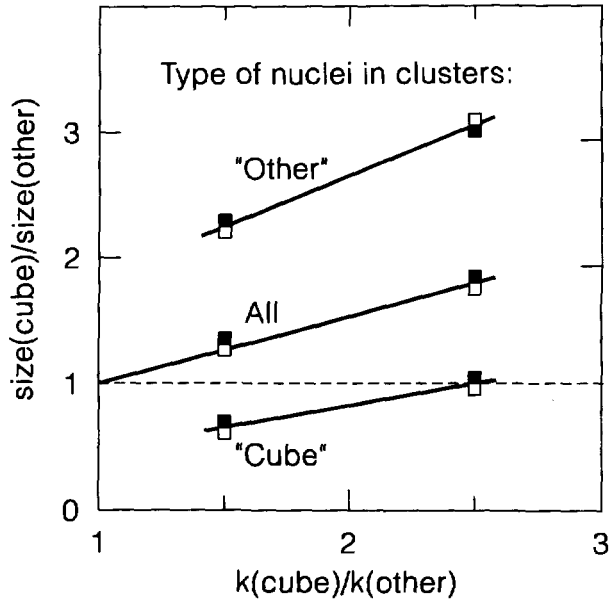

Fig. 3. Simulation of ratios between the average recrystallized grain size of cube and of other grains as a function of the relative growth advantage of the cube grains for various nucleation assumptions. The growth rates were assumed to follow the equation $\langle G \rangle = k\, t^{\alpha}$, and different k values were used in the simulation. The nucleation was assumed to appear clustered along random lines in the structure - 5 to 10 nuclei on each line. Top curve - all "other" nuclei were assumed to develop in clusters whereas cube nuclei form alone at random sites. Middle curve - all nuclei of both types develop in clusters. Bottom curve - only cube nuclei in clusters and all other nuclei form as single nuclei at random sites.

As it typically is fairly straight forward to separate recrystallized nuclei/grains from still-deformed matrix (for example using the EBSP technique based on the characteristics of the patterns, see section 2.1), $X_{(i)}$ and $A_{(i)}$ are readily determined. To calculate $\frac{dX_{(i)}}{dt}$ (see eq. (1) and (2)), a function which describes $X_{(i)}(t)$ well, has to be selected. Very often the Avrani equation is used. However in general this equation does not describe $X_{(i)}(t)$ too well over the entire annealing time interval (e.g. Doherty, Rollett and Scrolovitz 1986). An exponential function of the form

$$\log \ln \left(\frac{1}{1-X(t)} \right) = A - B \exp\left(-C\,(\log t - D)^{E}\right) \qquad (4)$$

where A, B, C, D and E are fitting constants, seems to be much more applicable. For a detailed discussion of this see Vandermeer and Juul Jensen (1994a).

Results obtained by this extended Cahn-Hagel method is summarized in Table 1 and shown in Fig. 4. So far, this type of investigations has been limited to heavily cold rolled Al and Cu. The data show that in these metals there is an orientation effect on growth.

This method to determine statistical growth rates is much more time consuming to use than the indirect methods described above; it typically takes several days of work to collect the necessary EBSP data, but it seems, at present, to be the best method available to study orientation effects on growth during recrystallization. As it is only the movement of the free-unimpinged boundaries which are included in the calculation, impingement does not cause problems. Furthermore, there are no assumptions about nucleation (spatial distributions or rates), and the growth may be anisotropic. The only requirement is that the test lines are selected randomly in the sample (3D).

To study movements of single boundaries, a new possibility is to use hard x-rays from synchrotron beam lines. The penetration depth depends on the synchrotron source and on the atomic number Z of the material, but is in the centimetre range for most standard metals. Furthermore the flux is very high. By proper collimation and focusing, the orientation within very small sample volumes (in the μm^3 range) in the bulk of a larger sample can be determined. This may allow in-situ studies of the growth of one or a few nuclei/grains of known orientation(s) in a small, selected, well characterized volume of the deformed matrix within the bulk of a larger sample. This technique and preliminary results are presented elsewhere in these Proceedings (Poulsen and Juul Jensen 1995).

3. GROWTH IN POLYCRYSTALS COLD DEFORMED TO HIGH STRAINS

The growth of nuclei/grains during recrystallization depends strongly on the deformation microstructure in which they are growing. Recently, significant progress has been achieved in the characterization of the deformation microstructures, and a framework for the microstructural development as a function of strain, common to fcc, medium to high SFE metals has been suggested (Bay, Hansen, Hughes and Kuhlmann-Wildsdorf 1992). Furthermore, local misorientations and orientation distributions within the deformed grains have been quantified (eg. Hansen and Hughes 1995, Hughes and Hansen 1995, Liu and Hansen 1995). In another keynote paper (Hughes 1995), the evolution of deformation microstructures and local orientations are reviewed, but main results very relevant for growth during recrystallization of heavily cold deformed polycrystals will be shortly summarised below.

It has been shown that the original grains at high strain are subdivided by dislocation boundaries such as lamellar boundaries, microbands, subgrain boundaries (and maybe shear bands) as well as ordinary cell boundaries. Typically the cell boundaries are of low misorientation, whereas the other types of boundaries are associated with large misorientations. As an example, misorientations measured across each dislocation boundary for a scan along ND in 90% cold rolled commercially pure Al is shown in Fig. 5. All together 20 or 22% of the 91 boundaries crossed are associated with a misorientation larger than 15°. Some of these - approximately 5 - are original grain boundaries, but the remaining ones have developed during the deformation.

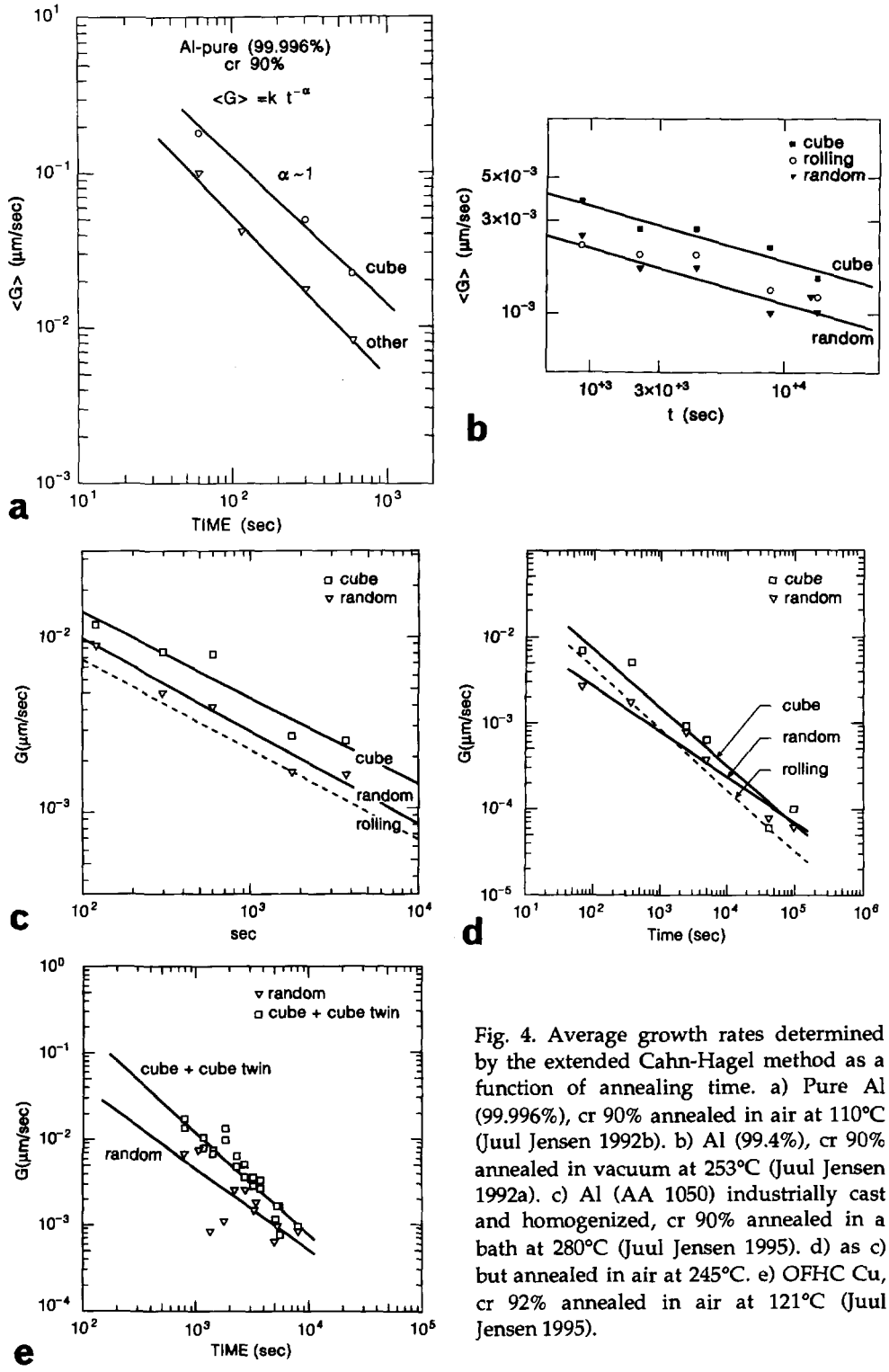

Fig. 4. Average growth rates determined by the extended Cahn-Hagel method as a function of annealing time. a) Pure Al (99.996%), cr 90% annealed in air at 110°C (Juul Jensen 1992b). b) Al (99.4%), cr 90% annealed in vacuum at 253°C (Juul Jensen 1992a). c) Al (AA 1050) industrially cast and homogenized, cr 90% annealed in a bath at 280°C (Juul Jensen 1995). d) as c) but annealed in air at 245°C. e) OFHC Cu, cr 92% annealed in air at 121°C (Juul Jensen 1995).

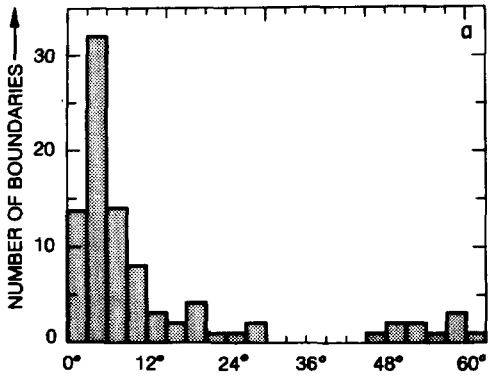

Fig. 5. Misorientation angles across dislocation boundaries in the deformed microstructure inspected in the longitudinal section in the aluminium of Fig. 4c and d (Hansen and Hughes 1995).

The high angle boundaries make sharp transitions between deformed material of very different orientations and they appear very close to each other. For example, in 90% cold rolled commercially pure Al, it has been found that the average distance between high angle boundaries (>15°) is 2.3 μm and 4.4 μm when measured along ND and RD respectively. A typical scan along ND is shown in Fig. 6.

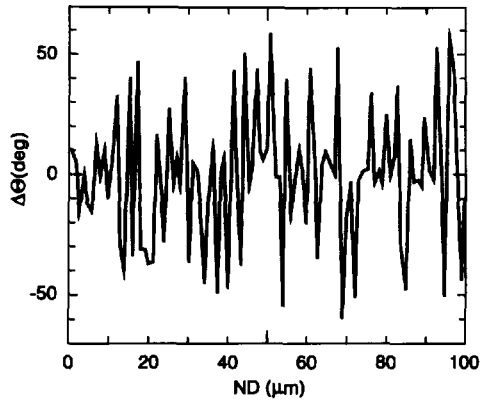

Fig. 6. Misorientation angles between neighbouring 1μm areas determined by an EBSP scan along ND in the cold deformed microstructure of the aluminium of Fig. 4c and d. The sign is determined from the corresponding rotation axis: if it is a right hand side triangle the sign is + and - if it is in the left hand side (Juul Jensen 1995).

It is clear that the growth of nuclei in such a heterogeneous matrix is very complex. Already when a nucleus is formed it is surrounded by matrix of different orientations at various places along its periphery. And during the growth, the nucleus will meet deformed material having very different orientations at various parts of its boundaries and at various stages during the annealing. Consequently, a wide spectrum of misorientation axes and angles between nuclei/grains and their surrounding deformed matrix must be expected. This has also been found experimentally (Sztwiertria and Haessner 1990, Juul Jensen 1995). An example is shown in Fig. 7. Here the misorientation between nuclei/grains and the surrounding matrix in a partly annealed 90% cold rolled commercially pure Al sample is shown. It can be seen that almost all possible axis/angle pairs are present. Also if the nuclei/grains are classified according to their orientations (eg. cube, rolling or random) no sharp peaks are observed in the misorientation distributions (see Fig. 8.).

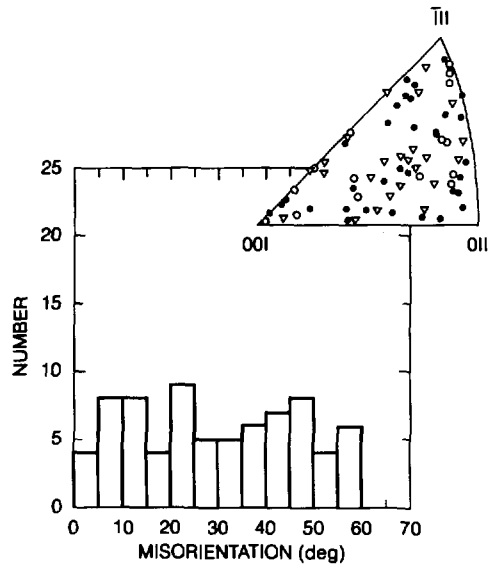

Fig. 7. Misorientations between growing nuclei/grains and the deformed matrix of the Al shown in Fig. 4c and d annealed for 180 sec. The misorientation angles are shown as histograms and the axes are shown in unit stereographic triangles. Different signatures are used for axes with different misorientation angles: • boundaries with high misorientation $\theta \geq 35°$, x medium misorientation $20° \leq \theta < 35°$ and o low misorientations $\theta < 20°$ (Juul Jensen 1995).

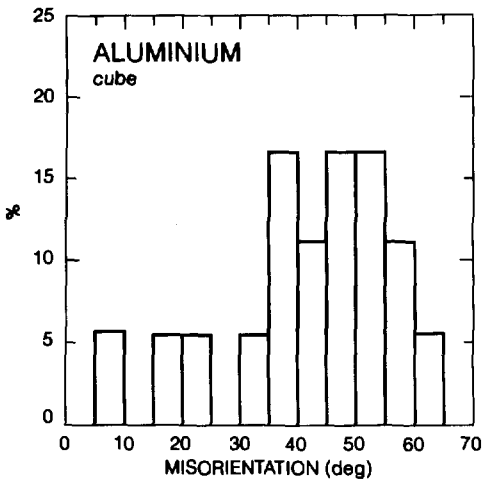

Fig. 8. Misorientation angles between growing cube nuclei/grains and the deformed matrix along ND and RD in the aluminium shown in Fig. 4c and d. The data include all annealing times (Juul Jensen 1995).

Single crystal experiments (e.g. Beck, Sperry and Hu 1950, Kohara, Parthasarathi and Beck 1958, Liebmann, Lücke and Masing 1956) and later bicrystal experiments (Gottstein and Shwindlerman 1992) have shown exceptionally high mobility of boundaries with specific misorientation relationships, for example with a near 40° <111> misorientation. This has led to the standard definition of "oriented growth", namely that nuclei/grains with a special misorientation relationship to the deformed matrix grow faster than other grains. For heavily deformed polycrystals this definition can however not (at least not in its standard form), be used to describe the growth of the nuclei/grains because of the large local orientation variations in the deformed matrix. (Not even, when a growth advantage of nuclei/grains of a specific orientation (often cube) is observed (see Fig. 4 and Table 1)). Oriented growth may of course take place locally when a segment of a nucleus/grain

boundary meets a (typically small) volume in the deformed matrix with which a preferential misorientation relationship exists. But to explain the observed growth advantages (eg. Fig. 4) also other possibilities have to be sought.

Such a possibility may relate to the presence of low angle boundaries between nuclei/grains of the various orientations and the surrounding deformed matrix. When twinning can be ignored, it is generally believed that nuclei develop with orientations already present in the deformed state. During their formation and growth they may therefore meet local volumes of the same, or almost the same orientation resulting in low angle boundary segments. As the mobility of low angle boundaries is low (e.g. Doherty 1978) such volumes will act as obstacles to the moving boundary and pin it (until the boundary has finally moved across or "unzipping" may have taken place). This effect, which in the following will be termed *orientation pinning*, is illustrated in Fig. 9. Here an imaginary nucleus of a given orientation A is shown. In the neighbouring deformed matrix, local volumes which could be cell blocks or subgrains, of A or near A orientation is shown in grey. In the sketched example, it is clear that the movement of top and right-hand side of the nucleus boundary will be hindered by orientation pinning whereas the lower part is more free to move. If nuclei/grains of given orientations (e.g. of retained rolling orientations) are more likely to meet deformed material of their own orientation than other types of grains (e.g. cubes) are, it is clear that orientation pinning will affect the relative growth rate of the two types of nuclei/grains (reducing more severely that of the retained rolling orientations).

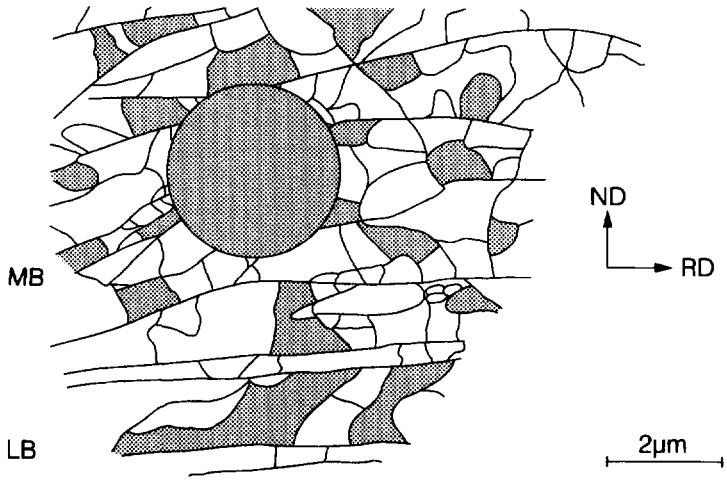

Fig. 9. Sketch illustrating orientation pinning. An imaginary circular nucleus is shown in a deformation microstructure typical for heavily cold rolled polycrystals. Areas of microbands and lamellas bands are marked by MB and LB respectively. When the nucleus grows into areas of nearly its own orientation, as those shown in grey, the boundary motion will be hindered in that direction by orientation pinning.

To illustrate the importance of orientation pinning, data from annealing of heavily deformed Al and Cu (Juul Jensen 1995) are summarised below. By a statistical investigation of misorientations between nuclei/grains of cube, rolling and random orientations and the surrounding matrix, it was found that the rolling and randomly oriented nuclei/grains in both Al and Cu were surrounded by about 10-25% low angle (≤10%) boundaries to the

deformed matrix whereas only 3-10% of the cube (and in Cu cube twin) boundaries were of low angle. The orientation pinning is therefore occurring about 3 times as often for rolling and random grains than for cube grains. This will clearly affect the relative growth rates, reducing more severely that of the rolling and random nuclei/grains. If it for simplicity is assumed that the low angle boundaries are completely immobile, and all other boundaries have identical mobilities, this would mean that the cube nuclei/grains will grow about 1.3 times as fast the other grains. Experimentally a cube growth advantage of about 1.6 is observed in Al (see Fig. 4). In this simple calculation, effects of orientation pinning on neighbouring segments of the boundary is not included. Orientation pinning together with "local oriented growth" (fast movement of boundary segments having a preferential orientation-relationship, e.g. 40° <111>) therefore seems to provide a reasonable explanation for the observed growth advantage.

4. GROWTH IN ALUMINIUM HOT DEFORMED TO HIGH STRAINS

Like for cold deformed polycrystals, in recent years major progress has been achieved in the characterization of the hot deformation microstructure. The identification of cube bands in hot deformed aluminium has shown to be very important both scientifically and industrially. In the following effects of the hot deformation microstructure with cube bands on growth will be discussed. Elsewhere in these Proceedings, 3 keynote papers are describing the effects of cube bands on nucleation and on processing of industrial aluminium (Doherty, Samajdar, Necker, Vatne and Nes 1995, Hirsch and Engler 1995 and Weiland 1995).

After hot rolling to high strains, the microstructure typically is a laminar structure with lamellar boundaries (LBs) approximately parallel to the rolling plane. Between the LBs are almost equiaxed subgrains with a very low interior dislocation density. An optical micrograph showing a typical microstructure in 86% plane strain compressed aluminium is shown in Fig. 10. The distance between the LBs is, in this case, in the range 5-15 μm, which

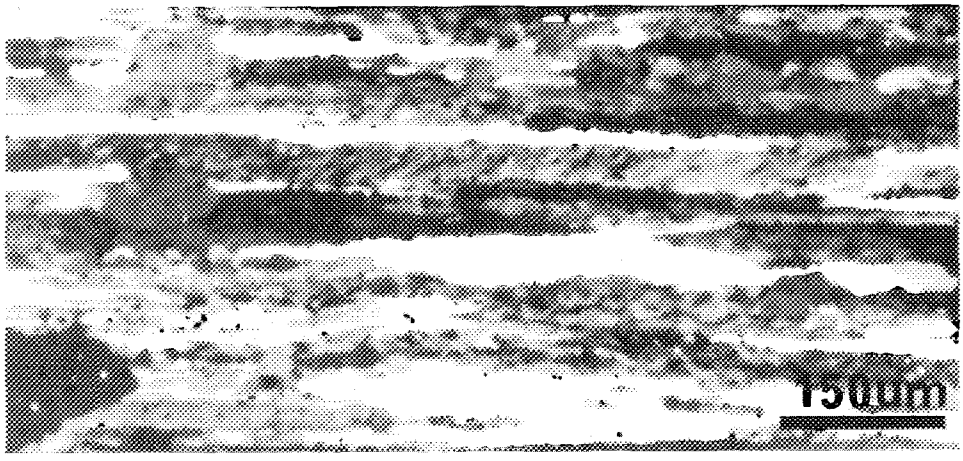

Fig. 10. Optical micrograph of partly annealed hot deformed Al. The starting material is identical to that of Fig. 4c and d but here it is hot deformed by plane strain compression at T = 400°, $\dot{\varepsilon}$ = 2.5 s^{-1} and ε = 2.0 at Pechiney. The sample has been annealed in a bath at 400°C for 300 sec.

matches the width of the (deformed) original 100 μm grains. The LBs are generally associated with high misorientations whereas there is little variations in the crystallographic orientation between the LBs. This can be seen in Fig. 11, where the misorientation between neighbouring points - 1 μm apart - are shown for an EBSP scan along ND.

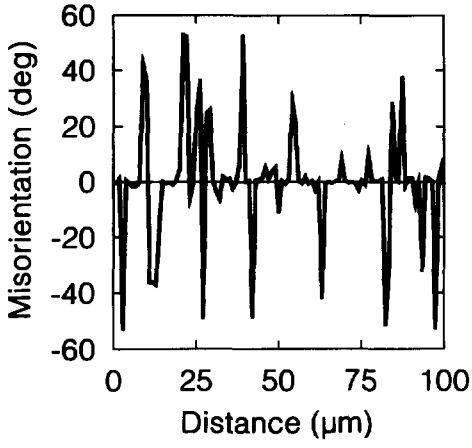

Fig. 11. Misorientation angles between neighbouring 1μm areas determined by an EBSP scan along ND in the hot deformed microstructure of the aluminium shown in fig. 10.

Of particular interest, is the cube orientation. Hot rolling of aluminium alloys have shown that the cube orientation is metastable and bands (lamellas) of cube orientations are seen in the microstructure even after heavy deformations (e.g. Weiland and Hirsch 1991, Vatne, Daaland and Nes 1994, Samajdar, Doherty, Panchanadeeswaran and Kunze 1994). For example, in Al 1Mn 1Mg hot rolled to a total reduction of 96%, the "cube bands" are 1-5 μm wide at this strain and can be seen quite close together - e.g. 10 μm apart (Daaland 1993). It is furthermore found that the subgrains within the cube bands are larger than other subgrains and that cube oriented nuclei develop in these cube bands (Samajdar and Doherty 1995, Vatne, Furu and Nes 1995). When a cube nuclei is formed in a cube band it is at least partly surrounded by low angle boundaries. An example of this has been seen in Al (AA 1050) deformed by plane strain compression at 400°C to $\varepsilon = 2.0$. Two samples annealed at 400°C for 180 and 300 seconds, respectively (corresponding to 17% and 35% recrystallization) were examined by EBSP and the misorientations between 15 arbitrary cube nuclei and the surrounding deformed matrix along RD and ND were determined. The result is shown in Fig. 12. It can be seen that approximately half the boundaries are relatively low angled whereas the others half are of very high misorientations. Also later, during their growth to the final recrystallized grain size (in this case 80 μm), the cube nuclei/grains may meet other cube bands creating new low angle boundaries.

The growth in direction of the low angle boundary segment will be hindered by orientation pinning as discussed for the cold deformed materials. This will be the case for cube nuclei/grains as well as for all other nuclei/grains of orientations similar to those in the deformation texture. So maybe orientation pinning will affect the growth of all types of nuclei more or less equally in the hot deformed materials. This is in agreement with size/orientation investigations, which all have shown that the orientation has no effect on the size of the recrystallized grains after hot deformation (see Table 1). In this context it would be of interest to examine growth rates in a series of samples deformed at different Zener-Holloman parameters, Z, and thereby study possible relationships between the

stability of cube bands (which are known to decrease at increasing Z) and the ratio between the growth rate of cube and of other grains.

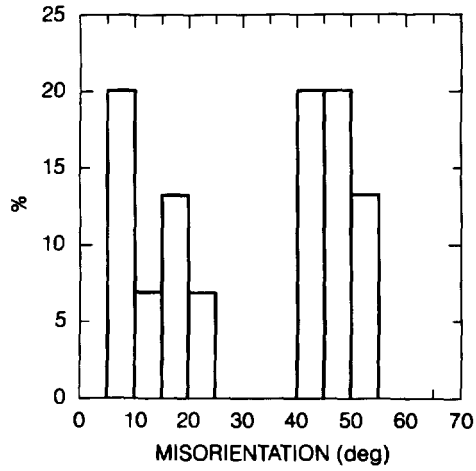

Fig. 12. Misorientation angles between 15 cube nuclei/grains and the neighbouring hot deformed matrix along ND and RD in the aluminium shown in Fig. 10 and 11. The data include annealing times of 120 and 300 seconds.

5. MODELLING RECRYSTALLIZATION INCLUDING ORIENTATION EFFECTS

A new trend in recrystallization modelling, is to include the orientations of the nuclei/grains (Tavernier and Szpunar 1991, Juul Jensen 1992b, Vandermeer and Juul Jensen 1994b, Furu, Vatne, Ørsund and Nes 1995). As an illustration of how this may be done, a combined analytical and numerical procedure developed at the Naval Research Laboratory in Washington DC and at Risø, will be shortly described below.

A schematic diagram showing the procedure is given in Fig. 13. At first a detailed experimental characterization is carried out. Using a local texture technique, like the EBSP technique, maybe supplemented by bulk texture measurements, it is fairly straightforward to determine the volume fraction of recrystallized material, X(t), the free unimpinged surface area of the recrystallized grains A(t), the texture, grain size distributions and interface area, R(t), between recrystallized grains for a series of partly recrystallized samples. All these parameters are categorized according to the orientation, i, of the recrystallized nuclei/grains.

The next step in the procedure is to analyse the $X_i(t)$ and $A_i(t)$ data by the microstructural path method (MPM). A detailed description of the MPM is given in another keynote paper elsewhere in these Proceedings (Vandermeer 1995). By a qualified trial and error procedure, nucleation and growth models are developed which fit the X_i and A_i data. The deduced models are expressed in terms of nucleation rates, growth rates and shapes for the individual orientation categories. They depend critically upon the impingement "rules" that are prescribed: do the nuclei form randomly in the structure, in clusters along lines on planes etc.? The result of this step is a set of nucleation and growth models which might be termed a "best guess".

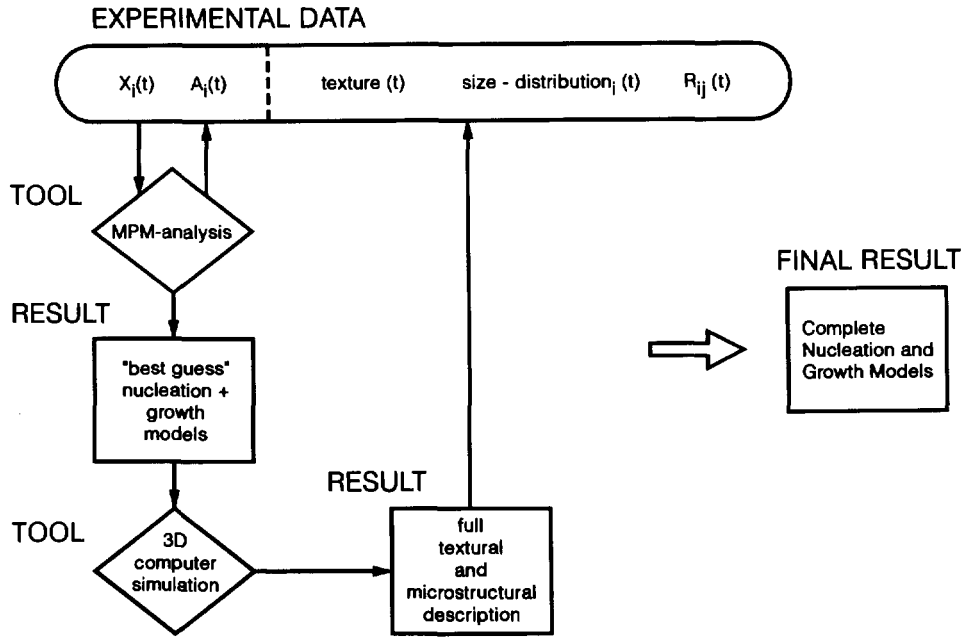

Fig. 13. Flow chart showing the combined MPM and simulation approach of recrystallization modelling.

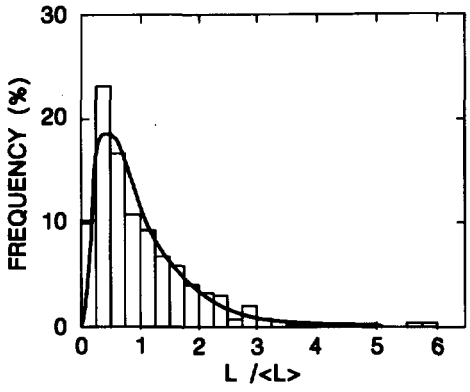

Fig. 14. Normalised grain size distribution (linear intercept values) for grains of all orientations. The histogram is experimental EBSP data and the full line is the simulated result (Juul Jensen and Vandermeer 1995).

A further validation of the "best guess" nucleation and growth models is obtained by 3D numerical computer simulations (Juul Jensen 1992b), which is the next step in the procedure (see Fig. 13). Here, effects of variations in the suggested input parameters from the MPM analysis, as well as effects of specific nucleation clustering are studied. Concerning the latter aspect, it is for example determined how large the clusters should be, how they should be

arranged in space and if nuclei of different orientation categories develop at separate clusters or mixed together within the individual clusters. The output is a full textural and microstructural description at any selected annealing time. The simulated results are then compared to the experimental results, and generally very good agreement can be obtained (Juul Jensen and Vandermeer 1995). An example of this is shown in Fig. 14. The final result of the combined MPM and simulation procedure is complete nucleation and growth models which are able to describe the recrystallization under the given materials and processing conditions.

6. CONCLUSIONS

Significant advances in the understanding of growth during recrystallization in heavily deformed polycrystals have been achieved using modern methods to measure growth rates and to characterize the development of deformation microstructures and microtextures. Findings very important for growth during recrystallization have been that in cold deformed polycrystals, the original grains are heavily subdivided by deformation induced high angle boundaries and in hot deformed aluminium, bands of cube orientation exist after deformation.

- The Cahn-Hagel method extended to include the crystallographic orientation of the nuclei/grains is at present the most powerful technique available to study statistically the growth rate of nuclei/grains with different orientations. In the not too far future, high energy synchrotron techniques may enable direct in-situ measurements of the movement of single selected boundaries in the bulk during recrystallization.

- Due to significant grain subdivision by high angle dislocation boundaries during deformation to high strains, a recrystallization nuclei/grain will be surrounded by many different orientations and the surroundings will change during the growth. Preferential growth misorientation relationships (e.g. a 40° <111> rotation) can therefore only exist locally in space and time.

- When the recrystallization nuclei/grains have orientations similar to components of the deformation texture, they may, during their formation and growth, meet deformed material of their own, or almost their own, orientation and then become partly surrounded by low angle boundaries. Since the mobility of low angle boundaries is low, this may cause local "orientation pinning" of the moving boundary.

- Depending on the volume fraction and distribution of the texture components in the deformed matrix, orientation pinning can affect differently the average growth rate of nuclei/grains with different orientations. Nuclei/grains with orientations alien to the deformed matrix will not be affected by orientation pinning resulting in a growth advantage of these grains. Examples of this are seen in cold deformed Al and Cu. "Orientation acceleration" of growth may occur locally when a preferential growth misorientation between a nucleus/grain and the matrix exists, and thus affect similarly the relative growth rates of nuclei/grains of different orientations.

- A future aim is to incorporate the characteristics of the deformation microstructure in the recrystallization modelling/simulation programmes to be able to simulate directly consequences of local oriented growth and orientation pinning on the recrystallization kinetics, texture and microstructure.

ACKNOWLEDGEMENTS

Niels Hansen and Roy A. Vandermeer are gratefully thanked for fruitful discussions. Lisbeth Larsen and Jytte Mortensen are thanked for carefully typing of this manuscript.

REFERENCES

Bay, B., Hansen, N., Hughes, D.A. and Kuhlmann-Wilsdorf, D. (1992). Evolution of fcc deformation structures in polyslip. Acta metall. mater. 40, 205-219.

Beck, P.A., Sperry, P.R. and Hu, H. (1950). The orientation dependence of the rate of grain boundary migration. J. Appl. Phys. 21, 420-425.

Bunge, H.J. and Köhler, U. (1992). Model calculations of primary recrystallization textures. Scripta metall. mater. 27, 1539-1543.

Böttcher, A., Hastenrath, M. Lücke, K. and Hjelen, J. (1991). Nucleation during primary recrystallization of RGO electrical steel sheet observed by the EBSP-method. ICOTOM 9 Textures and Microstructures 14-18, 673-678.

Cahn, J.W. and Hagel, W.C. (1962). Theory of the pearlite reaction. In: Decomposition of Austenite by Diffusional Processes. Edited by V.F. Zackay and H.I. Aaronson (Interscience, NY) 131-196.

Daaland, O. (1993) Development of microstructure and texture during rolling and annealing of commercial Al-Mn-Mg alloys. Ph.D. thesis Trondheim, pp 152.

Daaland, O., Dronen, P.F., Vatne, H.E., Naess, S.E. and Nes, E. (1993). On the growth rate of cube grains, rotated cube grains and rotated goss-grains in commercial aluminium alloys. ICOTOM 10 Mat. Sci. Forum. 113-115, 115-120.

Doherty, R.D. (1978). Nucleation. In: Recrystallization of metallic materials. Edited by F. Haessner. (Dr. Riederer-Verlag GmbH Stuttgart) 23-61.

Doherty, R.D., Gottstein, G., Hirsch, J.R., Hutchinson, W.B., Lücke, K., Nes, E. and Wilbrandt, P.J. (1988). Report of the panel on recrystallization textures: Mechanisms and experimants. ICOTOM 8. Edited by J.S. Kallend and G. Gottstein (TMS, Warrendale PA) 563-572.

Doherty, R.D., Kashyap, K. and Panchanadeeswaran, S. (1993). Direct observation of the development of recrystallization texture in commercial purity aluminium. Acta metall. mater. 41, 3029-3053.

Doherty, R.D., Rollett, A.R. and Srolovitz, D.J. (1986). Structural evolution during recrystallization. In: Proc. Risø Symp. 7th. Annealing Processes - Recovery, Recrystallization and Grain Growth. Edited by N. Hansen et al. (Risø, Denmark) 53-67.

Doherty, R.D., Samajdar, I., Necker, C.T., Vatne, H.E. and Nes, E. (1995). Nucleation of recrystallization in cold and hot deformed polycrystals. In these Proceedings.

Driver, J.H. (1995). Effect of crystal orientation on recrystallization. In these Proceedings.

Duggan, B.J., Lücke, K., Köhlhoff, G. and Lee, C.S. (1993). On the origin of cube texture in copper. Acta metall. mater. 41, 1921-1927.

Engler, O., Hirsch, J. and Lücke, K. (1995). Texture development in Al-1.8 wt% Cu depending on the precipitation state-II. Recrystallization textures. Acta metall. mater. 43, 121-138.

Engler, O. and Lücke, K. (1992). Mechanisms of recrystallization texture formation in aluminium alloys. Scripta metall. mater. 27, 1527-1532.

Furu, T., Vatne, H.E., Ørsund, R. and Nes, E. (1995). Modelling recrystallization after hot deformation of aluminium. Submitted to Mater. Sci. Techn.

Gastaldi, J. and Jourdan, C. (1984). Study of grain boundary migration using synchrotron white beam x-ray topography. In: Proc. Risø Symp. 5th. Microstructural characterization of materials by non-microscopical techniques. Edited by N. Hessel Andersen et al. (Risø, Denmark) 255-260.

Gottstein, G. and Shvindlerman, L.S. (1992). On the orientation dependence of grain boundary migration. Scripta metall. mater. 27, 1515-1520.

Habiby, F. and Humphreys, F.J. (1994). The effect of particle stimulated nucleation on the recrystallization texture of an Al-Si alloy. Scripta metall. mater. 30, 787-790.

Hansen, N. and Hughes, D.A. (1995). Analysis of large dislocation populations in deformed metals. Phys Stat. Sol b 149, 155-172.

Hirsch, J. (1986). Recrystallization of fcc metals as investigated by ODF analysis. In: Proc. Risø Symp. 7th. Annealing Processes-Recovery, Recrystallization and Grain Growth. Edited by N. Hansen et al. (Risø, Denmark), 349-360.

Hirsch, J. and Engler, O. (1995). Texture, local orientation and microstructure in industrial Al-alloys. In these Proceesings.

Hjelen, J., Ørsund, R. and Nes, E. (1991). On the origin of recrystallization textures in aluminium. Acta metall. mater. 37, 1377-1404.

Hughes, D.A. (1995). The evolution of deformation microstructures and local orientations. In these Proceedings.

Hughes, A.A. and Hansen, N. (1995). High angle boundaries and orientation distributions at large strains. Scripta metall. mater. in press.

Juul Jensen, D. (1995). Growth rates and misorientation relationships between growing nuclei/grains and the surrounding deformed matrix during recrystallization. Acta metall. mater. in press.

Juul Jensen, D. (1992a). Growth of nuclei with different crystallographic orientations during recrystallization. Scripta metall. mater. 27, 533-538.

Juul Jensen, D. (1992b). Modelling of microstructure development during recrystallization. Scripta metall. mater. 27, 1551-1556.

Juul Jensen, D., Hansen, N. and Humphreys, F.J. (1985). Texture development during recrystallization of aluminium containing large particles. Acta metall. mater. 33, 2155-2162.

Juul Jensen, D. and Vandermeer, R.A. (1995). Simulation of recrystallization microstructures and textures in multiple texture component materials. To appear in Proc. EUROMAT.

Kestens, L. and Jonas, J.J. (1995). Modelling texture change during the static recrystallization of IF steels. Submitted to Acta metall. mater.

Kohara, S., Parthasarathi, M.N. and Beck, P.A. (1958). Anisotropy of boundary mobility. J. Appl. Phys. 29, 1125-1126.

Krieger Lassen, N.C., Juul Jensen, D. and Conradsen, K. (1994). Automatic recognition of deformed and recrystallized regions in partly recrystallized samples using electron back scattering patterns. ICOTOM 10. Mat. Sci. Forum. 157-162, 149-158.

Liebmann, B.v., Lücke, K. and Masing, G. (1956). Untersuchungen über die Orientierungsabhängigkeit der Wachstumsgeschwindigkeit bei der primären Rekrystallisation von Aluminium-Einkristallen. Z. Metallkde. 47. 57-63.

Liu, Q. and Hansen, N. (1995). Geometrically necessary boundaries and incidental dislocation boundaries formed durig cold deformation. Scripta metall. mater. 32, 1289-1295.

Nes, E. and Solberg, J.K. (1986). Growth of cube grains during recrystallization of aluminium. Mat. Sci. Techn. 2, 19-21.

Poulsen, H.F. and Juul Jensen, D. (1995). Synchrotron radiation diffraction: a novel tool for recrystallization studies in bulk μm^3 sized local areas. In these Proceedings.

Rickert, T., Guldberg, S., Furu, T., Nes, E. and Lücke, K. (1991). The effect of particles on texture evolution in commercial AlMn. ICOTOM 9. Textures and Microstructures 14-18, 721-726.

Samajdar, I. and Doherty, R.D. (1995). Role of S [{123}<634>] orientations in the preferred nucleation of cube grains in recrystallization of fcc metals. Scripta metall. mater. 32 845-850.

Samajdar, I., Doherty, R.D., Panchanadeeswarans and Kunze, K. (1994). Direct observation of the nucleation and growth rates of cube and non-cube grains in warm plane-strain extruded commercially purity aluminium. ICOTOM 10 Mat. Sci. Forum 157-162, 2025-2030.

Sztwiertnia, K. and Haessner, F. (1991). The orientation characteristics of different recrystallization stages in copper. ICOTOM 9 Textures and Microstructures 14-18, 641-646.

Sztwiertnia, K. and Haessner, F. (1990). Discrete statistical treatment of recrystallization texture development. In Recrystallization '90. Edited by T. Chandra (TMS, Warrendale) 535-540.

Tavernier, Ph. and Szpunar, J.A. (1991). Modelling of recrystallization textures. Acta metall. mater. 39, 549-556.

Underwood, E.E. (1968). Surface area and length in volume. In: Quantitative microscopy. Edited by R.T. DeHoff and F.N. Rhines (McGraw-Hill Book Co NY) 77-127.

Vandermeer, R.A. (1995). Analytical modelling of the kinetics of recrystallization. In these Proceedings.

Vandermeer, R.A. and Juul Jensen, D. (1994a). On the estimation of Cahn-Hagel interface migration rates. Scripta metall. mater. 30 1575-1580.

Vandermeer, R.A. and Juul Jensen, D. (1994b).Modelling microstructural evolution of multiple texture components during recrystallization Acta metall. mater. 42, 2427-2436.

Vatne, H.E., Daaland, O. and Nes, E. (1994). On the formation of cube texture in aluminium. ICOTOM 10, Mat. Sci. Forum 157-162, 1087-1094.

Vatne, H.E., Furu, T. and Nes, E. (1995). Nucleation of recrystallised grains from cube bands in hot deformed commercially purity aluminium. Submitted to Mater. Sci. Techn.

Weiland, H. (1995). Nucleation and growth of recrystallized grains during industrial thermomechanical processing of aluminium alloys. In these Proceedings.

Weiland, H. and Hirsch, J.R. (1991). Microstructure and local texture in hot rolled aluminium. ICOTOM 9 Textures and Microstructures 14-18, 647-652.

Weiland, H., Rouns, T.N. and Liu, J. (1995). The role of particle stimulated nucleation during recrystallization of an aluminium-manganese alloy. Z. Metallkde. 85, 592-597.

Simulation of Recrystallization Microstructures and Textures: Effects of Preferential Growth

D. JUUL JENSEN

Three-dimensional (3-D) simulations of recrystallization were carried out using an approach where grains of different orientations are characterized by different nucleation and growth parameters. The aim was, by simulation, to study the effects of preferential growth on recrystallization under various nucleation assumptions. The simulations were based on the assumptions that (1) a material can be represented by two types of grains, one that grows 1.5 to 2.5 times faster than the other type; (2) the nucleation takes place either instantaneously when annealing is started or continuously during the annealing period; and (3) the nucleation sites are distributed either randomly or in clusters (around points, along lines, or on planes). These assumptions relate to common experimental observations. It was found that the nucleation and growth assumptions have very significant influences on the recrystallization characteristics. The preferential growth of one type of grain in particular affects the width of the recrystallized grain size distribution and the texture development. Furthermore, it was found that many different nucleation and growth assumptions can result in identical recrystallization microstructures and textures. The results of the simulations are discussed with reference to typical experimental findings.

I. INTRODUCTION

DURING recrystallization of deformed materials, nuclei develop and grow at the expense of the deformed matrix. The crystallographic orientation of the nuclei may be of importance for their growth, and there may be relations between the orientation of the nuclei and the site at which they develop. This has been shown experimentally using modern automated local orientation techniques, such as the electron back scattering pattern technique.[1,2] By this technique, statistically accurate average growth rates of grains of various crystallographic orientations can be determined.[3] It is often found that grains of special orientations grow faster than other grains.[3-6] Such preferential growth of one type of grain can have a large effect on recrystallization, on microstructural and textural development, and on kinetics. The magnitude of this effect, however, depends critically on the nucleation pattern, which determines the impingements among the various types of grains. If, for example, the fast growing nuclei develop in clusters and the other nuclei do not, the preferential growth effects will be limited.

By using local orientation techniques, it has been shown that nuclei of different crystallographic orientations may form at different types of sites.[7-9] However, to get statistically reliable data on nucleation rate and on the density and distribution of potential nucleation sites is not straightforward. In the present work, simulations are, therefore, used to calculate the effects of preferential growth under various nucleation assumptions. A similar approach was previously used by Frost and Thompson[10] for two-dimensional (2D) simulations of effects of nucleation conditions on the microstructural development. But in this work orientation effects were not considered. In the present work, the component method[11] is used for the simulations. Conditions, typical for recrystallization of heavily deformed, medium to high stacking fault energy fcc metals are selected. Typically, growth data are chosen, and nucleation conditions covering extremes of experimental observations are assumed in the simulations. In total, 59 types of recrystallization processes are simulated, and the effects of preferential growth on the recrystallization kinetics, texture, and microstructure under the various nucleation conditions are described and discussed.

D. JUUL JENSEN, Senior Scientist, is with the Materials Department, Riso National Laboratory, DK-4000 Roskilde, Denmark.

Manuscript submitted February 13, 1996.

II. SIMULATION APPROACH

A. *The Component Method*

The component method allows three-dimensional (3-D) simulation of recrystallization. It is possible to perform the simulation with as many texture components (grain orientations) as desired (and, therefore, the two components assumed in the present work), and it is straightforward to define nucleation and growth conditions for the different components. It is a geometrical method very similar to that introduced by Mahin *et al.*[12] but extended to include the various components. The component method has already been described.[11] However, new aspects, for example, concerning continuous nucleation, have been used for the first time in this work. Therefore, a short resumé will be given to introduce the method.

A cubic matrix (computer sample) is considered, the size of which is determined by the number of grains in the simulation (N_g) and the nucleation density. First, the N_g grains are distributed in the matrix. They may be distributed at wish (for example, one component may be at random sites and another clustered on two-dimensional (2-D) planes). For each nuclei, the following information is stored: (1) the nucleation position (x,y,z), (2) the crystallographic orientation (texture component number), and (3) the nucleation time. If a nuclei, n_i, is associated with a long nucleation time (*i.e.*, nucleated late) its site may become occupied by

Table I. Simulation Parameters (The Ones Marked by an Asterisk Are Variable, Changing from Simulation to Simulation; the Others Are Fixed at the Given Value for All the Simulations)

Nucleation	
Density	$2.4 \cdot 10^{-4}$ μm^{-3}
Size	4 μm
* Number of texture components	(1) 2
* Number of fractions of component 2 (type II)	10, 30 pct
* Sites (spatial distribution)	random or clusters
* Rate	instantaneous or continuous
Growth	
Shape	spherical
Rate	$G = k \cdot t^{\alpha}$
α	-0.5
k(I) (type I)	0.1 $\mu m/s^{(\alpha+1)}$
* k(II) (type II)	0.15 to 0.25 $\mu m/s^{(\alpha+1)}$
Statistical	
Number of grains (N_g)	5000
Number of inspection planes	3
Number of inspection lines in each plane	10

a neighboring grain (nucleated early). In that case, the nuclei, n_i, will never become active.

Then, the nuclei are allowed to grow. The growth rates may depend on sample direction (x,y,z), grain orientation (texture component number) and annealing time (t). It is assumed that growth stops when two grains impinge (in that direction) but continues unaffected in all other directions.

For all grid points in the computer sample, it is registered which of the N_g grains arrived there first and at what time. At any annealing time, it is therefore straightforward to calculate (1) the volume fraction of recrystallized material, (2) the textural composition, (3) the average grain size, and (4) the grain size distributions for the individual texture components and for all grains. As these results are available at any annealing time, the recrystallization kinetics are also fully described. The grain size data are obtained by the linear intercept method in selected planes in the computer sample. Thereby, data directly comparable to typical experimental microstructural measurements are obtained.

In the present work, the effects of the selected nucleation and growth parameters on only the simulated recrystallization grain size, grain size distribution, texture, and recrystallization kinetics have been described. In the simulated data, however, much more information is available, such as number of grain edges and grain corners and the unimpinged surface area of the grains in the partly recrystallized stages.

B. *Simulation Conditions*

The parameters for the simulations are given in Table I. The chosen values relate to common experimental observations explained later.

1. *Nucleation parameters*

a. *Nucleation density and nuclei size*

These parameters are chosen as typical values for heavily rolled Al.[4,13,14] These parameters determine the size scale and initial condition for recrystallization, but they are, relatively unimportant for the simulated results (which, when possible, are given as normalized results).

b. *Number of components*

In heavily deformed, medium to high stacking fault energy (SFE) fcc metals, it is often observed that grains of cube orientation behave significantly different from the other grains—they may nucleate at special sites[8,9] and grow faster than the other grains.[3–6] Therefore, two texture components (types of nuclei/grains) are selected. However, for purposes of comparison, simulations using only one "average" component were carried out.

c. *Nucleation rate*

It is either assumed that nucleation is instantaneous (site saturation at zero time), or that nucleation continues to take place during the recrystallization process. In the latter case, two rates, a fast rate (1 nucleation/s) and a slow rate (1 nucleation/2s), are assumed. In the continuous nucleation case, some of the potential nuclei will never nucleate. That is, a neighboring grain that has nucleated earlier has already grown to occupy the potential nuclei's position. This means that the nucleation density in the sample will be lower than in the instantaneous nucleation case. Depending somewhat on actual growth rates (k(II)/k(I)) and number of nuclei of the two orientations, about 80 and 70 pct of the potential nuclei will become active in the fast and slow nucleation rate situation, respectively.

d. *Nucleation distribution*

Various assumptions about the spatial distribution of the nuclei are used:

(1) All nuclei form at random positions over the entire sample volume.
(2) By particle simulated nucleation, nuclei are often developing in the deformation zone around a large second-phase particle.[7] This is simulated by assuming that the nuclei are formed in clusters around selected random points in the microstructure. From one to eight nuclei are assumed to form at each point (particle).
(3) Triple line junctions, where three original grains meet, are known to be potential nucleation sites.[15] This is simulated by letting nuclei develop in clusters along a line in the microstructure. These lines have random directions relative to the sample axes. One to ten nuclei are assumed to form at each nucleation line, and the distance between two neighboring nuclei was selected randomly in the range 0 μm to $rf/2$, where rf is the final average radius of the grains ($rf \simeq 10$ μm). One of the nucleation lines (with eight nuclei) is shown in Figure 1(a).
(4) Original grain boundaries or deformation-induced intragranular high angle boundaries stimulate nucleation.[8,16,17] After high strain deformation by rolling, these boundaries (as seen in 2-D sections) are planes which are mostly aligned along the rolling plane. To simulate this type of nucleation, the nuclei are formed in clusters on 2-D planes in the microstructure. The planes are selected to be parallel to the rolling plane. One to one hundred nuclei are assumed to form on each plane. They are formed at random arcs on rings around a random point. The distance between the rings is 2

Table II. Effects of Using Five Different Nucleation Seeds (Results Are Given for Two Different Recrystallization Process Assumptions)

Assumption	Seed Number	Average Grain Size (μm)	Average Size (II)/ Average Size (I)	Vol Pct (II)	$t_{1/2}$ (s)
Random nucleation,	1	12.3	1.63	51.2	695
10 pct type II nuclei,	2	12.5	1.65	53.7	698
k(II)/k(I) = 2.5	3	12.4	1.60	53.5	672
	4	12.3	1.57	50.8	676
	5	12.6	1.59	50.6	718
Type I nuclei on	1	14.1	3.00	92.7	460
clustered lines; type II	2	14.0	2.99	91.7	459
random nucleation,	3	13.5	2.96	89.5	462
30 pct type II nuclei,	4	13.2	3.04	91.6	468
k(II)/k(I) = 2.5	5	14.3	2.95	93.7	450

areas are still deformed matrix. The simulation is for 30 pct type-II nuclei growing 2.5 times as fast as type I. The sample is 66 pct recrystallized. Already, at this stage, the dominance of the fast-growing type-II grains is clear. The spherical growth assumption is apparent in the shape of the grains. In the following discussion, only the fully recrystallized microstructures will be described. Some of the simulated microstructures with different nucleation and growth conditions are shown in Figure 3. From the figure, it can be seen that the variation in nucleation and growth parameters and the introduction of two types, instead of one type, of grains have very significant effects. When only one type of grain is included in the simulation (Figure 3(a)), a homogeneous microstructure with straight boundaries appears, whereas in the two component cases (Figures 3(b) through (j)), a more inhomogeneous grain size distribution evolves, and the boundaries between the two components become curved due to the difference in growth rate.

Figures 3(b) through (d) show the changes in microstructure and texture composition as the growth rate of type-II grains (k(II)) increases relative to that of type-I grains (k(I)). When k(II)/k(I) is 1.5 (Figure 3(b)), the microstructure is still fairly homogeneous and dominated by type-I (red) grains. As the growth rate ratio increases, type-II (green) grains become larger and more dominating.

The effects of continuous instead of instantaneous nucleation are illustrated by Figures 3(e) and (f). Less type-I (red) grains are seen when the nucleation rate is fast (Figure 3(f)).

Examples of clustered nucleation are shown in Figures 3(g) through (j). Figure 3(g) shows the recrystallized microstructure when all nuclei are clustered around random points, and Figure 3(h) is a partly clustered case where type-I nuclei develop in clusters, but type-II (green) grains have nucleated as single unclustered nuclei at random sites. In the partly clustered case (Figure 3(h)), type-II (green) grains dominate more but have a smaller average and a more homogeneous size distribution than in the fully clustered case (Figure 3(g)).

In Figures 3(i) and (j) microstructures for nucleation along lines and on planes are shown. The microstructures appear stripy due to early impingement in one or two directions, respectively.

B. *Average Grain Sizes*

The average recrystallized grain size is plotted *vs* the growth advantage of type-II grains (k(II)/k(I)) for the various nucleation conditions in Figure 4. The four top diagrams are for instantaneous nucleation, whereas the bottom two diagrams are for continuous nucleation. Each column represents different types of nucleation sites: random, clustered around points, clustered on lines, and clustered on planes. The figure shows that, for all nucleation conditions, an increase in k(II)/k(I) leads to an increase in the average recrystallized grain size. Typically, this increase is about 20 pct. That there is not a simple direct correlation between the growth rate ratio and the size advantage in the sense that a growth rate ratio of for example 2.5 yield size advantages of only 1.5, related to the increased probability for impingement of the fast growing grains. If type-II nuclei are not clustered, but the other are clustered around points or lines, the increase in average grain size with increasing growth rate is larger. When the nucleation takes place continuously at random sites, the increase in average grain size is up to 37 pct. In most cases, the number of type-II nuclei (10 or 30 pct) does not have much effect.

The comparison with the average grain size data for nucleation on the aligned planes (the right column) is more complicated because the result (linear intercept value) now depends on the direction of the line. The results presented in Figure 4 are average values for scans along normal direction (ND) and rolling direction (RD), *i.e.*, perpendicular and parallel and to the direction of the nucleation planes. The grains grow relatively freely along the ND but experience early impingement along the RD and transverse direction. Because the line scans are only along the ND and RD, the results will overestimate the true 3-D grain size. However, as this would be a typical experimental measuring procedure, also experimentally one would get an overestimated grain size under these nucleation conditions. The data in Figure 4 show that, unlike the other clustered cases, a smaller average grain size is developed when the type-II nuclei are non-clustered. This relates to the fact that, in these partly unclustered conditions, the microstructure is completely dominated by the type-II grains that are spherical and not needle or stick shaped (and, therefore, not overestimated but measured correctly).

The ratios between average grain size of type-II and type-I grains are shown in Figure 5. An increase in type-II growth rate always leads to an increase in this size ratio. Typically, a growth rate advantage of 2.5 results in size advantages in the range of 1.5 to 1.8 (if both types of nuclei have similar nucleation conditions). That there is not a one-to-one relationship in the sense that a growth advantage of

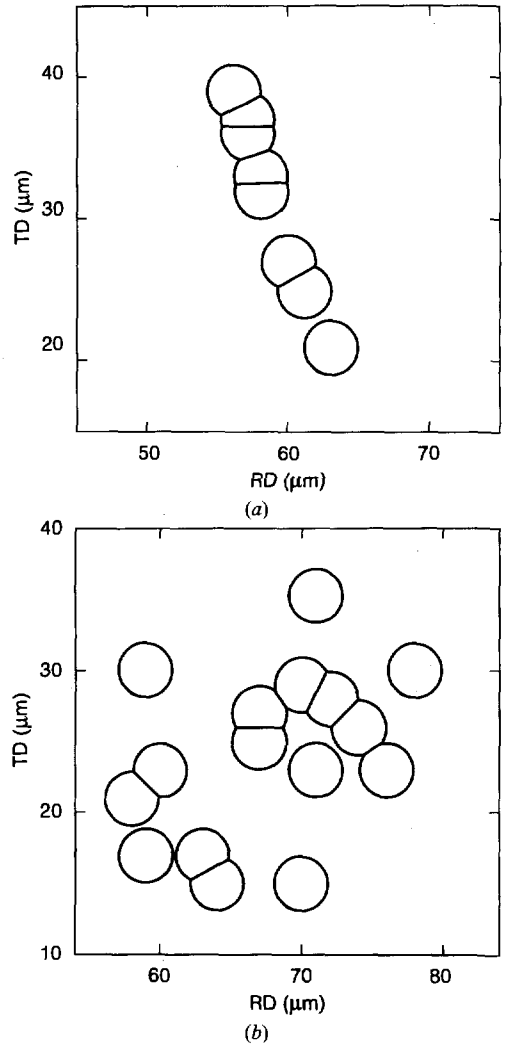

Fig. 1—Illustration of the spatial distribution of nuclei (*a*) along a line and (*b*) on a plane parallel to the rolling plane.

μm: one nuclei on the first ring, two on the next, *etc.* An example is shown in Figure 1(b)

In the clustered cases (2 through 4), it is assumed that the nuclei in the individual clusters form very close to each other (probably closer than in reality), and within each cluster, only one type of nuclei develops. Consequently, grains in the simulated microstructures are very small in one or two dimensions, and there are clusters of orientations. This is not often observed experimentally. Larger distances and mixed-type nucleation would lead to more typical microstructure. However, for the present purpose, it is considered better to somewhat exaggerate to be able to see the full effects of these types of clustered nucleation.

One further option is investigated for the clustered nucleation cases (2 through 4). Experimentally, it is observed that sometimes one type of nuclei develops in clusters, whereas others do not. For example, in heavily cold-rolled particles containing Al, randomly oriented (type I) nuclei develop in clusters near the large particles, whereas cube (type II) nuclei originate from other, less clustered sites in the microstructure. In the simulations, two options are therefore selected: (1) all nuclei develop in a number of clusters; and (2) only type-I nuclei are clustered, whereas type-II nuclei are free and nucleated randomly in the microstructure.

2. *Growth parameters*

a. *Grain shape*

Optical microscopy reveals that the grain shape in recrystallized, heavily cold-rolled metals like Cu and Al often is fairly equiaxed (also seen in the longitudinal sample section).[5] Therefore, spherical growth is chosen for the simulations.

b. *Growth rate*

Experimentally, it is generally observed that the average growth rate, $\langle G \rangle$, of free (unimpinged) boundaries decreases with annealing time, during recrystallization as[5,18]

$$\langle G \rangle = k \cdot t^{\alpha}$$

where k and α are constants.

In the few experimental investigations where $\langle G \rangle$ has been determined for different texture components, it is typically found that the slope at which the growth rate decreases as a function of t is similar for the different components.[3,19] For the present simulation, $\alpha = -0.5$ was selected.

The k values were also chosen to be representative for experimental observations of recrystallization of heavily cold-rolled Al and Cu.[4,5] For type I, $k = 0.1$ $\mu m/s^{(\alpha+1)}$, and for type II (*e.g.*, the cube component), $k = 0.15$ to 0.25 $\mu m/s^{(\alpha+1)}$ were chosen.

3. *Statistical parameters*

The statistical parameters were chosen to get reasonable computing times (<5 hours on a VAX* 4600) and converging results. For the various simulations, the random number in the program was always initiated in the same way. Thereby, the simulations could always be repeated with identical results. A different initiation of the random number generator changes the nucleation seeds, and because of the limited number of grains in the simulation, slightly different results may thus be obtained. The results for five different nucleation seeds and two different types of recrystallization process assumptions are listed in Table II. For the present purpose, the variations in results caused by the different nucleation seeds are considered to be of minor importance.

*VAX is a trademark of Digital Equipment Corporation, Maynard, MA.

III. RESULTS

A. *Microstructural Appearance*

The simulations give information about the microstructural appearance at any stage during the recrystallization. An example is shown in Figure 2. The red grains are type I and the green ones are the fast-growing type II. The white

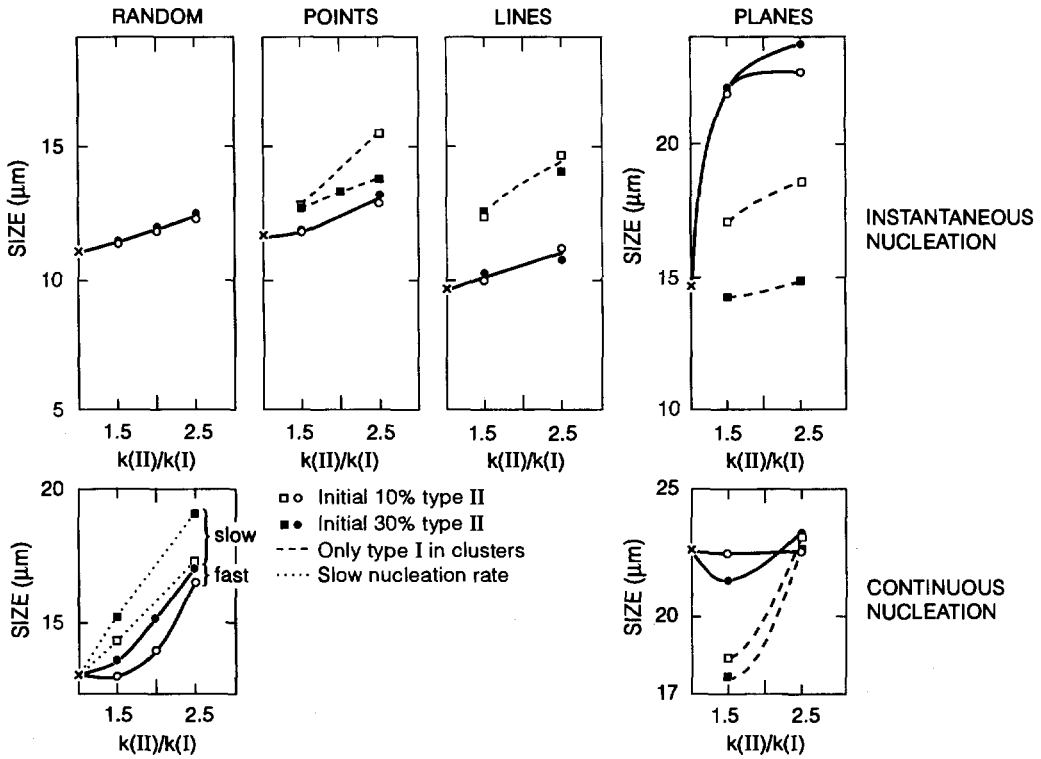

Fig. 4—Average recrystallized grain sizes (linear intercept values) as a function of the growth advantage of type II grains (*i.e.*, $k(II)/k(I)$) for the various nucleation conditions.

x times does not result in a size advantage of x times is due to the increased impingement probability for the fast-growing grains. If, however, only type-I nuclei are clustered and type II are free, the size advantage of type-II grains can become very significant: up to 3 times for the present nucleation and growth assumptions (Figure 5).

C. *Grain Size Distributions*

The size distributions are significantly affected by the growth and nucleation parameters. If instantaneous nucleation at random sites of only one type of grain is assumed, a narrow grain size distribution evolves (gray part of the histograms, Figure 6). For example, no grains have grown larger than 3 times the average grain size. Already, by introducing 10 pct type-II grains growing 2.5 times faster than type-I grains, the distribution widens significantly (Figure 6(a)). Now, 2.4 pct of the grains are larger than 3 times the average size, and the maximum size is 4 times the average. This result corresponds to the microstructure shown in Figure 3(d). Continuous, instead of instantaneous, nucleation leads to several large recrystallized grains and a large fraction of relatively small grains in the grain size distribution (compare Figures 6(a) and (b)). When the nuclei develop in clusters (partly or fully clustered), even wider distributions develop (Figures 6(c) and (d)). The maximum size in these cases is in the range of 4 to 9 times the average size.

D. *Texture*

Already, from the simulated microstructures (Figure 3), it is clear that the texture varies between extremes (from 10 to ~95 pct type-II texture). The results are summarized in Figure 7. The development is as expected in the sense that the faster type-II grains grow, the more these grains dominate the recrystallization texture. And if the type-II grains are free when nucleated, whereas type-I grains are not, strong type-II textures develop. It is, however, remarkable that only 10 pct type-II nuclei can give recrystallized textures in which these grains account for up to 95 vol pct.

The various assumptions about clustering of the nuclei (if all nuclei are clustered) do not have significant effects on the resulting texture, and also the nucleation rate does not affect the texture. This latter relates to the fact that both components (types I and II) are assumed to have identical nucleation rates in the simulations.

E. *Kinetics*

The Avrami equation[20] is generally used to describe experimental recrystallization kinetics data:

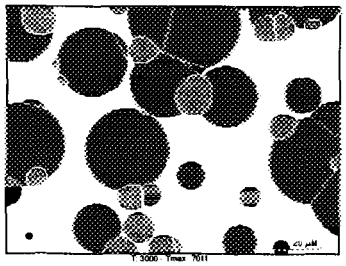

Fig. 2—Simulated partly recrystallized microstructure. Green grains are type II and red ones are type I. The input assumptions are 30 pct type II nuclei, continuous nucleation (1 nucleation/2 s) at random nucleation sites in the deformed microstructure, and $k(II)/k(I) = 2.5$. The spherical growth is very apparent.

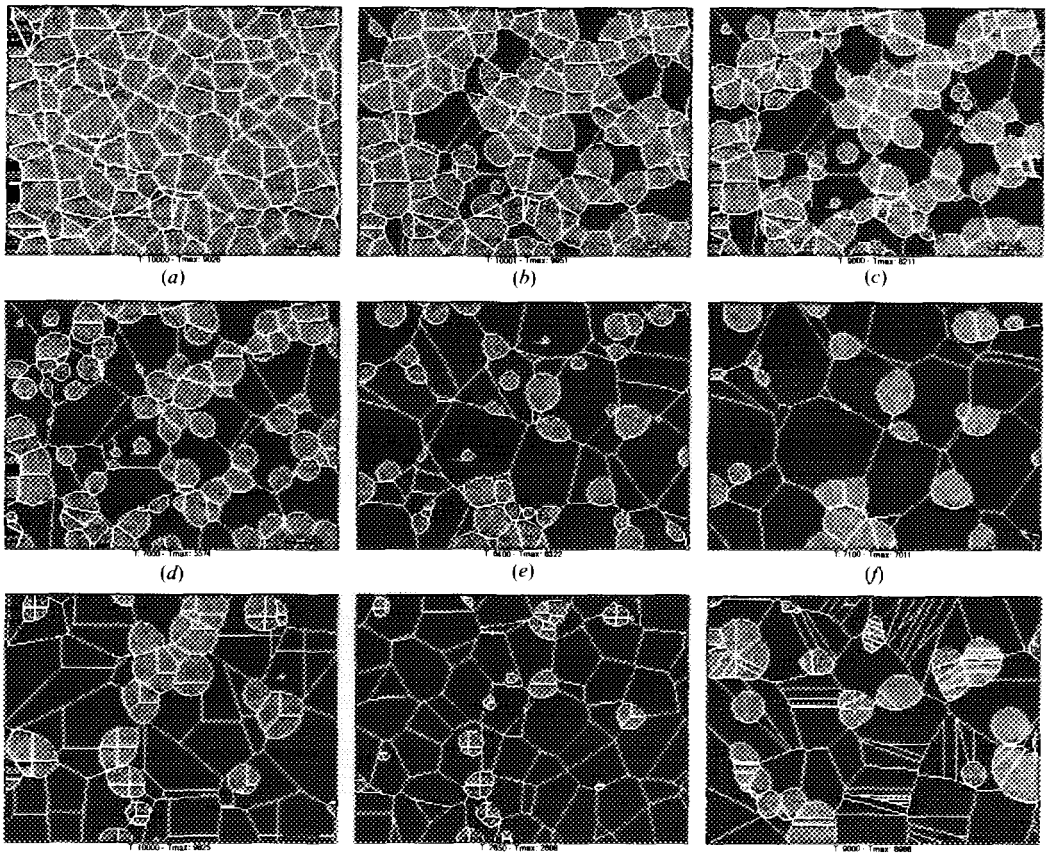

Fig. 3—Simulated fully recrystallized microstructures. Green grains are type II and red ones are type I. The input assumptions are as follows.

	Figures									
	(a)	*(b)*	*(c)*	*(d)*	*(e)*	*(f)*	*(g)*	*(h)*	*(i)*	*(j)*
Pct type II:	0	10	10	10	30	30	30	30	30	30
Nucleation rate:	I	I	I	I	C1	C2	I	I	I	I
Nucleation sites:	R	R	R	R	R	R	P	P(1)	L	A
$k(II)/k(I)$:	–	1.5	2.0	2.5	2.5	2.5	2.5	2.5	2.5	2.0

I: Instantaneous nucleation, C1: continuous nucleation with 1 nucleation/s, C2: continuous nucleation with 1 nucleation/2 s, R: random nucleation, P: nuclei sites clustered around points, P(1): type I nuclei clustered around points, L: nuclei clustered along lines, and A: nuclei clustered on planes.

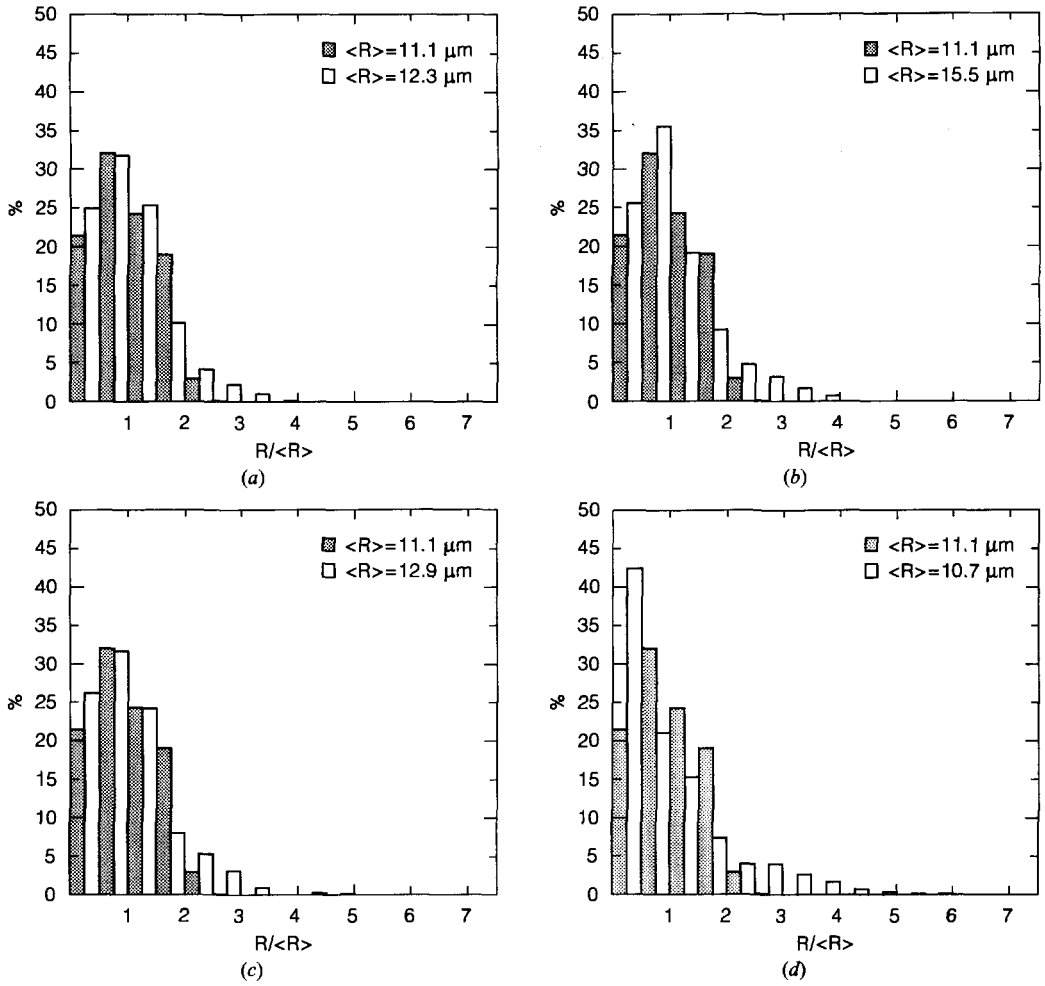

Fig. 6—Normalized grain size distributions. The gray shaded parts in all figures are for a simulation with only one texture component (instantaneous nucleation at random sites; also Fig. 3(a)). The white parts are for various conditions. The width of each bar in the histogram (grey or white) corresponds to 0.5 × R/<R>. (*a*) 10 pct type II nuclei, $k(II)/k(I) = 2.5$, instantaneous nucleation at random sites. (*b*) The same as (a) but with continuous nucleation 1 nucleation/s. (*c*) The same as (a) but with all nuclei developing in clusters around points. (*d*) The same as (a) but now with 30 pct type II nuclei, and the nuclei clustered along lines.

distributions that are too narrow compared to experimental findings. It is shown experimentally that for the heavily deformed materials referred to earlier, the maximum grain size is typically 5 to 7 times the average, and 5 to 10 pct of the grains are larger than 3 times the average.[3,24,25] One component simulation assuming instantaneous nucleation (site saturation) at random sites results in grain size distributions in which no grains are larger than 3 times the average size. By introducing preferential growth in a two-component simulation, broader grain distribution with maximum grain sizes in the range of 4 to 9 times the average is developed, thus covering the experimental range.

B. *Ambiguities*

A recrystallized material is often characterized by its texture and grain size. A notable result of the simulations is how many nucleation and growth conditions actually lead to identical textures and grain sizes. An example is given in Table III. Here, all the nucleation and growth conditions are listed which give a 45 vol pct type-II texture and a

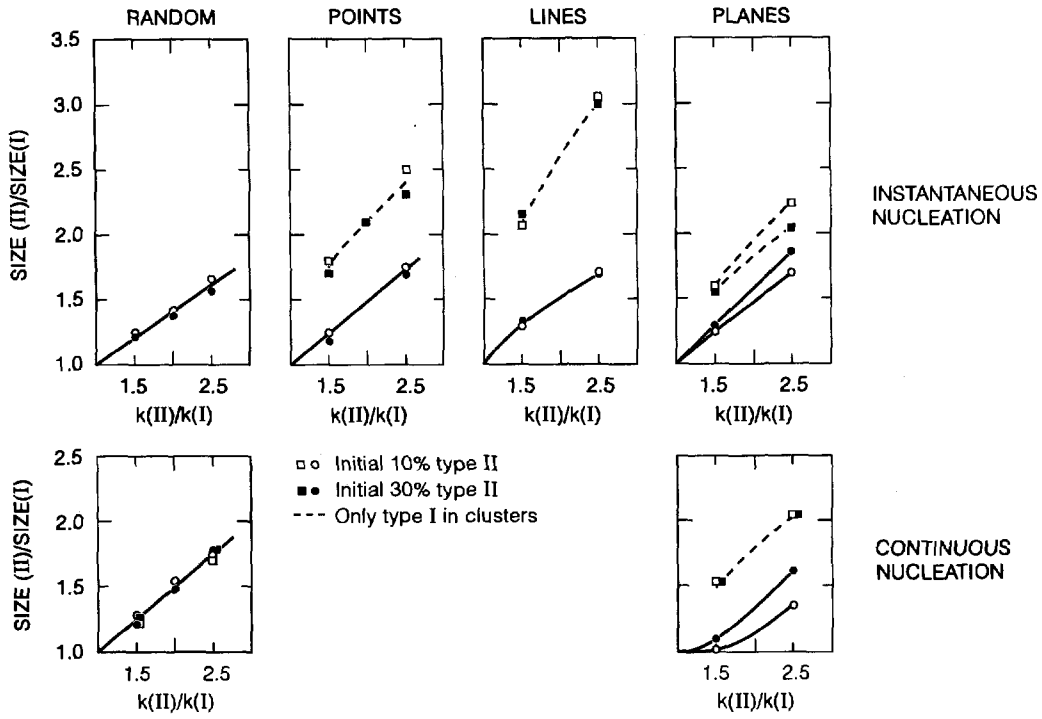

Fig. 5—Average recrystallized grain size of type II relative to type I grains as a function of $k(II)/k(I)$ for the various nucleation conditions.

$$X = 1 - \exp\left[-k(t/t_{1/2})^{\beta}\right]$$

where k, $t_{1/2}$, and β are constants characteristic of the process. However, it is often found that this equation does not give an adequate fit of the experimental data particularly at short and long annealing times.[21,22] This is also the case for the present simulated data. Two examples are shown in Figure 8. In the case of instantaneous nucleation at random sites, a deviation at short annealing times is observed. This is due to the fact that the nuclei are "born" with a finite size (2-μm radius). When the nucleation sites are clustered, larger deviations, also at long annealing times, are observed.

In spite of these deviations, the Avrami equation gives a reasonable determination of $t_{1/2}$ (not of β), and the simulated data are fitted to this equation to get an impression of the effects of preferential growth on the kinetics. The fitted results for $t_{1/2}$ are plotted in Figure 9. As can be seen, $t_{1/2}$ decreases when the growth rate of type-II grains is increased. The decrease is less significant when the nuclei appear in clusters or when the nucleation continues during the annealing process.

IV. DISCUSSION

A. *Effects of Preferential Growth*

The effects of preferential growth on the recrystallization texture, microstructure, and kinetics have been investigated. Experimentally, a growth advantage in the range 1.3 to 2.1 of cube-oriented grains compared to other grains has been observed in several heavily cold-rolled, medium to high SFE fcc metals.[3-6] Due to earlier impingements, the growth of these fast-growing grains will be relatively more hindered than that of the other grains. It is, therefore, not straightforward to estimate the effects of preferential growth based just on information about the growth advantage. In the present work, 3-D computer simulations are used to study preferential growth effects under various nucleation assumptions. It was found that an increase in the relative growth rate of one component (*e.g.*, type II) leads, as intuitively expected, to an increase in the average recrystallized grain size, a wider grain size distribution, a larger ratio of the average grain size of the two types of grains, a stronger (type II) texture, and faster kinetics. The magnitude of these effects depends strongly on the specific nucleation conditions. The most marked effects are seen on the texture: 10 pct type-II nuclei that grow 2.5 times as fast as the others result in recrystallization textures with 50 to 90 vol pct type-II grains (Figure 7). This agrees with the development of strong cube recrystallization textures in most heavily deformed, medium to high SFE fcc metals.[23]

Another important implication of preferential growth is a significant widening of the grain size distribution. Models assuming only one component, and therefore neglecting a possible preferential growth, in general predict grain size

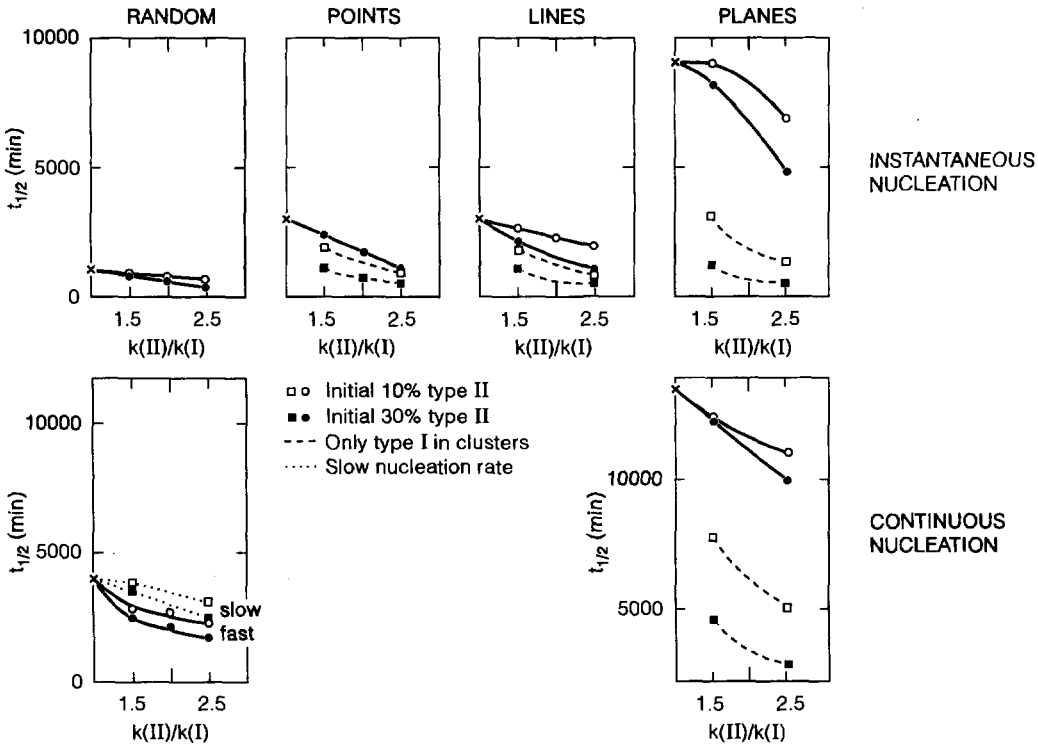

Fig. 9—Times for 50 pct recrystallization as a function of $k(II)/k(I)$ for the various nucleation conditions.

Table III. Nucleation and Growth Conditions Which All Result in a 45 Pct Type II Recrystallization Texture and Recrystallized Grain Size of 10 to 15 μm ("F" Refers to Only Type I Nuclei Being Clustered and Type II Nuclei Forming at Random Sites)

Nucleation Rate	Nucleation Sites	Pct of Type II Nuclei	$k(II)/k(I)$	Grain Size (μm)	>3× Average Grain Size
Instantaneous	*random*	*30*	*1.4*	*11.3*	*<1 pct*
		10	2.2	12.0	~1 pct
	clustered	30	1.4	11.7	~1 pct
	at points	10	2.3	12.6	~3 pct
		30 F	1.1	12.0	~1 pct
		10 F	1.4	12.5	~5 pct
	clustered	30	1.3	10.0	~5 pct
	along lines	10	2.2	10.8	~5 pct
		30 F	1.1	10.5	~4 pct
		10 F	1.4	12.0	~5 pct
	clustered	30 F	1.1	14.0	<1 pct
	on planes	10 F	1.3	15.0	~5 pct
Cont. (fast)	random	30	1.4	13.5	<1 pct
		10	2.2	14.5	~4 pct
Cont. (slow)	random	30	1.4	14.9	<1 pct

introduction of several "orientation components" can have very significant effects on all three recrystallization characteristics, and that, typically, several sets of nucleation growth assumptions lead to identical recrystallization textures and grain sizes.

The effects of preferential growth of grains of one orientation (referred to as type II) are studied. Experimentally, realistic growth rates were selected. It is shown that preferential growth leads to a very strong type-II texture development and a significant widening of the normalized grain size distribution. With only 10 pct type-II nuclei, recrystallization textures containing up to 50 to 90 vol pct of type-II grains develop, and grain sizes up to 9 times the average size are observed. The overall average grain size and the kinetics are somewhat affected by the preferential growth, here the nucleation assumptions are clearly more important. The simulations also illustrate that some of the discrepancies between experimental observations and more simple simulations like the width of the grain size distribution can be diminished, if not eliminated, if two or more orientation components and preferential growth are considered in the simulations.

ACKNOWLEDGMENTS

Jens V. Olsen is thanked for his assistance developing

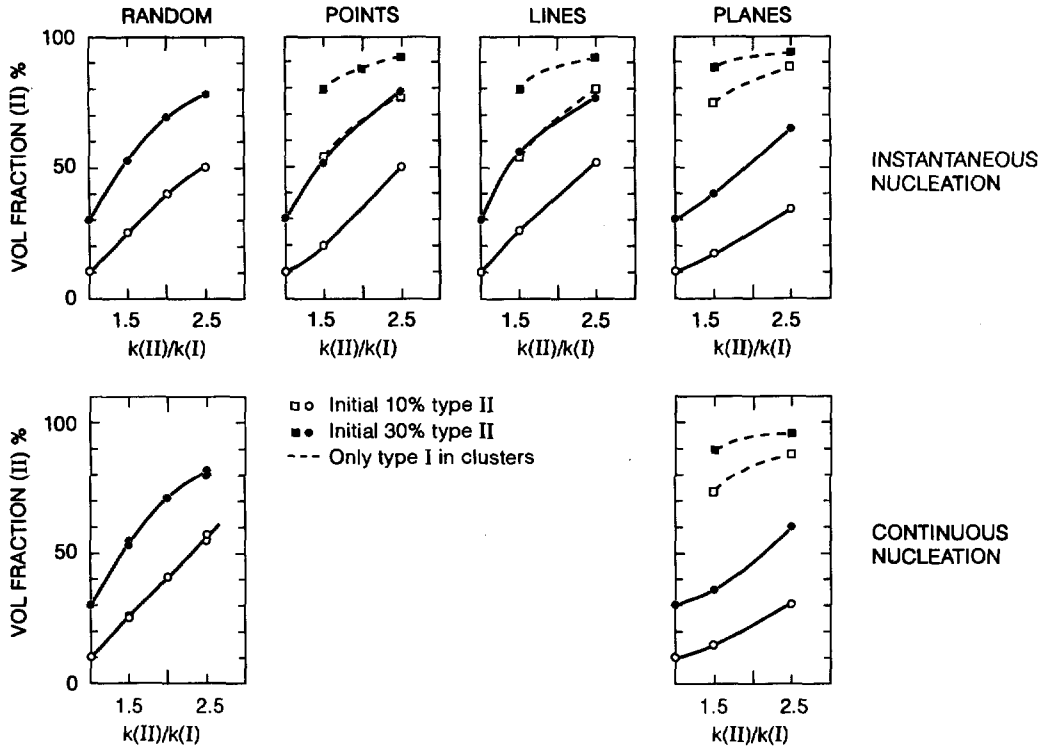

Fig. 7—Volume fraction of type II grains in the fully recrystallized state as a function of $k(II)/k(I)$ for the various nucleation conditions.

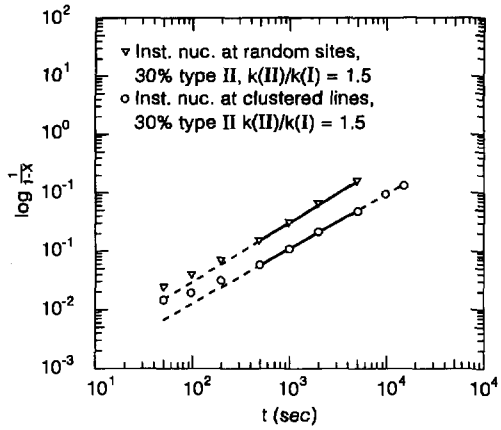

Fig. 8—Avrami plot of selected kinetic data.

recrystallized grain size of 10 to 15 μm. In total, 15 different sets of the selected nucleation and growth parameters (out of the original 59) give these results. Even if the size distribution is included, ambiguities still exist. For example, seven sets of parameters give distributions with ~1 pct of the grains larger than 3 times the average size. And, these many "solutions" are when only one nucleation density is assumed. If the nucleation density was also a free parameter in the simulation, the list would have been almost infinite.

It is, therefore, clear that when various recrystallization assumptions or a full recrystallization model have to be checked against experiments, additional, sensibly chosen recrystallization characteristics have to be included. When the test is on the possibility of preferential growth, additional sensitive characteristics are the average size of the fast-growing grains relative to the other grains together with information about clustering. This latter may be determined by measuring the free unimpinged surface area of the various grains as a function of the fraction recrystallized material (*i.e.*, the microstructural path function).[26]

V. CONCLUSIONS

A 3-D numerical method to simulate recrystallization is presented. It allows crystallographic aspects to be taken into account in the sense that nuclei/grains of different crystallographic orientations are treated individually and can be characterized by different nucleation and growth parameters. The simulations contain full information about the microstructure, texture, and kinetics. It is shown that the

software for visualizing the simulated microstructures. Drs. Niels Hansen and Roy A. Vandermeer are thanked for helpful discussions and comments.

REFERENCES

1. J.A. Venables and C.J. Harland: *Phil. Mag.*, 1973, vol. 35, pp. 1317-21.
2. D.J. Dingley: *Scan. Elec. Microsc.*, 1984, vol. 11, pp. 569-75.
3. D. Juul Jensen: *Scripta Metall. Mater.*, 1992, vol. 27, pp. 533-38.
4. R.A. Vandermeer and D. Juul Jensen: *Metall. Trans. A*, 1995, vol. 26A, pp. 2227-35.
5. D. Juul Jensen: *Acta Metall. Mater.*, 1995, vol. 43, pp. 4117-29.
6. D. Juul Jensen: in *Microstructural and Crystallographic Aspects of Recrystallization*, N. Hansen, D. Juul Jensen, Y.L. Liu, and B. Ralph, eds., Risø National Laboratory, Roskilde, 1995, pp. 119-37.
7. F.J. Humphreys, M. Ferry, C. Johnson, and P. Paillard: in *Microstructural and Crystallographic Aspects of Recrystallization*, N. Hansen, D. Juul Jensen, Y.L. Liu, and B. Ralph, eds., Risø National Laboratory, Roskilde, 1995, pp. 87-104.
8. R.D. Doherty, I. Samajdar, C.T. Necker, H.E. Vatne, and E. Nes: in *Microstructural and Crystallographic Aspects of Recrystallization*, N. Hansen, D. Juul Jensen, Y.L. Liu, and B. Ralph, eds., Risø National Laboratory, Roskilde, 1995, pp. 1-23.
9. H. Weiland: in *Microstructural and Crystallographic Aspects of Recrystallization*, N. Hansen, D. Juul Jensen, Y.L. Liu, and B. Ralph, eds., Risø National Laboratory, Roskilde, 1995, pp. 215-28.
10. H.J. Frost and C.V. Thompson: Acta Metall., 1987, vol. 35, pp 529-40.
11. D. Juul Jensen: *Scripta Metall. Mater.*, 1992, vol. 27, pp. 1551-56.
12. K.W. Mahin, K. Hanson, and J.W. Morris: *Acta Metall.*, 1980, vol. 28, pp. 443-53.
13. B. Bay and N. Hansen: *Metall. Trans. A*, 1979, vol. 10A, pp. 279-88.
14. D. Juul Jensen, N. Hansen, and F.J. Humphreys: *Acta Metall.*, 1985, vol. 33, pp. 2155-62.
15. R.A. Vandermeer and P. Gordon: *Trans. TMS-AIME*, 1959, vol. 215, pp. 577-88.
16. A.R. Jones, B. Ralph, and N. Hansen: *Proc. R. Soc. London*, vol. A368, pp. 345-57.
17. R.D. Doherty: in *Recrystallization and Grain Growth of Multi-Phase and Particle Containing Materials*, N. Hansen, A.R. Jones, and T. Leffers, eds., Risø National Laboratory, Roskilde, 1980, pp. 57-69.
18. A.T. English and W.A. Backofen: *Trans. TMS-AIME*, 1964, vol. 230, pp. 396-407.
19. R.A. Vandermeer and D. Juul Jensen: *Acta Metall. Mater.*, 1994, vol. 42, pp. 2427-36.
20. M. Avrami: *J. Chem. Phys.*, 1939, vol. 7, pp. 1103-12.
21. C.W. Price: *Scripta Metall.*, 1985, vol. 19, pp. 669-73.
22. R.D. Doherty, A.R. Rollett, and D.J. Srolovitz: *Annealing Processes—Recovery, Recrystallization and Grain Growth*, N. Hansen, D. Juul Jensen, T. Leffers, and B. Ralph, eds., Risø National Laboratory, Roskilde, 1986, pp. 53-67.
23. K. Lücke: *Proc. 7th Int. Conf. on Textures of Materials*, C.M. Brakman, P. Jongenburger, and E.J. Mittemeijer, eds., Zwijndrecht, The Netherland's Society for Materials Science, 1984, pp. 195-210.
24. K. Marthinsen, O. Lohne, and E. Nes: *Acta Metall.*, 1989, vol. 37, pp. 135-45.
25. T. Furu, K. Marthinsen, and E. Nes: *Mater. Sci. Technol.*, 1990, vol. 6, pp. 1093-1102.
26. A. Vandermeer: in *Microstructural and Crystallographic Aspects of Recrystallization*, N. Hansen, D. Juul Jensen, Y.L. Liu, and B. Ralph, eds., Risø National Laboratory, Roskilde, 1995, pp. 193-213.

Bibliographic Data Sheet **Risø-R-978(EN)**

Title and authors

Orientation Aspects of Growth during Recrystallization

Dorte Juul Jensen

ISBN	ISSN
87-550-2295-2	0106-2840

Department or group	Date
Materials Research Department	April 1997

Groups own reg. number(s)	Project/contract No(s)

Pages	Tables	Illustrations	References
81	4	41	153

Abstract (max. 2000 characters)

Recrystallization of heavily cold rolled aluminium and copper is studied with the aim of achieving information about effects of crystallographic orientation on the growth process. The potentials of several experimental techniques are analysed, and a method well suited for characterizing growth rates of grains with different orientations is developed. This method, which is referred to as the extended Cahn-Hagel method, is used for growth rate determinations in aluminium and copper deformed and annealed under five different conditions. In all the investigated cases, preferential growth of cube oriented grains is observed.

Recrystallization models, which simulates the orientational as well as microstructural development, are described. Selected models are applied for studies of recrystallization in aluminium and copper under specific deformation and annealing conditions as well as for more general studies of the effects of orientation dependent growth rates on the recrystallization microstructure and texture.

Finally, reasons for the observed orientation dependent growth rates are discussed. A new mechanism, orientation pinning, is suggested and it is shown that this mechanism is necessary for the understanding of experimental results.

Descriptors INIS/EDB

ALUMINIUM, ANNEALING, COLD WORKING, COPPER, DEFORMATION, GRAIN ORIENTATION, MICROSTRUCTURE, POLYCRYSTALS, RECRYSTALLIZATION, ROLLING, TEXTURE.

Available on request from Information Service Department, Risø National Laboratory, (Afdelingen for Informationsservice, Forskningscenter Risø), P.O.Box 49, DK-4000 Roskilde, Denmark. Telephone +45 46 77 46 77, ext. 4004/4005, Telex 43 116, Telefax +45 46 75 56 27

Collage of ingredients important for this work, including optical micrographs of partially recrystallized aluminium, an electron back-scattering pattern, a (111) pole figure, a simulated microstructure, reflections on growth rate determination, the furnace for neutron texture measurements, a cold rolled aluminium plate and a beverage can.

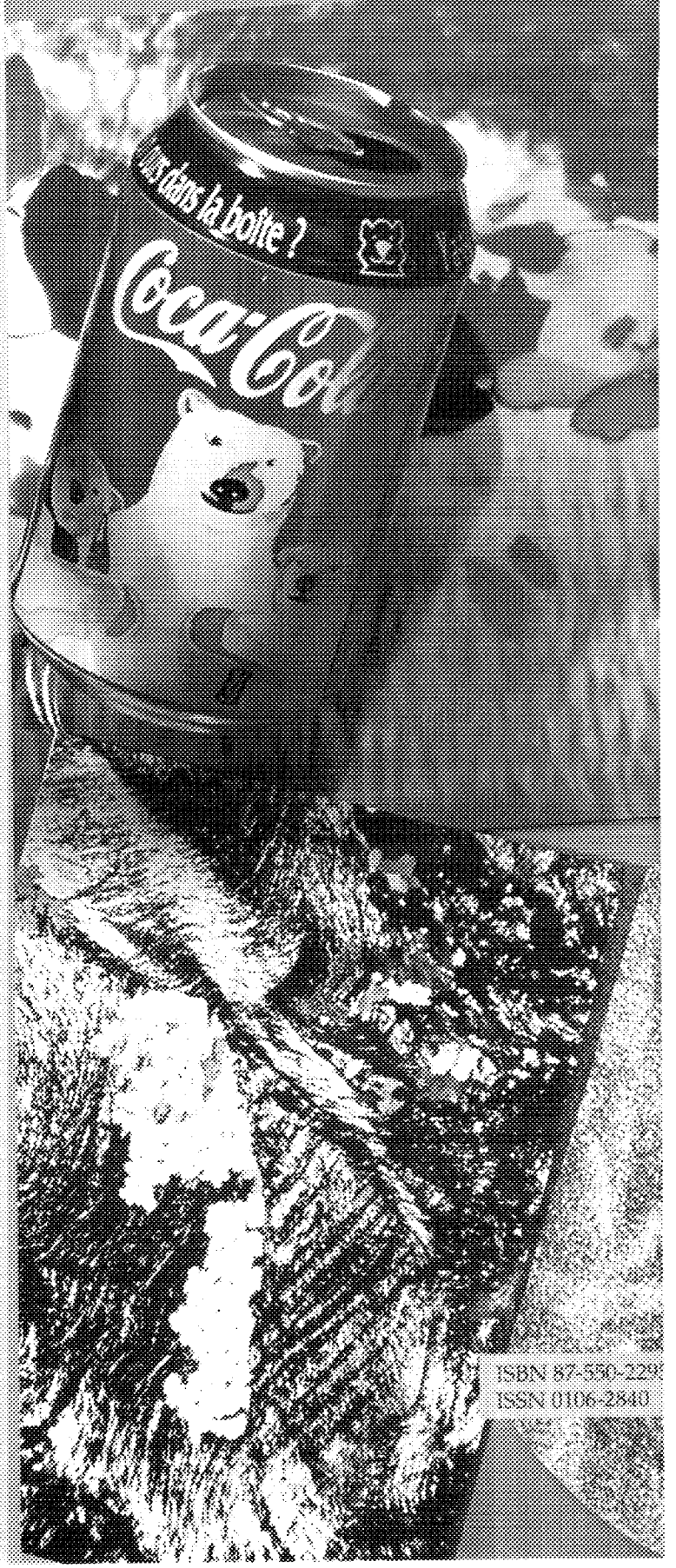

Materials Research Department
Risø National Laboratory
DK-4000 Roskilde
Denmark
Phone: +45 4677 5700
Fax: +45 4635 1173
e-mail: materials@risoe.dk

ISBN 87-550-229
ISSN 0106-2840